Groundwater in and Around Cambay Basin, Gujarat: Some Geochemical and Isotopic Investigations

A Thesis Submitted to
The Maharaja Sayajirao University of Baroda, Vadodara

For the Award of the Degree of
Doctor of Philosophy
in
Geology

By
R.D. Deshpande

Physical Research Laboratory
Ahmedabad, INDIA

November 2006

DECLARATION

This is to certify that the contents of this thesis comprise original research work of the candidate and have at no time been submitted for any other degree.

(R.D. Deshpande)
Candidate

(Dr. S. K. Gupta)
Guide

(Dr. S. J. Patel)
Co-Guide

Acknowledgements

I wish to express my profound gratitude to Dr. S.K. Gupta for introducing me to the exciting subject of hydrology. I am pleased to acknowledge that whatever understanding of hydrological systems that I have developed today, is largely because of my scientific interaction over the last fifteen years of my association with him. He taught me not only the isotope hydrology but various other conventional and modern hydrological aspects related to water resource development and management. I thank him not only for guiding me throughout the Ph.D. work but for transforming me into an explorer of the hydrological changes induced by global climate change and engineered structures.

I thank Dr. Satish Patel of the M.S. University of Baroda for agreeing to be co-guide of this thesis. His untiring help in guiding me and his encouragement and cooperation in various scientific and administrative issues have been of immense value.

Dr. P. Sharma took a lot of pains in editing the entire manuscript to improve its linguistic as well as scientific presentation. I sincerely thank him for his kindness not only during my studies but throughout my association with him.

The aspects of stable isotope systematics taught by Prof. R. Ramesh during my pre-doctoral coursework at Physical Research Laboratory (PRL) and by Prof. S.K. Bhattacharya during informal discussions helped me considerably in understanding water isotope systematics. I sincerely thank both of them for educating me. Discussions with Prof. R. Ramesh also motivated me to read the basic physics enabling me to visualise not only the large scale geohydrological processes from a hydrologic perspective but also atomic and molecular scale processes from a perspective of physics.

Prof. S. Krishnaswami has been a source of continuous inspiration and encouragement, particularly during setting up of the CFC laboratory. I have greatly benefited from informal yet very informative and enlightening discussions with him. I sincerely thank him for all that he did for me. It was indeed due to him that I could visit some of the distinguished scientists, namely, Prof. Peter S. Liss and Dr. P. Dennis (University of East Anglia, Norwich); Dr. T. C. Atkinson and Dr. Yuan Zhao (University College, London); and Dr. W. G. Darling and Dr. D.C. Goody (Institute of Hydrology, British Geological Survey, Wallingford). Interactions with these researchers significantly improved my perspective about application of tracer techniques to hydrology. I thank them all for their guidance.

Dr. Ed. Busenberg and Dr. J. Cassile of the Reston CFC laboratory, US Geological Survey responded to a large number of my emails despite the fact that I never met them. They provided some critical inputs while setting up the CFC laboratory. I sincerely thank both of them.

I also thank Prof. Shyam Lal, Mr. S. Venkataramani and Mr. T.K. Sunilkumar for providing important guidance and help during initial stages of setting up the CFC laboratory.

Inputs from Prof. M.M. Sarin about the chemistry of ground waters and the dry deposition of salt and dust particles have been useful in formulating some of the interpretations of the data presented in this thesis. I thank him for his help.

Informal interaction with Prof. A.K. Singhvi inspired me to organise the laboratory as well as to manage the field trips efficiently. I thank him for his encouraging words of advice. Prof. S.V.S. Murty responded positively every time I approached him with some request concerning logistics. I also thank him for his kind cooperation.

Mr. M.H. Patel (PRL) and Mr B.R. Raval (GWRDC) helped me in the fieldwork and in mobilising the support of local people for permission to work in their farms. Mr. D.K. Rao and Mr. R.A. Jani helped significantly in isotopic analyses of water samples. Dr. Meetu Agarwal, then a PDF in hydrology group assisted me in the fieldwork and also analysed the groundwater samples for the ^{222}Rn activity. My former colleague Mrs. Vasanti Somayajulu helped me in analysing some of the samples and in other laboratory activities. I thank them all for their great help.

Mr. Pranav Adhyaru set up the automated electronic system for remotely actuating the Valco Rotary Valves coupled with External Event Control Card of the Gas Chromatograph. Dr. M.G. Yadava measured the ^{14}C activity in the carbonate precipitates provided to him. Dr. Navin Juyal has been a valuable resource person for geological and palaeoclimatic aspects of the study area. I sincerely thank all of them for their very important contributions.

I would also like to thank Mr. Y.M Trivedi, Mr. K.K. Patel, Mrs. Parulben and Mr. Ghanshyambhai for extending the necessary administrative and logistic support during several field trips. My thanks are also due to Mr. D.R. Ranpura who took the photographs for this thesis.

I can not imagine how the life at PRL would be without Tea club members, namely *V.G. Shah, Pandian, Shiva, Padia, Ramakant, Hitesh, Renga, Kamesh, Jani, Madhusudan and Pranav.* The ten minutes intermission spent in their company provided a refreshing change in my hectic work schedule. I am happy to acknowledge a large number of my friends and colleagues, namely *Anil, Amish, Bhas, Bhushan, Bobra, Deepu, Dilip Angom, GG Dholakia, AP Gohil, RS Gupta, Ishwarbhai, Jitesh Bhatt, Jyoti, Jigar, KK Patel, Pauline, Modh, Narayanan, Nishthaben, Rama, Raghu, Sunil, Subbu, SK Shah, Somkumar, Suthar and Vishal* for their constant encouragement and support. I sincerely thank all of them for being with me.

There are colleagues at PRL too numerous to be named individually for their direct or indirect help during this work. I do remember all of them and express my sincere gratitude.

The encouragement from my family has been the motivating force to sustain me through the difficult times during this work. I thank all the members of my extended family at Baroda, Gandhinagar and Ahmedabad for excusing me for not being with them when they needed me the most.

I have no words to thank my son -*Amol* and my wife -*Uma*. Their lonely evenings and weekends are hidden throughout this thesis.

-R.D. Deshpande

Table of Contents

Page

List of Figures

Page

Chapter 1. Introduction

Chapter 2. Theory

Chapter 3. Experimental Procedures

Chapter 4. Results and Discussions

Lists of Tables

Pages

Chapter 2. Theory

Chapter 3. Experimental Procedure

Chapter 4. Results and Discussion

List of Abbreviations

AEU:	Air Equilibration Unit
bdl:	Below Detection Limit
bgl:	Below Ground Level
bl:	Boundary Layer
CBGW:	Cambay Basin Ground Water
CFC:	Chlorofluorocarbon
DCB:	Dug cum Bore well
DW:	Dugwell
EC:	Electrical Conductivity
ECBBF:	Eastern Cambay Basin Bounding Fault
GC:	Gulf of Cambay
GMWL:	Global Meteoric Water Line
GNIP:	Global Network for Isotopes in Precipitation
GWRDC:	Gujarat Water Resources Development Corporation
HP:	Hand Pump
IAEA:	International Atomic Energy Agency
kaBP:	Kilo Annum Before Present (1000 years before present)
Lat.:	Latitude
LGM:	Last Glacial Maxima
LMWL:	Local Meteoric Water Line
Long.	Longitude
LRK:	Little Rann of Kachchh
mS:	mili Siemens
MW:	Molecular Weight (g mol^{-1})
NGC:	North Gujarat Cambay
NS:	Nalsarovar
PA:	Peak Area
PFM:	Piston Flow Model
pmC:	Percentage Modern Carbon
PPM:	Parts Per Million
RSD:	Relative Standard Deviation
RT:	Retention Time
SIRM:	Stable Isotope Ratio Mass-spectrometer
T:	Tubewell
TA:	Artesian Tubewell
TDIC:	Total Dissolved Inorganic Carbon
TS:	Thermal Spring
WCBBF:	Western Cambay Bounding Fault
WMO:	World Meteorological Organization
WMRM:	Well Mixed Reservoir Model

Abstract

The NGC region is characterized by a unique combination of geological, hydrological, tectonic and climatic features, namely, (i) two major deep seated faults, namely the East Cambay Basin Bounding Fault (ECBBF) and the West Cambay Basin Bounding Fault (WCBBF) defining the Cambay Graben with several other sympathetic faults parallel and orthogonal to these; (ii) more than 3 km thick sedimentary succession forming a regional aquifer system in the upper part; (iii) higher than average geothermal heat flow; (iv) intermittent seismicity; (v) emergence of thermal springs and thermal artesian wells in some cases with high helium concentrations; (vi) arid climate with high rate of evapotranspiration; and (v) significant mining of groundwater over the past few decades.

During the last couple of decades, along with declining piezometric levels a progressive increase in groundwater fluoride concentrations was observed. This prompted the belief that high fluoride in groundwater of the region was associated to long residence time of the mined groundwater and/ or subsurface injection of thermal waters. This study aimed to (i) determine the distribution of various geochemical tracers that could help identify the origin of groundwater fluoride; (ii) determine the direction and rate of movement of groundwater in the regional aquifer system; (iii) relate the reported high helium and temperature anomalies with the tectonic framework of the region; and (iv) search for hydrological proxies of past climates.

- A survey of dissolved groundwater fluoride and electrical conductivity (EC) was undertaken to identify areas of high concentration of fluoride, and to understand its origin. Dissolved fluoride and EC of modern rainfall were also measured to understand the role of dry deposition and/ or amount of rain in controlling the fluoride and EC of rainwater.
- A survey of dissolved helium and temperature of groundwater in the NGC region was undertaken to delineate areas with anomalies in these parameters and to understand their inter-relationship with the regional tectonics. Simple procedures were developed and standardized for (i) sample collection and storage, and (ii) measurement of helium concentrations in soil-gas and groundwater using commercially available helium leak detector.
- Groundwater dating was undertaken employing ^{14}C decay, ^{4}He accumulation and $^{4}He/^{222}Rn$ ratio methods to determine regional groundwater flow parameters. Laboratory and field procedures for carbonate precipitation (for ^{14}C method) and

water sample collection, storage and analyses for other groundwater dating methods were developed and standardized.

- Oxygen and hydrogen isotope ratios ($\delta^{18}O$ and δD) in thermal springs and groundwater samples were measured to identify the possible signatures of the past aridity and to identify the source of thermal spring water. Isotopic analyses of modern precipitation were also carried out to provide a reference for interpretation of the groundwater data.
- A groundwater CFC laboratory was set up as part of this study. Field and laboratory procedures for sample collection, storage, extraction of dissolved CFCs and injection for gas chromatographic analyses were standardized.

Important observations from the above investigations and conclusions drawn are summarized in the following.

The regional aquifer system of NGC region comprises a sequence of unconfined and confined sub-aquifers. The recharge area of the confined aquifers lies in the foot hills of the Aravalli Mountains in the east. The confinement of aquifers becomes effective only towards west of the ECBBF. Beyond the region of effective confinement, the groundwater in the aquifer system preserves the geochemical and isotopic characteristics acquired at the time of recharge in the recharge area. The groundwater ages progressively increase from <2 kaBP in the Aravalli foothills to > 35 kaBP in the low lying tract linking the Little Rann of Kachchh (LRK), the Nalsarovar (NS) and the Gulf of Cambay (GC). This defines the general flow direction along WSW.

Overlying the intersecting basement faults, deeper crustal fluids get injected into the aquifer system and significantly alter some of the geochemical properties of the groundwater of the region, namely, temperature, dissolved helium, water isotopes, fluoride and EC of groundwater in certain pockets. The localization of these pockets along intersecting deep seated basement faults on the two flanks of the Cambay basin is conceptualised in the form of a tectono-hydrothermal model of the NGC region. This model involves hydrothermal circulation of water of meteoric origin into deeper crustal layers, its interaction with deeper fluids and return flow to shallow depths, either into groundwater or as thermal springs. The faults and fractures provide the pathways for (i) downward percolation of shallow groundwater (of meteoric origin) as also (ii) for the upward migration of return flow with changed geochemical properties.

The high groundwater fluoride and EC in NGC region around an E-W trending line from around the thermal springs of Lasundra and Tuwa towards the Nalsarovar is explained by a continuous injection throughout Late Quaternary of hydrothermal fluids and the regional groundwater flow in the aquifer system. This mechanism, however, does not explain the observed distribution of enhanced groundwater fluoride around the three nearly parallel lines trending NNW-SSE with intervening areas of low fluoride and EC. This distribution is explained by: (i) predisposition of this semi-arid region to high groundwater fluoride arising from mineral assemblage in surface soils and in aquifer matrix, aided by general aridity particularly in the recharge area; (ii) enhanced aridity around the LGM leading to recharge of groundwater enriched in fluoride resulting from enhanced evaporation as well as dry deposition and flow of this groundwater to its present location around a line within the Cambay Basin, during the past 20 ± 5 kaBP; and (iii) evaporative enrichment of stagnant surface water in the low lying LRK-NS-GC convergence zone and infiltration of a part of it into groundwater.

Additional hydrological signal of past aridity were also observed in the distribution of stable isotopes in the groundwater of the region in the form of high $\delta^{18}O$ and low *d*-excess nearly coinciding with the central belt of high fluoride and high EC. The ^{14}C ages of this belt around LGM (20 ± 5 kaBP) relate this to a period of enhanced aridity in the palaeoclimatic history of the NGC region.

Some additional studies as follow up of this work have also been proposed.

Chapter 1. Introduction

Groundwater aquifers are being exploited indiscriminately throughout the world to meet the ever increasing water demand. It has been estimated that global groundwater mining (i.e. exploitation in excess of natural and artificial replenishment) is about 160 km^3 per year (The United Nations World Water Development Report; available at URL: http://www.unesco.org/water/wwap/wwdr). This volume of groundwater mining may appear insignificant compared to the total volume (~11 x 10^6 km^3) of fresh groundwater on the earth (Fitts, 2002). However, from the point of sustainability, the large scale mining of groundwater is of concern. This is because it has led to significant decline of piezometric levels at many places in the world resulting in increased cost of pumping the groundwater from progressively deeper layers. The alluvial aquifer systems usually have much higher porosity compared to hard rock aquifers and therefore, have higher groundwater potential. Since major agricultural zones and urban agglomerates are located in the alluvial plains, the alluvial aquifers are also the most exploited ones. In the late seventies, it was realised by water managers and planners that the easy option of exploiting the local groundwater to meet the increasing water demand will not be sustainable in the longer run. This realisation came from general observations about declining water levels, increasing cost of pumping, progressively deteriorating groundwater quality, salinity ingression in response to reduced hydrostatic pressure in the coastal aquifers, anthropogenic contamination due to application of chemical fertilisers & pesticides, and discharge of municipal and industrial effluents. It was also realised that exploitation of groundwater can not be stopped at the cost of economic development of a region but it must be judiciously and intelligently restricted. This required complete description of the regional aquifer system using both conventional geohydrological investigations and the modern geochemical and isotopic investigations that can address specific hydrological issues of a given region. The United States Geological Survey (USGS) completed (1978-1995) a nationwide programme of Regional Aquifer System Analyses (RASA) in collaboration with multidisciplinary researchers. Some of the details of this comprehensive investigation of twenty five regional aquifer systems in USA can be found at URL: http//www.usgs.org. This investigation not only generated scientific knowledge necessary for sustainable water resource development and management but also equipped the concerned agencies with an infrastructure to monitor the hydrological response to exploitation, engineered structures and global climate change. Similar large scale studies of regional aquifers systems have also been undertaken by some other developed nations (Edmunds, 2001).

In India, such a nationwide investigation of regional aquifer system is yet to be initiated but the geochemical and isotopic investigations of a regional aquifer system in Western India, presented in this thesis, offer a possible model for a nationwide replication with region specific adaptations. This study also highlights the role of modern isotopic tracers in strengthening the conventional geohydrological technique for addressing specific hydrological problems of a region.

1.1 The Research Problem

The North Gujarat - Cambay (NGC) region of Gujarat State in Western India is characterised by a unique combination of geological, hydrological, tectonic and climatic features, namely, (i) two major bounding faults, defining the Cambay Graben, and several other sympathetic faults parallel and orthogonal to these; (ii) more than 3 km thick sedimentary succession, formed by syndepositional subsidence in the Cambay Graben, acting as a reservoir for the oil and gas at deeper levels and a regional aquifer system at shallower depths; (iii) higher than average geothermal heat flow; (iv) intermittent seismicity; (v) emergence of thermal springs; and (vi) arid climate with high rate of evapotranspiration.

The surface soils in the region are loamy to sandy loam type and provide high agricultural productivity when water is available. But, the streams flowing through the region are only seasonal; therefore groundwater mining has been resorted to in some parts. This has lead to decline in piezometric levels - at more than 3 m/yr during the last couple of decades.

During the same period, it has also been noticed that fluoride concentrations in groundwater in some parts particularly, Banaskantha, Mehsana and Ahmedabad districts have progressively increased leading to endemic fluorosis. Based on the assumption that deeper ground waters have been in contact with the aquifer material for relatively longer periods, it has been argued that high groundwater fluoride of the region is due to its slow leaching from the mineral grains comprising the aquifer matrix (Patel, 1986; Ramakrishnan, 1998). Some studies have also indicated that thermal springs in the region have both high concentration of fluoride and dissolved helium. Therefore, it has also been suggested that higher concentrations of fluoride may be related to subsurface injection of thermal waters (Chandrasekharam and Antu, 1995).

It has long been recognised that helium and radon produced by radioactive decay of uranium and thorium in rocks and minerals are steadily released from grains by etching, dissolution, fracturing and alpha recoil during weathering and then subsequently released into the atmosphere by diffusion and temperature variations. Anomalously high amounts of dissolved helium and radon in groundwater from some parts of the region have been reported earlier (Datta et al, 1980). However, relationship of these dissolved gases with the tectonic framework of the region has not been studied.

There are several known thermal springs and flowing artesian wells in and around the Cambay Basin. The geothermal gradient in parts of Cambay Basin is known to be in excess of 60°C/km (Gupta, 1981; Panda, 1985; Ravi Shankar, 1988; Negi et al, 1992). Based on reports of ground waters with high temperature, anomalous helium and high fluoride, it is believed that these might be related to each other (Chandrasekharam and Antu, 1995; Minisalle et al, 2000; Gupta and Deshpande, 2003). However, detailed geographical distribution, range of variation and inter-relationship between these groundwater parameters is not known.

The average annual relative humidity at present is only ~50% in northern part of Cambay Basin; therefore water loss by evapotranspiration is expected to be very high. The Late Quaternary sedimentary record of the region, however, suggests episodes of both wetter and drier periods (Prasad and Gupta, 1999; Pandarinath et al, 1999b; Wasson et al, 1983; Juyal et al, 2003). Since, during the process of evaporation, a water mass undergoes kinetic fractionation in oxygen and hydrogen isotopes, the imprints of relatively more arid/ humid phases of the past could have been recorded in ground waters recharged during those palaeoclimatic phases. However, these possible climatic imprints on isotope composition of groundwater and modern precipitation have not been investigated.

To overcome the general scarcity of water, a community and the State driven movement for groundwater recharge is presently underway in the region. Several groundwater recharge structures have been constructed but doubts about their usefulness and efficiency persist. In recent decades, Chlorofluorocarbons (CFCs) have emerged as useful tracers of young ground waters (Busenberg and Plummer, 1992; Plummer and Busenberg, 1999). Monitoring of dissolved CFCs in the vicinity of the recharge structures provides an easy way of identifying the modern groundwater recharge and to estimate its quantity. Away from the recharge structures, the CFC concentration in groundwater can also be used to estimate the time since the water became isolated from the unsaturated zone during the past few decades. Presence of detectable CFC signal in groundwater indicates mixing of modern water with that recharged prior to 1945. Such investigations can identify the regions where modern waters have infiltrated. Though successfully employed elsewhere in world, India did not have a laboratory for analysing CFCs in groundwater. Therefore, a need for having such laboratory facility had been long felt, particularly for studying the effectiveness of groundwater recharge structures.

Based on the above considerations, it was decided to undertake a multi-parameter geohydrological investigation in the NGC region to understand the roles of (i) geohydrological; (ii) palaeoclimatic (iii) topographic and (iv) tectonic processes/ features in controlling the chemical and isotopic composition of groundwater, its interaction with aquifer matrix and movement in the regional aquifer system. In the following, some more specific information about the study area is provided followed by specific objectives and the methodology adopted to achieve these objectives.

1.2 The Study Area

1.2.1 Geography

The study area is located in the State of Gujarat in Western India between the 21.5°–24.5°N latitudes and 71.5°–74°E longitudes. The important rivers and other landmarks within the study area covering an area of approximately 90,000 km^2 are shown in Figure 1.1. The urban hubs of the Gujarat State, namely Ahmedabad, Vadodara and Mehsana, and some smaller towns such as Tharad in the NW, Ambaji in the North, Godhra in the east, Bharuch in the south and the Bhavnagar in the SW are also marked in Figure 1.1. The prominent geographic features of the study area include Nalsarovar (NS), Little Rann of Kachchh (LRK) and Gulf of Cambay (GC).

1.2.2 Geology

The rocks exposed in Aravalli foothills in the Eastern part of the study area comprise Proterozoic succession that include the Delhi Supergroup and the Aravalli Supergroup. The Delhi Supergroup includes Pre-Erinpura (Mafic) and Ambaji Granites, Sirohi and Kumbhalgarh Groups. These are intruded by the Erinpura, Post-Erinpura (Mafic) and Godhra Granites. The Aravalli Supergroup includes Champaner, Lunawada, Rakhabhdev (Ultramafic) and Jharol Groups. The geological map of the study area is shown in Figure 1.2.

A small patch of Mesozoic sedimentary rocks is exposed in the study area in the western part. These rocks comprise marine to fluvio-marine sedimentaries (Surendranagar and Wadhwan Formations) of the Uppermost Jurassic to Lower Cretaceous age. Outside the study area in north-eastern part of the Saurashtra, these occupy large area (~ 5000 km^2).

The Deccan Traps formed by the outpouring of the huge volume of basalt, marking the Cretaceous-Tertiary boundary are exposed only in a small part of the study area both on the east and west flanks of the Cambay Basin in the southern part. These outcrops rest either over Precambrian or over the Cretaceous sedimentary rocks. In the east-central part small inliers of Deccan Traps are also seen in the alluvium and soils in the vicinity of the Aravalli Foothills.

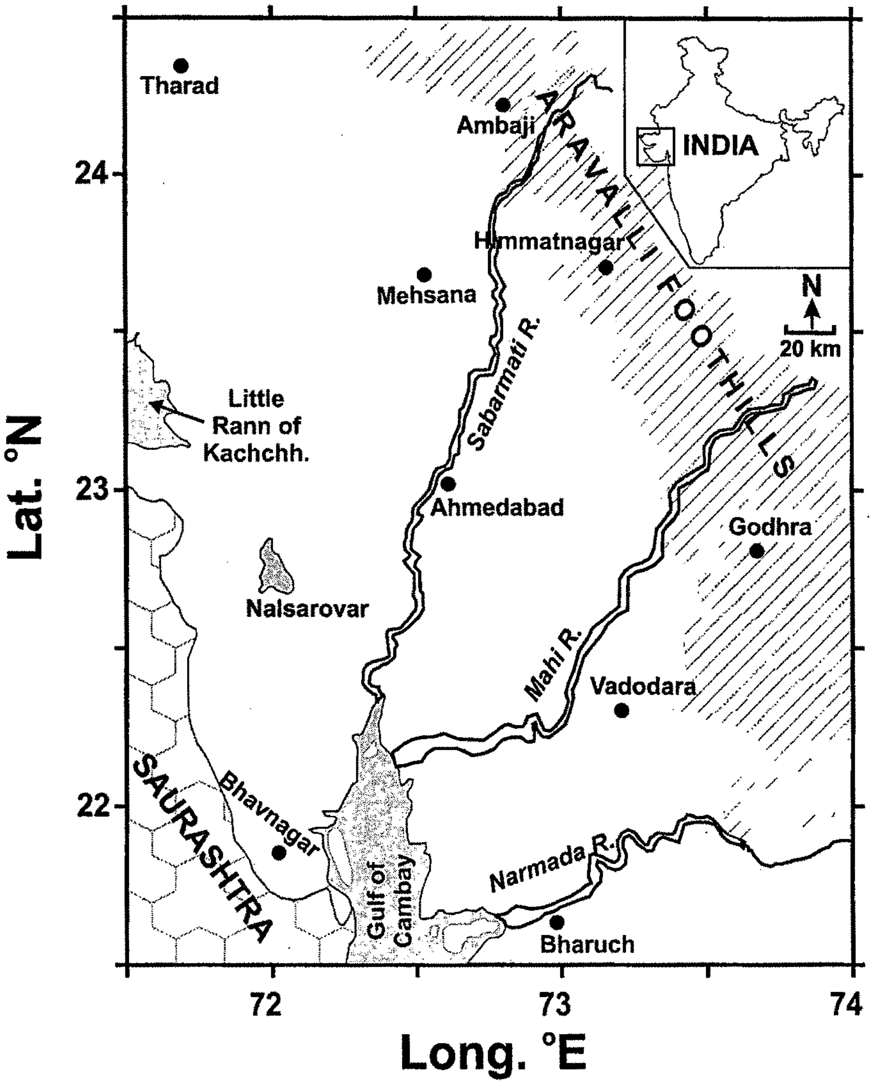

Figure 1.1 Map showing study area and the geographical locations of some important landmark features such as major rivers, towns, lakes etc. The inset map shows location of the study area.

The outcrops of Laterites are found only at a few locations within the study area, overlying the Deccan Trap in southern part, both in south Gujarat as well as Saurashtra. The Laterites are believed to have been formed by in situ decomposition of pyroclastic material or by brecciated and fractured lava flows.

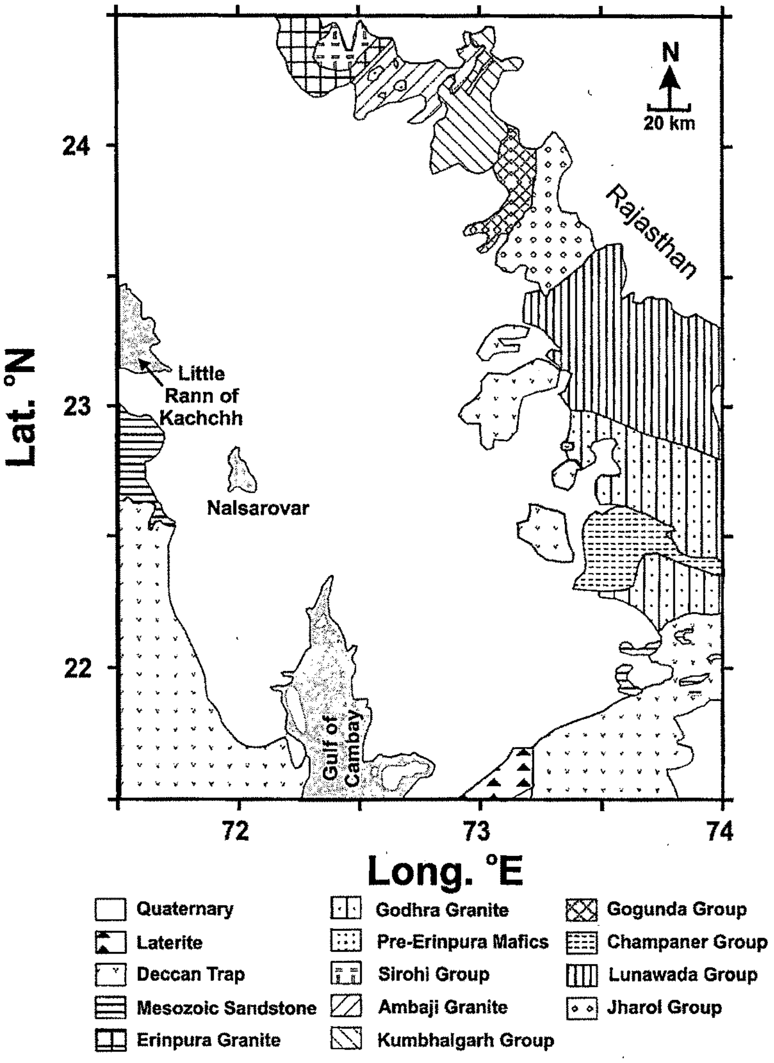

Figure 1.2 The Geological Map of the study area. A large part of the area is covered by Quaternary alluvium. Proterozoic rocks (mainly granitic) lie along the Aravalli foothills in the east and the upper Cretaceous Deccan Traps in the SW and SE corner. A small patch of Mesozic sandstone is also seen towards the west. A sub-surface lithological section along AA' is shown in Figure 1.6.

The Quaternary sediments, also referred to as Gujarat Alluvium, occupy the largest part of the study area and cover the Cambay Basin and a large area on either flanks. Regional stratigraphy based on the subsurface data shows that nearly 500 m thick Quaternary sediments comprising thick layered sequences of sediments of fluvio-marine and fluvio-aeolian origins overlie the Tertiary basement (Biswas, 1987; Merh, 1993; Merh and Chamyal, 1993; Maurya et al, 1995; Tandon et al, 1997; Prasad et al, 1998; Srivastava et al, 2001). Shallow marine sediments were also deposited in the low-lying tract between the Gulf of Cambay (GC) and the Little Rann of Kachchh (LRK) during the Late Quaternary.

A model of Late Quaternary deposition related to westward migration of a depositional front caused by marine regression and/ or tectonic uplift of the east flank was presented by Prasad et al (1997), Prasad and Gupta (1999) and Pandarinath et al (1999a). The alternating phases of humid and arid climates in this region during Quaternary period, is known to have influenced fluvial and aeolian regimes and is reflected in the mode of occurrence, extent, lithology, soil types, structure and texture of the successive horizons of the sediments. These Quaternary alluvial sediments with alternating sand and silty-clay layers constitute the regional aquifer system extending up to the low lying tract linking the Little Rann of Kachchh (LRK) – Nalsarovar (NS) – Gulf of Cambay (GC) region and having its recharge area in the foothills of Aravalli Mountains.

1.2.3 Tectonic Framework and Sedimentation

Cambay Basin of the NGC region is one of the three major marginal rift basins in the western margin platform of the Indian craton; the other two being Kachchh and Narmada basins. Earlier, Burke and Dewey (1973) identified the region of convergence of Cambay and Narmada rift basins with West Coast (WC) fault in the Gulf of Cambay (also known as Gulf of Khambhat) as a 'triple junction'. Another major tectonic structure in the south, namely the 'Kukdi-Ghod lineament zone', also converges into the triple junction (Figure 1.3). Repeated block faulting along these tectonic structures has broken the lithosphere into several blocks separated by major or minor faults running parallel as well as orthogonal to each other. The intersecting network of faults has given rise to such a tectonic configuration that movement of any lithospheric block along a particular fault is propagated along other faults. Many of these faults and fissures within these major structures seem to extend to the lower lithosphere (Ravi Shankar, 1995) and several hot springs lie along them (GSI, 2000).

Tectonic framework of the study area is shown in Figure 1.4. The Cambay basin is an intracratonic slightly asymmetrical fault bounded Graben and is defined by two major bounding faults, namely, Eastern Cambay Basin Bounding Fault (ECBBF) and the Western Cambay Basin Bounding Fault (WCBBF). This system of major bounding faults additionally comprises several successive sympathetic faults that run parallel along NNW-SSE and many orthogonal cross cutting faults (Merh, 1995). This NNW-SSE alignment of this narrow Graben (55–100 km) takes a swing in NNE-SSW direction into the Gulf of Cambay around 21.75 °N. This tectonic depression is flanked (Figure 1.3) by Kathiawar (Saurashtra) Uplift in the west and Aravalli Range in the east (Biswas, 1982;

1987). The Cambay Basin also extends along the west coast of India through the Gulf of Cambay parallel to Precambrian Dharwar trend. In the south, the Cambay Basin merges with the EW trending Narmada Graben and the Surat (Danahu) Depression where a tipple junction is formed. Though the Cambay Basin originated in the Late Mesozoic, it has mainly evolved during the Tertiary as revealed by the huge thickness of Cenozoic sediments (Merh, 1995).

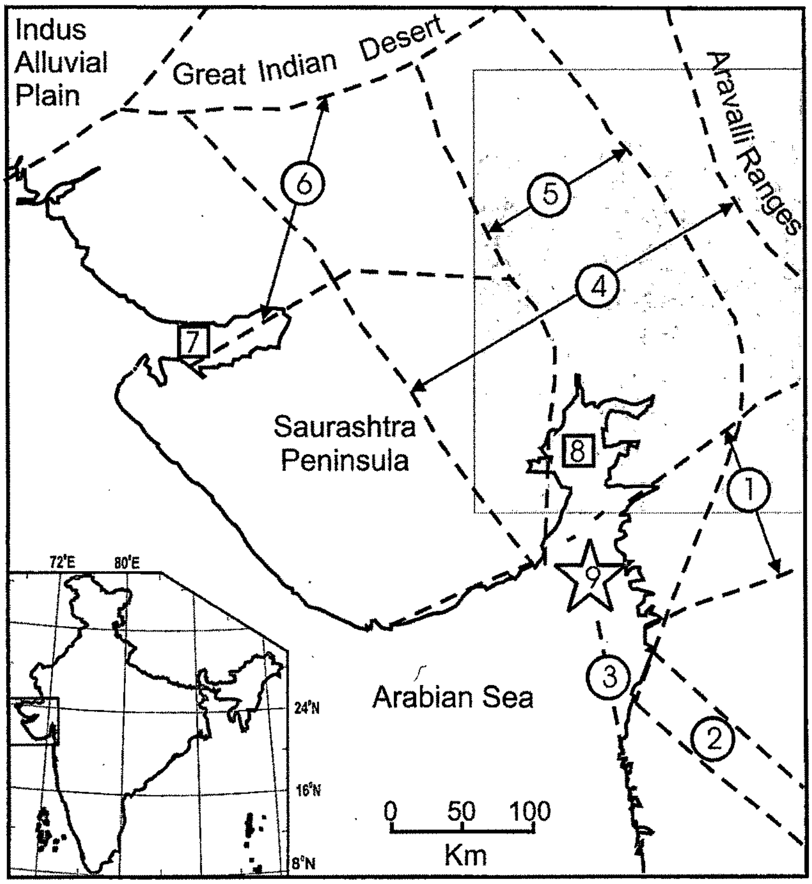

Figure 1.3 Tectonic framework of the Gujarat State in western India showing major linear tectonic structures based on Burke and Dewey (1973), Biswas (1987), Misra (1981; 2001). The various structural elements are: 1. Narmada Tapti Tectonic Zone; 2. Kukdi-Ghod Lineament Zone; 3. West Coast Fault; 4. Cambay Structure; 5. Cambay Graben; 6. Kachchh Rift; 7. Gulf of Kachchh; 8. Gulf of Khambhat; 9. Triple Junction of 1, 2 and 5. The study area is shown in grey shade.

The Cambay Graben is underlain by an uncertain thickness of pre-Deccan, terrigenous, Late Jurassic to Early Cretaceous sediments. Deccan Trap volcanics directly overlie this and are present throughout the extent of the Graben. They are thickest in the axial part of the Graben where their thickness is up to 2000 m (Kaila, 1988). The Tertiary sedimentary formations with productive oil and gas reservoirs overlie the Deccan volcanics. About 300 to 800 m thick Quaternary fluvial and alluvial sediments overlie the Tertiary sediments thus forming about 3500 to 4000 m thick Cenozoic sedimentary succession within the Cambay Graben for most of its length (Gombos et al, 1995). The thickness of the sedimentary cover, however, reduces to a few metres on both the east and the west flanks of Cambay Basin.

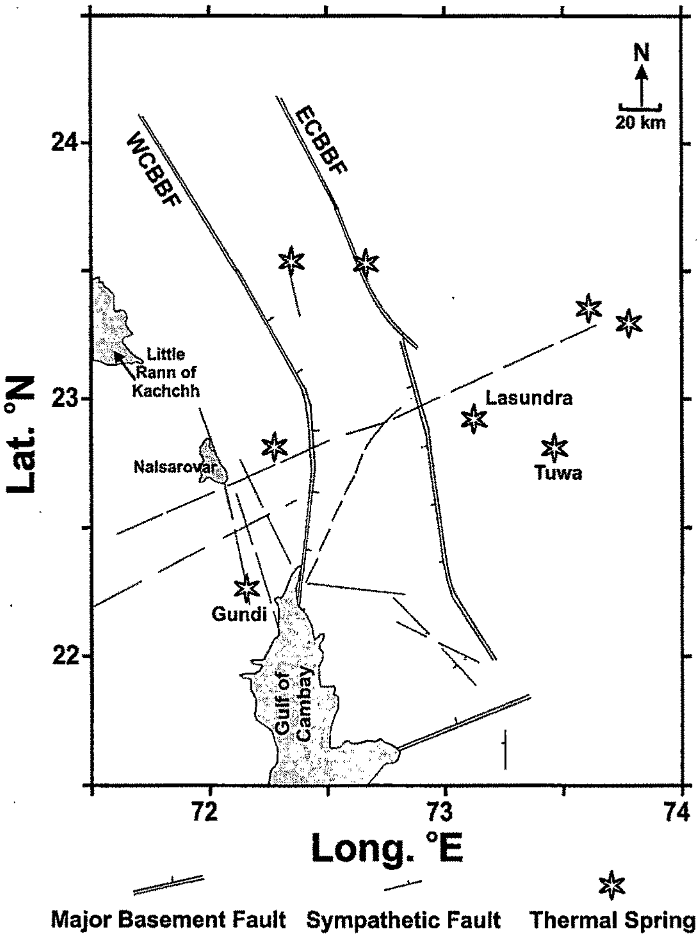

Figure 1.4 Tectonic framework of the NGC region. Two major bounding faults, namely, the ECBBF and the WCBBF define the Cambay Basin. Several sympathetic faults parallel or orthogonal to the major faults also exist. Most thermal springs are seen to be located in the vicinity of known basement faults.

The Cambay Basin seems to have subsided episodically since the formation of Graben structure in the Late Mesozoic with varying rates and finally during Quaternary the rate of subsidence slowed down. However, it can not be ruled out that the Quaternary basin experienced considerable reactivation of the pre-existing faults (Maurya et al, 1995). A variety of soft sediment deformation structures documented in the Lower Mahi River basin are slumps and slides, syn-tectonic folds, faulting, slickenside and pseudo-nodules and indicate syn-tectonic sedimentation and differential subsidence of the basin along the sympathetic step faults that developed parallel to ECBBF (Maurya et al, 1997). Based on lineament and drainage studies, Sareen et al (1993) showed that present Sabarmati River flows in NNE-SSW direction deviating from the regional slope of NE-SW. This was attributed to the neo-tectonic activity in the basin. Geomorphologic studies have indicated recent movements along many faults in this region (Srivastava et al, 2001).

1.2.4 Geothermal Regime

Cambay Basin region is characterised by higher than average heat flow and geothermal gradient which has been explained in the context of a thick high density (3.02 g cm^{-3}) igneous layer underlies the crust in this region. It has also been hypothesised that underlying the accreted igneous layer, a low velocity zone of hot mantle and/or a zone of intense interaction between lower crust and upper mantle has been identified beneath the area of triple junction (Arora and Reddy, 1991). This configuration is compatible with high geothermal regime (heat flow 55-90 mWm^{-2}; temperature gradient 36-58 ^{0}C km^{-1}) in the region (Gupta 1981; Panda 1985; Ravi Shankar 1988; Negi et al, 1992). Therefore, the lithosphere beneath the triple junction and the three arms, namely the Cambay Graben, Narmada-Tapti rift zone and West Coast fault, is now much warmer, thinner, relatively ductile and less viscous compared to the margins (Pandey and Agrawal, 2000). Based on deep seismic soundings (Kaila et al, 1981; Kaila et al, 1989; Kaila and Krishna 1992) and gravity surveys (Singh and Meissner, 1995; Singh, 1998), it has been suggested that these structures reach up to the mantle (~ 40 km in depth; Kaila et al, 1989) in the Narmada-Tapti rift system and the Cambay Basin areas. This regional tectonic fabric seems to be responsible for higher geothermal regime in the Cambay Basin region.

The higher geothermal gradient in the region is also manifested in several thermal springs (Figure 1.4) and thermal artesian wells some of which are free flowing type (GSI, 2000). Existence of these thermal springs along geologically well defined structures (Section 1.2.3 above), with frequent earthquakes of moderate intensity, suggests that the associated structures may be active even presently. This was also suggested by the signatures of neotectonic movements in the Quaternary sediments and from the geomorphic studies of the region (Sridhar et al, 1994; Maurya et al, 1995; Maurya et al, 1997; Tandon et al, 1997, Srivastava et al, 2001).

1.2.5 Topography and Drainage

A surface elevation and drainage map of the study area is shown in Figure 1.5. The elevations in the study area range from >300m in the NE part to <25m near the Gulf of Cambay in the south.

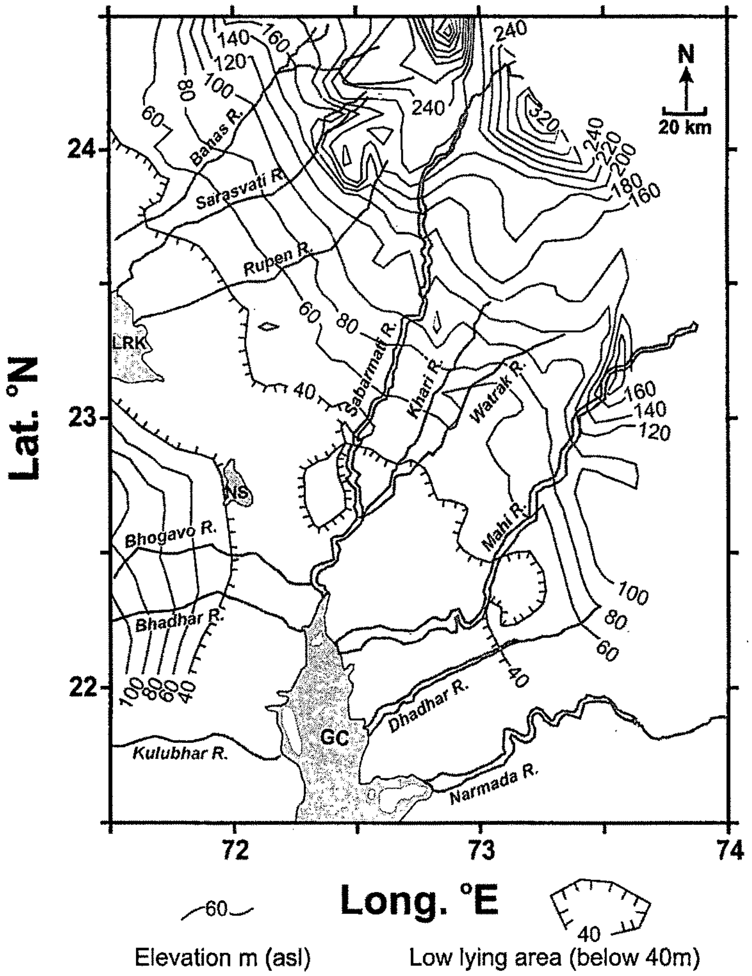

Figure 1.5 Map showing River drainage and surface elevation in the NGC region. The low lying belt linking LRK-NS-GC is less than 40 m in elevation and forms the zone of convergence for surface drainage from both the sides.

The Aravalli foothills occupy the intermediate elevation (~100-200 m) trending the NW-SE. The lowest elevations are found in the tract linking LRK-NS-GC. The elevations increase to >100m further southwest of this low lying tract. The control of surface elevation gradient on the drainage pattern is evident from Figure 1.5. It is seen that the low lying tract linking LRK-NS-GC forms the zone of convergence wherein the streams from both the sides of higher elevations converge. The rivers originating from the Aravalli hills, namely, Banas, Saraswati, Rupen and Sabarmati flow south-westward towards the LRK-NS-GC tract. The rivers (Bhogavo, Bhadar and Kulubhar) originating from Saurashtra highlands flow NE towards the LRK-NS-GC tract.

The Rupen, Saraswati and Banas rivers drain into the Ranns of Kachchh. These are seasonal rivers which carry water only during the monsoon months (June – September). The Mahi and Sabarmati are the two most important rivers that have shaped the present landform of the major part of the study area. The Mahi River originates in the Malwa region of Madhya Pradesh, flows for ~180 km in the study area before debauching into the Gulf of Cambay. The Sabarmati River originating in the south-western part of the Aravalli hills traverses a distance of ~400 km (NE to SW) across the Cambay Basin and outfalls in the Gulf of Cambay. It was suggested by Zeuner (1950) that the Sabarmati River had shifted its course gradually towards the east during the Pleistocene. Contrary to NE-SW regional slope of the alluvial plain, Sabarmati River follows N-S to NNE-SSW path attributed to neotectonic activity (Sareen et al, 1993). On the basis of sedimentological and geomorphologic studies, it was suggested (Sridhar et al, 1994) that the volume of Quaternary sedimentation in the Sabarmati basin could not be accounted for by the modern day flow of the river and a super fluvial system during Quaternary was postulated. However, it was subsequently indicated, based on sedimentological analyses, that upper fluvial sedimentary sequence is deposited by the meandering of the same river system but during a persistently wetter phase (Srivastava et al, 2001). The region between Sabarmati and Mahi is drained by a number of tributaries of Sabarmati namely, Khari, Shedhi, Majham, Andheri, Meswo and Vatrak. The Bhadar and Bhogavo are two major rivers flowing eastwards from Saurashtra draining into the Gulf of Cambay. Bhogavo, however, joins Sabarmati at its mouth before draining into the Gulf of Cambay.

1.2.6 Climate

The study area falls in the sub-tropical climate zone with the tropic of Cancer passing through the middle. The northern part of the study area comprises districts of Banaskantha and western part of Sabarkantha having arid to semi-arid climate, with less than 400 mm of average annual rainfall. In the southern part around Ahmedabad and parts of Saurashtra, the average annual rainfall is ~750 mm. Most of the rainfall is received during the southwest monsoon in the month of June to September. The average annual relative humidity is low (~50-60 %) throughout the year excepting the areas in the vicinity of the Gulf of Cambay. The area lies between the average annual isotherms of 35 °C and 45 °C indicating that, in general, aridity prevails in most part of the study area.

The area is known to have recorded palaeoclimatic fluctuations in form of various proxies in sedimentary deposits. The palaeoclimatic significance of sedimentary deposits in the Sabarmati, Mahi and Narmada basins was recognised by Zeuner (1950) and he postulated that climate in this region alternated between wet and dry during the Pleistocene. The arid excursions have also been documented in several other studies. Prasad and Gupta (1999) reported the presence of a thick gypsum layer, representing periods of extreme aridity, corresponding to estimated luminescence age ~20-30 ka, in a sediment core from Nalsarovar. Based on the crystallinity index of illite, Pandarinath et al (1999b) have also indicated aridity for this layer. Regional evidences of aridity have also been reported in the form of enhanced dune building activity which began ~20 ka in N. Gujarat (Wasson et al, 1983; Juyal et al, 2003, 2006).

1.2.7 Groundwater Hydrology

The groundwater occurrence in the study area can be grouped under three physiographic settings, namely: (i) hilly area of Aravalli foothills in the northeast and east; (ii) alluvial plains including Cambay Basin and it's both flanks; and (iii) part of the Saurashtra upland in the study area.

In the hilly region of Aravalli foothills where hard rocks are either exposed on the surface or are at a very shallow depth of few meters, groundwater is found in the secondary porosity zones resulting from weathering, joint planes, cracks and fissures. The water table in this terrain is generally at relatively shallow depths of less than 10 m. The groundwater level rises considerably in the post monsoon period due to direct infiltration of rainwater in the secondary porosity. The sediments in the foothill region are relatively coarse and this zone between Aravalli hills in the east and the alluvial plains in the west forms the principal recharge area for the confined groundwater in the Cambay Basin area. Using tritium tagging of soil moisture annual recharge to groundwater in the recharge area has earlier been estimated to ~15% of average annual precipitation (Gupta and Sharma, 1984).

A thick succession of Quaternary alluvial deposits comprising multilayered sequences of sediments of fluvio-marine and fluvio-aeolian origin forms the regional aquifer system which extends from the Aravalli foothills in the northeast and east to the Little Rann of Kachchh and Saurashtra highlands in the west (Figure 1.2). A subsurface lithological cross-section across the Cambay Basin from Nayaka to Chadotar (along the line AA' in Figure 1.2), based on drilling logs obtained from Gujarat Water Resources Development Corporation Ltd (GWRDC), is shown in Figure 1.6.

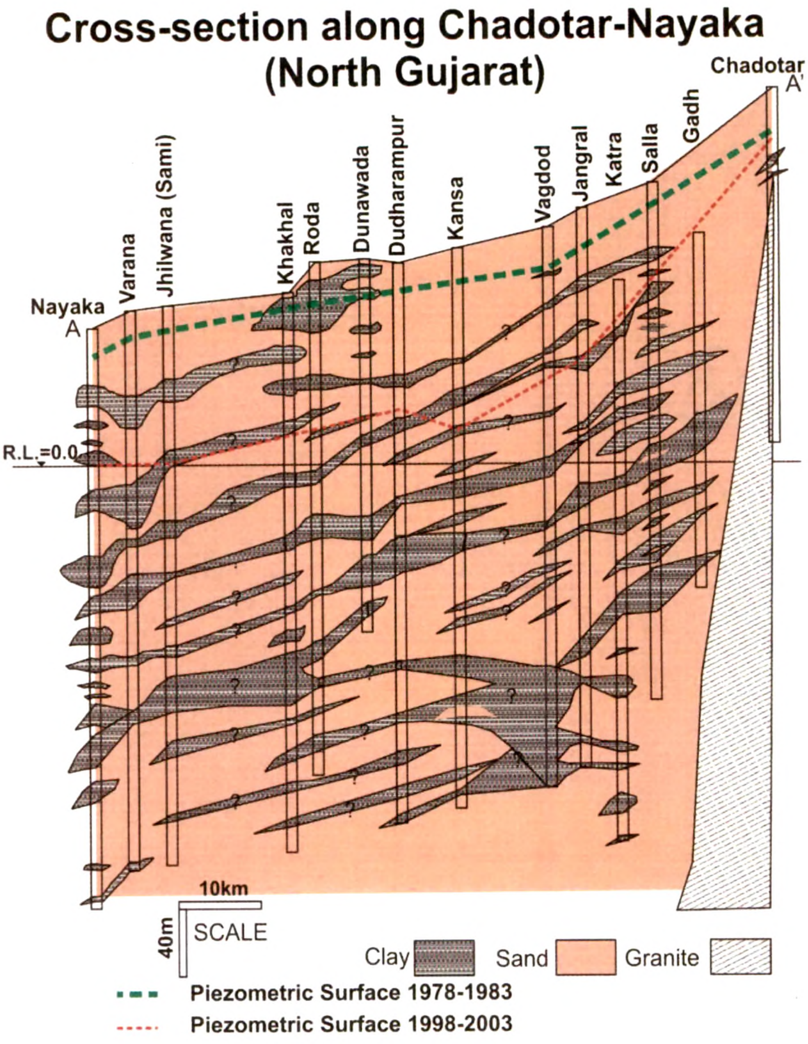

Figure 1.6 Sub-surface lithological cross-section along line AA' (in Figure 1.2) from Nayaka to Chadotar. The sandy layers forming aquifer horizons are seen to be laterally continuous and vertically interspersed with thin semi-permeable clay/silt layers that may not have lateral continuity over a large area. The uncertainty of continuity in view of large separation is indicated by (?). Tubewells tap all water bearing horizons up to their maximum depth.

As can be seen, the thickness of the alluvium rapidly increases westwards away from the Aravallis and a sand-clay/silt succession replaces the coarse sediments of the foothill. The sandy layers forming aquifer horizons are seen to be laterally continuous and vertically interspersed with thin semi-permeable clay/silt layers that may not have lateral continuity over a large area. It is also seen that various sub-aquifers are roughly inclined parallel to the ground surface; so that at different locations, a given depth below ground level (bgl) reaches approximately the same sub-aquifer within the Cambay Basin. According to Patel (1986), the deeper aquifers are under artesian condition. Towards their western extension, the deeper aquifers abut against a thrust plane little north of LRK. Along the LRK-NS-GC belt, tubewells tapping the deeper aquifers exhibit free flowing condition at ground have high water temperature and saline water. Recently, excess dissolved helium has also been recorded from groundwater of these wells (Datta et al, 1980).

The upper aquifers are under semi-confined condition. They receive recharge (i) directly by seepage from the overlying unconfined aquifer; and (ii) by lateral flow from the recharge zone of Aravalli foothills in the east. The shallow unconfined aquifer receives direct recharge from (a) rainfall infiltration, (b) nearby stream flow, and (c) by return flow from irrigation.

The groundwater development in the region can be sub-divided in three phases:

1. Pre-1935 phase - Groundwater at shallow depths (5-10 m), obtained from dug wells by bullocks and manual lifting.
2. 1935-1955 Phase - Groundwater levels declined to 10-30 m and dug-cum-bore wells became prevalent and diesel pump sets were used for lifting.
3. Post 1955 Phase - Groundwater levels began to decline rapidly and from sixties onwards the decline has been between 1-3 m per year. Deep tubewells fitted with electric motors have been used to lift groundwater from 100-250 m depth.

Deterioration in the groundwater quality almost parallels the post 1955 phase, when, with the advent of tubewells and electric motors, the groundwater extraction increased many folds. Gradually, the soil fertility was affected by irrigation from high TDS groundwater and several native crops disappeared. Presently, cash crops of cotton, *bajari* and *jowar* are grown in the region.

In recent years, the deeper groundwater from this regional aquifer system, particularly in the Cambay Basin region, is being exploited to meet agricultural, domestic and industrial water demands. Since extensive withdrawal of deeper groundwater is not made up by natural or artificial groundwater recharge, the water levels in most of the study area have declined at a rate of 3-4 m/yr (see piezometric surfaces in Figure 1.6). In some parts of the NGC region, the groundwater levels have declined to >400 m depth and the water is being pumped at progressively increasing cost.

1.3 Specific Objectives of the Study

The hydro-geological and climatic conditions (temperature, rainfall, evaporation etc) prevailing in the recharge zone govern chemical and isotopic properties (e.g. temperature, pH, dissolved ions, oxygen and hydrogen isotopic compositions and dissolved gases) of the infiltrating water. During groundwater flow in the aquifer, these properties can be modified by subsurface processes such as evaporation from the capillary zone, leaching from the aquifer matrix, venting of thermal fluids, release of gases such as helium etc.

Thus, geochemical and isotopic investigation of groundwater can provide insight into a variety of surface and sub-surface processes operating during recharge and movement in the aquifers. With this background, following specific objectives have been defined:

1. To identify the regions of groundwater recharge to the regional aquifer system of NGC region.
2. To determine direction and rate of groundwater movement within the regional aquifer system.
3. To estimate groundwater ages employing ^{14}C, ^{4}He and $^{4}He/^{222}Rn$ methods and to understand their relationship with various ionic and isotopic properties of groundwater from the recharge towards the discharge area.
4. To determine regions of anomalous helium, temperature and fluoride in groundwater and to explain the origin of observed variation in terms of tectonic framework and geothermal regime of the study area.
5. To identify the possible ionic or isotopic signatures of past climatic changes.
6. To set up a laboratory for analysing dissolved Chlorofluorocarbons (CFCs) in groundwater.

1.4 Motivation and Approach

Motivation for identification of the above as specific objectives of this study and the methodology adopted to achieve these is introduced in the following:

1.4.1 Groundwater Dating

Based on general topography, geology, the lithologs of drilled tubewells and the water level/ piezometric level data, recharge area of the regional aquifer system in the study area was identified in the foothills of the Aravalli Mountains in the NE. The low lying LRK-NS-GC region has been identified as the area of convergence both for surface- and ground-water beyond which the groundwater may be discharging into the Gulf of Cambay.

However, this inference of groundwater recharge and discharge areas, based on topographic and lithological parameters, needs to be strengthened and refined by determining the age of groundwater, its direction and rate of movement in the aquifer. The radiometric dating methods provide information on age and residence time of groundwater, exchange between shallow and deep aquifers and interaction with the aquifer matrix. Therefore, groundwater dating employing ^{14}C decay, ^{4}He accumulation and $^{4}He/^{222}Rn$ methods, was undertaken. Laboratory and field procedure for water sample collection, carbonate precipitation, storage and analyses were developed for various groundwater dating methods.

1.4.2 Groundwater Helium and Temperature Anomalies

It has long been recognised (Golubev et al, 1975; Dikum et al, 1975) that helium (^{4}He) produced by α-decay of U and Th series nuclide in rocks and minerals get liberated during convective circulation, rock dilation and fracturing. Since the Cambay region has several deep seated faults, anomalously high amounts of this liberated helium may be escaping from these faults, either directly or as component of injected deeper fluids. Before escaping to atmosphere, injected gases, including helium, are trapped by omnipresent groundwater at shallower levels. Therefore, if groundwater acquires additional ^{4}He from deep subsurface sources, its dissolved ^{4}He concentration can be in excess of atmospheric equilibration value plus that acquired from radioactivity in the host aquifer matrix.

High concentrations of dissolved helium and high temperature of groundwater in some parts, particularly around thermal springs, was reported earlier (Datta et al, 1980). However, geographic distribution and interrelationship between these two parameters and their relationship with deep seated faults in the region were not known.

Therefore, a survey of dissolved helium and temperature of groundwater in the study area was undertaken. As part of the investigations, simple standardised procedures were also developed for sample collection, storage and measurement of helium concentrations in soil-gas and groundwater samples using commercially available helium leak detector.

1.4.3 High Fluoride in Groundwater

In response to extensive groundwater mining during the past 2-3 decades it has been noticed that fluoride concentrations in groundwater in some parts particularly, Banaskantha, Mehsana and Ahmedabad districts increased progressively leading to endemic fluorosis. Evidences of dental and skeletal fluorosis in many parts of this region have been reported (Gupta and Deshpande, 1998).

Although knowledge concerning fluoride-affected parts of Gujarat is available (Vasavada, 1998; Gujarat Water Supply and Sewerage Board, unpublished data, 1997), little is understood about the origin of high groundwater fluoride in affected areas though several hypotheses exist.

None of these hypotheses were tested, except the self evident geographical coincidence of high fluoride ground waters zones in arid parts of the globe.

Therefore, a survey of dissolved fluoride in groundwater was undertaken to understand the origin of high concentration of groundwater fluoride in terms of depth of source water, age of groundwater, proximity to fluoride rich source rock and hydrothermal springs. In addition to a purely academic enquiry, understanding the origin of fluoride in regional groundwater could be useful in devising water exploitation and management strategies. Since electrical conductivity (EC) is a proxy of total ionic concentration of water, EC was also measured along with fluoride concentration, temperature, pH, Eh and chloride (at some locations) in groundwater samples from the various depth zones ranging from shallow dug wells, geothermal springs, hand-pumps, tubewells and flowing artesian wells up to 450 m depth.

1.4.4 Isotopes in Groundwater: Palaeoclimatic Imprints

The stable isotopes of oxygen and hydrogen constituting water, due to isotopic fractionation processes accompanying precipitation and groundwater recharge, record the climatic signatures. Some studies based on this premise have been reported from other parts of the world (see Clark and Fritz, 1997; Kendall and McDonnell, 1998).

With a view to identify the possible signatures of the past aridity and to identify the source of thermal spring water, oxygen and hydrogen isotope ratios ($\delta^{18}O$ and δD) in the thermal springs and groundwater samples were measured. Isotopic analyses of modern precipitation were also carried out to provide reference for interpretation of the groundwater data.

In this Chapter, after introducing the research problem, specific objectives were defined. This was followed by enunciation of the motivation and approach. In the Chapter 2, theoretical aspects related to various geochemical and isotopic investigations undertaken are described.

Chapter 2. Theory

In this Chapter, basic information about some geochemical and isotopic parameters and their behaviour in geo-hydrological environment is provided. Principles of various groundwater dating methods, such as ^{14}C, ^{4}He and $^{4}He/^{222}Rn$ (employed in this study) and CFCs (for which a new laboratory was set up), are also discussed.

2.1 Helium

Helium (^{4}He) is the second most abundant element in the known Universe after hydrogen and constitutes 23% of the elemental mass of the Universe. It is the second lightest element in the periodic table after hydrogen. It is a colourless, odourless, non-toxic, and virtually inert mono-atomic gas. It was discovered in 1868 by J. Norman Lockyear in the spectrum of a solar eclipse. The fact sheet of helium is given in the Table 2.1.

Table 2.1 The fact sheet of Helium (compiled from CRC handbook)

Name (Symbol)	Helium (He)
Atomic Number	2
Atomic mass	4.002602 g/mol
Chemical series	Noble gases
Group, period, block	18, 1, s
Electronic configuration	$1s^2$
Electrons per shell	2
Stable isotopes (Natural abundance)	^{4}He (99.999863%), ^{3}He (0.000137%)
Radioactive isotopes	^{5}He ,^{6}He , ^{7}He, ^{8}He, ^{9}He, ^{10}He
Atmospheric concentration	5.3 parts per million (ppm) by volume
Diffusivity in water at 25^0C	$7.78x10^{-5}$ cm^2s^{-1}
Recoil path length	30–100 μm

Although there are eight known isotopes of helium, only two isotopes namely ^{4}He (2 protons and 2 neutrons) and ^{3}He (2 protons and 1 neutron) are stable. The remaining six isotopes are all radioactive and extremely short lived. The isotopic abundance of helium, however, varies greatly depending on its origin. On earth, helium is produced by the radioactive decay of much heavier elements such as Uranium and Thorium. The alpha particles produced during radioactive alpha-decay are nothing but fully ionised ^{4}He nuclei. In the ^{238}U, ^{235}U and ^{232}Th series, the decay chains yield respectively 8, 7 and 6 atoms of ^{4}He (Figure 2.1).

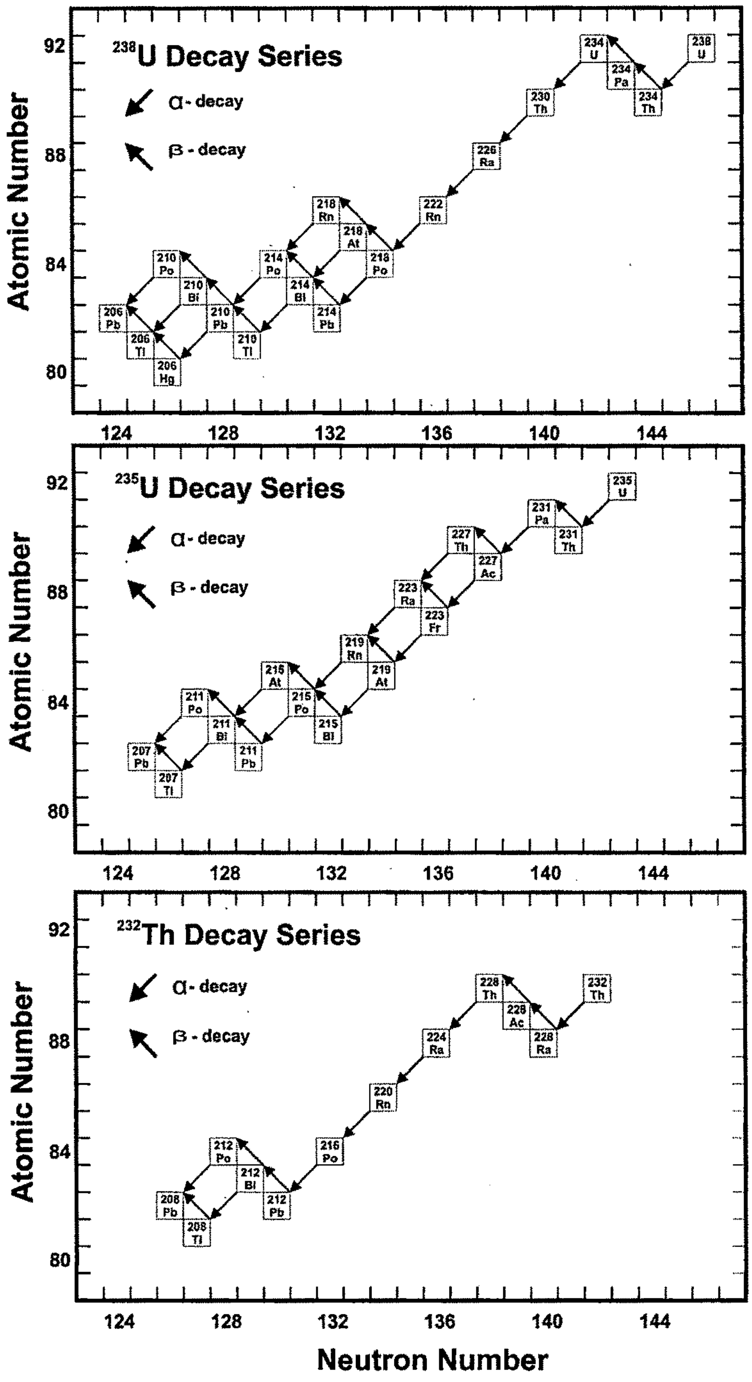

Figure 2.1 Radioactive decay series of Uranium and Thorium showing production of α particles (the helium nucleus) and the ^{222}Rn. Note that 8, 7 and 6 helium atoms are produced in the decay chains of ^{238}U, ^{235}U and ^{232}Th respectively. ^{222}Rn is produced in the decay chain of ^{238}U.

Helium so produced is released from grains by their etching, dissolution and fracturing and by alpha recoil and then exhaled into the atmosphere by diffusion and temperature variations. Since helium is produced in rocks and soils within earth and escapes to outer space from the top of the atmosphere due to its inertness and low mass, its concentration shows a gradient decreasing towards the ground-atmosphere interface. In the Earth's atmosphere, the concentration of helium is only ~5.3 parts per million (ppm) by volume.

Water in solubility equilibrium with the atmosphere usually shows low concentrations of helium because of its low solubility (~1%) and low atmospheric concentration. In ground waters, however, dissolved helium can be high due to its radioactive production and release from earth materials. Since its diffusivity in water is low (7.78×10^{-5} cm^2s^{-1} at 25^0C; CRC handbook), it gets trapped in groundwater and collects additional radiogenic helium from the aquifer matrix while moving through it till groundwater comes in contact with atmosphere. This provides the basis for groundwater dating by the helium method using the knowledge of helium production rate in the aquifer matrix from its uranium and thorium content (Fröhlich and Gellermann, 1987; Torgersen, 1980; 1992; Mazor and Bosch, 1992; Clark et al, 1998; Castro et al, 2000). Presence of fractures and fissures, particularly in hard rocks, provide preferential pathways for migration of radiogenic helium from the subsurface interconnected spaces between the grains. Therefore, depending on the collection volume of a particular fracture or fissure, helium concentration in the groundwater residing in the particular fracture zone can be significantly higher than its production from the rock volume in contact with groundwater. This then forms the basis of delineating the deep structural zones (Kulongoski et al, 2005; Kulongoski et al, 2003; Gupta and Deshpande, 2003a; Gülec et al, 1987; Minisalle et al, 2000; Filippo et al, 1999). Moreover during and just before earthquakes, enhancement in helium concentration in some ground waters has been noticed (Reimer, 1984; Barsokov et al, 1984; Rao et al, 1994). This is possibly due to rock dilation and fracturing during incipient fault movements and forms the basis for using helium monitoring as a tool for earthquake prediction. The important point to be noticed is that all the radiogenic helium may not be released from the rock matrix in the normal course giving a release factor of less than unity. This may have implications for groundwater dating using helium and helium/radon dating as discussed subsequently (see Sections 2.6.2 and 2.6.3). When the groundwater has dissolved helium in excess of atmospheric equilibration value, the groundwater is referred to as having 'helium anomaly' or 'excess helium'. Ground waters may have 'excess helium' also due to other factors, viz., (i) occurrence of uranium mineralization within a particular aquifer zone or in its vicinity – forming basis for radioactive mineral exploration (Reimer, 1976); and (ii) occurrence of natural gas reservoir, below the aquifer system, which can have high concentration of helium – forming basis for petroleum exploration using helium surveys (Jones and Drozd, 1983; Weismann, 1980). In addition, depending on the physical nature of capillary fringe zone just above the saturated zone, air bubbles ca be entrapped and transported into the saturated zone. The air bubbles can also be entrapped by rapid rise in the water table due to occasional heavy rainfall in semi arid regions. Entrapment and subsequent dissolution of such air bubbles into the groundwater introduces excess-air and consequently all its components including helium. This contributes additional helium to groundwater over and above atmospheric equilibration value (Heaton, 1981; Heaton and Vogel, 1981; Andrews et al, 1985).

2.2 Radon

Radon (Rn) is a chemically inert, radioactive noble gas formed by the disintegration of Ra (radium) in the decay chains of Uranium and Thorium (Figure 2.1). It was discovered in 1900 by Friedrich Ernst Dorn. There are twenty known radioactive isotopes of radon but it does not have any stable isotope. Among its isotopes, ^{222}Rn formed by decay of ^{226}Ra (in the ^{238}U decay series; Figure 2.1), has the longest half-life of 3.8235 days and decays to ^{218}Po (Polonium) by emitting an α–particle. The fact sheet of Radon is given in the Table 2.2.

Table 2.2 The fact sheet of Radon (compiled from CRC handbook)

Name (Symbol)	Radon (Rn)
Atomic Number	86
Atomic mass	222 g/mol
Chemical series	Noble gases
Group, period, block	18, 6, p
Electronic configuration	[Xe] $4f^{14}$ $5d^{10}$ $6s^2$ $6p^6$
Electrons per shell	2, 8, 18, 32, 18, 8
Stable isotopes	None
Radioactive isotopes	^{195} Rn to ^{228} Rn (only 20 natural)
Natural abundance	^{222}Rn (100%)
Atmospheric activity	~7x10^{-4}dpm/l
Diffusivity in water at 25^{0}C	1.33x 10^{-5} cm^{2}s^{-1}
Recoil path length	~0.05 μm

Natural radon concentration in the earth's atmosphere is very low (1 in 10^{21} molecules of air) due to its radioactive decay though it has been shown to accumulate in the air if there is a meteorological inversion. The natural waters in equilibrium with the atmosphere has low concentration of ~7x10^{-4} dpm/l (Gupta et al, 2002).

Ground waters can have higher concentration of ^{222}Rn due to release from subsurface production. Due to its diffusion into the atmosphere, radon content of unsaturated zone, in common with other inert gases, is lower than in the saturated zone. The mobility of radon in ground waters is to some extent linked to its parent radium, which is particle and salinity sensitive (Krishnaswami et al, 1991).

As with helium, the faults and fractures in the crust act as preferential pathways for migration of radon. Unlike helium that can go on accumulating in stationary or confined ground waters (Gupta et al, 2002), radon is expected to be in a steady state between production, decay and mobilisation from rock/soil matrix. Though, during and for a short time following any disturbance, such as an earthquake, the steady state conditions may not prevail. Similar to helium anomalies, the radon anomalies have also been used as seismic precursors (Shapiro, 1981; Virk et al, 2001), delineation of active fracture zones (Reddy et al, 2006), radioactive mineral exploration (Jones and Drozd, 1983; Weismann, 1980) and in groundwater dating using helium/radon ratio (Gupta et al, 2002; Agarwal et al, 2006). In this last application due to the fact that both radiogenic gases are produced from the decay of ^{238}U, their ratio is independent of uranium concentration (Torgersen, 1980).

Radon is one of the heaviest gases at room temperatures and can accumulate in buildings, and drinking water, and cause lung cancer (BEIR, 1999). Therefore, it is considered to be a health hazard. It is probably the most significant contaminant in indoor air quality worldwide.

2.3 Fluoride

In aqueous solution, element fluorine (F) commonly occurs as the fluoride ion (F^-). In ground waters fluoride is one of the most important environmental pollutant due to natural and/or anthropogenic factors. Pure fluorine (F_2) is a corrosive pale yellow gas that is a powerful oxidizing agent. It is the most reactive and electronegative of all the elements, and readily forms compounds with most other elements including noble gases. The fact sheet of fluorine is presented in Table 2.3.

The ill effects of excessive fluorine/ fluoride ingestion on human health have been extensively studied (WHO, 1970; 1984; Gupta and Deshpande, 1998; Luke, 1997; Zero et al, 1992). The occurrence and development of endemic fluorosis has its roots in the high fluoride content in water, air and soil, of which water is perhaps the major contributor. Bureau of Indian Standards (BIS, 1990) has suggested the permissible limit of fluoride in drinking water as 1 part per million (ppm), which is lower then the WHO (1984) drinking water limit of 1.5 ppm. Gupta and Deshpande (1998) have described the hazardous effects on human and cattle health from ingestion of excessive fluoride in the NGC region where it was observed that ingestion of excessive fluoride has adverse effect on teeth and bones (known as dental and skeletal fluorosis).

Table 2.3 The fact sheet of Fluorine (compiled from CRC handbook)

Name (Symbol)	Fluorine (F)
Atomic Number	9
Atomic mass	18.9984032 g/mol
Chemical series	Halogens
Group, period, block	17, 2, p
Electronic configuration	$1s^2 2s^2 2p^5$
Electrons per shell	2, 7
Stable isotopes	^{19}F
Radioactive isotopes	^{14}F to ^{31}F (although there are many radioactive isotopes of fluorine, they all have such a short half-life that fluorine is generally considered mono-isotopic element.
Permissible limit in drinking water	1.5 ppm (Parts per Million or mg/l); WHO, 1984. 1.0 ppm; BIS, 1990.

The normal fluoride content in the atmospheric air is reported between 0.01–0.4 µg/m^3. However, in industrial areas, it is known to range from 5 to 111 µg/m^3 (Oelschläger, 1965; Bowen, 1966). Average fluoride content of precipitation varies from almost nil to 0.089 mg/l with as high as 1 mg/l (Gmelin, 1959; Sugawara, 1967) in industrial areas. The fluoride content of rivers also varies greatly depending on the fluoide content of effluent discharges of groundwater feeding the stream and on the amount of precipitation and runoff. The fluoride content in surface water is generally higher during dry period due to evaporative concentration (Deshmukh et al, 1995b). The mean concentration of fluoride in ocean waters ranges from 0.03 to 1.35 mg/l and is seen to increase with depth in many cases (Bewers, 1971; Riley, 1965). The groundwaters, particularly in the arid/ semiarid regions throughout the globe are known to have high fluoride concentration (Handa, 1977).

The fluoride content of groundwater greatly depends on the type of soil/rocks/aquifer it comes in contact with. There are more than 150 fluorine bearing minerals in the form of silicates, halides and phosphates (Strunz, 1970; Wedepohl, 1974). Fluorite (CaF_2) is the most widely distributed fluorine bearing mineral in nature while fluorapatite ($Ca_5 F (PO_4)_3$) is a very common member of the immiscible phase generated during early differentiation of mafic and ultramafic magmas, forming apatite-magnetite rocks. In advanced stage of differentiation, fluorine is enriched into the residuum and therefore rocks like granitoids or pegmatites have very high content of apatite resulting in average fluorine content of up to 2.97 % (by weight) in these rocks. In sedimentary rocks, in addition to fluorite and fluorapatite in clastic component, clay sized minerals like micas (muscovite, biotite, phlogopite, zinnwaldite and lepidolite) and clay minerals (montrmorillonite, illite and kaolinite) have high content of fluorine due to replacement of OH^- by F^- or due to admixture of skeletal debris in which hydroxyl bonds are replaced by fluorine in the hydoxy-apatite structure (Carpenter, 1969). Out of the total fluorine content of the clay sized particles, 80 to 90 % is hosted in the micaceous minerals and remainder is associated with clay minerals (Koritnig, 1951). The fluorine content of soils depends mainly on the rocks from which they have been derived and the climatic regime in which the soil is formed. However, in warm and humid climate decomposition of organic remains can be principal source of fluorine. The average fluorine content in the soil ranges between 90 to 980 ppm (Fleischer and Robinson, 1963). The leaching of fluoride from soils and aquifer matrix into groundwater involves adsorption-desorption and dissolution-precipitation processes. Since the solubility of fluorite and fluorapatite is very low in natural waters (Deshmukh et al, 1995a), in the leaching process it is dissolved slowly by the circulating water but fluoride from mica is leached out rapidly. However, on account of the ionic strength of complex forming ions, solubility of fluorite can be drastically modified. Calcium and sulphate ions significantly lower the fluorite solubility in natural waters, often causing precipitation of fluorite (Handa, 1977; Perel'man, 1977; Deshmukh et al, 1993). The distribution of Ca and F in groundwater is therefore, antipathic (Handa, 1977; Deshmukh et al, 1995a; Dev et al, 1995; Srivastava et al, 1996). Fluorine from the clay minerals is readily desorbed in the alkaline environment. Fluoride to hydroxyl ion exchange in clay minerals depends upon concentration of fluoride ion and pH of circulating water (Hubner, 1969 a; b). Thus, solubility of fluorine bearing minerals is governed by various parameters like pH, alkalinity, ionic strength, calcium and sulphate ion concentration etc.

It is seen from the global map (Figure 2.2) of endemic fluorosis reproduced from UNICEF website (http://www.unicef.org/programme/wes/info/fl_map.gif) that most of the fluoride affected regions have arid to semiarid climate. In India, fluoride rich ground waters are found in the arid parts, especially Rajasthan, Gujarat and interior parts of the southern peninsula characterised by episodic rainfall separated by extended dry periods (Agrawal et al. 1997; Vasavada, 1998; Jacks et al. 1993). Fluoride poisoning is also reported from the arid climatic regime (Yong and Hua, 1991) in North China.

The fluoride content of thermal springs can increase with temperature due to increased rock-water interaction at elevated temperature (Chandrasekharam and Antu, 1995) and /or scavenging from the large volume during hydrothermal circulation (Minissale et al, 2000; Gupta and Deshpande 2003a) but this is not observed as a rule. There are thermal springs with as low concentraion of fluoride as <0.15 mg/l and as high concentration as 55.4 mg/l (Gmelin, 1959; Sugawara, 1967).

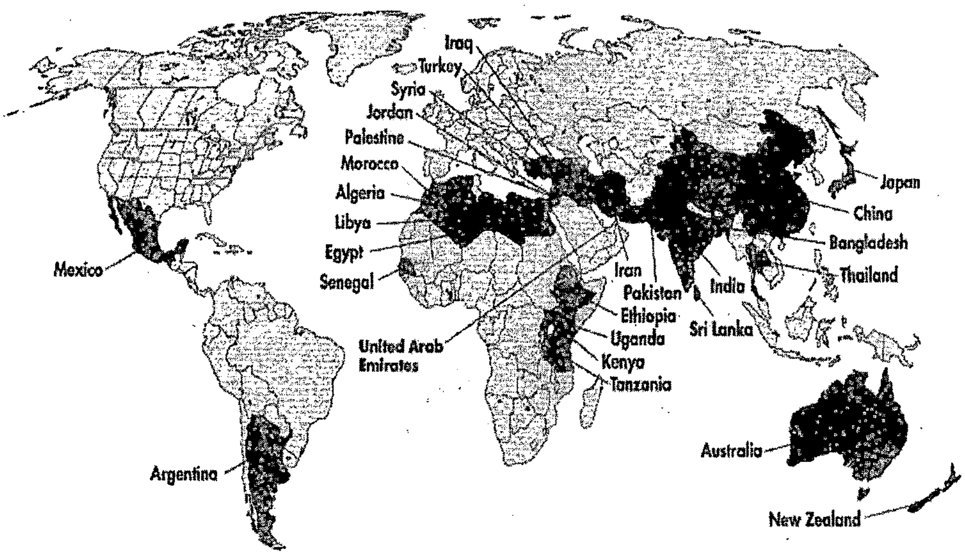

Figure 2.2 Global distribution of endemic fluorosis. Note that the most affected areas are in arid/ semiarid regions. Source-http://www.unicef.org/programme/wes/info/fl_map.gif.

2.4 Stable Isotopes of Oxygen and Hydrogen

Among various isotopes used as tracers in hydrology, stable isotopes of oxygen (^{18}O) and hydrogen (^{2}H, also known as deuterium; D) are the most important. Since these form integral parts of water molecules; these are ideally suited to follow the movement of water throughout the hydrological cycle. The basic fact sheet of these isotopes is given in Table 2.4.

In hydrological parlance, the two isotopes are also referred to as water isotopes. Importance and applications of water isotopes to hydrological studies have been discussed at length and demonstrated in several parts of the world (Dincer et al, 1974; Salati et al, 1979; Gonfiantini, 1986; Gat and Matsui, 1991; Rozanski et al, 1993; Clark and Fritz, 1997; Kendall and Mcdonnell, 1998; Araguas-Araguas et al, 1998). Several Indian case studies have been reported over the last few decades (Kumar et al, 1982; Bhattacharya et al, 1985; Das et al, 1988; Krishnamurty and Bhattacharya, 1991; Datta et al, 1991; Chandrasekharan et al, 1992; Navada et al, 1991, 1993; Datta et al, 1994,1996; Yadava, 1997; Sukhija et al, 1998; Bhattacharya et al, 2003; Deshpande et al, 2003; Shivanna et al, 2004) and in recent years by Gupta and Deshpande (2003 c; 2005 a, b, c) and Gupta et al (2005b).

Table 2.4 The fact sheet of Oxygen and Hydrogen (compiled from CRC handbook)

Name (Symbol)	Oxygen (O)	Hydrogen (H)
Atomic number	8	1
Atomic Mass	15.9994 g/mol	1.00794 g/mol
Chemical Series	Non-metals, chalcogens	non-metals
Group, period, block	16, 2, p	1, 1, s
Electronic configuration	$1s^2\ 2s^2\ 2p^4$	$1s^1$
Electrons per shell		1
Stable isotopes (Natural Abundance)	^{16}O (99.76%) ^{17}O (0.038%) ^{18}O (0.21%)	^{1}H (99.985%) ^{2}H (0.015%)
Radioactive isotopes	Fourteen isotopes from ^{12}O to ^{28}O excepting ^{16}O, ^{17}O and ^{18}O. All radioactive isotopes have half-life less than 3 minutes	^{3}H (tritium) With half-life of 12.3 years. ^{3}H beta-decays to ^{3}He.

Isotopic compositions are normally expressed in δ–notation, as deviations of heavy to light isotopic ratios relative to an international standard of known composition, in units of parts per thousand or per mil (denoted as ‰). The δ values are calculated as:

$$\delta \text{ (in ‰)} = (R_x / R_s - 1) \times 1000 \qquad \text{Eq. (2.1)}$$

where R_x and R_s denote the ratio of heavy to light isotope (e.g. $^{18}O/^{16}O$ or D/H) in the sample and standard respectively. Both, δD and $\delta^{18}O$ values, are normally reported relative to SMOW (Standard Mean Ocean Water; Craig, 1961a) or the equivalent VSMOW (Vienna-SMOW; Gonfiantini, 1978) standard.

Isotopic fractionation occurs mainly by (i) equilibrium isotopic exchange reactions and (ii) kinetic processes. Equilibrium exchange reactions involve redistribution of the isotopes between the products and reactants (or the two phases during phase change) in contact with each other. As a 'rule of thumb', among different phases of the same compound (e.g. H_2O), the denser the material, the more it tends to be enriched in the heavier isotope (D and ^{18}O).

In systems out of equilibrium, forward and backward reaction rates are not identical, and isotope reactions become unidirectional, e.g., when reaction products are physically isolated from the reactants. Such reactions are called kinetic. A third reaction type where fractionation of isotopes occurs is the diffusion of atoms or molecules across a concentration gradient. This can be diffusion within another medium or diffusion of a gas into vacuum. In this case fractionation arises from the difference in diffusive velocities of isotopic molecular species.

The isotope fractionation is expressed by a fractionation factor (α), which is the ratio of the isotope ratios for reactant and product ($\alpha = R_{reactant}/R_{product}$). For example, in case of water→ vapour system, the fractionation factor is given by;

$$\alpha^{18}O_{(water \rightarrow vapour)} = \left({}^{18}O/{}^{16}O\right)_{water} \Big/ \left({}^{18}O/{}^{16}O\right)_{vapour}$$

Eq. (2.2)

Craig (1961b) showed that in spite of the great complexity in different components of the hydrological cycle, $\delta^{18}O$ and δD in fresh waters correlate on a global scale. Craig's global meteoric water line or GMWL defines the relationship between $\delta^{18}O$ and δD in global precipitation as:

$$\delta D = 8 \times \delta^{18}O + 10 \quad (‰\ SMOW)$$

Eq. (2.3)

This equation indicates that the isotopic composition of meteoric waters behave in fairly predictable fashion. The GMWL is average of many local or regional meteoric water lines, which may somewhat differ from each other due to varying climatic and geographic parameters. A Local Meteoric Water Line (LMWL) can differ from global line in both slope and deuterium intercept. Nonetheless, GMWL provides a reference for interpreting the hydrological processes and provenance of different water masses.

Improving the precision of the Craig's GMWL, Rozanski et al (1993) compiled the precipitation isotope data from 219 stations of the IAEA/WMO operated Global Network for Isotopes in Precipitation (GNIP). This refined relationship between ^{18}O and D in global precipitation (Figure 2.3) is given by:

$$\delta D = 8.17(\pm 0.07) \times \delta^{18}O + 11.27(\pm 0.65) \quad (‰\ VSMOW)$$

Eq. (2.4)

The evolution of $\delta^{18}O$ and δD values of meteoric waters begins with evaporation from the oceans, where the rate of evaporation controls the water - vapour exchange and hence the degree of isotopic equilibrium. Increased rates of evaporation impart a kinetic or non-equilibrium isotope effect to the vapour. Kinetic effects are influenced by surface temperature, wind speed (shear at water surface), salinity and, most importantly humidity. At lower values of humidity, evaporation becomes an increasingly non-equilibrium process.

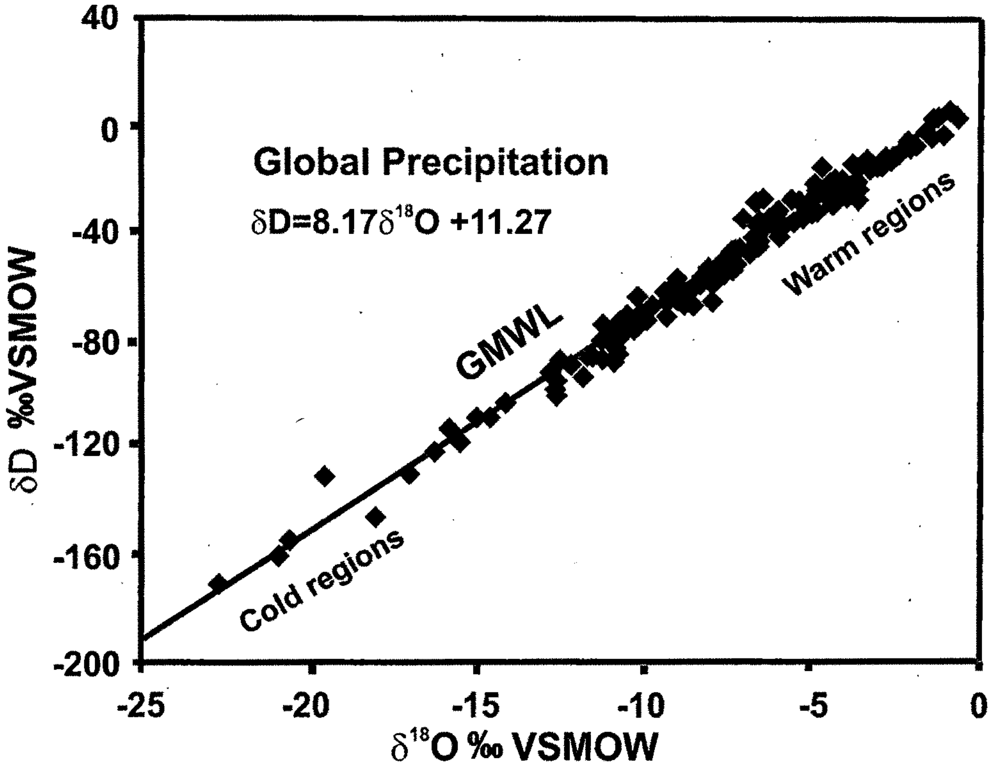

Figure 2.3 The linear regression line between $\delta^{18}O$ and δD of global precipitation samples. Data are weighted average annual values for precipitation monitored at 219 stations of IAEA/WMO global network. Redrawn from Rozanski et al (1993).

The most accepted model for non-equilibrium evaporation from a water body involves diffusion of water vapour across a hypothetical microns thin boundary layer (bl) over the liquid water interface. The boundary layer has virtually 100% water saturation. This layer is in isotopic equilibrium with the underlying water column. Between the boundary layer and the mixed atmosphere above is a transition zone through which water vapour is transported in both directions by molecular diffusion. It is within the transition zone that non-equilibrium fractionation arises due to the fact that diffusivity of ${}^{1}H_2{}^{16}O$ in air is greater than that of ${}^{2}H^{1}H^{16}O$ or $H_2{}^{18}O$. The additional isotopic enrichment ($\Delta\varepsilon$) of evaporating water due to kinetic fractionation at relative humidity (h; fractional) is approximated by the following two empirical relationships (Gonfiantini, 1986) that ignore all other controlling factors except the humidity:

$$\Delta\varepsilon^{18}O_{\text{bl-v}} = 14.2 \times (1 - h)\ ‰$$

Eq. (2.5)

$$\Delta\varepsilon^{2}H_{\text{bl-v}} = 12.5 \times (1 - h)\ ‰$$

Eq. (2.6)

It is seen from the above equations that relative magnitude of kinetic fractionation for oxygen isotopes is significantly higher than that for hydrogen isotopes. The total enrichment between water column and open air is the sum of the enrichment factor for equilibrium water vapour exchange ($\varepsilon_{l\rightarrow v}$) and the kinetic factor ($\Delta\varepsilon_{\text{bl-v}}$). For ^{18}O, this would be:

$$\delta^{18}O_l - \delta^{18}O_v = \varepsilon^{18}O_{l\rightarrow bl} + \Delta\varepsilon^{18}O_{bl\rightarrow v}$$

Eq. (2.7)

Because the boundary layer is at 100% saturation, $\varepsilon^{18}O_{l\rightarrow bl}$ corresponds to equilibrium fractionation in water→vapour system. This calculation represents the enrichment of water with respect to vapour. The depletion in vapour with respect to water is the negative enrichment. Under conditions of 100% humidity ($h = 1$), the vapour is in isotopic equilibrium with seawater ($\Delta\varepsilon^{18}O_{\text{bl-v}} = 0$). When humidity is low (e.g., $h = 0.5$) the vapour is strongly depleted in ^{18}O compared to D. The global atmospheric vapour forms with an average humidity around 85% ($h = 0.85$). That is why the Craig's GMWL has deuterium intercept of 10 ‰.

Thus, formation of atmospheric vapour masses is a non-equilibrium process due to effects of lower than saturation humidity. However, the reverse process – condensation to form clouds and precipitation – takes place in an intimate mixture of vapour and water droplets with near saturation humidity so that equilibrium fractionation between vapour and water is easily achieved. As a result isotopic evolution of precipitation during rainout is largely controlled by temperature. Because of this, the slope of GMWL (8) is largely in agreement with that given by the ratio of equilibrium fractionation factors for D and ^{18}O.

$$S \approx \frac{10^3 \ln \alpha D_{v\rightarrow l}}{10^3 \ln \alpha^{18} O_{v\rightarrow l}} = 8.2 \text{ at } 25^\circ C$$

Eq. (2.8)

However, the slopes of various LMWLs vary from 9.2 to 8.0 with average temperature of condensation between 0 to 30°C. It is thus seen that the relationship between ^{18}O and D in meteoric waters arises from a combination of non-equilibrium fractionation from the ocean surface (at ~85% humidity) and equilibrium condensation from the vapour mass. However, during rainout, further partitioning of ^{18}O and D between different regions is governed by the Rayleigh distillation equation.

As an air mass moves from its vapour source area along a trajectory and over continents, it cools and loses its water content through the rainout process. During rainout, ^{18}O and D in vapour and the condensing phases (rain or snow), within the cloud, partition through equilibrium fractionation. But along the trajectory, as each rainout removes the vapour mass, the heavy isotopes from the vapour are preferrentially removed so that remaining vapour becomes progressively depleted in ^{18}O and D. Whereas each rainout gives isotopically enriched rain (or snow) with respect to its immediate parent vapour. It will, however, be depleted with respect to earlier rainiout, because the vapour from which it formed was isotopically depleted with respect to the vapour of the earlier rainout. One can model this isotope evolution during rainout according to Rayleigh distillation equation as below.

$$R_V = R_{V0} f^{(\alpha - 1)} \quad \text{Eq. (2.9)}$$

Because $R_l / R_v = \alpha = R_{l0} / R_{v0}$; this equataion can also be written in terms of liquid water, i.e.

$$R_l = R_{l0} f^{(\alpha - 1)} \quad \text{Eq. (2.10)}$$

In above equation, R_{V0} is initial isotope ratio ($^{18}O/^{16}O$ or D/H) of vapour in the cloud and R_V the ratio after a given proportion of the vapour has rained out to yield the precipitation with the isotopic ratio R_l from liquid equilibrium value (R_{l0}) corresponding to R_{V0}. The residual fraction in vapour reservoir is denoted by 'f'. The factor 'α' denotes the equilibrium water→vapour fractionation factor at the prevailing *in-cloud* temperature.

Along the trajectory, when part of the rained out vapour is returned to the atmosphere by means of evapotranspiration, this simple Rayleigh law, however, is not applicable. The downwind effect of the evapotranspiration flux on the isotopic composition of the atmospheric vapour and precipitation depends on the details of the evapotranspiration process. Transpiration returns precipitated water essentially un-fractionated back to the atmosphere, despite the complex fractionation in leaf water (Zimmermann et al, 1967; Forstel, 1982). Thus transpiration, by returning vapour mass with isotopic composition R_V (= R_l/α) in the downwind direction, in a way restores both the vapour mass and the heavy isotope depletion caused by the rainout in such a way that the next rainout event is not as depleted as it would have been without the transpiration flux. Under such circumstances, the change in the isotopic composition along the air mass trajectory is only due to the fraction 'f_{net}', representing the net loss of water from the air mass, rather than being a measure of the integrated total rainout. This causes apparent reduction in the downwind isotopic gradient. The evaporated water, on the other hand, is usually depleted in heavy species relative to that of transpired vapour (i.e $<R_V$), thus restoring the vapour mass to the downwind cloud but reducing its isotopic composition. This causes apparent increase in the downwind isotopic gradient.

The isotopic imprints of evaporation are also recorded in the form of a parameter *d*-excess (discussed below), in the evaporating water body, the evaporated vapour and the precipitation from the admixture of atmospheric vapour and the evaporated flux. Since the kinetic fractionation for ^{18}O is more than that for D, as seen from Eq. (2.5) and Eq. (2.6), the relative enrichment of the residual water for an evaporating water body is more for ^{18}O than for D. Correspondingly, for the resulting vapour the depletion is more for ^{18}O than for D. The extent to which ^{18}O is more fractionated compared to D can be represented by a parameter *d*-excess defined by Dansgaard (1964) as below:

$$d\text{-excess} = d = \delta D - 8 \times \delta^{18}O \ (‰) \qquad \text{Eq. (2.11)}$$

The *d*-excess as defined above represents the excess δD than 8 times $\delta^{18}O$ for any water body or vapour. Since magnitude of equilibrium fractionation for D is about 8 times that for ^{18}O, any value of δD in vapour, in excess of 8 times $\delta^{18}O$ signifies the effect of kinetic fractionation due to evaporation. As mentioned earlier, the intercept (~10‰) of GMWL also signifies the kinetic fractionation during evaporation but the difference between intercept and *d*-excess is that the intercept of a meteoric or any other water line is valid for an entire dataset whereas, the *d*-excess parameter can be calculated for a single water sample whose δD and $\delta^{18}O$ values are known.

As the evaporation proceeds, because of relatively higher enrichment of ^{18}O in the residual water, the *d*-excess of the evaporating water body decreases and that of the resulting vapour increases. Therefore, if the original water was meteoric in origin, the residual water not only gets enriched in heavier isotopes but also shows progressively lower *d*-excess values as the evaporation proceeds i.e. its position on the $\delta^{18}O - \delta D$ plot will be below the Local Meteoric Water Line. The resulting vapour on the other hand shows the opposite effect. Further, since condensation and consequentially rainout is an equilibrium process (with slope ~8), it does not significantly alter the *d*-excess. Thus, *d*-excess provides an additional handle on identifying vapours of different histories and their mixing. Due to the effect of evaporation, most meteoric and subsurface processes shift the $\delta^{18}O$–δD signatures of water to a position below the LMWL. It is rare to find precipitation or groundwaters that plot above the LMWL, i.e., showing higher *d*-excess. However, in low-humidity regions, re-evaporation of precipitation from local surface waters and/or soil water/ water table creates vapour masses with isotopic content that plots above the LMWL. If such vapours are re-condensed in any significant quantity before mixing with the larger tropospheric reservoir, the resulting rainwater will also plot above LMWL (Clark and Fritz, 1997), along a condensation line with slope ~8. It is however, important to recall that recycling of water back to the atmosphere in the form of vapour from soil moisture by plant transpiration is a non-fractionating process that does not affect the *d*-excess.

A small fraction of rain percolates down through the soil layer eventually to become groundwater. For many ground waters, their isotopic composition has been shown to equal the mean weighted annual composition of precipitation (Krishnamurty and Bhattacharya, 1991; Bhattacharya et al, 1985; Hamid et al, 1989; Douglas, 1997; Rank et al, 1992). However, significant deviations from precipitation are also found in several cases. Such deviations from local precipitation are more pronounced in arid zones due to extensive evaporation from the unsaturated zone or even evaporative losses from water table (Dincer et al, 1974; Allison et al, 1983). Considering that only a small percentage of precipitation actually reaches the water table in most situations, the meteoric signal in ground water can get significantly modified. Isotope variations in precipitations get attenuated and seasonal biases in recharge are imparted to the newly formed ground water. This bifurcation of the hydrological cycle between precipitation and surface water on one hand and groundwater on the other ends where groundwater discharges and rejoins surface runoff in streams and rivers. Environmental isotopes play a significant role in quantifying relative contribution of groundwater to stream flow and in understanding the hydraulic processes operating in a catchment area.

2.5 Chlorofluorocarbons

Chlorofluorocarbons (CFCs) are non-flammable, non-corrosive, non-explosive, non-carcinogenic, very low toxic and stable halogenated alkanes synthesised first in early 1930s as safe alternatives to ammonia and sulphur dioxide in refrigeration and air-conditioning. Because of such peculiar physical properties, CFCs are suitable for a wide range of industrial applications such as blowing agents in foams, insulation, packing materials, propellants in aerosol cans solvents, in vapour degreasing and cold immersion cleaning of microelectronic components and in surface cleaning procedure. There are several CFC compounds produced commercially for industrial applications but the three most important CFC species that provide as excellent hydrological tracers are Trichloro-fluoromethane (CFC-11 or F-11), Dichloro-difluoromethane (CFC-12 or F-12) and Trichloro-trifluoroethane (CFC-113 or F-113) (Busenberg and Plummer, 1992; Dunkle et al, 1993; Cook and Solomon, 1995, 1997). The basic fact sheet of these compounds, is given in Table 2.5 which is compiled from Volk et al, 1997; Plummer and Busenberg, 1999 and Busenberg and Plummer, 1992.

Table 2.5 The basic fact sheet of important CFC species.

	CFC-11	**CFC-12**	**CFC-113**
Produced since (year)	1936	1931	1945
Name	Trichloro-fluromethane	Dichloro-difuoromethane	Trichloro-trifluoroethane
Formula	$CFCl_3$	CF_2Cl_2	$C_2F_3Cl_3$
Molecular Wt. (g/mol)	137.5	121	187.5
Boiling Point	24 ^{0}C	–29 ^{0}C	48 ^{0}C
Air mixing ratios (pptv)	249.6 pptv (NH) 247.8 pptv (SH)	538.7 pptv (NH) 538.6 pptv (SH)	78.1 pptv (NH) 78.0 pptv (SH)
Atmospheric life time	45 ± 7 years	87 ± 17 years	100 ± 32 years
(NH) = Northern Hemisphere; (SH) = Southern Hemisphere;			

The atmospheric build up of CFCs in southern and northern hemispheres is shown in Figure 2.4 It is seen that atmospheric concentration of CFCs rose rapidly through the 1970s and 1980s. This observation is in accordance with the fact that annual production of CFC-11 and CFC-12 peaked in 1987 and that of CFC-113 peaked in 1989 (AFEAS, 1997). With the realisation that CFCs are a prime contributor to stratospheric ozone depletion, Montreal Protocol (1987) on "Substances that Deplete the Ozone Layer" was signed by 37 nations which agreed to limit the release of CFCs and to reduce the CFC emissions to 50% by the year 2000. In 1990, this protocol was strengthened, requiring industrial countries to completely phase out CFCs by the year 2000, and developing countries by 2010. The Protocol received a major boost in 1992 when 90 countries agreed to cut off the production of CFCs by 1996. With various degrees of compliance with these agreements, the atmospheric concentration of CFCs started falling. As seen in Figure 2.4, air mixing ratios of CFC-11 and CFC-113 peaked around 1993 and 1994 respectively. Elkins et al. (1993) have reported peak values of 275.1 and 85.4 pptv respectively for CFC-11 and CFC-113, in North America. The air mixing ratio of CFC-12 is seen to peak in year 2003 and declines slowly thereafter.

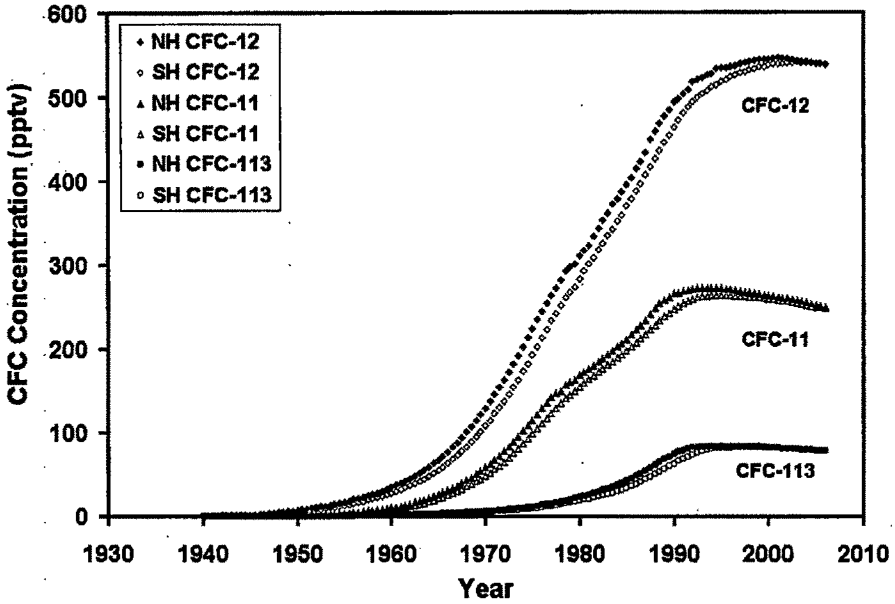

Figure 2.4 Atmospheric mixing ratios of CFC-11, CFC-12 and CFC-113 for Northern and Southern Hemisphere (NH and SH) atmosphere. Redrawn from United States Geological Survey (URL: http://water.usgs.gov/lab/software/air_curve/).

Atmospheric concentrations of CFC-11, -12 and -113 increased up to the minimum detection levels from about 1941, 1947 and 1955 respectively. CFCs dissolve in water in equilibrium with atmospheric air proportional to their mixing ratios and are subsequently carried underground by infiltrating water. Therefore, by measuring concentrations of CFC-11, CFC-12 and CFC-113, it is possible to identify groundwater recharged since about 1941, 1947 and 1955. The possibility of employing CFCs as tracers of recent recharge and indicators of groundwater age was first recognised in the 1970s (Thompson et al, 1974; Schults et al, 1976; Randall and Schultz, 1976). The progressive development in applicability of CFCs as hydrological tracers since 1970s has been described by Plummer and Busenberg (1999).

After isolation from the unsaturated zone and the soil atmosphere, newly recharged water may carry dissolved CFCs, into the aquifer. Thus, the CFC concentrations in groundwater at any location can, in principle, be traced back to atmospheric partial pressure of CFCs at the time of recharge. Therefore, the time elapsed since the groundwater lost contact with the atmosphere can be estimated. However, there may be exchange between gases dissolved in equilibrium with atmosphere and gases in the unsaturated zone invalidating the inherent assumption of no addition or removal of CFCs to or from the recharged water.

The isolation of a parcel of water from the unsaturated zone air is a function of several factors including (i) recharge rate; (ii) porosity of the unsaturated zone; (iii) aqueous and gaseous diffusion coefficients; and (iv) magnitude of water table fluctuation. There is evidence of loss of dissolved gases such as ^{3}He during vertical transport of water (Schlosser et al, 1989; Solomon et al, 1993). However, Cook and Solomon (1997) pointed out that CFCs have higher solubility and lower diffusion coefficients than ^{3}He. An investigation of CFC concentration in air and shallow groundwater revealed that groundwater during seasonal water table low preserved the CFC concentration formed when water table was near land surface and in equilibrium with atmosphere (Cook et al, 1995). Further, the molecular diffusion coefficients of gases in water are some 5 orders of magnitude smaller than in air. Thus, despite possibility of molecular diffusion, the shallow groundwater remains closed to gas exchange and CFC confinement is thought to occur fairly rapidly (Cook and Solomon, 1997).

The CFC concentrations can also be affected by various physical and chemical processes such as degradation and sorption during transit within the unsaturated zone and the soil zone. Soil-gas CFCs concentrations and the ratio of CFC-11 to CFC-12 are reported to decrease with depth indicating that various dissolved CFCs can be unequally retarded during their downward movement in unsaturated zone depending on tortuosity, sorption and dissolution in pore water (Weeks et al, 1982; Khalil and Rasmusen, 1989; Brown, 1980). These studies also indicate that CFCs are absorbed by soils in a magnitude decreasing with increasing fluorine content. The magnitude of absorption is dependent on the organic content of soil and is independent of mineralogy. The CFCs absorbed by dry soils can be subsequently released when soils become wet again.

The dissolved CFC concentration can also be modified by microbial degradation particularly in an anoxic environment. There is experimental evidence of microbial degradation of CFCs mainly after completion of denitrification reactions which indicate that microbial population other than denitrifiers are responsible for degradation of CFCs and rate of biodegradation is inversely related to fluorine content of halocarbons (Semprini et al, 1990). The microbial degradation, however, is not observed in the oxic environments. Additional CFCs, over and above atmospheric equilibration value, can also be introduced into groundwater due to entrapment and subsequent dissolution of air bubbles (See section 2.1), similar to that for helium (Heaton, 1981; Heaton and Vogel, 1981; Andrews et al, 1985).

Despite various factors that may give rise to uncertainties in the interpretation, CFCs in groundwater have been used advantageously to (i) identify the recent recharge;

(ii) estimate the time of recharge; and also (iii) explain differences in apparent ages in an aquifer (Busenberg and Plummer, 1992; Dunkle et al, 1993).

Over the last three decades there has been advancement in the analytical techniques, sampling and storage procedure and reliability and adequacy of data such as reconstructed atmospheric mixing ratios, Henry's solubility constants etc (Plummer and Busenberg, 1999). As a result, CFCs are now increasingly employed as tracers for studying oceanic circulation, ventilation and mixing, unsaturated zone processes and for identifying recent recharge and dating of young (~50 years time scale) ground waters (Plummer and Busenberg, 1999). It must, however, be stated that analyses of CFCs in water still remains quite tricky and cumbersome. Therefore, there are only a few functional laboratories in the world to measure dissolved CFCs.

2.6 Groundwater Dating

In an aquifer system, ensemble of water molecules arriving at a particular location within the aquifer comprises molecules that spend various time durations between recharge and their reaching a particular location. The concept of groundwater dating involves estimating the average time spent by the molecules before reaching a given location. The age of groundwater at a particular location is the estimated average time spent by the water molecules in the aquifer since the time of recharge and before arriving at that location. Depending on the conceptual mathematical model of the aquifer system, the age can give different additional information about the aquifer system. The various conceptual models in common use are: (i) the Piston Flow Model (PFM); (ii) the Well-Mixed Reservoir Model (WMRM); and (iii) the Dispersion-Advection Model (DAM).

The most commonly used groundwater flow model for estimating groundwater age assumes that as groundwater moves away from the recharge area, there are no flow lines of different velocities and that hydrodynamic dispersion as well as molecular diffusion of water molecules are negligible. Thus, water moves from the recharge area very much like a parcel pushed by a piston with mean velocity of groundwater (Piston Flow Model; PFM). This implies that a radiotracer which appears at the sampling point at any time "t" has entered the system at a time "t-T", and from that moment its concentration has decreased by radioactive decay during the time span "T" spent in the aquifer. Therefore:

$$C_{out}(t) = C_{in}(t-T) \,.\, \exp(-\lambda T)$$

Eq. (2.12)

This equation describes a dynamic system and is mathematically equivalent to describing the concentration of a radioisotope in a static water parcel separated since its recharge, whereby:

$$C_t = C_0 \, . \, \exp(-\lambda T)$$

Eq. (2.13)

Here, "t" is the radiometric age of the water and corresponds to "T" of the dynamic system. If "x" is the distance from the recharge boundary, T = x/u can be used to estimate the flow rate (u) of groundwater in the aquifer.

$$C_t = C_0 \exp(-\lambda x/u)$$

Eq. (2.14)

Unlike in the PFM, if it is assumed that the recharge flux completely mixes with the entire volume of the reservoir before outflow, we get another extreme situation and the model is known as Well Mixed Reservoir (WMR) model. In applying this model to an aquifer system, it is assumed that the well-mixed reservoir comprises the entire volume between the recharge area and the sampling point. Under this condition for a radiotracer,

$$C_t = C_0 / (1+\lambda\tau)$$

Eq. (2.15)

In Eq. (2.15), "λ" is the radioactive decay constant and "τ" is the ratio of the reservoir volume to the flux into the reservoir and represents the estimated mixing time (or the mean residence time) between the recharge area and the sampling location. It is seen that τ estimated from the tracer data actually represents a dynamic parameter – the mixing time.

$$\tau = \frac{1}{\lambda}\left(\frac{C_0}{C_t} - 1\right)$$

Eq. (2.16)

The phenomenon of mixing accompanying the movement of water molecules through porous media can also be described by a diffusion-advection equation in which the diffusion coefficient is replaced by a dispersion coefficient (Scheidegger, 1961; Gupta, 2001). For a radiotracer, the one dimensional continuity equation in groundwater flow system may be written as (Guymon,1972):

$$\frac{\delta C}{\delta t} = \frac{\delta\left(D \, {}^{\delta C}\!/_{\delta x} - uC\right)}{\delta x} + W_1 - W_2$$

Eq. (2.17)

In the above equation, "D" is the diffusion coefficient of the tracer, and as in the case of PMF, "x" is the distance from the recharge boundary, "u" is the bulk flow velocity, "W_1" and "W_2" are the rates of the introduction and removal of the tracer respectively. With further assumptions of u and D not being function of x and in case of steady state (i.e. dC/dt = 0), the above equation reduces to:

$$D\frac{\partial^2 C}{\partial x^2} - u\frac{\partial C}{\partial x} W_1 - W_2 = 0$$

Eq. (2.18)

In case of radioactive tracers, the term W_2 will include, in addition to radioactive decay, loss of tracer from water due to non-radioactive processes (e.g. adsorption on the aquifer matrix). Dealing with the case of loss of tracer by radioactive decay alone and for $W_1 = 0$, the above equation can be rewritten as:

$$D\frac{\partial^2 C}{\partial x^2} - u\frac{\partial C}{\partial x} - \lambda C = 0$$

Eq. (2.19)

This equation for the case of D = 0, and the boundary condition $C = C_0$ at $x = 0$ give the solution for the piston flow Eq. (2.14).

In case of finite dispersion, the solution of Eq. (2.19) for the boundary conditions $C = C_0$ at $x = 0$ and $C = 0$ at ∞, is given by Gupta et al (1981).

$$C/C_0 = \exp\left[\frac{xu}{2D}\left\{1 - \left(1 + 4\lambda D/u_2\right)^{1/2}\right\}\right]$$

Eq. (2.20)

The tracer concentration decreases exponentially with distance similar to the case of PFM. Therefore, a simplistic application of the PFM would give an apparent velocity:

$$u_a = \frac{u}{2}\left\{1 - \left(1 + 4\lambda D/u^2\right)^{1/2}\right\}$$

Eq. (2.21)

There are several other mathematical models in use that conceptualize the flow of groundwater in aquifer system differently depending on specific understanding of the geometry, and flow paths. But for confined aquifers with a definite recharge area, the above models are most frequently used to interpret the environmental isotopic data and to determine the groundwater age evolution from recharge to discharge regions. This, though, is still a challenging task for hydro-geochemists because sampling locations are often randomly distributed over an area where water from an aquifer is pumped from various depths or where springs bring water to the surface. Several environmental tracers (including radio nuclides) find application in determining direction and magnitude of groundwater flow, hydro-geological parameters of the aquifer and age of groundwater (Andrews et al., 1989; Cserepes and Lenkey, 1999).

In regional aquifer systems, groundwater ages may range up to 10^3 ka and more. Radiocarbon, with half-life ($t_{1/2}$) of 5.73 ka, can be used for groundwater dating up to ~35 ka (Geyh, 1990). The other available radio nuclides such as ^{36}Cl ($t_{1/2}$ = 3.01x 10^2 ka; Andrews and Fontes, 1992), ^{81}Kr ($t_{1/2}$ = 2.1x10^3 ka; Lehmann et al., 1991) and ^{234}U ($t_{1/2}$ = 2.45x10^2 ka; Fröhlich and Gellermann, 1987) enable groundwater age determination well beyond the radiocarbon dating range. On the other hand, the range of groundwater ages that can be estimated by radiogenic ^4He is 1–100 ka (Torgersen, 1980; 1992; Mazor and Bosch, 1992; Clark et al., 1998; Castro et al., 2000). When combined with ^{222}Rn activity measurements, the $^4He/^{222}Rn$ systematics also provides estimation of groundwater age in the range 1–1000 ka (Torgersen, 1980; Gupta et al, 2002). Another advantage of both ^4He and $^4He/^{222}Rn$ methods is that measurements of ^4He and ^{222}Rn are relatively simple. However, some complications also exist.

2.6.1 ^{14}C Dating Method

The radiocarbon (^{14}C) dating method for groundwater is based on measuring the residual activity of ^{14}C, in total dissolved inorganic carbon (TDIC) of a given groundwater sample. The groundwater age is estimated using:

$$\text{Age}(t) = -\frac{1}{\lambda_{14}} . \ln\left(\frac{A_t}{A_0}\right)$$

Eq. (2.22)

In Eq. (2.22), ^{14}C activities are expressed in terms of percent modern carbon (pmC). The activity of 'modern Carbon' is defined as 95% of the ^{14}C activity in 1950 of the NBS oxalic acid standard. This is close to the activity of wood grown in 1890 in a fossil-CO_2-free environment and equals 13.56 dpm/g carbon. Thus, expressed in pmC, A_t refers to ^{14}C activity of TDIC in groundwater at the time of sampling and A_0 the initial activity in the recharge area; λ_{14} is the radioactive decay constant for ^{14}C and t is the estimated age.

Two key assumptions made in this method are: (i) A_0 is known and has remained constant in time; and (ii) the system is closed to subsequent gain or loss of the parent, except by the radioactive decay. In the case of radiocarbon dating of vegetal remains, A_0 can be taken as equal to 100 pmC since the only source of ^{14}C is atmospheric CO_2. However, in the case of ground waters, A_0 in TDIC depends on contribution from soil CO_2 and from soil carbonates which can have any value of ^{14}C activity between zero (radioactively dead carbon) to 100 pmC. Depending on the contribution from soil carbonates, A_0 can have any value between 50–100 pmC. This is because, of the two carbon atoms in the molecule of $Ca(HCO_3)_2$ in TDIC, $[CaCO_3 + H_2O + CO_2 \leftrightarrow Ca(HCO_3)_2]$, one is derived from soil CO_2 and the other from soil carbonate. There is further complication due to isotopic exchange between TDIC and the soil CO_2 and carbonate material. There are several models that attempt to estimate the contribution of soil carbonates to the TDIC and estimate the applicable value of A_0. This is done either through a stoichiometry approach for the various chemical reactions involving carbon or by estimating dilution of active carbon using an isotope mixing approach based on ^{13}C content of each species involved or a combination of the two approaches. Various methods for estimating A_0 can be found in Mook (1976) and Fontes and Garnier (1979). The error due to incorrect estimation of A_0, however, is $<t_{½}$ of ^{14}C, except in some special case of carbonate aquifers where continuous exchange between TDIC and the aquifer matrix may reduce A_0 to <50 pmC. Since most of the chemical and isotope exchange occurs in the unsaturated soil zone during the process of groundwater recharge, and between TDIC and the soil CO_2, the A_0 in several ground waters has been found to be 85±5 pmC (Vogel, 1967; 1970).

In the present investigation, the theoretical value of A_0 after equilibrium between soil $CO_{2,}$ soil carbonate (at $^{14}C = 0$ pmC; $\delta^{13}C = 0‰$) and infiltrating water has been achieved, is estimated using the following equation (Münnich, 1957; 1968):

$$A_0 \quad = \quad \frac{\delta^{13}C_{TDIC}}{\delta^{13}C_{soil} - \varepsilon} 100$$

Eq. (2.23)

Where, $\delta^{13}C_{TDIC}$ is the $\delta^{13}C$ value of the groundwater TDIC, $\delta^{13}C_{soil}$ is the $\delta^{13}C$ of soil CO_2 (~–22‰) and ε is equilibrium fractionation between the soil CO_2 and the TDIC of groundwater (~–9‰). This is done with the knowledge that application of any other model would give radiocarbon ages differing by < ± 2ka. Also because, in regional aquifers, the difference in groundwater ages between any two locations, after the confinement of the groundwater in the aquifer becomes effective, depends little on the applicable value of A_0.

2.6.2 ^{4}He Dating Method

The Helium-4 dating method for groundwater is based on estimating the amount and rate of accumulation of *in situ* produced radiogenic ^{4}He in groundwater (Andrews and Lee, 1979; Stute et al, 1992a). If secular equilibrium and release of all the produced ^{4}He atoms in the interstitial water are assumed, the groundwater ages can be calculated from the annual ^{4}He production rate estimated as (Torgersen, 1980):

$$J'_{He} = 0.2355 \times 10^{-12}\, U^*$$

Eq. (2.24)

where,

$$U^* = [U]\{1+0.123([Th]/[U]-4)\}$$

Eq. (2.25)

J'_{He} = production rate of ^{4}He in cm^3 STP g^{-1} rock a^{-1}; [U] and [Th] are concentrations (in ppm) of U and Th respectively in the rock/sediment.

Accumulation rate (AC'_{He}) of ^{4}He in cm^3 STP cm^{-3} water a^{-1} is therefore, given by:

$$AC'_{He} = J'_{He}.\rho.\Lambda_{He}.(1-n)/n$$

Eq. (2.26)

Where, Λ_{He} = helium release factor; ρ = rock density (g cm^{-3}); n = rock porosity.

Since the helium measurements were actually made on equilibrated headspace air samples, in the present study, the dissolved helium concentrations (cm^3 STP cm^{-3} water) are expressed in terms of Air Equilibration Units (AEU) which expresses the dissolve helium in terms of the corresponding equilibrium dry gas phase mixing ratio at 1 atmospheric pressure and 25°C. As a result, water in equilibrium with air containing 5.3 ppmv helium is assigned dissolved concentration of 5.3 ppmAEU. Water of meteoric origin will have a minimum helium concentration ($^4He_{eq}$) of 5.3 ppmAEU, acquired during its equilibration with the atmosphere. Excess helium ($^4He_{ex}$) represents additional helium acquired by groundwater either from *in situ* produced radiogenic ^{4}He or any other subsurface source.

Using a dimensionless Henry Coefficient (H_x) of 105.7 for helium at 25°C (Weiss, 1971), 5.3 ppmAEU corresponds to a moist air equilibrium concentration of 4.45×10^{-8} cm^3 STP He. cm^{-3} water. Therefore,

$$AC_{He} = AC'_{He} .10^6 . H_X.(T/T_0).P_0/(P_0 - e)$$

Eq. (2.27)

where, AC_{He} = accumulation rate of ^4He in ppmAEU a^{-1}; T_0 = 273.15° K; P_0 = 1 atm and e = saturation water vapour pressure (0.031 atm) at 25°C, H_x = 105.7.

For an average [U] = 1 ppm for alluvial sedimentary formations and [Th]/[U] = 4 (Ivanovich, 1992), n = 20 %; Λ_{He} = 1; ρ = 2.6 g cm^{-3}, *in situ* ^4He accumulation rate (AC_{He}) of 2.59×10^{-4} ppmAEU a^{-1} is obtained. Therefore, from the measured helium concentration of the sample (^4He_s), the age of groundwater can be obtained by using:

$$\text{Age (t)} = {}^4He_{ex} / AC_{He}$$

Eq. (2.28)

where, $^4He_{ex}$ is obtained by subtracting $^4He_{eq}$ (= 5.3 ppmAEU at 25°C and 1 atmospheric pressure) from the measured concentration in groundwater sample (^4He_s).

The above formulae, however, ignores 'excess air' helium ($^4He_{ea}$) due to supersaturation of atmospheric air as the groundwater infiltrates through the unsaturated zone. Various models have been proposed for estimating this component in groundwater studies (Aeschbach–Hertig et al., 2000; Kulongoski et al., 2003) based on measurement of other dissolved noble gases. Since measurement of dissolved noble gases has not been made in this study, it has not been possible to correct for this effect. However, from other studies (Holocher et al., 2002) it appears that $^4He_{ea}$ can be up to 10–30% of $^4He_{eq}$ giving a possible overestimation of groundwater age up to ~ 6 ka.

Further, (^4He_s) can contain other terrigenic helium components (Stute et al., 1992a) that can cause overestimation of groundwater age. These terrigenic components are: (i) flux from an external source e.g. deep mantle or crust, adjacent aquifers etc. (Torgersen and Clarke, 1985); and (ii) release of geologically stored ^4He from young sediments (Solomon et al., 1996). Depending upon the geological setting, particularly in regions of active tectonism and/or hydrothermal circulation, the contribution of these sources may exceed the *in situ* production by several orders of magnitude (Stute et al., 1992a; Minissale et al., 2000; Gupta and Deshpande, 2003a). Additional measurements/ data (e.g. $^3He/^4He$, other noble gases) are required to resolve these components. For recent reviews on terrigenic helium, reference is made to Ballentine and Burnard (2002) and Castro et al. (2000). However, in many cases it seems possible to rule out major contribution from terrigenic He sources since the helium flux may be shielded by underlying aquifers that flush the Helium out of the system before it migrates across them (Torgersen and Ivey, 1985; Castro et al., 2000). According to Andrews and Lee (1979), with the exception of a few localised sites and for very old ground waters, 'excess He' in groundwater is due to *in situ* production only and is often used for quantitative age estimation within the aquifer if the U and Th concentrations of the aquifer material are known. But, in case, there is evidence of deep crustal ^{4}He flux (J_0) entering the aquifer, the Eq. (2.28 gets modified to (Kulongoski et al, 2003):

$$\mathrm{Age}(t) = {}^{4}\mathrm{He}_{Ex} / [(J_0 / n Z_0 \rho_w) + AC_{He}] / 8.39\mathrm{x}10^{-9}$$

Eq. (2.29)

where, Z_0 is the depth (m) at which the ^{4}He flux enters the aquifer and ρ_w is the density of water (1 g cm^{-3}).

2.6.3 ^{4}He/^{222}Rn Dating Method

Since both ^{4}He and ^{222}Rn have a common origin in groundwater, being produced by the α decay of U and/or Th in the aquifer material, their simultaneous measurements in groundwater can also be utilized for calculating its age (Torgersen, 1980).

As in case of ^{4}He, the ^{222}Rn accumulation rate (AC_{Rn}) in cm^{3} STP cm^{-3} water a^{-1} is given by:

$$AC_{Rn} = J'_{Rn} . \rho . \Lambda_{Rn} . (1-n)/n$$

Eq. (2.30)

$$\text{where, } J'_{Rn} = 1.45 \times 10^{-14} [U]$$

Eq. (2.31)

and J'_{Rn} = production rate of ^{222}Rn in cm^{3} STP g^{-1} rock a^{-1} and [U] = concentration (in ppm) of U in the rock/sediment.

Thus, computing accumulation rate ratio of ^{4}He and ^{222}Rn (= AC_{He}/AC_{Rn}), the age of groundwater can be calculated as follows:

$$\mathrm{Age}(t) = (\Lambda_{Rn}/\Lambda_{He})(AC_{Rn}/AC_{He})(C_4/A_{222})$$

Eq. (2.32)

where, $\Lambda_{Rn}/\Lambda_{He}$ is the release factor ratio for radon and helium from the aquifer material to groundwater; C_4 is concentration (atoms l^{-1}) of ^{4}He and A_{222} is activity (disintegration l^{-1} a^{-1}) of ^{222}Rn in groundwater. From Eq. (2.24) to Eq. (2.26) and Eq. (2.30) to Eq. (2.32) it is seen that ^{4}He/^{222}Rn ages are independent of porosity, density and U concentration, but do require a measure of [Th]/[U] in the aquifer material. The ratio $\Lambda_{Rn}/\Lambda_{He}$ depends upon grain size and recoil path length of both ^{222}Rn (~0.05μm) and ^{4}He (30–100μm) (Andrews, 1977). Release of ^{222}Rn by α–recoil from the outer surface (~0.05μm) of grain (~2–3mm) has been estimated to be ~0.005% (Krishnaswami and Seidemann, 1988). Apart from α–recoil, both ^{222}Rn and ^{4}He can diffuse out from rocks/ minerals through a network of 100–200Å wide nanopores throughout the rock or grain body (Rama and Moore, 1984). Radon release factor (Λ_{Rn}) ranging from 0.01–0.2 has been indicated from laboratory experiments for granites and common rock forming minerals (Krishnaswami and Seidemann, 1988; Rama and Moore, 1984). On the other hand, Torgersen and Clarke (1985), in agreement with numerous other authors, have shown that most likely value of $\Lambda_{He} \approx 1$. Converting C_4 (atoms l^{-1}) to C_{He} (ppmAEU) units and A_{222} (disintegration l^{-1} a^{-1}) to A'222 (dpm l^{-1}) units, Eq. (2.32) can be rewritten as:

$$\text{Age (t)} = 4.3\times10^{8}\cdot(\Lambda_{Rn}/\Lambda_{He})\cdot(AC_{Rn}/AC_{He})\cdot C_{He}/A'_{222}$$

Eq. (2.33)

Here, 1 ppmAEU ^{4}He concentration corresponds to 2.26×10^{14} atoms of ^{4}He l^{-1} of water. Another inherent assumption of ^{4}He/^{222}Rn dating method is that both ^{4}He and ^{222}Rn originate from the same set of parent grains/rocks and their mobilization in groundwater is similarly affected.

Andrews et al. (1982) used following one–dimensional equation for calculating diffusive transport of ^{222}Rn in granites:

$$C_x = C_0 \exp(-\sqrt{\lambda/D}.X)$$

Eq. (2.34)

where, C_0 and C_x are concentration of ^{222}Rn from an arbitrary x = 0 and at x = x respectively; D = diffusion coefficient in water (~10^{-5} cm^2 s^{-1}); and λ = decay constant for ^{222}Rn. They calculated that C_x/C_0 = 0.35 at a distance equal to one diffusion length (X = $[D/\lambda]^{1/2}$ i.e. 2.18 cm). Therefore, even at high ^{222}Rn activity its diffusion beyond few metres distance is not possible. The average radon diffusion co–efficient in soils with low moisture content and composed of silty and clayey sand is even lower ~2×10^{-6} cm^2 s^{-1} (Nazaroff et al., 1988). Therefore, ^{222}Rn measurements of groundwater depend essentially on U in the pumped aquifer horizons in the vicinity of the sampled tubewell.

Therefore, for ground waters that may have a component external to the aquifer, the measured ^{222}Rn because of its short half–life ($t_{1/2}$ = 3.825 d) is indicative of local mobilisation only. Whereas ^{4}He, being stable, might have been mobilized from the entire flow–path. In such cases, the resulting $^{4}He/^{222}Rn$ ages for groundwater samples having high ‘excess He’ might be over estimated.

2.6.4 CFC Dating Method

Groundwater dating with CFCs is possible because: (i) the atmospheric mixing ratios of CFCs are known or have been reconstructed over the past 50 year; (ii) the Henry's law solubility of CFCs in water are known; and (iii) technology to measure low concentrations of CFCs in water has been developed. CFC age of groundwater actually estimates the time since the water became isolated from the air in unsaturated zone. However, in view of possibility of modifications of dissolved CFC concentration during transit, it is more appropriate to use the term ‘CFC-model age’ or ‘CFC-apparent age’. The basic assumption in assigning the model age is the piston flow model (PFM; See Section 2.6 above). The inferred model age assumes that the concentration of the CFC was not altered by the transport processes from the point of entry to the measurement point in the aquifer. Most of the apparent CFC ages referred to in the literature are based on PFM (Plummer and Busenberg, 1999).

The scope of the present work is limited to setting up of the groundwater CFC laboratory at PRL for future application. Therefore, further details including the mathematics involved in groundwater dating with CFCs are not presented here.

In Chapter 3 next, details of the field and laboratory procedures for sample collection, storage, instrument calibration and analyses using CFC standard are described. Also described in Chapter 3 are similar details for other tracer techniques used in this study.

Chapter 3. Experimental Procedures

The specific field protocols for collection and storage of groundwater samples for analyses of dissolved helium, radon, fluoride and precipitation of inorganic carbon for radiocarbon dating were developed and standardized as part of this work. The protocols were validated in the laboratory before field application. Purge and trap system for extracting dissolved CFCs in groundwater was also developed and tested. The existing analytical facilities at PRL were used for measuring stable isotope ratios of oxygen and hydrogen, and activities of ^{14}C and ^{222}Rn.

Groundwater samples in this study were collected from tubewells, hand pumps, dug wells and thermal springs ranging in depth from 3m to 350m. Prior to sampling, the hand pumps and tubewells were purged long enough (>3 well volumes) to flush out any stagnant water. The standard water quality parameters like temperature, pH and electrical conductivity (EC) were measured in the field during sampling using the µ-processor based water analysis kit (Brand: Century: CMK-731).

Sampling, storage and analytical techniques for some geochemical and isotopic parameters as developed as part of this work are described in the following.

3.1 Helium in Soil-air and Groundwater

3.1.1 Soil air and Groundwater Sampling

Soil air samples were collected from 1 m below ground. A 1.2-metre long copper tube ($\Phi = 5$ mm) with perforation on 15-cm of its lower end was inserted into the soil. The ground surface near the upper end of the copper tube was then hammered and moistened to effectively seal the hole from direct contact with atmosphere. The upper end of the copper tube was connected to a hand-operated suction pump by a Tygon tube. The pump was operated sufficiently long to ensure removal of atmosphere/ soil-air mixture from the copper tube and the surrounding soil-air. The upper end of Tygon tube was then closed using a 3-way stopcock for accumulating soil-air inside the tubes. After about 12 hours, the hypodermic needle fitted to the third end of the stopcock was made to pierce the rubber stopper of a 1.2-litre pre-evacuated soda-lime glass bottle for soil-air sample collection. Withdrawal of the hypodermic needle, quickly, from rubber stopper effectively sealed the soil-air sample.

Groundwater samples were collected directly from the pump outlet using a PVC tube ($\Phi = 8$ mm) to divert the water flow and to transfer the same to the bottom of a 1.2-litre soda-lime glass sample bottle, pre-rinsed with groundwater from the same source being sampled. It was ensured that the tubewell was pumping at least for half an hour prior to sampling. In case of a hand pump, it was operated at least for 15 minutes before sampling.

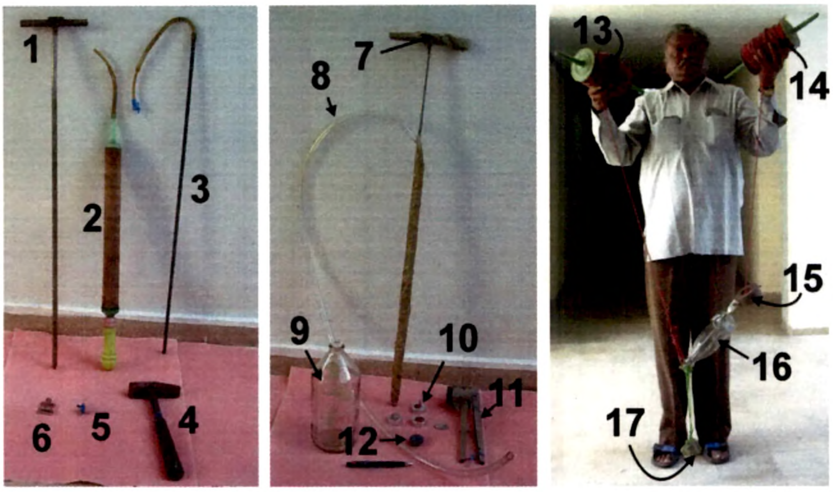

Figure 3.1 Various tools and gadgets used for sampling of groundwater and soil air. 1 – Metallic rod; 2 – Hand operated suction pump; 3 – copper tube perforated at the bottom; 4 – Hammer; 5 –Three-way valve; 6 – Pinch cock; 7 & 8 – Metallic rod with a PVC tube tied on it for diverting groundwater flow from pump outlet; 9 – 1.2-litre soda-lime glass bottle; 10 – three layers of the aluminium seal; 11 – Hand operated crimping tool for aluminium seal; 12 – Bromo-butyl synthetic rubber stopper; 13 & 14 – Nylon ropes connected to mouth and base of the collection glass bottle for extraction of water from the desired depth of the water column in dug wells, lakes and streams; 15 – Heavy weight tied to the base of the glass bottle; 16 – The water collection glass bottle ; 17 – Heavy weight tied to the mouth of the bottle. Weights (15 and 17) are meant to keep the bottle vertical while lowering or lifting and for reverting the bottle at the desired depth in the water column.

After allowing the sample bottle to overflow for a while and when no bubbles were visually seen, the PVC tube was withdrawn and the sample volume was reduced to a factory -marked position on the sampling bottle leaving 98 ml of air above water surface. The bottle was then sealed within few seconds with a rubber stopper and triple aluminium protection cap using a handheld crimping tool. Wherever pumping facility did not exist (e.g. a dug well), the sample was collected by immersing an inverted (mouth down) empty 2-litre glass bottle inside the water with the help of a rope and suitable weight attached to keep it inverted. After the bottle reached the required sampling depth, it was reverted (mouth up) for water sampling. The collected sample was then transferred to a 1.2-litre soda-lime bottle and sealed as above.

The bottles filled with water sample were stored in corrugated hardboard box with compartments made to accommodate one bottle per compartment. The bottles were stored in inverted position to minimise any loss of helium from the stopper. The air in the bottle got equilibrated with water by movement during transportation and additionally by shaking for sometime in laboratory before analysing helium concentration by the standardised procedure described in the following (Section 3.1.3). The various field implements used for sampling helium from soil air and the groundwater are shown in Figure 3.1.

3.1.2 Sample Storage

Helium permeates readily through many materials, it is therefore important to carefully choose the containers in which the soil-air and groundwater samples intended for subsequent helium analyses are to be stored. The optimal material for such containers is oxygen free high conductivity (OFHC) copper tubing in which samples for helium analyses are sealed by crimping at both ends (Craig and Lupton, 1976; Lupton et al. 1977). Gupta et al. (1990) showed that loss of dissolved helium from thick walled soda-lime glass bottles, with conventional laboratory rubber stopper was less than 3% during a storage period of 24 h.

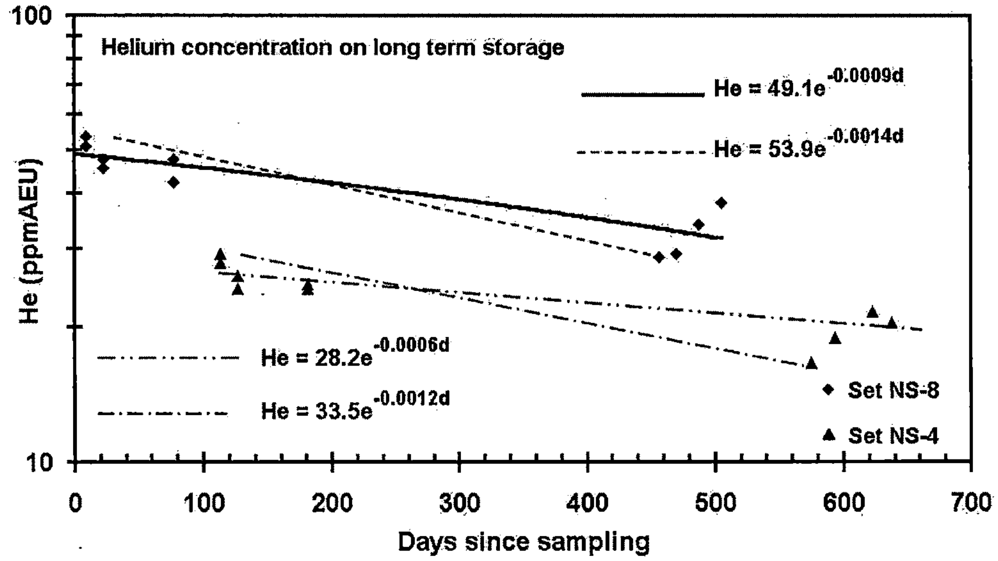

Figure 3.2 Residual helium concentrations on long term storage in soda-lime glass sampling bottles with bromobutyl rubber stopper and triple aluminium protection seal. Two separate sets of multiple samples were collected from two different sources. Individual samples were analysed subsequently at various intervals during a period of 20 months after the sample collection. The maximum observed loss of helium is given by the steepest line on this log-linear plot which corresponds to a loss of <0.15 % per day. The average loss, obtained by averaging the rates from the two best fit lines is, however, 0.075% per day.

This storage method, however, was not suited for soil-air and for equilibration measurement techniques of helium. Therefore, thick (3 mm) walled soda-lime glass bottles with bromobutyl synthetic rubber stopper manufactured according to guidelines of U.S. Pharmacopoeia standard II (USP Std-II) and secured by additional triple aluminium cap fixed by hand held crimping tool in the field were used for sample collection and storage. The synthetic rubber stopper was easily pierced by hypodermic needle and seals effectively when the needle was withdrawn. Each bottle used for sampling is pre-checked for maintenance of vacuum by evacuating the same and measuring the air pressure inside after 10 days. Bottles showing pressure > 2 torr were rejected. To test the integrity of samples against leakage and diffusion of helium, two identical sets of water samples (ten each) each were simultaneously collected from the same source following the procedure described previously. Helium concentrations in these sets of sample bottles were measured over a period of 20 months. The measured concentrations were then plotted on a log-linear plot (Figure 3.2) It was assumed that the loss during storage is a first order rate process; like radioactive decay, depending on the concentration. The slope of the steepest line through any particular set of data points corresponds to the highest loss rate and the best fit line corresponds to the average loss rate. It is seen from Figure 3.2 that the maximum loss of helium during storage was given by the line (He=53.94*exp(–0.0014d) for NS-8). Applying the standard concept of half life; a value of 495 days was obtained corresponding to 50 % helium loss using this equation. This corresponds to a loss of <0.15 % per day.

3.1.3 Analytical Procedure

A helium leak detector (ALCATEL Model ASM 100 HDS) comprising a tuned mass-spectrometer for helium ions (m/e = 4) was used for helium measurements by connecting an inlet port to its sniffer probe. This system was in many ways similar to the one used by Friedman and Denton (1975) and Reimer (1984). Equilibrated air samples (Figure 3.3a) were drawn from the head space of the bottles by piercing their rubber seal using a 20 ml syringe (Syringe-1). As the sample was drawn, an equal amount of air from another syringe (Syringe-2) entered the bottle and mixed with the sample gas. The test sample drawn in Syringe-1 was injected first into a pre-evacuated Syringe-3 by piercing the rubber septum on the inlet port and then allowed to be sucked into the leak detector through a moisture trap connected to the sniffer probe (Figure 3.3). The system response, directly proportional to the partial pressure of helium in the air /gas flowing through the analyser was recorded as voltage output on a data logger and chart recorder. The measured helium concentrations were corrected for (i) volume of headspace, (ii) water volume, (iii) volume of air drawn in during analysis and (iv) duration of storage. The average loss, obtained by averaging the rates from the two best fit lines is, however, 0.075% per day as shown in Figure 3.2.

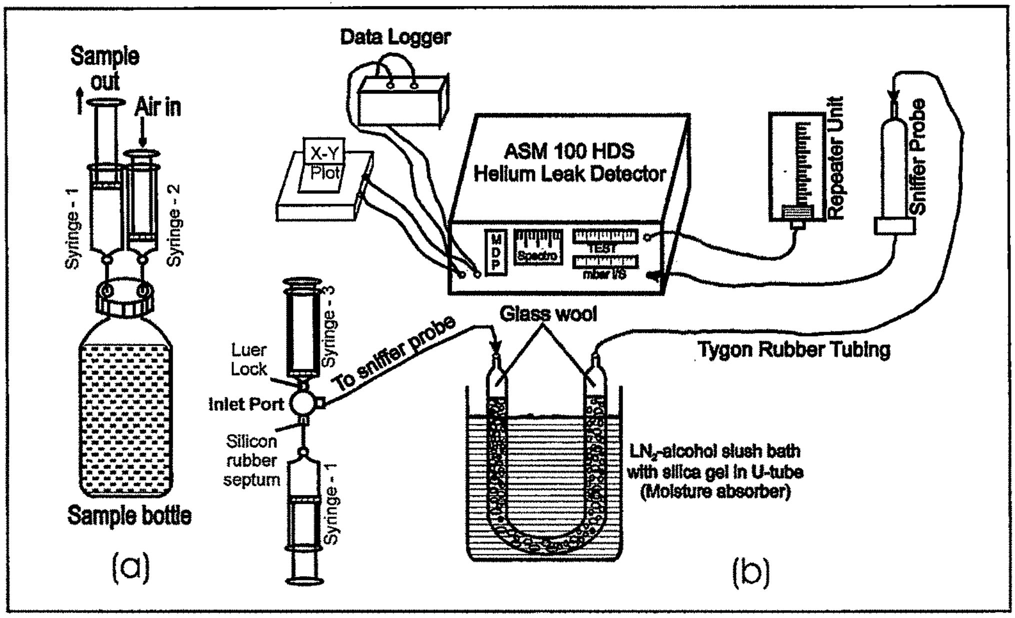

Figure 3.3 Schematic diagram showing layout of (a) drawing of equilibrated air sample and (b) helium measurement through helium leak detector for water/ air/ gas samples.

As mentioned in Section 2.6.2, helium measurements in this study are expressed in terms of Air Equilibration Units (AEU) because these were actually made on equilibrated headspace air samples.

3.1.3.1 Calibration of Helium Leak Detector

The helium leak detector was calibrated using atmospheric air with He concentration of 5.3-ppmv. The standard calibration curve for the chart recorder reading (set at 10 V range) is given by the expression:

$$\mathrm{He} = \mathrm{Const}_1 . \exp(\mathrm{Const}_2 * D_s) \qquad \text{Eq. (3.1)}$$

where, D_s is the number of chart recorder divisions at the 10 V full-scale setting and He is the concentration of helium (in ppmv).

If the chart recorder divisions are measured as deviation/ difference from the atmospheric background reading, the above equation can be rewritten as;

$$\mathrm{He} = 5.3 \exp(\mathrm{Const}_2 * (D_s - D_{bkg})) \qquad \text{Eq. (3.2)}$$

where, $(D_s - D_{bkg})$ is the difference between the chart recorder reading of the sample and the atmospheric background.

The calibration checks carried out for this study were designed to verify the combination of factory calibration and modifications made subsequently in the input port and to verify the robustness of procedure specified in Section 3.1.3 above for helium assay in air/ gas samples. For this purpose two experiments were carried out, (i) repeated dilution of an arbitrary helium concentration sample with fixed volume of atmospheric air; and (ii) determination of Henry's law constant for helium.

3.1.3.2 Dilution by Atmospheric Air

A fixed volume $(=V_A)$ of air is drawn from the head space (volume $= V_0$) of storage bottle using a hypodermic syringe. As the sample is drawn, equal volume of atmospheric air is allowed to enter the sampling bottle through another hypodermic syringe (Figure 3.3a). As a result, helium concentration in the air sample, being drawn from the head space, varies continuously in response to dilution by atmospheric air and mixing with remaining air in the bottle. If drawing of sample and resulting dilution is repeated several times, a recursive equation can be obtained as under (Gupta and Deshpande, 2003):

$$C_{Mn} = \frac{C_0 \quad e^{-(n-1)f}}{f}(1-e^{-f}) - \frac{C_A e^{-(n-1)f}}{f}(1-e^{-f}) + C_A$$

Eq. (3.3)

where, C_{Mn} = measured helium concentration after n^{th} dilution;

C_0 = original helium concentration in volume V_0;

C_A = is the helium concentration of incoming atmospheric air; and

$f = V_A/V_0$.

For $C_A << C_0$, $$C_{Mn} = \frac{C_0 \quad e^{-(n-1)f}}{f}(1-e^{-f})$$

Therefore,

$$\frac{C_{Mn}}{C_{M(n-1)}} = e^{-f}$$

Eq. (3.4)

Thus, the measured helium concentration will decrease by a factor e^{-f} after every dilution. In the standard experiments for this study, the volume of sample air drawn (V_A) was 20 ml; and volume of the head space (V_0) was 56 ml, governed by the factory made marking on the bottle.

Calibration of the instrument and the entire analytical procedure, starting with air/gas sample with any arbitrary helium concentration, can be experimentally checked using Eq. (3.4). A graph of two separate experiments showing measured and calculated helium concentration variation involving repeated dilution with atmospheric air is given in Figure 3.4a. The close agreement between the measured and calculated values not only confirms the correctness of the calibration procedure but also of the experimental procedures followed.

3.1.3.3 Estimation of Henry's Law Constant

Henry's Law states that the solubility of any sparingly soluble gas in water is proportional to the partial pressure of that gas in the air, in equilibrium with water. For n^{th} equilibration, the relation derived for determination of Henry's law constant by repeated equilibration of atmospheric air with water containing dissolved helium is (Gupta and Deshpande, 2003):

$$\log C_{Gn} = \log C_{G0} - n\log(1+FH_x) \qquad \text{Eq. (3.5)}$$

Where; C_{Gn} = Concentration of helium in gas phase after n^{th} equilibration

C_{G0} = Original concentration of helium in gas phase

$F = V_G/V_L$ = Volume of gas phase / Volume of liquid phase

H_x = Henry's law constant

Plot of 'log C_{Gn}' vs 'n' (equilibration number) would be a straight line with its intercept = $\log C_{G0}$ and slope = $-\log(1+F H_x)$.

In these experiments, while the values of C_O were arbitrarily varied, the values of V_G and V_L were 50 ml each. Figure 3.4b shows measured helium concentration in equilibrated air against the number of equilibrations in several experiments involving different initial helium concentrations. The average estimated value of Henry's law constant for six sets of similar experiments is 98 against the reported values of 105.7 at 25°C (Weiss, 1971) and 94.5 at 25°C (Fry et al, 1995; Perry, 1984). Agreement between the values obtained in different experiments and between estimated and reported values reconfirms the validity of calibration procedure adopted in the entire experimental set up and the robustness of the procedure standardised for estimation of helium concentration in air /water sample.

Reproducibility of measured helium values was checked by repeated analyses on a set of 4 samples collected at the same time in two different bottles in the concentration range of 5.3 to 340 ppmAEU. The results of these experiments (Table 3.1) show that the analytical precision of measurement of helium concentration is better than 5%.

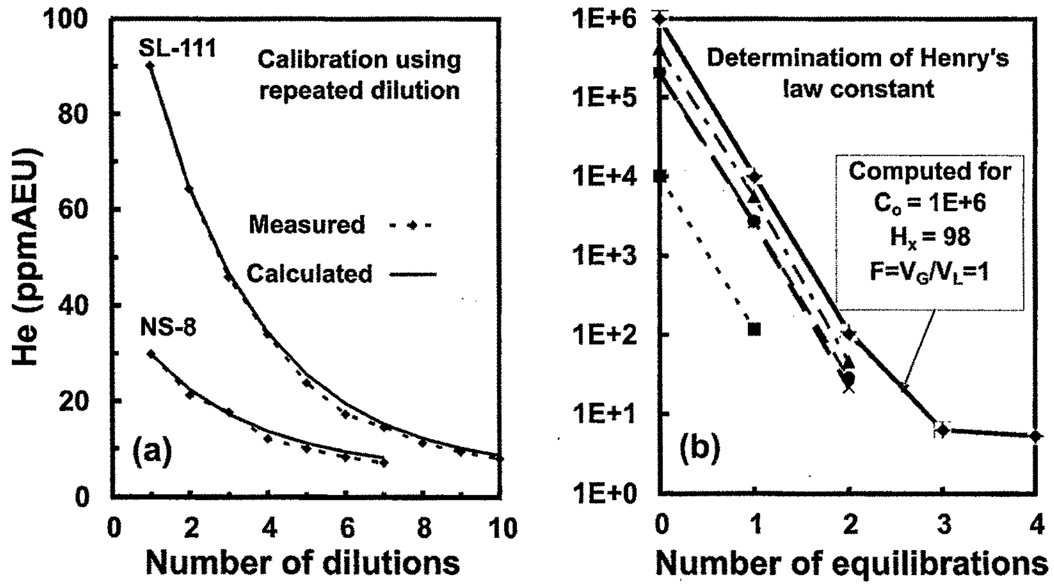

Figure 3.4 (a) Comparison of measured and calculated dilution curves; and (b) the results of a set of six experiments undertaken for estimation of Henry's law constant for water-helium system. The experimental values are similar to the known value of 105.7 at 25oC (Weiss, 1971). These experiments validate the calibration of the helium measurements and the robustness of the analytical procedure.

Table 3.1 Reproducibility of measured helium concentration in groundwater samples.

Sample location	Helium Concentration (ppmAEU)		Variability (%)
	Sample-1	Sample-2	
Ranip	6.17	6.20	1
Bagodra	339.7	339.7	0
Roika	24.3	24.8	2
Tilaknagar	5.3	5.3	0

3.2 Radon in Groundwater

For ^{222}Rn measurements, groundwater from pump outlet was piped directly into 630-ml PVC bottles (Brand: Tarson) by a PVC tube and allowed to overflow for >> 3 bottle volumes to minimise atmospheric contamination during sampling. The bottles were completely filled up to the brim and capped immediately and sealed with parafilm (Brand: AMERICAN Can Company) to prevent escape of dissolved gases.

^{222}Rn was measured, within 5 days of sample collection, by counting 609 keV gamma rays produced by the decay of its short-lived daughter ^{214}Bi using a high purity germanium (HPGe) gamma ray spectrometer. The background in the ^{214}Bi peak was

0.062 ± 0.001 cpm. The counting efficiency of ^{214}Bi, determined using a ^{226}Ra source of known activity (107.4 ± 0.4 dpm) in the same configuration as the sample bottle, was 0.31 ± 0.01%. Repeated counting for some samples after a period of more than three weeks confirmed that ^{222}Rn was unsupported by the decay of ^{226}Ra present in the groundwater. Values of ^{222}Rn activity were decay corrected to the time of collection, with errors quoted as one standard deviation based on counting statistics. Total uncertainty of ^{222}Rn measurements, based on repeat analyses and counting statistics, is <10%. The radon measurements were made by Dr. Meetu Agarwal (see Agarwal et al, 2006).

3.3 Fluoride in Groundwater

The groundwater samples for analyses of dissolved fluoride were collected in 1.2 litre soda-lime glass bottles after thoroughly rinsing with the sample water. All the procedures and precautions for sampling remain the same as mentioned in case of helium (Section 3.1.1). To ensure the integrity of stored water for fluoride contamination from the sampling bottles, de-ionised water was stored in several sample bottles over a period of one year. No measurable fluoride was detected in the stored water.

The fluoride concentrations were measured in the laboratory by colorimetry within a few days of the sample collection, using 580 nm tuned colorimeter (Model: Hach) using the SPADNS reagent method. The Hach colorimeter used for this study is a high quality filter photometer designed for single parameter colorimetry. The instrument was calibrated to measure fluoride in water samples ranging in concentration from 0 to 2.0 mg/l using borosilicate vials with high degree of transparency and optical uniformity. The borosilicate vials and other glassware were first cleaned with 1:1 HNO_3 and followed by thoroughly rinsing with deionised water. The identified borosilicate vials and other glassware were used exclusively for fluoride analyses to avoid contamination and to maintain identical transparency and optical uniformity between set of samples analysed at different times.

The instrument was recalibrated before analysing every set of 10 samples, using two-point calibration facility provided in the instrument. For any fluoride measurement, including that for calibration, 10 ml of liquid to be analysed (sample water, deionised water or standard solution) was poured into the borosilicate vials using high precision volumetric dispenser. Thereafter, 2 ml of SPADNS Reagent was dispensed into the same vial. The vial was tightly capped and swirled thoroughly for homogenisation. The fluoride ions in the liquid reacted with SPADNS Reagent which is a red zirconium-dye solution. The fluoride ion combines with part of the zirconium ion to form a colourless complex, thus bleaching (discolouring) the red colour of the solution in proportion to the fluoride concentration. This reaction is generally completed within a minute; therefore, the vials were left aside for a few minutes after adding SPADNS Reagent and swirling thoroughly. The degree of discolouration of the solution is directly proportional to the fluoride concentration of the sample.

The vial was then placed in the cell holder of the instrument with a light emitting diode (wavelength 580 nm) on one side and a silicon detector cell (filter bandwidth 15nm; absorbance range 0-1Å) on the other. The liquid crystal display of the instrument provided a direct readout of fluoride concentration (in mg/l). The precision of fluoride measurements was better than 0.1 ppm.

There are various ions and compounds (e.g. chloride, ferric iron, ortho-phosphates, sulphates, aluminium and alkalinity as $CaCO_3$, etc.) that can interfere with fluoride in the colorimetric analyses of water samples. Any natural water sample can have variety of such elements which can interfere with fluoride and result in systematic error in the estimated concentration of fluoride. The error introduced due to interference by various ions and compounds in the colorimetric analyses of fluoride as provided by the Hach Company is given in Table 3.2.

Table 3.2 Colorimetric interference of selected ions and compounds

Ion/Compound	**Concentration (mg/l)**	**Error introduced (± mg/l F^-)**
Alkalinity (as CaCO3)	5000	–0.1
Aluminium	.01	–0.1
Chloride	7000	+0.1
Ferric Iron	10	–0.1
Ortho-phosphate	16	+0.1
Sodium Hexametaphosphate	1.0	+0.1
Sulphate	200	+0.1

It is seen from the Table 3.2 that at a precision level better than 0.1ppm, very high concentrations of interfering ions are required to affect the measurements. Such high values of alkalinity, chloride and sulphates were not found (at 27 locations where these parameters were measured as part of sampling protocol for radiocarbon dating; Table 4.6). Also the unpublished data of routine surveys, conducted by Gujarat Water Resources Development Corporation Ltd. (GWRDC), did not report high values of these parameters. In view of this, any error in fluoride measurements due to the interfering ions and compounds was ignored.

Figure 3.5 (a) Picture showing a specially designed foldable stand with conical aluminium base which holds the high density PVC bag filled with 100 litre of water sample. The supernatant water is decanted by piercing the bag after the carbonate precipitates settle in the conical base of the bag; (b) Carbonate precipitates are transferred from PVC bag into 1.2-litre soda-lime glass bottle without exposure to atmosphere.

3.4 Groundwater Radiocarbon Dating

For ^{14}C dating, about 100 litre of groundwater is piped directly into a collapsible high density PVC bag through a narrow opening. The PVC bag is kept in the folded condition in a stand designed specifically for this purpose and assembled from its prefabricated parts at the site (Figure 3.5a). The PVC bag unfolds only when the groundwater gets filled into it. Before piping in the groundwater, a few pellets of NaOH (~10g) were added to the PVC bag to raise the solution pH to >10 for immobilising the dissolved CO_2 in the form of CO_3^{2-} and its eventual precipitation as barium carbonate. At pH greater than 10.3 most of the dissolved CO_2 is in the form of CO_3^{2-} since at this pH, activity of HCO_3^- drops and activity of CO_3^{2-} rises rapidly (Drever, 1997).

Depending upon the alkalinity and sulphate concentration of groundwater samples (measured in the field), a pre-determined amount of barium chloride ($BaCl_2$) was then added to the 'groundwater-NaOH' solution to ensure complete precipitation of dissolved carbonates (Clark and Fritz, 1997). Following vigorous stirring, the mixture was left undisturbed for precipitates to settle in the conical base of the PVC bag (Figure 3.5a).

It usually takes 4-5 hours for the precipitates to settle. After decanting the supernatant liquid, precipitates were transferred to glass bottles (Figure 3.5b) and sealed by capping the bottle with a bromobutyl synthetic rubber stopper and triple aluminium protective cover on it using a hand held crimping tool. Care was taken to prevent/minimise sample exchange with atmospheric CO_2 during the entire field procedure.

On reaction with orthophosphoric acid, barium carbonate precipitates liberate CO_2. The liberated CO_2 was first converted to acetylene and then trimerised into benzene (C_6H_6) and the ^{14}C activity in the benzene counted by liquid scintillation spectroscopy (Gupta and Polach, 1985). A small aliquot of the sample CO_2 was sealed in glass ampoules for $\delta^{13}C$ measurement using SIRM (PDZ Europa Model GEO 20-20). The processing and analyses of the CO_2 liberated from the groundwater samples was done by Dr. M.G. Yadava in the ^{14}C laboratory of PRL.

3.5 Chlorofluorocarbons (CFCs) in Groundwater

3.5.1 Sample Collection and Storage

Sample collection and storage of groundwater for CFC analyses is the most critical aspect of employing CFCs as hydrological tracer. This is because: (i) inadvertent introduction of as little as 0.01 cc of modern air can be detected in the highly sensitive chromatographic analyses and can introduce significant error in estimating the groundwater recharge age, particularly of old ground waters; and (ii) there are severe restrictions on availability of suitable material for storing the water sample. All the conventionally used containers like glass bottles with rubber stopper, high density plastic-rubber-polymer bottles, glass flasks with stopcock, glass syringes with luer locks, polypropylenes syringes with luer locks, syringes with neoprene or Teflon plungers, tubes made up of stainless steel, copper or aluminium etc, are not really suitable for sample collection and storage for CFC analyses. Most of the materials used in construction of these conventional containers either absorb the CFCs from atmosphere/ water or leach/ release significant amounts of CFCs or other chlorinated compounds. In addition, CFCs can diffuse from the air through the polymers into the sample (Reynolds et al, 1990; Bullister, 1984). Significant uptake of halocarbons by aluminium and stainless steel occurs within an hour and a week respectively. However, all these materials and methods have been used earlier by various researchers with known limitations of the respective method (Thompson et al, 1974; Schultz, 1976; Warner and Weiss, 1985; Bullister and Weiss, 1988; Bu and Warner, 1995; Jean-Baptiste et al, 1994; Wilkowske and Solomon, 1997; Hofer and Imboden, 1998). No uptake of halocarbons, however, was observed even after 5 weeks of storage in borosilicate vials (Reynolds et al, 1990). Busenberg and Plummer (1992) designed an involved procedure for collection and storage of water samples in the field.

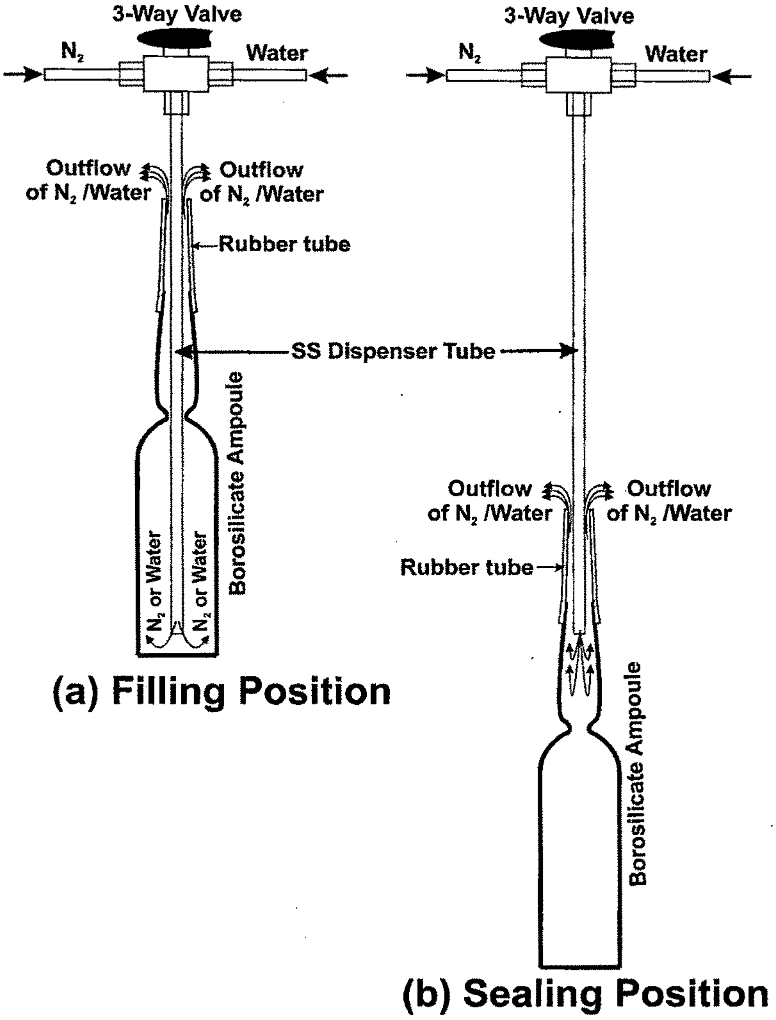

Figure 3.6 The groundwater sampling system for CFC analyses. (a) Relative position of 3-way valve and ampoule for flushing the ampoule with ultrapure nitrogen and filling with groundwater sample. (b) Relative position of 3-way valve and ampoule for evacuating the neck of ampoule and sealing it. (see the text for details)

As part of this work, a specific field procedure of water sample collection for CFC analyses was developed and tested for its integrity. The groundwater samples were collected in specially designed 60-ml borosilicate glass ampoules with constriction at the top and a tubular mouth (Figure 3.6). The sampling system comprises a 3-way valve (OD – 3.2 mm/ 1/8"), a borosilicate ampoule and a metallic stand that can hold these two at variable heights. Figure 3.6 depicts how water sample was collected in the borosilicate ampoules.

As seen in Figure 3.6(a), one port of a 3-way Swagelok valve is supplied with ultrapure nitrogen and the second port of the valve is supplied with groundwater from the pump outlet. A 60-cm long SS tube (OD – 3.2 mm/ 1/8") is connected to the third port of the 3-way valve that acts as a dispenser of ultrapure nitrogen gas or water as required. The 3-way valve and the borosilicate ampoule (with a 30-cm long rubber tube tightly fixed on its tubular neck) are firmly held in the metallic stand such that the SS dispenser passes through the rubber tube and reaches the bottom of the ampoule. Since even a minute amount of atmospheric air can contaminate the water sample, the ampoule is thoroughly flushed with ultrapure nitrogen for 5 minutes at a flow rate of ~300 ml/ min. The water sample is then introduced into the ampoule by turning the 3-way valve towards water port. After the vial is completely filled with water, sufficient volume (~1 litre) of water is allowed to overflow from the rubber tube leaving no trace of atmospheric air inside the ampoule and the rubber tube. While water is overflowing, the ampoule along with the attached rubber tube is slowly pulled down to the level at which the lower end of SS dispenser tube reaches just above the tubular mouth of the ampoule (Figure 3.6b). The nitrogen flow is then restarted in this position (Figure 3.6b) by turning the 3-way valve towards gas port. The stream of nitrogen immediately starts displacing the water from the tubular mouth of the ampoule via rubber tube. When the water is completely displaced from the tubular part of the ampoule, it is wiped from outside with a tissue paper and the tubular mouth of ampoule is then fused with sharp, violet flame of LPG-Oxygen mixture. After ampoule is cooled to room temperature, it is checked for perfection in sealing. This is done by trying to see if any water droplets come out of ampoule by jerking. If water droplets come out of ampoule due to jerking, the ampoule is rejected. As a matter of abundant precaution for any inadvertent loss of sample during transportation or analyses, it is advisable to collect at least three ampoules of each groundwater sample.

3.5.2 Purge and Trap System for Extraction of CFCs

Since water samples can not be directly injected and vaporised into the injection port of Gas Chromatograph, the dissolved CFCs from these are extracted in a separate Purge and Trap system and injected into analytical column for subsequent Gas Chromatographic analyses. A new purge and trap system was designed and built following Busenberg and Plummer (1982). The photograph of the complete CFC analytical system including newly built purge and trap system is shown in Figure 3.7 and Figure 3.8. The line drawing of the entire analytical set up is given in Figure 3.9. The purge and trap system is used not only for extraction and injection of the CFCs from water sample but also for injecting the standard gas mixture or any other gas injected from pressurised cylinder or large volume syringes.

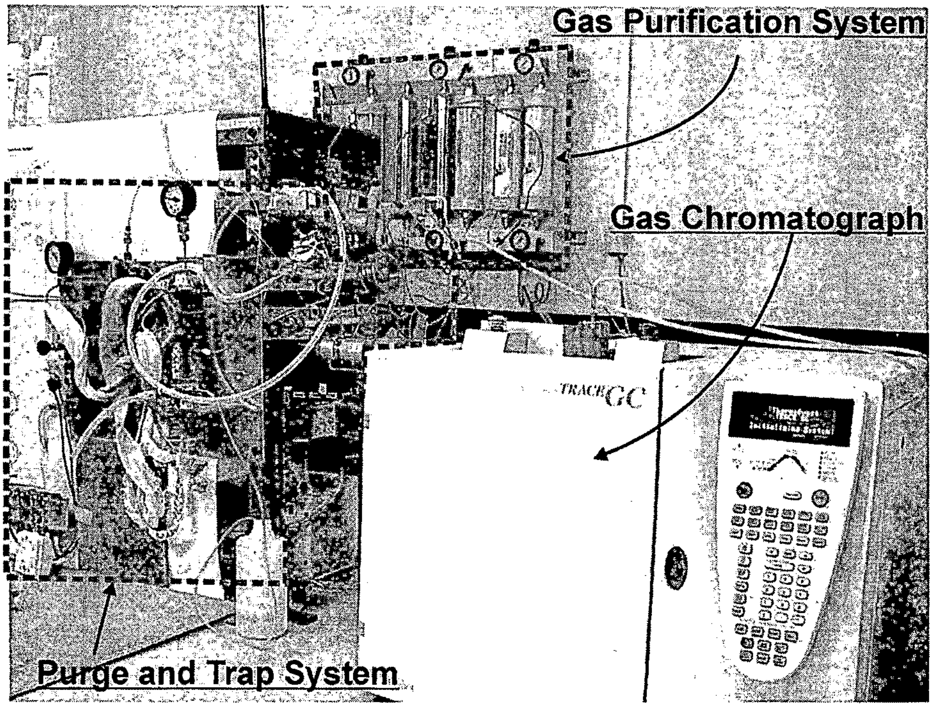

Figure 3.7 A gas purification subsystem, purge and trap subsystem and the gas chromotograph are the major components of the Groundwater CFC Laboratory. A blow up of the purge and trap system is shown in Figure 3.8. Complete line drawing of the CFC analytical set up is shown in Figure 3.9.

As seen in Figure 3.8 and Figure 3.9, the CFC analytical system is a complex network comprising various valves, gauges, purge tower, purge housing etc. The valves V-2, V-3, V-4, and V-6 are 6-port Valco Rotary Valves and V-7 is a 4-port Valco Rotary Valve. The Valco valves can be electrically actuated either through remote switches operated manually or by programmable computer command during gas chromatographic run. The valves V-1 and V-5 are manually operated 5-port Swagelok valves. The valves V-8, V-9, V-10, V-11 and V-12 are manually operated 3-port Swagelok valves. The direction of gas flow through various parts of the CFC analytical system is indicated by the arrows. With the help of these valves various sections of the analytical system can either be isolated or connected and the desired stream of gas can be made to flow through.

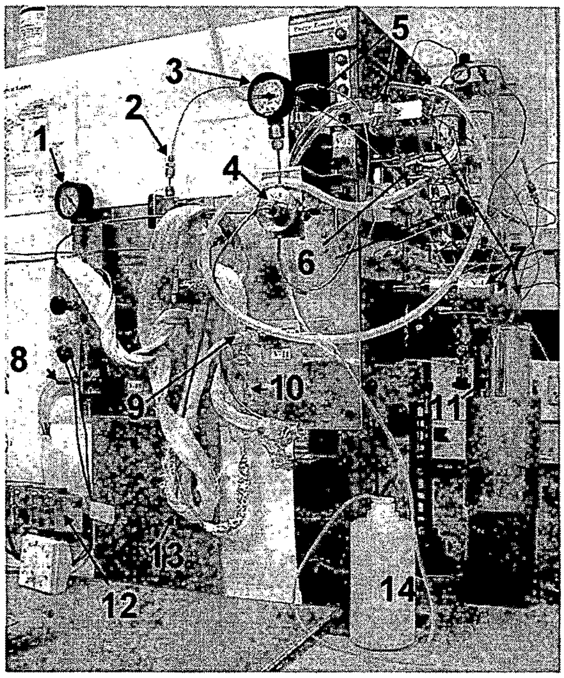

Figure 3.8 Blow up of the Purge and Trap System showing its constituents. 1 – Vacuum gauge; 2 – Carrier gas injection port; 3 – Pressure gauge; 4 – Multi-port valve; 5 – Bubblers; 6 – Gas sampling loops; 7- Valco valves; 8 – Suction port; 9 – Water inlet port; 10 – Purge tower; 11 – CFC trap in Dewar flask; 12 – Switch for Valco valves; 13- heating tape; 14 – Drain collector.

For extraction of dissolved CFCs from water, the borosilicate ampoule with water sample is connected to water sample port of V-11 with a Tygon tube (Figure 3.8). The purge tower and the Tygon tube connecting to ampoule are evacuated through suction port (V-10) using the rotary vacuum pump. After the desired level of vacuum is generated in the purge tower, it is isolated from the vacuum pump. On breaking the flame fused tip of the ampoule, the water sample is sucked into the purge tower. When 30 ml of water enters the purge tower (with pre-scored volume marks), the inflow is stopped by the valve V-11. The stream of purging gas (Ar/CH_4) is started by switching V-4 and the purging is done for 4 minutes. During the four minutes of purging, the dissolved CFCs and other gases purged from the water sample, together with moisture, are carried by purging gas. The moisture is trapped in two Magnesium Perchlorate [$Mg(ClO_4)_2$] moisture traps. The CFC-11, CFC-12 and CFC-113 are trapped on the CFC-trap (Figure 3.9) held at –40 °C. Other unimportant dissolved species (of no interest) are carried out of the system by the purging gas. The trapped CFCs are released by heating the trap with boiling water bath. A stream of carrier gas (Ar/CH_4) flowing into detector is then diverted through the CFC-trap for 30 seconds by programmed PC commands which operate the V-4 valve. Within 30 seconds, the gases released from CFC-trap are transported into the analytical column through the pre-column. The purpose of the pre-column is to prevent the late eluting compounds from entering the analytical column. Such compounds are trapped on the pre-column and flushed out of the system by a stream of Ar/CH_4 in the opposite direction. Detailed specifications of the CFC-trap, analytical column and pre-column are given in Table 3.3.

Table 3.3 Technical specifications of various packed columns

Sr. No.	Column Type	Purpose	Technical Specification
1	CFC Trap Column	To trap the three CFC Species (F-11, F-12 and F-113) simultaneously on a single column	▪ Packed column ▪ (200 mm) 8" long, (3.2 mm)1/8" OD, (2.2 mm) 0.085" ID, SS - 304 type stainless steel tube ▪ Glass wool plug and 1 inch length of glass beads on either end. ▪ Packed with equal length of Porapak-T (80/100 mesh) and Porous-Sil C (80/100 mesh) separated by small amount of glass beads.
2	Pre-column	To prevent the late eluting compounds entering the analytical column	▪ (150 mm) 6" long, (3.2 mm)1/8" OD, (2.2 mm) 0.085" ID, SS - 304 type stainless steel tube ▪ Packed with Porous-Sil C (80/100 mesh), with a small glass wool plug at each end.
3	Analytical column	For chromatographic separation of three CFC Species (F-11, F-12 and F-113) simultaneously using a single column	▪ (3.05 m) 10' long, (3.2 mm)1/8" OD, (2.2 mm) 0.085" ID, SS - 304 type stainless steel tube ▪ Packed with Porous-Sil C (80/100 mesh), with a small glass wool plug at each end

The procedure for analysing CFCs in stripping gas (for background), standard gas mixture, atmospheric air as well as water samples involve a sequence of about 30 operations like evacuation of purge tower, cooling or heating of traps, switching of valves for diverting the stream of gas or isolating a particular portion of the analytical system etc. Each step is equally important for a reproducible analysis. The sequence of operations involved in analysing CFCs in stripping gas (for background), CFC standard, atmospheric air, and water sample are given respectively in Table 3.4, Table 3.5, Table 3.6 and Table 3.7.

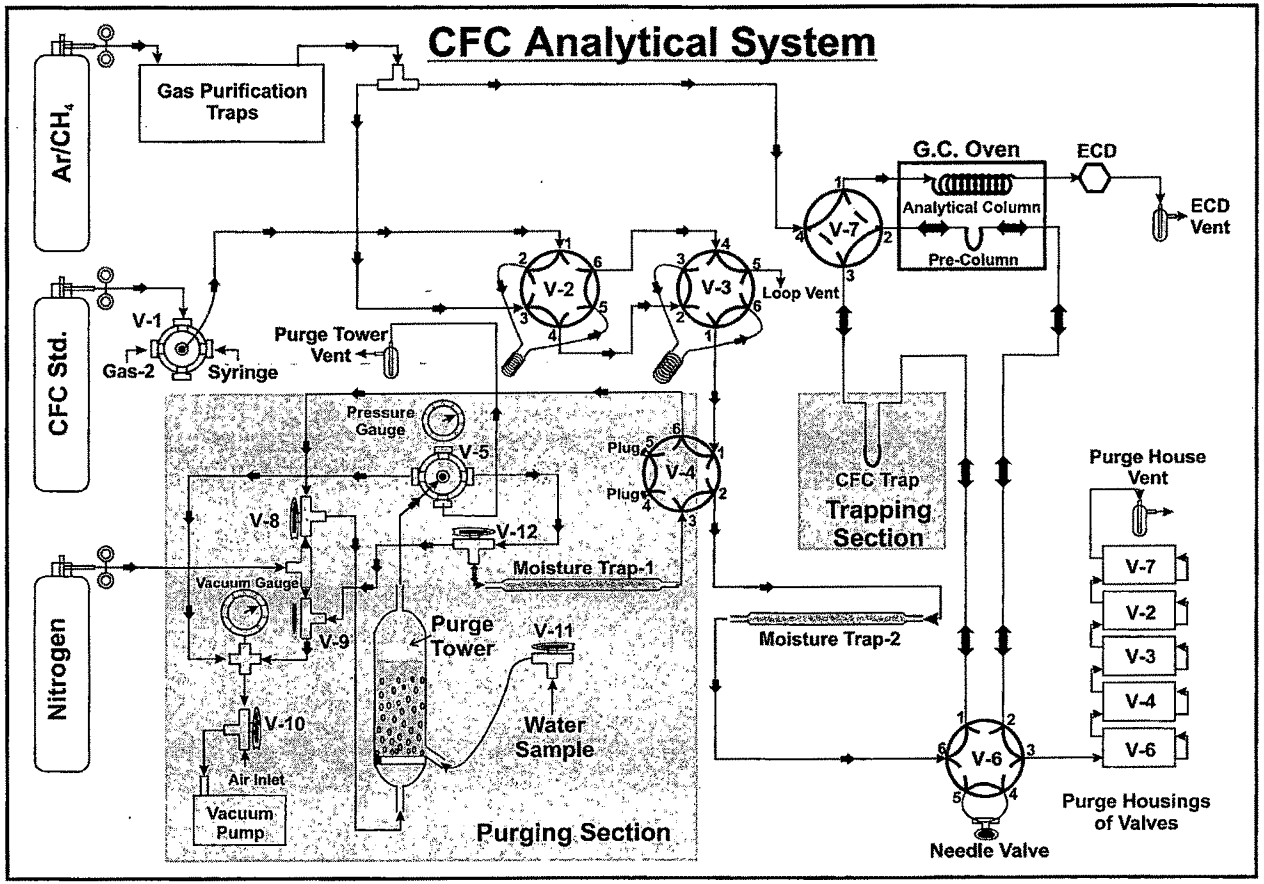

Figure 3.9 Line drawing of the complete CFC analytical system.

Table 3.4 Sequence of operations for analysing Ar/CH_4 stripper gas as background.

STEP	SEQUENCE OF ACTIONS
1.	Prepare the -40^0C slush (LN_2 + alcohol) and Set the valves as follows: V-1 → DOWN (Blind); V-2, V-3, V-4, and V-6 → LOAD; V-5 → RIGHT (Towards V-12) V-7 → INJECT; V-8 → UP (Stripper Gas side); V-12 → RIGHT (Towards V-5)
2.	Ensure the Stripper Gas flow rate of ~100 cc/min at Purge Housing vent
3.	V-4 → INJECT (Purging section is isolated from the rest of the stripping flow line)
4.	Switch on the Vacuum pump and set the valves as follows: V-10 → UP (Towards Vacuum Gauge); V-9 → DOWN (Towards Vacuum Gauge) V-5 → LEFT (Connecting purge tower to Suction line) V-12 → LEFT (Connecting Moisture Trap-1 to Suction line)
5.	Wait till Vacuum Gauge shows –29.5 (In Hg , black scale)
6.	V-5 → UP (Secondary evacuation of Pressure Gauge by Purge Tower)
7.	V-5 → LEFT (Connecting purge tower to Suction line)
8.	V-5 → RIGHT (Secondary evacuation up to V-12 by Purge Tower)
9.	V-5 → LEFT (Connecting purge tower to Suction line)
10.	Wait till Vacuum Gauge shows –29.5 (In Hg, black scale).
11.	V-5 → UP (Purge Tower connected to Pressure Gauge)
12.	V-6 → INJECT (CFC Trap and Pre-column isolated)
13.	Needle Valve at V-6 → CLOSE (system isolated from atmosphere at V-6)
14.	V-4 → LOAD (Stripper gas starts filling the Purge Tower; Moisture Trap-2 connected to suction line through Moisture Trap-1)
15.	Evacuate purge tower (by switching V5 → left) 3 times at 1 atmosphere. Wait till pressure gauge shows 2 kg/cm^2
16.	V-12 → RIGHT (Moisture Trap-1 connected to V-5)
17.	V-5 → RIGHT (Stripping gas from pressurised Purge Tower flows into Moisture Traps)
18.	Wait for 15 seconds for stripping gas to fill the evacuated moisture traps
19.	V-6 → LOAD (stripping gas flows out at purge housing vent through CFC Trap and Pre-column)
20.	Needle Valve at V-6 → OPEN 2 turns; Wait till flow through purge house vent is stabilised
21.	V-6 → INJECT (CFC Trap and Pre-column isolated)
22.	Immerse the CFC Trap in slush at -40^0C and Start the stopwatch. (Pre-cooling for 1 min.)
23.	At 1 min. V-6 → LOAD
24.	Switch on the Kettle and keep the boiling water ready.
25.	At 5 min. in stopcock, V-6 → INJECT
26.	Immerse the CFC Trap in boiling water bath and start stopwatch. Complete the next two steps in less than a min.
27.	Open the "View sample being acquired" window, set the scale of 0-3 mV
28.	Start Auto-zero function and register the output and offset in logbook
29.	At 1.5 min. Press "PREP RUN" button. When in "READY TO INJECT" state, Press "START"
30.	At start of the run V-7 automatically switches to LOAD and returns to INJECT after 30 sec.
31.	When V-7 returns to INJECT position: V-6 → LOAD (stripping gas starts back flushing the Pre-column)
32.	Switch off the Vacuum pump and V-10 → DOWN (Air inlet)
33.	When the run ends, the indicator returns to "STANDBY/PREP RUN" mode. Evaluate the Chromatogram, adjust the scale of view and take printout

Table 3.5 Sequence of operations for analysing CFC Standard.

STEP	SEQUENCE OF ACTIONS
1.	Prepare the –40^{0}C slush (LN$_2$ + alcohol) and Set the valves as follows: V-1 → DOWN (Blind); V-2, V-3, V-4, and V-6 → LOAD; V-5 → RIGHT (Towards V-12) V-7 → INJECT; V-8 → UP (Stripper Gas side); V-12 → RIGHT (Towards V-5)
2.	Ensure the Stripper Gas flow rate of ~100 cc/min at Purge Housing vent
3.	V-4 → INJECT (Purging section is isolated from the rest of the stripping flow line)
4.	Switch on the Vacuum pump and set the valves as follows: V-10 → UP (Towards Vacuum Gauge); V-9 → DOWN (Towards Vacuum Gauge) V-5 → LEFT (Connecting purge tower to Suction line) V-12 → LEFT (Connecting Moisture Trap-1 to Suction line)
5.	Wait till Vacuum Gauge shows –29.5 (In Hg, black scale)
6.	V-5 → UP (Secondary evacuation of Pressure Gauge by Purge Tower)
7.	V-5 → LEFT (Connecting purge tower to Suction line)
8.	V-5 → RIGHT (Secondary evacuation up to V-12 by Purge Tower)
9.	V-5 → LEFT (Connecting purge tower to Suction line)
10.	Wait till Vacuum Gauge shows –29.5 (In Hg, black scale)
11.	V-6 → INJECT (CFC Trap and Pre-column isolated)
12.	Needle Valve at V-6 → CLOSE (system isolated from atmosphere at V-6)
13.	V-4 → LOAD (Stripper gas starts filling the Purge Tower; Moisture Trap-2 connected to suction line through Moisture Trap-1)
14.	Remove the Glass plug at the loop-vent and connect it to bubbler
15.	Open Primary knob of CFC Cylinder
16.	V-1 → CFC Std input side (Let CFC std flow out from Loop Vent for 2 minutes)
17.	V-3 (2 ml) or V-2 (10 ml) → INJECT (stripping gas by-passes the loop and CFC std flows through sample loop)
18.	Flush the purge tower (by switching V5 → UP and LEFT) with stripping gas 3 times at 1 atmosphere. Wait till pressure gauge shows 2 kg/cm^2.
19.	V-12 → RIGHT (Moisture Trap-1 connected to V-5)
20.	V-5 → RIGHT (Stripping gas from pressurised Purge Tower flows into Moisture Traps)
21.	Wait for 15 seconds for stripping gas to fill the evacuated moisture traps
22.	V-6 → LOAD (stripping gas flows out at purge housing vent through CFC Trap and Pre-column)
23.	Needle Valve at V-6 → OPEN 2 turns; Wait till flow through purge house vent is stabilised
24.	V-6 → INJECT (CFC Trap and Pre-column isolated)
25.	Immerse the CFC Trap in slush at –40^{0}C and start stopwatch. (Pre-cooling for 1 min.)
26.	At 1 min. V-1 → DOWN (blind). Close Primary knob of CFC Cylinder.
27.	When the bubbling stops at the loop-vent: V-6 → LOAD; V-3 (2cc) or V-2 (10cc) → LOAD (Stripper flows through the respective loop and carries the CFC std from the loop). Start stopwatch.
28.	Switch on the Kettle and keep the boiling water ready.
29.	At 4 min.: V-6 → INJECT
30.	Immerse the CFC Trap in boiling water bath and start stopwatch. Complete the next two steps in less than a min.
31.	Open the "View sample being acquired" window, set the scale of 0-3 mv.
32.	Start Auto-zero function and register the output, offset and sample number in logbook
33.	At 1.5 min. Press "PREP RUN" button. When in "READY TO INJECT" state, Press "START"
34.	At start of the run V-7 automatically switches to LOAD and returns to INJECT after 30 sec.
35.	When V-7 returns to INJECT position: V-6 → LOAD (stripping gas starts back flushing the Pre-column)
36.	Switch off the Vacuum pump and V-10 → DOWN (Air inlet)
37.	When the run ends, the indicator returns to "STANDBY/PREP RUN" mode. Evaluate the Chromatogram, adjust the scale of view and take printout

Table 3.6 Sequence of operations for analysing atmospheric air.

STEP	SEQUENCE OF ACTIONS
1.	Prepare the -40^{0}C slush (LN_2 + alcohol) and Set the valves as follows: V-1 → DOWN (Blind); V-2, V-3, V-4, and V-6 → LOAD; V-5 → RIGHT (Towards V-12) V-7 → INJECT; V-8 → UP (Stripper Gas side); V-12 → RIGHT (Towards V-5)
2.	Ensure the Stripper Gas flow rate of ~100 cc/min at Purge Housing vent
3.	V-4 → INJECT (Purging section is isolated from the rest of the stripping flow line)
4.	Switch on the Vacuum pump and set the valves as follows: V-10 → UP (Towards Vacuum Gauge); V-9 → DOWN (Towards Vacuum Gauge) V-5 → LEFT (Connecting purge tower to Suction line) V-12 → LEFT (Connecting Moisture Trap-1 to Suction line)
5.	Wait till Vacuum Gauge shows –29.5 (In Hg, black scale)
6.	V-5 → UP (Secondary evacuation of Pressure Gauge by Purge Tower)
7.	V-5 → LEFT (Connecting purge tower to Suction line)
8.	V-5 → RIGHT (Secondary evacuation up to V-12 by Purge Tower)
9.	V-5 → LEFT (Connecting purge tower to Suction line)
10.	Wait till Vacuum Gauge shows –29.5 (In Hg, black scale)
11.	V-6 → INJECT (CFC Trap and Pre-column isolated)
12.	Needle Valve at V-6 → CLOSE (system isolated from atmosphere at V-6)
13.	V-4 → LOAD (Stripper gas starts filling the Purge Tower; Moisture Trap-2 connected to suction line through Moisture Trap-1)
14.	Connect the rubber tube from loop-vent to Air-inlet port of V-10
15.	V-1 → UP (Atmosphere inlet side)
16.	V-3 (2 ml) or V-2 (10 ml) → INJECT (stripping gas by-passes the loop and atmospheric air fills the loop)
17.	V-10 → DOWN (Atmospheric air sucked in through loop-vent); V-10 → UP
18.	Disconnect the rubber tube from V-10 and connect it to bubbler.
19.	Flush the purge tower (by switching V5 → UP and LEFT) with stripping gas 3 times at 1 atmosphere. Wait till pressure gauge shows 2 kg/cm^2.
20.	V-12 → RIGHT (Moisture Trap-1 connected to V-5)
21.	V-5 → RIGHT (Stripping gas from pressurised Purge Tower flows into Moisture Traps)
22.	Wait for 15 seconds for stripping gas to fill the evacuated moisture traps
23.	V-6 → LOAD (stripping gas flows out at purge housing vent)
24.	Needle Valve at V-6 → OPEN 2 turns; Wait till flow through purge house vent is stabilised
25.	V-6 → INJECT (CFC Trap and Pre-column isolated)
26.	Immerse the CFC Trap in slush at -40^{0}C and start stopwatch. (Pre-cooling for 1 min.)
27.	At 1 min. V-1 → DOWN (blind).
28.	V-6 → LOAD; V-3 (2cc) or V-2 (10cc) → LOAD (Stripper flows through the respective loop and carries the atmospheric air from the loop). Start stopwatch.
29.	Switch on the Kettle and keep the boiling water ready.
30.	At 4 min.: V-6 → INJECT
31.	Immerse the CFC Trap in boiling water bath and start stopwatch.
32.	Open the "View sample being acquired" window set the scale of 0-3 mv.
33.	Start Auto-zero function and register the output, offset and sample number in logbook
34.	At 1.5 min. Press "PREP RUN" button. When in "READY TO INJECT" state, Press "START"
35.	At start of the run V-7 automatically switches to LOAD and returns to INJECT after 30 sec.
36.	When V-7 returns to INJECT position: V-6 → LOAD (back flushing of Pre-column)
37.	Switch off the Vacuum pump and V-10 → DOWN (Air inlet)
38.	When the indicator returns to "STANDBY/PREP RUN" mode. Evaluate the Chromatogram, adjust the scale of view and take printout

Table 3.7 Sequence of operations for analysing Water Sample.

STEP	SEQUENCE OF ACTIONS
1.	Prepare the -40^0C slush (LN_2 + alcohol) and Set the valves as follows: V-1 → DOWN (Blind); V-2, V-3, V-4, and V-6 → LOAD; V-5 → RIGHT (Towards V-12) V-7 → INJECT; V-8 → UP (Stripper Gas side); V-12 → RIGHT (Towards V-5)
2.	Ensure the Stripper Gas flow rate of ~100 cc/min at Purge Housing vent
3.	Ensure that the wire-mesh is placed at the end of rubber tube connected to V-11
4.	Fix the inverted sample ampoule in the stand and connect it to V-11 through rubber tube
5.	V-4 → INJECT (Purging section is isolated from the rest of the stripping flow line)
6.	Switch on the Vacuum pump and set the valves as follows: V-10 → UP (Towards Vacuum Gauge); V-9 → DOWN (Towards Vacuum Gauge) V-5 → LEFT (Connecting purge tower to Suction line) V-12 → LEFT (Connecting Moisture Trap-1 to Suction line) V-11 → LEFT (Connecting rubber tube to purge tower)
7.	Wait till Vacuum Gauge shows –29.5 (In Hg , black scale)
8.	Check for leakage or moisture by closing V-10. If pressure increases rectify the rubber tube connection or remove the moisture by heating.
9.	V-5 → UP (Secondary evacuation of Pressure Gauge by Purge Tower)
10.	V-5 → LEFT (Connecting purge tower to Suction line)
11.	V-5 → RIGHT (Secondary evacuation up to V-12 by Purge Tower)
12.	V-5 → LEFT (Connecting purge tower to Suction line)
13.	Wait till Vacuum Gauge shows –29.5 (In Hg, black scale).
14.	V-5 → UP (Purge Tower connected to Pressure Gauge)
15.	V-6 → INJECT (CFC Trap and Pre-column isolated)
16.	Needle Valve at V-6 → CLOSE (system isolated from atmosphere at V-6)
17.	V-4 → LOAD (Stripper gas starts filling the Purge Tower; Moisture Trap-2 connected to suction line through Moisture Trap-1)
18.	Flush purge tower (by switching V5 → left) 3 times at 1 atmosphere. Wait till pressure gauge shows 1 kg/cm^2
19.	V-12 → RIGHT (Moisture Trap-1 connected to V-5)
20.	V-5 → RIGHT (Stripping gas from pressurised Purge Tower flows into Moisture Traps)
21.	After 15 Seconds V-6 → LOAD (stripping gas flows out at purge housing vent through CFC Trap and pre-column)
22.	Needle Valve at V-6 → OPEN 2 turns
23.	V-12 → CENTRE; V-8 → CENTRE; V-4 → INJECT; V-6 → INJECT
24.	Immerse the CFC Trap in slush at -40^0C for pre-cooling of the CFC-trap
25.	Evacuate Purge Tower and rubber tube connected to ampoule by switching V-5 → LEFT
26.	Secondary evacuation of pressure gauge and tube up to V-12 (step 9 to 12)
27.	V-5 → RIGHT
28.	Crush the tip of the Ampoule and introduce the water in purge tower. When 30 ml of water is introduced: V-11 → RIGHT
29.	Needle Valve at V-6 → CLOSE (system isolated from atmosphere at V-6)
30.	V-4 → LOAD; V-8 → UP (Bubbling starts in the purge tower); V-12 → RIGHT After 15 Seconds V-6 → LOAD and start stopwatch. ((Stripping gas flows out at purge housing vent through pre-cooled CFC trap and pre-column)
31.	Needle Valve at V-6 → OPEN 2 turns
32.	Switch on the Kettle and keep the boiling water ready.

Table continues on next page

Table continues from previous page

33. At 4 min., V-6 → INJECT
34. Immerse the CFC Trap in boiling water bath and start stopwatch. Finish next two steps in less than 1 min.
35. Open the "View sample being acquired" window, set the scale of 0-3 mV
36. Start Auto-zero function and register the output and offset in logbook
37. At 1.5 min. Press "PREP RUN" button.
    When in "READY TO INJECT" state, Press "START"
38. At start of the run V-7 automatically switches to LOAD and returns to INJECT after 30 sec.
39. After V-7 returns to INJECT
    V-4 → INJECT; V-6 → LOAD; V-5 → UP; V-8 → CENTRE; V-12 → LEFT
40. Remove the ampoule from rubber tube at V-11 and drain the water out of Purge Tower by switching V-11 → LEFT
41. Open the Nitrogen cylinder (< 2 atm. Pressure); V-8 → DOWN; Start the Nitrogen gas flow in Purge Tower and let it flow out through V-11 until no bubbling is visible from the frit of the Purge Tower.
42. V-5 → LEFT; V-11 → RIGHT
43. Start the heating coil and use the hot air blower to remove the moisture.
44. When no water drop is visible in Purge Tower stop the nitrogen gas flow.
45. When the run ends, the indicator returns to "PREP RUN" mode. Evaluate the Chromatogram, adjust the scale of view and take printout
46. Switch off the Vacuum pump and V-10 → DOWN (Air inlet)

3.5.3 Analytical Technique for Measurement of CFCs

The CFCs from water sample, stripper gas, CFC standard or atmospheric air trapped on the CFC trap by purge and trap system are injected into the analytical column of a Gas Chromatograph (GC) and analysed by an Electron Capture Detector (ECD).

An analytical method for simultaneous chromatographic separation of F-11, F-12 and F-113 was developed. The oven temperature, inlet port temperature, carrier gas flow rate and back flushing time are critical parameters in developing the analytical method for CFCs. The optimum values of these parameters established after several hundred experimental analytical runs are given in Table 3.8.

Table 3.8 Optimised analytical method for chromatographic separation of CFCs.

GC Parameter	Values
Oven	70 ^{0}C
Packed Inlet Port	65 ^{0}C
Carrier Gas	Ar (95%)/CH_4(5%)
Carrier Gas Flow rate	25 cc/min
Detector Base body	250 ^{0}C
ECD	270 ^{0}C
Runtime	10 minutes
Heating Steps	Isothermal

With a view to ensure the identical injection and back flushing time in each analysis, the operation of valves responsible for injection and back-flushing, is automated with the help of external event control facility in the GC. As shown in Figure 3.9, when position of valve V-7 is changed (from Inject to Load), the carrier gas passes through heated CFC trap and transports the trapped gases into GC. Thus, loading of V-7 at a fixed time in every analytical run ensures reproducible retention time. After the analysis has started, when position of valve V-7 is changed (from Load to Inject), the carrier gas passes directly into GC without carrying any more residues from CFC traps or pre-column. Thus, injecting of carrier gas from V-7 at a fixed time in every analytical run prevents late eluting compounds from entering into the analytical column. Therefore, these two operations of V-7 were automated.

Different injection volumes of stripper gas, CFC standard gas mixture and atmospheric air have been analysed by the above method. Some representative chromatograms for 2 ml, 5 ml and 10 ml injections of CFC standard gas mixture are shown respectively in Figure 3.10, Figure 3.11 and Figure 3.12. It is seen that all the three CFC species of interest can be identified in the injected gases based on their sequence of elution and characteristic retention time (RT). The values of peak area and retention time along with the relevant statistics for these representative chromatograms are given in Table 3.9.

The retention time and elution sequence are governed by different factors. The retention time of a compound on the column is governed by several factors such as: (i) length of column; (ii) chemical composition of the material packed in the column; (iii) the oven temperature and (iv) the carrier flow rate. In a particular system the adjustable parameters are optimised to achieve good separation of the peaks of interest within the reasonable run time. The system specifications and the optimised analytic method have been given in Table 3.3 and Table 3.8 respectively. The gases with progressively higher molecular weight (MW) elute progressively slower, therefore, the heavier gases elute later in the sequence of elution. Thus, sequence of elution is governed by molecular weighs of constituent gases in a mixture. In the present study, the observed elution sequence is: N_2O (MW = 44 g.mol^{-1}; RT = ~1.6 min), F-12 (MW = 121g.mol^{-1}; RT = ~2.27 min), (MW = 137.5 g.mol^{-1}; RT = ~3.8 min) and lastly F-113 (MW = 187.5 g.mol^{-1}; RT = ~6.1 min).

Because the parameter governing the elution sequence and RT remain constant (except when deliberately varied), the RT was found to be reproducible within ±0.1 minutes during large number of repeated analyses. Due to dependence of peak area on factors that vary unintentionally between different experiments, namely, (i) detector sensitivity (indicated by value of baseline output voltage); (ii) quality of carrier gas (that can change when new cylinder is installed); (iii) bleeding of analytical column; and (iv) efficiency of moisture trap, considerable variation (up to 15%) in the this was observed between similar experiments carried out at different times. To achieve better reproducibility, it is therefore necessary to further automate and effectively control the unintentional variables. Peak Area calibration curve for estimating concentrations of various CFC species in unknown samples is shown in Figure 3.13.

Table 3.9 Values of peak area and retention time along with the relevant statistics for the chromatograms shown in Figure 3.10, Figure 3.11 and Figure 3.12.

RT: Retention Time; PA: Peak Area; Avg: Average; SD: Standard Deviation; %RSD = Percentage Relative Standard Deviation = SD*100/Avg

2 ml Injection of CFC Standard Mixture (See chromatograms in Figure 3.10)

Sample No.	**N_2O**		**F-12**		**F-11**		**F-113**	
	RT (minute)	PA (μv*min)	RT (minute)	PA (μv*min)	RT (minute)	PA (μv*min)	RT (minute)	PA (μv*min)
PRL-623	1.617	146214	2.267	14583	3.770	117668	6.065	11142
PRL-625	1.600	150418	2.267	12141	3.783	109864	6.100	11621
PRL-627	1.617	154807	2.267	15369	3.783	110161	6.083	12424
Avg	1.611	150480	2.267	14031.0	3.779	112564	6.083	11729
SD	0.010	4297	0.000	1683.3	0.008	4422	0.018	648
% RSD	0.609	2.9	0.000	12.0	0.199	3.9	0.288	5.5

5 ml Injection of CFC Standard Mixture (See chromatograms in Figure 3.11)

Sample No.	**N_2O**		**F-12**		**F-11**		**F-113**	
	RT (minute)	PA (μv*min)	RT (minute)	PA (μv*min)	RT (minute)	PA (μv*min)	RT (minute)	PA (μv*min)
PRL-615	1.610	272911	2.275	29779	3.803	285776	6.183	14170
PRL-617	1.610	263789	2.275	32565	3.803	273242	6.148	10454
PRL-619	1.617	279123	2.283	29743	3.817	276283	6.167	12092
Avg	1.612	271941	2.278	30696	3.808	278434	6.166	12239
SD	0.004	7713	0.005	1619	0.008	6538	0.018	1862
% RSD	0.251	2.8	0.203	5.3	0.212	2.3	0.284	15.2

10 ml Injection of CFC Standard Mixture (See chromatograms in Figure 3.12)

Sample No.	**N_2O**		**F-12**		**F-11**		**F-113**	
	RT (minute)	PA (μv*min)	RT (minute)	PA (μv*min)	RT (minute)	PA (μv*min)	RT (minute)	PA (μv*min)
PRL-634	1.600	846732	2.280	60682	3.813	687932	6.173	48771
PRL-636	1.600	941932	2.280	61745	3.813	698601	6.160	51241
PRL-638	1.583	971362	2.280	66645	3.813	738038	6.160	49461
Avg	1.594	920009	2.280	63024	3.813	708190	6.164	49824
SD	0.010	65143	0.000	3181	0.000	26394	0.008	1274
% RSD	0.616	7.1	0.000	5.0	0.000	3.7	0.122	2.6

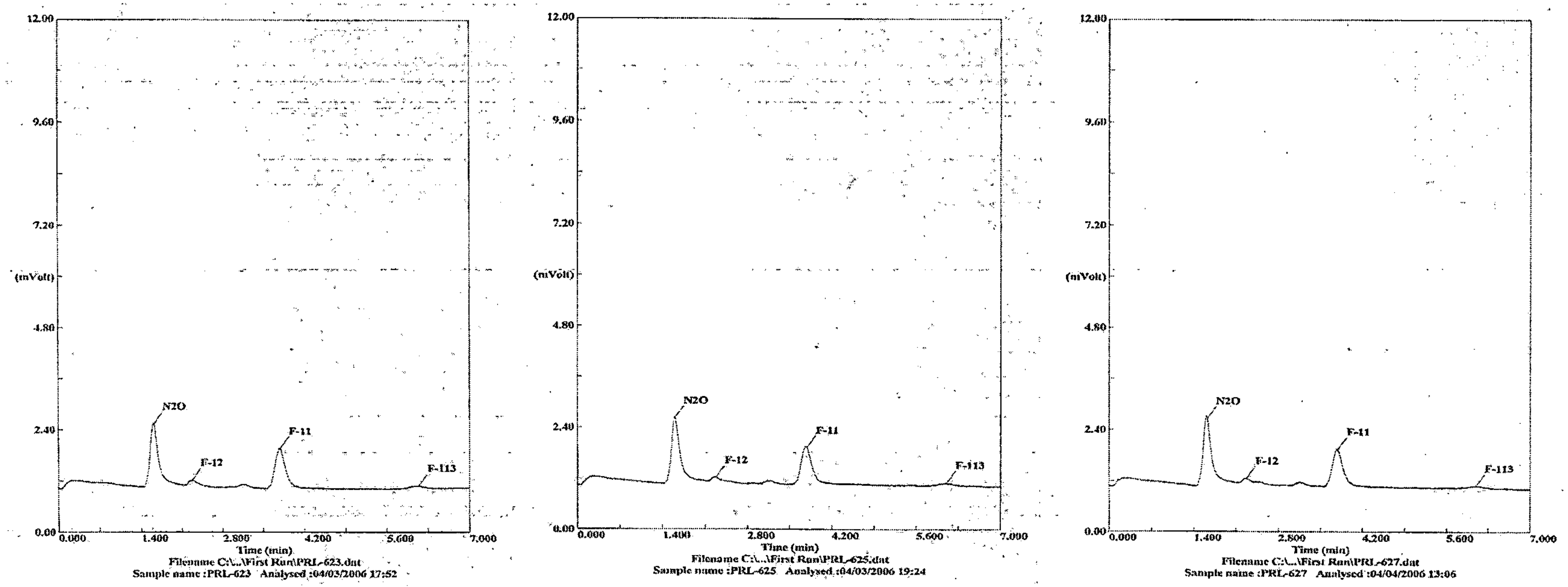

Figure 3.10 Three different chromatograms for 2 ml injection of CFC standard. Two CFC species of interest (F-12 and F-11) are identifiable from known elution time but F-113 peak is barely visible though it also can be identified from its known retention time.

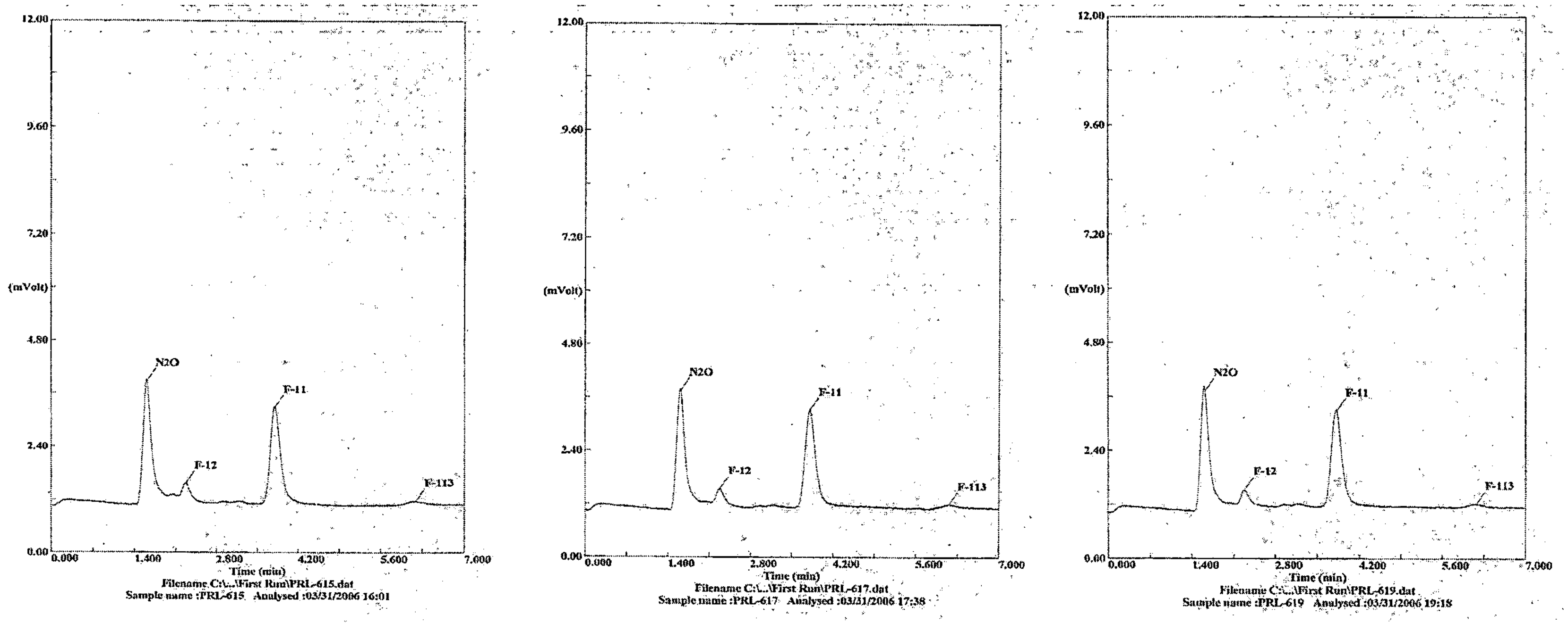

Figure 3.11 Three different chromatograms for 5 ml injection of CFC standard. Three CFC species of interest (F-12, F-11 and F-113) can be identified from their known retention time. Though identifiable, F-113 peak is small.

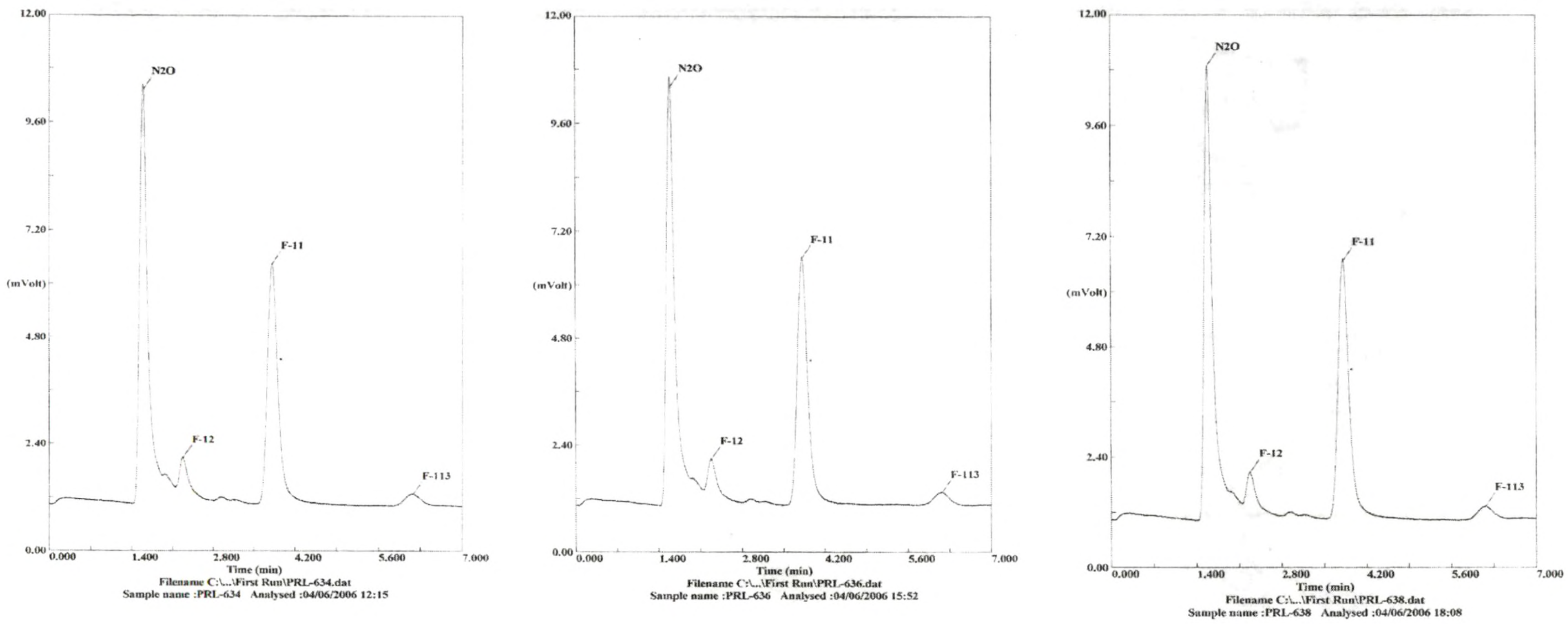

Figure 3.12 Three different chromatograms for 10 ml injection of CFC standard. All the three CFC species of interest (F-12, F-11 and F-113) can be identified from their known retention times.

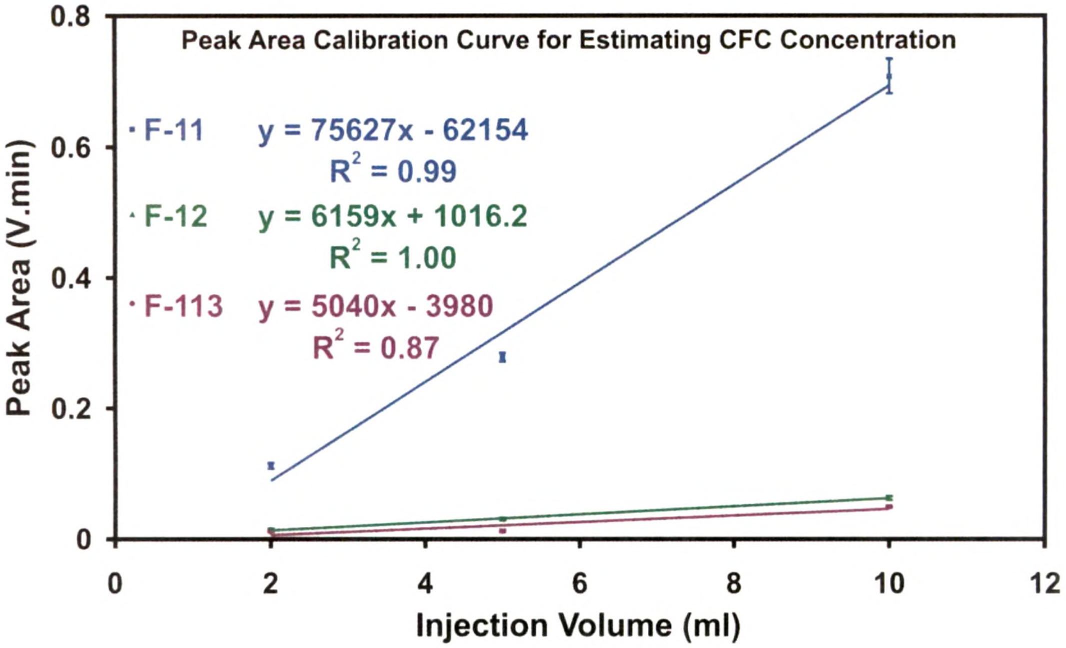

Figure 3.13 Peak area calibration curve for estimating CFC concentration in the injected gas sample. Concentration in the standard gas mixture used for calibration corresponds to: F-12 (4.834E-10 $ml.ml^{-1}$); F-11 (2.303E-10 $ml.ml^{-1}$); F-113 (7.3E-11 $ml.ml^{-1}$).

Additionally, it is also necessary to undertake peak area calibration experiments by analysing different volumes of CFC standard mixture before initiating the analyses of water samples after every few water samples and to include a background run before and after every analysis.

This completes the objective of setting up of the CFC laboratory and establishing the field and laboratory protocol for CFC analyses. Since the field sampling and analyses of groundwater samples did not form part of this study, no results of CFC analyses of groundwater have been included in Chapter 4. Results of various other field and laboratory investigations undertaken using other tracer techniques are, however, reported in Chapter 4.

Chapter 4. Results and Discussion

In this Chapter, results from various geochemical and isotopic investigations are presented both in tabular and graphical forms and salient features of the observed variations are described. This is followed by the interpretation and discussion leading to specific conclusions.

4.1 Results

4.1.1 Groundwater Helium and Temperature

Details of (i) the sampled well locations; (ii) well type; values of (iii) 'Excess helium' concentration (He_{ex}); and (iv) temperature of groundwater are given in Table 4.1. A map showing isolines of He_{ex} in groundwater (see Section 2.6.2 for definition of excess helium) of the NGC region is given in Figure 4.1. The isolines of groundwater temperature are shown in Figure 4.2.

Of the 12 soil-gas samples analyzed, only one sample ~100 m away from the thermal springs of Tuwa showed helium concentration (7.0 ppmv) higher than the atmospheric background. All other soil gas samples had helium concentrations close to atmospheric value.

It is seen from Figure 4.1 that groundwater with very high values of He_{ex} is found in the region west of the WCBBF where a set of intersecting orthogonal basement faults are located (See Figure 1.3). The highest He_{ex} value (2843 ppmAEU) was observed at Zinzawadar (CBGW-120; Table 4.1; Figure 4.1) located close to the western extremity of the longest orthogonal fault cutting across Cambay Basin. High He_{ex} in groundwater is also found at some locations on the eastern flank of the Cambay basin, associated with thermal springs of Lasundra (L) and Tuwa (T). The highest He_{ex} value (1163 ppmAEU) on the east flank of Cambay basin was observed in a groundwater sample from a hand pump near the thermal spring at Tuwa, located close to the Aravalli foothills (CBGW-21; Table 4.1; Figure 4.1). It is also seen from Figure 4.1 that the isoline of 5 ppmAEU He_{ex} lies close to the WCBBF.

The groundwater temperature in the study area ranged from 28°–61°C with an average value of 30°C. It is seen from Figure 4.2 that within the Cambay basin (having thick sedimentary cover), the groundwater temperatures are around 30°C. Along the WCBBF and on the west flank of Cambay basin a large area shows high groundwater temperature (>35°C), associated with thermal artesian wells and thermal springs. On the east flank, the groundwater temperatures >40°C are seen in and around the thermal springs tapping the Precambrian granitic basement. The highest groundwater temperature (61°C) was found in one of the eight sampled vents (CBGW-18; Table 4.1) of the thermal springs at Tuwa (T).

Table 4.1 Details of groundwater sampling sites together with values of He_{ex} and calculated ^{4}He ages using helium release factor (Λ_{He}) of 1 and 0.4. Calculations of ^{4}He ages are based on Th = 7.54±3.5; U = 1.07±0.41; ρ =2.6 g cm^{-3}; n = 20%. [TW = tubewell; DCB = dug cum bore; DW = dug well; HP = handpump; TA = thermal artesian; TS = thermal spring; He_{ex} = (measured – 5.3) ppmAEU].

CBGW Sample no.	Location name	Well type	Lat. (°N)	Long. (°E)	Depth bgl (m)	Temp. (°C)	He_{ex} ppmAEU	^{4}He ages (kaBP) (Λ_{He} =1)	^{4}He ages (kaBP) (Λ_{He} =0.4)
1	Gandhinagar	TW	23.24	72.68	55	---	0	0	0
2	Prantij	DCB	23.44	72.85	18	---	0	0	0
3	Prantij	TW	23.45	72.86	30	---	0	0	0
4	Shikha	DCB	23.39	73.23	30	---	0	0	0
5	Bayad	TW	23.22	73.21	18	---	0	0	0
6	Gundela	DW	23.12	73.36	9	---	0	0	0
7	Rojawa	TW	22.91	73.33	34	---	0	0	0
8	Lasundra	DW	22.91	73.14	6	52	186	547	1368
9	Lasundra	DW	22.91	73.14	6	---	55	162	404
10	Sinhuj	DCB	22.82	72.86	24	---	0	0	0
11	Dakore	TW	22.76	73.16	37	---	0	0	0
12	Ladvel	HP	22.91	73.12	12	---	0.2	1	1
13	Kapadvanj	DCB	23.04	73.10	38	---	0	0	0
14	Kunha	TW	23.01	72.77	91	---	0	0	0
15	Lasundra	TW	22.92	73.15	85	---	221	650	1625
16	Anghadi	DCB	22.81	73.30	24	---	0	0	0
17	Timba	HP	22.82	73.40	12	---	0	0	0
18	Tuwa	TS	22.80	73.46	1	61	137	403	1007
19	Tuwa	TS	22.80	73.46	1	47	96	282	706
20	Tuwa	TS	22.80	73.46	1	28	475	1397	3493
21	Tuwa	HP	22.80	73.46	12	51	1163	3421	8551
22	Tuwa	DW	22.80	73.46	6	---	0	0	0
23	Godhara	DW	22.78	73.60	7	---	0	0	0
24	Godhara	TW	22.76	73.61	30	---	0	0	0
25	Baska	HP	22.47	73.45	18	---	0	0	0
26	Baroda	TW	22.27	73.19	30	---	0	0	0
27	Jarod	HP	22.44	73.35	12	---	0	0	0
28	Khadki	HP	22.65	73.52	12	---	0	0	0
29	Dabhoi	HP	22.13	73.41	12	---	0	0	0
30	Sathod	TW	22.07	73.38	53	---	0	0	0
32	Adalaj	TW	23.17	72.58	229	---	0.1	0	1
33	Kaloi	TW	23.26	72.47	183	---	0.1	0	1
34	Malharpur	HP	22.81	72.62	18	---	0.1	0	1
35	Marala	DCB	22.62	72.64	30	---	0.1	0	1
36	Khambhat	TW	22.33	72.62	91	---	0.8	2	6
37	Nadiad	TW	22.56	72.82	30	---	0.1	0	1
38	Bhadran	TW	22.37	72.9	67	---	0.4	1	3
39	Masar Rd.	TW	22.11	72.89	61	---	5.2	15	38

Table 4.1 continues

CBGW Sample no.	Location name	Well type	Lat. (°N)	Long. (°E)	Depth bgl (m)	Temp. (°C)	He_{ex} ppmAEU	^{4}He ages (kaBP) (Λ_{He} =1)	^{4}He ages (kaBP) (Λ_{He} =0.4)
40	Kalak	DCB	22.02	72.76	21	---	0.1	0	1
43	Manglej	TW	22.09	73.17	76	---	0.1	0	1
44	Dholka	TW	22.69	72.43	107	---	0.5	1	4
45	Dholera	TA	22.25	72.19	168	43	109	321	801
50	Rampara	TW	22.11	71.89	76	---	2.7	8	20
51	Dhandhuka	DCB	22.38	71.98	15	---	0.2	1	1
52	Bawala	TW	22.83	72.36	198	33	6.3	19	46
53	Bagodra	TA	22.64	72.2	335	41	88	259	647
54	Bagodra	TA	22.64	72.2	335	41	190	559	1397
55	Gundi	TA	22.55	72.23	290	40	234	688	1721
56	Batod	HP	22.16	71.66	37	---	0.1	0	1
58	Vejalka	DCB	22.4	71.72	53	---	6.3	19	46
59	Wadhwan	TW	22.72	71.68	91	35	0.2	1	1
60	Bajana	TW	23.12	71.78	175	---	16	47	118
61	Dashada	TW	23.32	71.84	168	---	49	144	360
62	Sachana	TW	23.08	72.17	21	34	2.7	8	20
63	Vithalpur	TW	23.37	72.05	198	---	1	3	7
64	Umerkhaya	DW	22.90	72.02	13	---	0.2	1	1
65	Shiyala	TA	22.70	72.16	274	38	73	215	537
66	Ruhika	TA	22.66	72.23	457	41	157	462	1154
67	Sarala	TA	22.67	72.2	274	40	89	262	654
68	Vithalgadh	DW	22.99	71.97	15	---	0.2	1	1
69	Nardipur	TW	23.25	72.56	200	29	0	0	0
70	Santej	TW	23.11	72.47	274	29	0	0	0
71	Rancharda	TW	23.08	72.45	213	---	0	0	0
72	Nardipur	TW	23.25	72.56	200	29	0	0	0
73	Santej	TW	23.11	72.47	274	29	0	0	0
74	Rancharda	TW	23.08	72.45	213	---	0	0	0
75	Ananddham	TW	22.99	72.52	--	---	0	0	0
76	Sarkhej	TW	22.99	72.49	91	---	0	0	0
77	Sarkhej	TW	22.99	72.49	18	---	0	0	0
78	Collet	TW	22.97	72.43	229	33	1	3	7
79	Collet	TW	22.98	72.44	61	30	0	0	0
80	Sanand	TW	23.00	72.38	229	29	0.4	1	3
81	Thol	TW	23.13	72.38	183	32	0	0	0
82	Thol	HP	23.15	72.37	24	31	0	0	0
83	Rangpurda	TW	23.25	72.30	183	31	0.5	1	4
84	Kadi	TW	23.30	72.31	213	31	0	0	0
85	Bhoyani	TW	23.36	72.23	244	32	0.4	1	3
86	Katosan Road	TW	23.40	72.24	244	32	0.4	1	3
87	Navdeep Ind.	TW	23.01	72.34	244	30	0.8	2	6
88	Vansa	DCB	23.02	72.33	244	28	0.1	0	1
89	Sachana	TW	23.08	72.16	12	39	34	100	250
90	Hansalpur	TW	23.10	72.07	213	33	22	65	162
91	Viramgam	TW	23.10	72.06	110	34	66	194	485
92	Juna Padhar	TW	23.19	72.04	229	40	62	182	456
93	Endla	TW	23.29	72.04	244	38	23	68	169
94	Sitapur	TW	23.45	71.99	265	34	16	47	118

Table 4.1 continues

CBGW Sample no.	Location name	Well type	Lat. (°N)	Long. (°E)	Depth bgl (m)	Temp. (°C)	He_{ex} ppmAEU	^{4}He ages (kaBP) (Λ_{He} =1)	^{4}He ages (kaBP) (Λ_{He} =0.4)
95	Sitapur	TW	23.44	71.98	183	38	21	62	154
96	Valevda	TW	23.46	71.94	299	32	2.8	8	21
97	Valevda	TW	23.45	71.94	213	40	17	50	125
98	Dhanap	TW	23.26	72.75	262	31	0.2	1	1
99	Majara	TW	23.36	72.8	213	29	0.1	0	1
100	Talod	TW	23.35	72.93	122	28	0	0	0
101	Tajpur Camp	HP	23.37	73.03	46	29	0.2	1	1
102	Vadagam	HP	23.33	73.17	24	29	0.2	1	1
103	Ramnagar	HP	23.39	73.23	9	28	0	0	0
104	Dhamanya	HP	23.34	73.25	14	29	0	0	0
105	Kamaliya	HP	23.33	73.31	30	28	0	0	0
106	Ranmalgadh	TW	22.98	72.34	61	33	0.7	2	5
107	Rethal	TW	22.88	72.19	152	34	12	35	87
108	Shahpur	HP	22.88	72.02	168	29	2	6	15
109	Vasvelia	TW	23.00	72.04	18	37	131	385	963
110	Bhojva	TW	23.15	72.03	168	31	2.3	7	17
111	Malanpur	TW	23.25	71.93	61	35	56	165	412
112	Zainabad	TW	23.26	71.68	274	34	112	329	824
113	Zainabad	HP	23.26	71.68	213	29	0	0	0
114	Zinzuvada	TW	23.35	71.65	15	35	31	91	228
115	Zinzuvada	HP	23.35	71.66	198	28	0	0	0
116	Changodar	HP	22.93	72.44	15	29	0.3	1	2
117	Kalayangdh	TW	22.72	72.27	9	27	1.4	4	10
118	Limbdi	HP	22.57	71.81	61	28	0	0	0
119	Vadod	TW	22.56	71.63	14	29	1.6	5	12
120	Zinzawadar	TW	22.45	71.69	53	34	2843	8362	20904
121	Zinzawadar	HP	22.45	71.69	285	29	0	0	0
122	Chuda	TW	22.49	71.69	46	31	1290	3794	9485
123	Vekaria	HP	22.82	72.06	183	29	0.4	1	3
124	Fulgam	HP	22.54	71.54	12	31	0.2	1	1
125	Shekhpur	TW	22.70	71.56	55	31	0.2	1	1
126	Vana	HP	22.87	71.71	55	---	0	0	0
127	Rangpur	DW	22.41	71.93	12	27	0.6	2	4
128	Vagad	DW	22.36	71.87	11	29	0	0	0
129	Nagnesh	TW	22.36	71.76	18	31	2	6	15
130	Nagnesh	HP	22.36	71.76	61	31	1.1	3	8
131	Alampur	DW	22.30	71.66	17	28	0	0	0
132	Paliyad	HP	22.25	71.56	46	30	0	0	0
133	Paliyad	TW	22.25	71.56	91	32	0.7	2	5
134	Botad	HP	22.17	71.66	49	---	0	0	0
135	Tatam	TW	22.06	71.62	64	31	0.8	2	6
137	Ahmedabad	TW	22.98	72.62	233	35	0	0	0
138	Hathijan	TW	22.94	72.64	137	35	0.5	1	4
139	Onthwari	DCB	22.82	72.80	61	35	0	0	0
140	Ran Na Muvada	DCB	22.84	72.95	85	35	3.6	11	26
141	Porda	DCB	22.92	73.00	67	33	0.2	1	1
147	Sarangpur	HP	22.16	71.77	61	34	0	0	0
149	Panavi	TW	22.08	71.89	125	41	1624	4776	11941
150	Keriya Dhal	TW	22.11	71.89	183	35	0	0	0
151	Vaya	DW	22.20	71.87	30	30	0	0	0

Table 4.1 continues

CBGW Sample no.	Location name	Well type	Lat. (°N)	Long. (°E)	Depth bgl (m)	Temp. (°C)	He_{ex} ppmAEU	^{4}He ages (kaBP) (Λ_{He} =1)	^{4}He ages (kaBP) (Λ_{He} =0.4)
152	Devthal	DCB	22.75	72.13	10	35	4.4	13	32
153	Devthal	TW	22.76	72.12	274	35	116	341	853
154	Kanera	TW	22.81	72.62	137	33	1.4	4	10
155	Sokhada	TW	22.74	72.68	98	34	0.3	1	2
156	Matar	TW	22.71	72.68	110	35	0.1	0	1
157	Nar	TW	22.48	72.71	107	35	0.7	2	5
158	Jogan	DCB	22.45	72.79	34	32	0.1	0	1
159	Bharel	TW	22.41	72.83	61	34	0.1	0	1
160	Dededa	DW	22.46	72.91	58	32	0.3	1	2
161	Anand	TW	22.53	72.96	46	32	0	0	0
162	Uttarsanda	TW	22.66	72.9	55	32	0	0	0
163	Sojitra	TW	22.55	72.74	140	35	1.8	5	13
164	Jedwapura	TW	22.55	72.83	91	34	0	0	0
165	Bedva	DCB	22.55	73.04	37	---	0	0	0
166	Ode	TW	22.62	73.11	47	32	0.7	2	5
167	Lingda	HP	22.69	73.08	20	31	0.5	1	4
168	Alindra	HP	22.70	72.97	55	34	0.5	1	4
169	Vaghasi	TW	22.54	73.00	49	---	0	0	0
170	Bhetasi	TW	22.43	73.02	61	33	0	0	0
171	Samiala	TW	22.26	73.12	113	33	0.1	0	1
172	Dabhasa	TW	22.25	73.05	76	34	0	0	0
173	Vadu	DCB	22.21	72.98	51	33	0.2	1	1
174	Vadu	TW	22.22	72.98	130	37	3.5	10	26
175	Gavasad	TW	22.19	72.97	130	35	0.1	0	1
176	Jambusar	TW	22.05	72.81	73	34	1	3	7
179	Karjan	TW	22.05	73.12	107	34	0	0	0
184	Kanara	TW	22.08	73.4	183	34	0	0	0
185	Mandwa	TW	22.01	73.43	46	35	0.1	0	1
186	Chandod	TW	22.99	73.46	122	34	0	0	0
187	Ankhi	TW	22.13	73.2	91	33	4.6	14	34
188	Kayavarohan	TW	22.08	73.24	99	33	0	0	0
189	Dantiwada	HP	24.17	72.48	36	34	0	0	0
190	Dantiwada	T	24.16	72.48	101	31.5	0.4	1	3
191	Gola	DCB	24.19	72.78	37	28	0.2	1	1
192	Dharoi	HP	24.00	72.85	12	29	0.1	0	0
193	Mumanvas	DW	24.04	72.83	18	27	0.4	1	3
194	Mathasur	HP	23.80	73.01	46	30	0.2	1	1
195	Himmatnagar	HP	23.72	72.96	27	29	0.3	1	3
196	Dalpur	DCB	23.51	72.95	21	29	0	0	0
202	Math	HP	23.43	73.82	15	28	0.2	1	1
203	Aritha	HP	23.14	73.65	15	29	0.1	0	1
204	Limbodra	HP	23.19	73.60	15	29	0.3	1	2
205	Ghaliya Danti	HP	23.36	73.51	18	29	0.1	0	1
206	Shehra	HP	22.95	73.63	18	29	0.1	0	1
207	Popatpura	HP	22.79	73.45	18	29.5	0.2	1	1
208	Maniyor	TW	23.82	72.96	74	35	0.1	0	1
209	Dharewada	TW	23.98	72.39	212	35	2	6	15
210	Ganguva	TW	24.16	72.73	85	33	0	0	0
211	Chadotar	TW	24.21	72.39	63	32	0	0	0

Table 4.1 continues

CBGW Sample no.	Location name	Well type	Lat. (°N)	Long. (°E)	Depth bgl (m)	Temp. (°C)	He_{ex} ppmAEU	^{4}He ages (kaBP) (Λ_{He} =1)	^{4}He ages (kaBP) (Λ_{He} =0.4)
212	Bhadath	TW	24.34	72.2	141	32	0.3	1	2
213	Kuwarva	TW	24.04	71.9	187	35	0.3	1	2
214	Kuwarva	TW	24.05	71.9	122	33	0.3	1	2
215	Tharad	TW	24.41	71.64	299	42	30	88	221
216	Jitoda	TW	23.74	72.15	313	35	0.6	2	4
217	Jitoda	TW	23.74	72.15	427	42	9.7	29	71
218	Sami	TW	23.70	71.78	299	44	64	188	471
219	Wavadi	TW	23.92	72.52	145	34	0	0	0
220	Pilwai	TW	23.53	72.69	235	39	17	50	125
221	Pilwai	TW	23.54	72.68	152	37	0.5	1	4
222	Heduva	TW	23.57	72.34	267	37	1.8	5	13
223	Vaghpur	TW	23.68	73.42	86	33	23	68	169
224	Edla	TW	23.54	72.06	289	40	11	32	81
225	Sherisa	TW	23.20	72.48	232	35	0.3	1	2
312	Diyodar	TW	24.10	71.75	207	33	1.9	6	14
313	Diyodar	TW	24.10	71.75	207	33	1.2	4	9
314	Tharad	TW	24.41	71.64	201	39	30	88	221
316	Agathala	TW	24.29	71.88	137	31	0	0	0
317	Sujanipur	TW	23.89	72.11	91	31	0	0	0
318	Sujanipur	TW	23.90	72.12	326	37	16	47	118
319	Sujanipur	TW	23.91	72.12	40	29	0	0	0
320	Kuwarva	TW	24.04	71.9	187	32	0	0	0
321	Kharia	TW	23.94	71.83	158	30	0	0	0
322	Sami	TW	23.7	71.78	299	41	45	132	331
323	Hedva	TW	23.57	72.34	82	33	1.5	4	11
324	Kuder	TW	23.70	71.87	262	34	1.5	4	11
325	Patan	TW	23.84	72.11	198	31	0	0	0
326	Patan	TW	23.84	72.11	130	32	0	0	0
327	Patan	TW	23.84	72.11	60	29	0	0	0
328	Jitoda	TW	23.74	72.15	313	33	0.3	1	2
329	Jitoda	TW	23.74	72.15	448	39	10	29	74
330	Kamboi	TW	23.67	72.02	213	32	6.4	19	47
331	Muthia	TW	23.09	72.69	142	31	0.3	1	2
332	Paliya	TW	23.18	72.83	119	31	0.3	1	2
333	Punsari	TW	23.39	73.10	32	30	0	0	0
334	Dalani Muwadi	TW	23.36	72.88	91	31	12	35	88
335	Rojad	HP	23.35	73.09	29	29	0	0	0
336	Vadrad	TW	23.42	72.89	58	31	0	0	0
337	Tejpur	TW	23.39	72.81	160	30	0	0	0
338	Navalpur	TW	23.60	72.90	122	32	0.6	2	4
339	Dhanap	TW	23.26	72.75	168	32	0	0	0
340	Indroda Park	TW	23.19	72.65	107	31	0.3	1	2
341	Rupawati	TW	23.00	72.30	213	37	0	0	0
342	Sokali	TW	23.10	72.11	93	32	0.6	2	4
343	Dudapur	TW	23.02	71.58	61	32	44	129	324
355	Salajada	TW	22.80	72.39		35	0.9	3	7
356	Salajada	TW	22.79	72.39	198	35	0.9	3	7
357	Salajada	TW	22.79	72.39	93	31	0	0	0
358	Gundi	TA	22.55	72.23	>290	42	178	524	1309
359	Shiyal	TA	22.68	72.16	274	42	230	676	1691

Table 4.1 continues

CBGW Sample no.	Location name	Well type	Lat. (°N)	Long. (°E)	Depth bgl (m)	Temp. (°C)	He_{ex} ppmAEU	^4He ages (kaBP) (Λ_{He} =1)	^4He ages (kaBP) (Λ_{He} =0.4)
360	Padgol	TW	22.59	72.84	137	32	1.4	4	10
361	Morad	TW	22.54	72.86	91	31	0	0	0
362	Gumadia	TW	22.76	73.23	49	31	0.3	1	2
363	Tuwa	TS	22.80	73.46	1	50	405	1191	2978
364	Tuwa	TS	22.80	73.46	1	43	229	674	1684
365	Tuwa	TS	22.80	73.46	1	36	265	779	1949
366	Tuwa	TS	22.80	73.46	1	33	253	744	1860
367	Dholera	TA	22.25	72.19	168	45	443	1303	3257

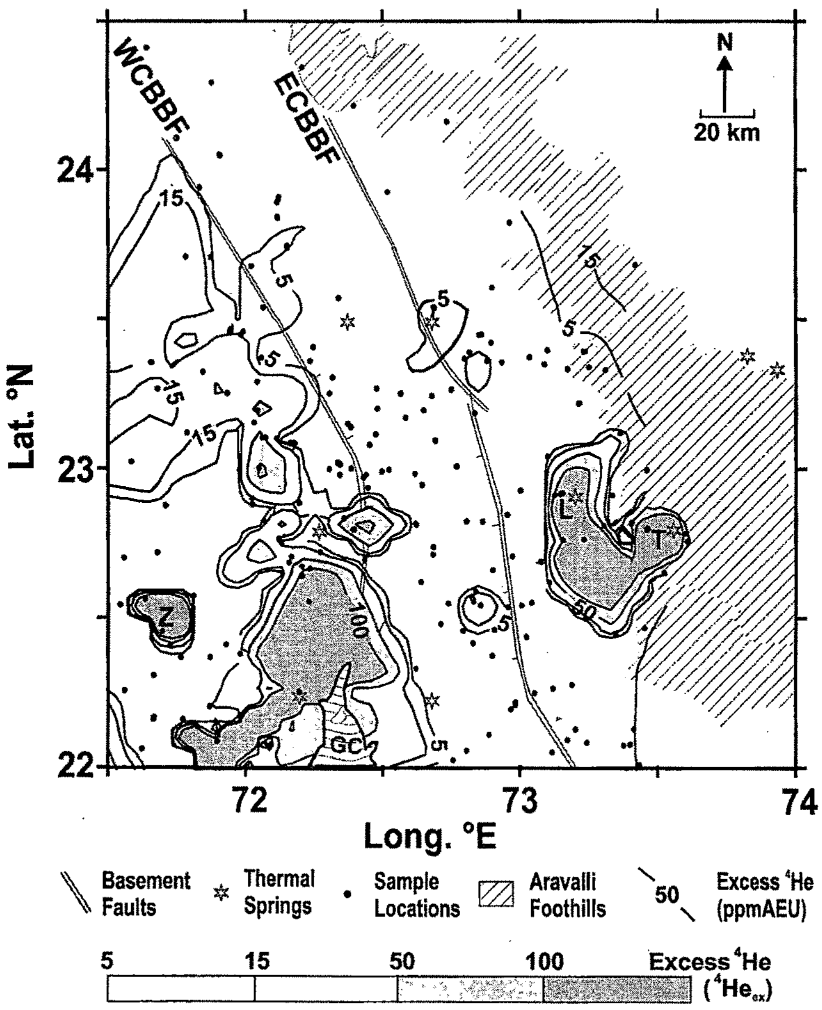

Figure 4.1 Isoline map of He_{ex} in groundwater of the NGC region. The isoline of 5 ppmAEU He_{ex} runs almost along the WCBBF. Pockets of He_{ex} >50 ppmAEU overlap with pockets of high (>40°C) groundwater temperature (Figure 4.2). Sampling locations are indicated by dots. L, T and Z respectively indicate the locations of thermal springs at Lasundra, Tuwa and a tubewell in Zinzawadar.

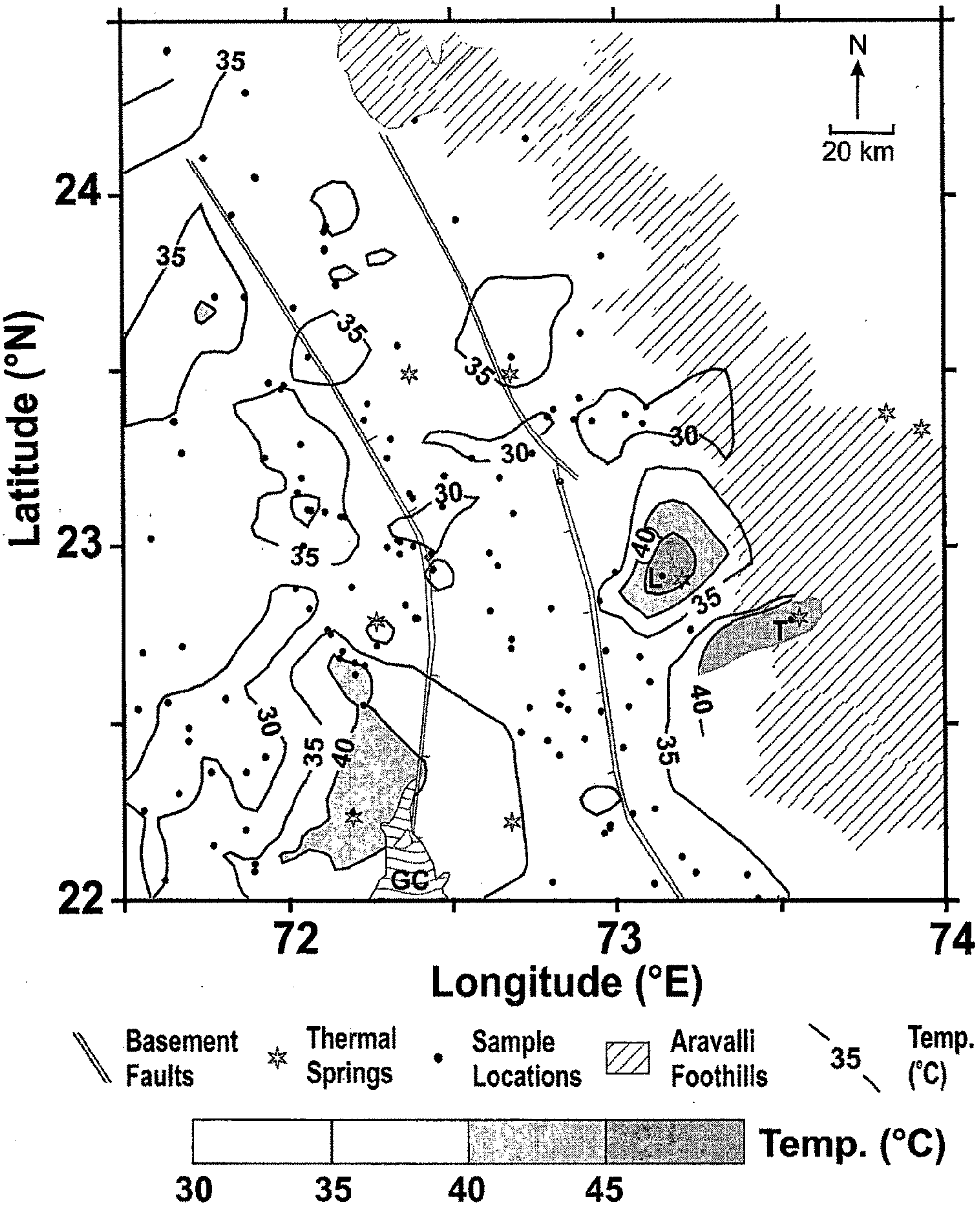

Figure 4.2 Isoline map of groundwater temperature in the NGC region. Large areas on both east and west flanks of the Cambay basin show groundwater temperature >35°C. Temperatures >40°C are seen around thermal springs. Sampling locations are indicated by dots. L and T respectively indicate locations of thermal springs at Lasundra and Tuwa

It is seen from Figure 4.1 and Figure 4.2 that areas with very high He_{ex} (>50 ppm AEU) in groundwater overlap with areas having high (>40°C) groundwater temperatures. In general, areas of high He_{ex} (>15 ppmAEU) are associated with high groundwater temperature (>35°C). However, on a plot of He_{ex} vs. temperature (Figure 4.3) no quantitative relationship is observed. It may also be noticed that even for different vents within the small region around the thermal springs at Tuwa no quantitative relationship is observed between temperatures (28°–61°C) and He_{ex} (137-475 ppmAEU). Also, no correlation was found between depth below ground level of sampled well and He_{ex} in groundwater in the NGC region (Figure 4.4).

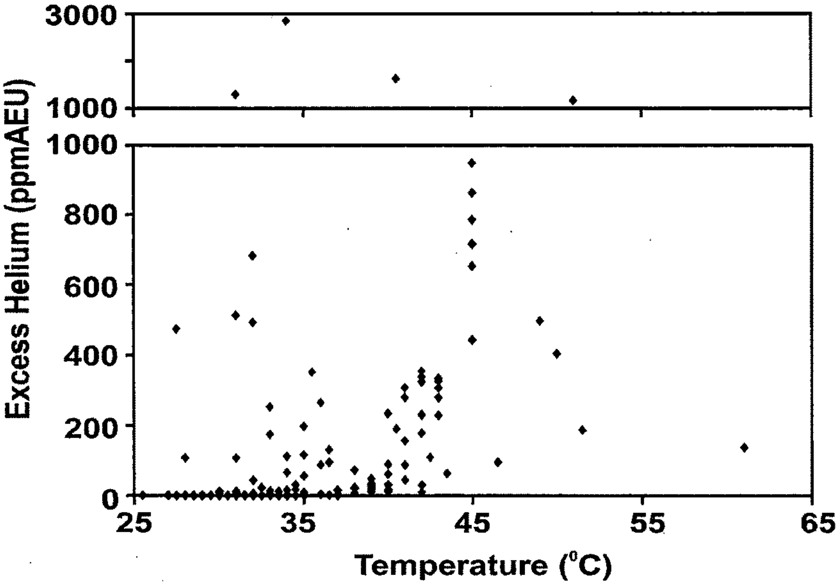

Figure 4.3 Groundwater temperature vs. He_{ex} in groundwater from NGC region.

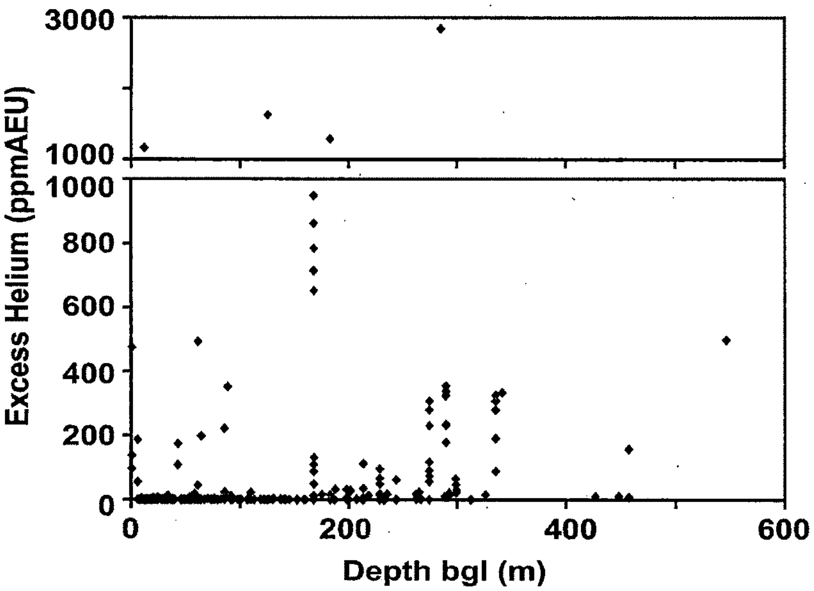

Figure 4.4 Depth of the sampled wells (bgl) vs. He_{ex} in groundwater in NGC region.

4.1.2 Groundwater Fluoride

Details of (i) the sampled well location; (ii) well type; and (iv) measured values of fluoride concentration are given in Table 4.2. The geographical distribution of fluoride in groundwater from the NGC region is shown in Figure 4.5.

Table 4.2 Details of groundwater sampling sites together with measured values of fluoride concentration and Electrical Conductivity. (TW = tubewell; DCB = dug cum bore; DW = dug well; HP = hand pump; TA = thermal artesian; TS = thermal spring; bgl = below ground level; CBGW = Cambay Basin Ground Water; EC = Electrical Conductivity)

CBGW No.	Location name	Well type	Lat. (°N)	Long. (°E)	Depth bgl (m)	Fluoride (ppm)	EC (mS)
1	Gandhinagar	TW	23.24	72.68	54.9	1.6	0.5
2	Prantij	DCB	23.44	72.85	18.3	1.2	0.5
3	Prantij	TW	23.45	72.86	30.5	0.9	0.5
4	Shikha	DCB	23.39	73.23	30.5	0.4	0.6
5	Bayad	TW	23.22	73.21	18.3	0.9	4.8
6	Gundela	DW	23.12	73.36	9.1	1.3	0.8
7	Rojawa	TW	22.91	73.33	33.5	1.7	2.0
8	Lasundra	DW	22.91	73.14	6.1	3.4	7.4
9	Lasundra	DW	22.91	73.14	6.1	3.3	7.6
10	Sinhuj	DCB	22.82	72.86	24.4	2.4	2.3
11	Dakore	TW	22.76	73.16	36.6	4.3	2.4
12	Ladvel	HP	22.91	73.12	12.2	1.5	0.7
13	Kapadvanj	DCB	23.04	73.10	38.1	1.0	0.9
14	Kunha	TW	23.01	72.77	91.4	1.3	1.0
15	Lasundra	TW	22.92	73.15	85.3	1.1	2.0
16	Anghadi	DCB	22.81	73.30	24.4	0.6	0.7
17	Timba	HP	22.82	73.40	12.2	1.2	1.9
18	Tuwa	DW	22.80	73.46	0.9	3.4	3.4
19	Tuwa	DW	22.80	73.46	0.9	3.5	6.2
20	Tuwa	DW	22.80	73.46	0.9	3.3	6.2
21	Tuwa	HP	22.80	73.46	12.2	3.4	4.7
22	Tuwa	DW	22.80	73.46	6.1	0.8	0.7
23	Godhara	DW	22.78	73.60	7.3	0.8	0.8
24	Godhara	TW	22.76	73.61	30.5	0.8	0.5
25	Baska	HP	22.47	73.45	18.3	0.4	2.3
26	Baroda	TW	22.27	73.19	30.5	0.1	2.3
27	Jarod	HP	22.44	73.35	12.2	0.6	0.5
28	Khadki	HP	22.65	73.52	12.2	1.2	1.1
29	Dabhoi	HP	22.13	73.41	12.2	1.4	2.0
30	Sathod	TW	22.07	73.38	53.3	0.7	1.2
31	Sinor	TW	21.93	73.34	76.2	0.4	1.1
32	Adalaj	TW	23.17	72.58	228.6	0.8	2.1
33	Kalol	TW	23.26	72.47	182.9	0.6	2.3
34	Malharpur	HP	22.81	72.62	18.3	0.9	2.7
35	Marala	DCB	22.62	72.64	30.5	0.6	0.8
36	Khambhat	TW	22.33	72.62	91.4	0.8	2.8
37	Nadiad	TW	22.56	72.82	30.5	0.6	1.9
38	Bhadran	TW	22.37	72.90	67.1	1.3	2.2
39	Masar Rd.	TW	22.11	72.89	61.0	0.9	4.2

Table 4.2 continues

CBGW No.	Location name	Well type	Lat. (°N)	Long. (°E)	Depth bgl (m)	Fluoride (ppm)	EC (mS)
40	Kalak	DCB	22.02	72.76	21.3	1.1	2.2
41	Valu	HP	21.76	72.93	36.6	0.6	3.1
42	Baruch	TW	21.72	72.99	33.5	0.5	3.9
43	Manglej	TW	22.09	73.17	76.2	0.6	1.6
44	Dholka	TW	22.69	72.43	106.7	1.7	3.1
45	Dholera	TA	22.25	72.19	167.6	0.3	6.9
46	Bhavnagar	DW	21.80	72.07	12.2	3.4	59.6
47	Bhavnagar	TW	21.81	72.07	126.5	0.4	1.6
48	Bhavnagar	TW	21.81	72.07	228.6	0.7	2.9
49	Vallabhipur	TW	21.88	71.88	15.2	2.8	8.8
50	Rampara	TW	22.11	71.89	76.2	2.2	1.3
51	Dhandhuka	DCB	22.38	71.98	15.2	1.7	3.1
52	Bawala	TW	22.83	72.36	198.1	0.7	1.6
53	Bagodra	TA	22.64	72.20	335.3	0.3	1.9
54	Bagodra	TA	22.64	72.20	335.3	0.2	1.4
55	Gundi	TA	22.55	72.23	289.6	0.2	1.5
56	Batod	HP	22.16	71.66	36.6	0.5	1.0
57	Raliyana	TW	21.91	71.56	167.6	0.5	1.3
58	Vejalka	DCB	22.40	71.72	53.3	1.2	0.9
59	Wadhwan	TW	22.72	71.68	91.4	2.4	1.9
60	Bajana	TW	23.12	71.78	175.3	1.2	1.6
61	Dashada	TW	23.32	71.84	167.6	0.2	1.2
62	Sachana	TW	23.08	72.17	21.3	0.7	1.1
63	Vithalpur	TW	23.37	72.05	198.1	0.6	1.5
64	Umerkhaya	DW	22.90	72.02	12.8	9.9	7.6
65	Shiyala	TA	22.70	72.16	274.3	0.3	3.4
66	Ruhika	TA	22.66	72.23	457.2	0.2	3.0
67	Sarala	TA	22.67	72.20	274.3	0.2	2.6
68	Vithalgadh	DW	22.99	71.97	15.2	5.1	5.9
69	Nardipur	TW	23.25	72.56	199.6	0.8	1.2
70	Santej	TW	23.11	72.47	274.3	2.0	1.2
71	Rancharda	TW	23.08	72.45	213.4	0.9	1.1
72	Nardipur	TW	23.25	72.56	199.6	0.8	1.2
73	Santej	TW	23.11	72.47	274.3	2.0	1.2
74	Rancharda	TW	23.08	72.45	213.4	0.9	1.1
75	Ananddham	TW	22.99	72.52		1.8	2.1
76	Sarkhej	TW	22.99	72.49	91.4	2.0	1.9
77	Sarkhej	TW	22.99	72.49	18.3	2.0	2.2
78	Collet	TW	22.97	72.43	228.6	0.7	1.6
79	Collet	TW	22.98	72.44	61.0	2.4	3.6
80	Sanand	TW	23.00	72.38	228.6	1.6	3.2
81	Thol	TW	23.13	72.38	182.9	1.2	3.2
82	Thol	HP	23.15	72.37	24.4	1.3	3.2
83	Rangpurda	TW	23.25	72.30	182.9	1.3	2.3
84	Kadi	TW	23.30	72.31	213.4	2.0	1.6
85	Bhoyani Derasar	TW	23.36	72.23	243.8	0.6	2.4
86	Katosan Road	TW	23.40	72.24	243.8	1.2	2.9
87	Navdeep	TW	23.01	72.34	243.8	1.3	2.4
88	Vansa	DCB	23.02	72.33	12.2	1.6	1.4

Table 4.2 continues

CBGW No.	Location name	Well type	Lat. (°N)	Long. (°E)	Depth bgl (m)	Fluoride (ppm)	EC (mS)
89	Sachana	TW	23.08	72.16	213.4	0.3	1.7
90	Hansalpur	TW	23.10	72.07	109.7	2.7	2.3
91	Viramgam	TW	23.10	72.06	228.6	0.3	1.8
92	Juna Padhar	TW	23.19	72.04	243.8	0.2	1.6
93	Endla	TW	23.29	72.04	265.2	0.3	1.6
94	Sitapur	TW	23.45	71.99	182.9	0.6	1.8
95	Sitapur	TW	23.44	71.98	299.0	0.2	1.5
96	Valevda	TW	23.46	71.94	213.4	1.0	4.3
97	Valevda	TW	23.45	71.94	262.1	0.4	1.8
98	Dhanap	TW	23.26	72.75	213.4	1.4	1.0
99	Majara	TW	23.36	72.80	121.9	1.3	1.2
100	Talod	TW	23.35	72.93	45.7	0.5	1.3
101	Tajpur Camp	HP	23.37	73.03	24.4	2.1	1.6
102	Vadagam	HP	23.33	73.17	9.1	0.3	0.5
103	Ramnagar	HP	23.39	73.23	13.7	0.6	0.6
104	Dhamanya	HP	23.34	73.25	30.5	0.5	0.7
105	Kamaliya Kampa	HP	23.33	73.31	61.0	1.4	1.5
106	Ranmalgadh	TW	22.98	72.34	152.4	0.8	1.5
107	Rethal	TW	22.88	72.19	167.6	1.3	1.5
108	Shahpur	HP	22.88	72.02	18.3	7.1	8.5
109	Vasvelia	TW	23.00	72.04	167.6	0.2	2.3
110	Bhojva	TW	23.15	72.03	61.0	4.7	3.0
111	Malanpur	TW	23.25	71.93	274.3	0.6	2.0
112	Zainabad	TW	23.26	71.68	213.4	0.3	2.3
113	Zainabad	HP	23.26	71.68	14.9	3.9	0.9
114	Zinzuvada	TW	23.35	71.65	198.1	0.4	2.6
115	Zinzuvada	HP	23.35	71.66	15.2	0.9	0.7
116	Changodar	HP	22.93	72.44	9.1	2.7	1.7
117	Kalayangdh	TW	22.72	72.27	61.0	2.4	5.2
118	Limbdi	HP	22.57	71.81	13.7	5.0	3.4
119	Vadod	TW	22.56	71.63	53.3	1.1	1.5
120	Zinzawadar	TW	22.45	71.69	285.0	0.8	3.5
121	Zinzawadar	HP	22.45	71.69	45.7	0.4	1.3
122	Chuda	TW	22.49	71.69	182.9	1.2	3.9
123	Vekaria	HP	22.82	72.06	12.2	5.0	6.6
124	Fulgam Jn	HP	22.54	71.54	54.9	0.9	1.1
125	Shekhpur	TW	22.70	71.56	54.9	2.3	5.3
126	Vana	HP	22.87	71.71	12.2	8.4	6.0
127	Rangpur	DW	22.41	71.93	10.7	1.3	9.0
128	Vagad	DW	22.36	71.87	18.3	1.8	3.7
129	Nagnesh	TW	22.36	71.76	61.0	1.2	2.2
130	Nagnesh	HP	22.36	71.76	38.1	2.2	2.3
131	Alampur	DW	22.30	71.66	16.8	0.7	0.6
132	Paliyad	HP	22.25	71.56	45.7	0.7	2.3
133	Paliyad	TW	22.25	71.56	91.4	0.6	1.4
134	Botad	HP	22.17	71.66	48.8	0.6	0.9
135	Tatam	TW	22.06	71.62	64.0	4.6	1.1
136	Gadhda	TW	21.96	71.58	61.0	0.5	2.2
137	Ahmedabad	TW	22.98	72.62	233.2	1.3	1.5
138	Hathijan	TW	22.94	72.64	137.2	1.8	1.1

Table 4.2 continues

CBGW No.	Location name	Well type	Lat. (°N)	Long. (°E)	Depth bgl (m)	Fluoride (ppm)	EC (mS)
139	Onthwari	DCB	22.82	72.80	61.0	1.7	2.0
140	Ran Na Muvada	DCB	22.84	72.95	85.3	1.0	1.5
141	Porda	DCB	22.92	73.00	67.1	1.4	0.8
142	Dhasa	TW	21.80	71.51	91.4	0.3	1.7
143	Mandva	HP	21.81	71.58	36.6	0.7	0.8
144	Dedakdi	TW	21.81	71.71	57.9	0.8	2.1
145	Umrala	HP	21.84	71.80	45.7	1.4	1.0
146	Kanpar	TW	21.96	71.88	21.3	5.9	2.4
147	Sarangpur	HP	22.16	71.77	61.0	0.7	2.2
148	Navagam	TW	21.96	71.90	61.0	2.9	3.2
149	Panavi	TW	22.08	71.89	125.3	0.4	6.0
150	Keriya Dhal	TW	22.11	71.89	182.9	2.5	0.8
151	Vaya	DW	22.20	71.87	30.5	3.8	1.0
152	Devthal	DCB	22.75	72.13	9.8	3.1	9.6
153	Devthal	TW	22.76	72.12	274.3	0.3	2.6
154	Kanera	TW	22.81	72.62	137.2	2.6	3.2
155	Sokhada	TW	22.74	72.68	97.5	1.6	5.7
156	Matar	TW	22.71	72.68	109.7	3.9	0.9
157	Nar	TW	22.48	72.71	106.7	0.5	2.5
158	Jogan	DCB	22.45	72.79	33.5	3.5	0.9
159	Bharel	TW	22.41	72.83	61.0	0.9	0.9
160	Dededa	DW	22.46	72.91	57.9	0.8	1.4
161	Anand	TW	22.53	72.96	45.7	0.6	0.8
162	Uttarsanda	TW	22.66	72.90	54.9	1.2	1.2
163	Sojitra	TW	22.55	72.74	140.2	0.7	1.5
164	Jedwapura	TW	22.55	72.83	91.4	0.7	2.3
165	Bedva	DCB	22.55	73.04	36.6	0.4	0.8
166	Ode	TW	22.62	73.11	47.2	0.6	0.8
167	Lingda	HP	22.69	73.08	19.8	1.5	0.7
168	Alindra	HP	22.70	72.97	54.9	0.6	0.6
169	Vaghasi	TW	22.54	73.00	48.8	1.2	0.9
170	Bhetasi	TW	22.43	73.02	61.0	1.0	1.2
171	Samlala	TW	22.26	73.12	112.8	0.8	0.9
172	Dabhasa	TW	22.25	73.05	76.2	0.7	1.0
173	Vadu	DCB	22.21	72.98	51.2	0.6	1.4
174	Vadu	TW	22.22	72.98	130.5	0.8	2.1
175	Gavasad]	TW	22.19	72.97	129.5	0.7	0.9
176	Jambusar	TW	22.05	72.81	73.2	0.9	3.4
177	Nahiyer	TW	21.96	72.88	61.0	0.5	3.9
178	Haldarva	TW	21.89	73.07	70.1	0.4	2.4
179	Karjan	TW	22.05	73.12	106.7	0.5	2.0
180	Saring	DCB	21.89	73.12	36.6	0.4	1.7
181	Arjanpura	DCB	21.87	73.16	48.8	0.4	1.4
182	Garudeshwar	TW	21.89	73.66	88.4	1.4	0.8
183	Garudeshwar	TW	21.89	73.66	64.0	1.3	0.7
184	Kanara	TW	22.08	73.40	182.9	0.6	1.0
185	Mandwa	TW	22.01	73.43	45.7	0.4	0.7
186	Chandod	TW	22.99	73.46	121.9	0.3	0.8
187	Ankhi	TW	22.13	73.20	91.4	0.5	2.4
188	Kayvarohan	TW	22.08	73.24	99.1	0.3	1.2

Table 4.2 continues

CBGW No.	Location name	Well type	Lat. (°N)	Long. (°E)	Depth bgl (m)	Fluoride (ppm)	EC (mS)
189	Dantiwada	HP	24.17	72.48	36	0.3	0.5
190	Dantiwada	TW	24.16	72.48	100.6	0.8	0.6
191	Gola	DCB	24.19	72.78	36.6	0.4	0.7
192	Dharoi	HP	24.00	72.85	12.2	1.6	0.6
193	Mumanvas	DW	24.04	72.83	18.3	1.5	0.9
194	Mathasur	HP	23.80	73.01	45.7	1.6	1.2
195	Himmatnagar	HP	23.72	72.96	27.4	1.6	0.9
196	Dalpur	DCB	23.51	72.95	21.3	0.2	0.6
202	Math	HP	23.43	73.82	15.2	0.6	0.4
203	Aritha	HP	23.14	73.65	15.2	0.8	0.5
204	Limbodra	HP	23.19	73.60	15.2	0.8	0.7
205	Ghaliya Danti	HP	23.36	73.51	18.3	0.8	0.8
206	Shehra	HP	22.95	73.63	18.3	1.1	0.5
207	Popatpura	HP	22.79	73.45	18.3	1.3	0.6
208	Maniyor	TW	23.82	72.96	73.9	3.1	1.9
209	Dharewada	TW	23.98	72.39	212.3	0.2	3.5
210	Ganguva	TW	24.16	72.73	85.5	0.7	0.5
211	Chadotar	TW	24.21	72.39	63.4	0.9	1.0
212	Bhadath	TW	24.34	72.20	140.9	1.1	0.4
213	Kuwarava	TW	24.04	71.90	186.6	1.9	1.7
214	Kuwarava	TW	24.05	71.90	121.9	1.9	0.0
215	Tharad	TW	24.41	71.64	299.1	0.8	3.4
216	Jitoda	TW	23.74	72.15	312.7	2.0	2.3
217	Jitoda	TW	23.74	72.15	426.7	1.0	0.0
218	Sami	TW	23.70	71.78	298.7	0.4	3.9
219	Wavadi	TW	23.92	72.52	144.9	1.6	1.0
220	Pilwai	TW	23.53	72.69	235.4	0.6	1.6
221	Pilwai	TW	23.54	72.68	152.4	0.7	1.3
222	Heduva	TW	23.57	72.34	266.7	0.8	2.3
223	Vaghpur	TW	23.68	73.42	85.8	1.0	1.4
224	Edla	TW	23.54	72.06	288.7	0.7	2.6
225	Sherisa	TW	23.20	72.48	232.3	1.1	1.7
312	Diyodar	TW	24.10	71.74	207.3	0.7	1.8
313	Diyodar	TW	24.10	71.74	207.3	0.6	4.1
314	Tharad	TW	24.41	71.64	201.2	0.3	2.4
316	Agathala	TW	24.29	71.88	137.2	1.0	1.8
317	Sujanipur	TW	23.89	72.11	91.4	2.0	9.5
318	Sujanipur	TW	23.90	72.12	326.1	0.9	3.6
319	Sujanipur	TW	23.91	72.12	39.6	3.1	5.3
320	Kuwarva	TW	24.04	71.90	186.6	1.7	1.9
321	Kharia	TW	23.94	71.83	158.5	2.3	1.0
322	Sami	TW	23.70	71.78	298.7	0.3	4.7
323	Hedva	TW	23.57	72.34	82.3	0.8	3.1
324	Kuder	TW	23.70	71.87	262.1	2.9	2.5
325	Patan	TW	23.84	72.11	198.1	3.1	2.0
326	Patan	TW	23.84	72.11	129.5	3.5	1.8
327	Patan	TW	23.84	72.11	60.0	2.1	3.4
328	Jitoda	TW	23.74	72.15	312.7	1.6	3.3

Table 4.2 continues

CBGW No.	Location name	Well type	Lat. (°N)	Long. (°E)	Depth bgl (m)	Fluoride (ppm)	EC (mS)
329	Jitoda	TW	23.74	72.15	448.1	0.7	4.3
330	Kamboi	TW	23.67	72.02	213.4	1.2	2.8
331	Muthia	TW	23.09	72.69	141.7	1.7	1.4
332	Paliya	TW	23.18	72.83	118.9	0.8	1.6
333	Punsari	TW	23.39	73.10	32.3	0.6	0.7
334	Dalani Muwadi	TW	23.36	72.88	91.4	0.8	1.6
335	Rojad	HP	23.35	73.09	28.7	0.6	1.7
336	Vadrad	TW	23.42	72.89	57.9	1.4	1.6
337	Tejpur	TW	23.39	72.81	160.0	0.7	1.7
338	Navalpur	TW	23.60	72.90	121.9	0.8	1.5
339	Dhanap	TW	23.26	72.75	167.6	1.3	1.7
340	Indroda Park	TW	23.19	72.65	106.7	1.0	1.2
341	Rupawati	TW	23.00	72.30	213.4	0.8	2.1
342	Sokali	TW	23.10	72.11	93.0	2.0	4.6
343	Dulapur	TW	23.02	71.58	61.0	1.8	3.5
355	Salajada	TW	22.80	72.39	168.0	0.6	2.3
356	Salajada	TW	22.79	72.39	198.4	0.6	2.3
357	Salajada	TW	22.79	72.39	93.0	1.6	4.9
358	Gundi	TA	22.55	72.23	289.6	0.3	4.1
359	Shiyal	TW	22.68	72.16	274.3	0.2	4.6
360	Padgol	TW	22.59	72.84	137.2	0.4	1.8
361	Morad	TW	22.54	72.86	91.4	0.3	1.2
362	Gumadia	TW	22.76	73.23	48.8	0.7	1.3
363	Kund-9	TS	22.80	73.46	1.0	3.0	7.2
364	Kund-13	TS	22.80	73.46	1.0	3.2	7.4
365	Kund-20	TS	22.80	73.46	1.0	3.1	7.1
366	Kund-28	TS	22.80	73.46	1.0	3.5	8.0
367	Dholera	TA	22.25	72.19	168.0	0.3	7.2

It is seen (Figure 4.5) that pockets of high groundwater fluoride concentration in NGC region are approximately aligned around four linear belts marked PP', QQ', RR' and SS'. The pockets of very high fluoride concentration values (4 to 8 ppm) are aligned around PP' linking LRK-NS-GC, roughly in the North-South direction. To the east of PP', there is another linear belt around QQ' within the Cambay Basin with patches of high fluoride concentration values (1.5 to 4 ppm). On the eastern most part lies the linear belt around RR', almost in the recharge area in the Aravalli foothills and is roughly parallel to it, with several small and isolated pockets of fluoride concentration >1.5 ppm. The fourth linear belt of high fluoride concentration (4 to 8 ppm) is around SS', roughly in the East-West direction, linking the region of thermal springs of Tuwa and Lasundra in the east to the Nalsarovar in the west.

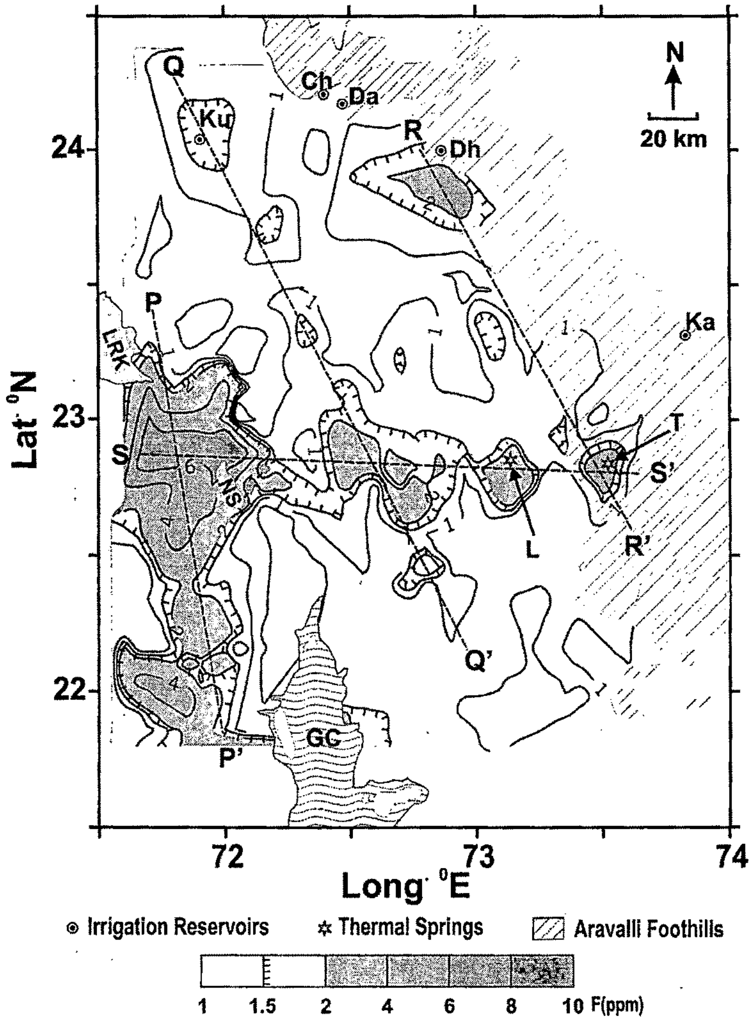

Figure 4.5 Isoline map of the fluoride concentration in groundwater – NGC region. Patches of high fluoride concentration (>1.5 ppm) appear to be aligned around four lines (PP', QQ', RR' and SS') separated by areas with low fluoride. Acronyms: Ch –Chadotar; Ku –Kuwarva; Da –Dantiwada; Dh –Dharoi; Ka –Kadana; L –Lasundra; T –Tuwa.

Figure 4.6(a) shows depth below ground level (bgl) of the sampled wells vs. fluoride concentration in groundwater in the NGC region. Very high fluoride concentrations are found even in shallow (depth <20 m) wells in some locations and low concentrations are found in very deep (depth >300 m) wells in other locations in the region. In some other locations inverse relationship is also observed. A similar plot using the same dataset but only taking samples with fluoride concentration >1.5 ppm is shown in Figure 4.6(b). Samples belonging to aquifers from different parts of the study area, namely, (i) along LRK-NS-GC tract, (ii) on the flanks of the Cambay Basin, and (iii) within Cambay Basin, are also identified in Figure 4.6(b).

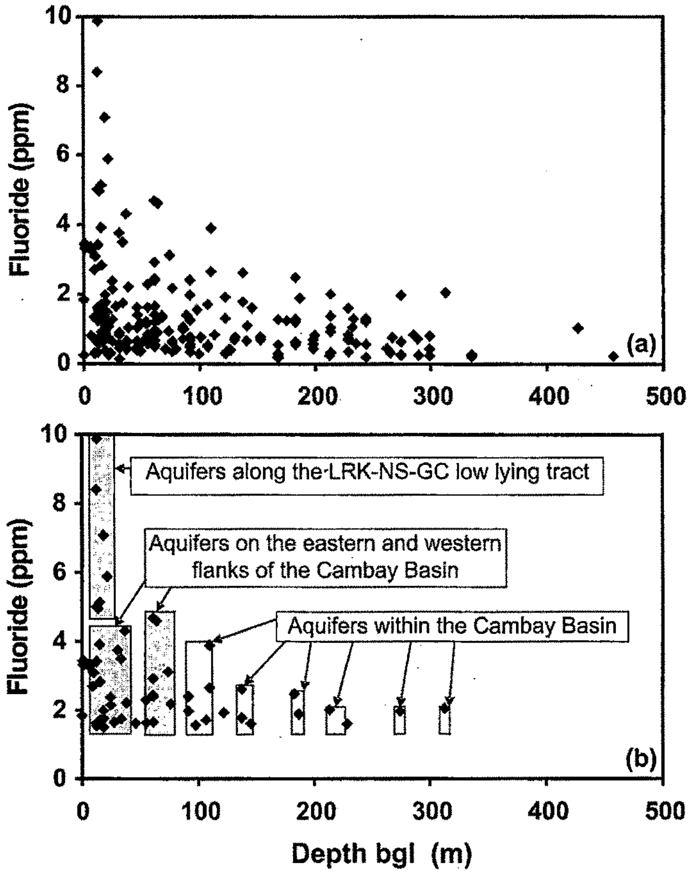

Figure 4.6 (a) Depth of sampled wells (bgl) vs. fluoride concentration for all sampled wells. (b) Samples with fluoride concentration <1.5 ppm area removed from plot (a). Several aquifer depth zones with >1.5ppm groundwater fluoride are identified within the Cambay basin.

Most fluoride-rich ground waters from the depth zone up to 40 m occur on the west flank of Cambay Basin where aquifers comprise either fluvio-marine sediments deposited in the LRK-NS-GC tract or Mesozoic sandstones farther west. Tubewells shallower than ~40 m and showing fluoride concentration <1.5 ppm are mainly located on the east flank of Cambay Basin. Tubewells tapping the depth zones of 53-76 m and yielding groundwater with fluoride concentration >1.5 ppm are located on both east and west flanks of the Cambay Basin. All fluoride rich tubewells with depth ranging from 90 m to ~310 m are located within the Cambay Basin. It is also noted that in the Cambay Basin fluoride rich groundwater is limited only to certain depth zones. It is possible, to identify six fluoride rich sub-aquifer depth zones (Table 4.3) within the Cambay Basin.

Table 4.3 Sub-aquifer depth zones having high fluoride in the Cambay Basin.

Zone	Depth range (m)	Zone	Depth range (m)
I	90-110	IV	210-230
II	135-145	V	~275
III	180-190	VI	~310

Identifying these fluoride rich sub-aquifer depth zones, based on groundwater fluoride concentration in samples across a large area within Cambay Basin, has an inherent assumption of the continuity of these sub-aquifers at approximately the same depth (bgl) throughout the Cambay Basin. This assumption seems reasonabe considering the subsurface lithological cross-section (Figure 1.6), wherein it is seen that at a particular depth (bgl) generally the same sub-aquifer is encountered at different locations along the profile within the Cambay Basin. This is also seen in several other cross sections drawn across the Cambay Basin by the GWRDC (unpublished data). It seemed possible that if these fluoride rich sub-aquifers are tapped by a particular tubewell (which may also be tapping other sub-aquifers), the fluoride concentration in the overall groundwater pumped from this tubewell may be relatively higher.

To verify the above possibility, a tubewell (marked A in Figure 4.7) in Chadotar village outside the Cambay Basin and four other tubewells in the vicinity of each other (marked B to E) in Kuwarva village (~50 km away from Chadotar) within the Cambay Basin were examined for any correlation between fluoride content in groundwater from these tubewells and fluoride rich sub-aquifers tapped (see Figure 4.5 for locations of these villages). The fluoride concentration in groundwater from these tubewells, the depth (bgl) of sampled well and the fluoride rich sub-aquifer depth zones (see Table 4.3) tapped by these tubewells are shown in Figure 4.7. It is seen that the shallowest (63 m) Tubewell – A at Chadotar does not tap any of the fluoride rich sub-aquifers and has a low fluoride content of 0.9 ppm. The Tubewell-B, tapping fluoride rich sub-aquifer Zone–I and Zone–II, has the highest fluoride concentration of 2.2 ppm. Tubewell – C taps only fluoride rich sub-aquifer Zone–I and its fluoride content is 1.9 ppm. Tubewell – D tapping three fluoride rich sub-aquifer Zones (I, II and III) has groundwater fluoride concentration of 1.9 ppm. The deepest Tubewell-E (185 m) tapping only a small part of fluoride rich zone–I and two other fluoride rich Zones (II and III) has fluoride content of 1.5 ppm. It is thus seen that Tubewell (A), not tapping any of the high fluoride sub-aquifers has the lowest fluoride content. Tubewells tapping any of the fluoride rich sub-aquifer depth zones, in general, have higher fluoride content.

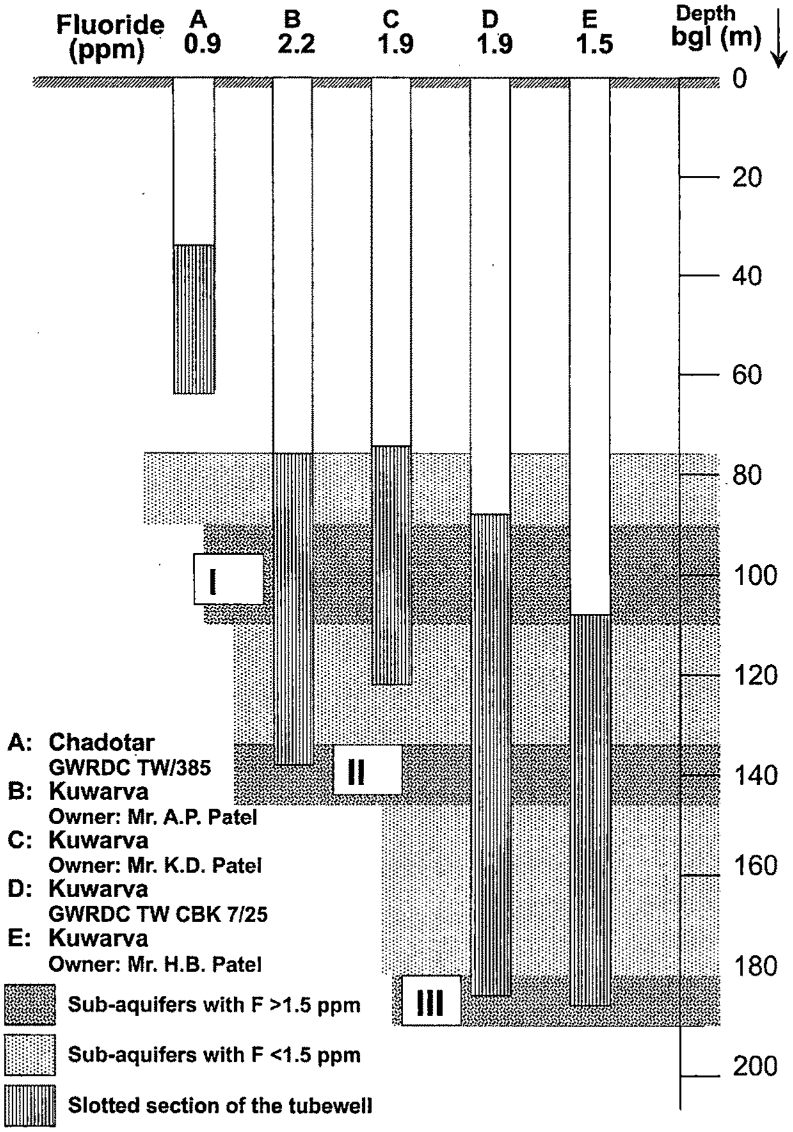

Figure 4.7 A comparison of groundwater fluoride content and fluoride rich sub-aquifer depth zones tapped in selected five tubewells. The shallowest tubewell–A does not tap any of the fluoride rich sub-aquifer depth zones and has the lowest fluoride content in groundwater. Tubewell–B, tapping zones I and II, has the highest fluoride in groundwater. The deepest tubewell E, which taps sub-aquifers from depth zones –II and –III but does not tap zone–I, has comparatively lower fluoride content of 1.5 ppm.

However, due to limited number of available tubewells providing suitable conditions (such as at Chadotar and Kuwarva) for verification, the possibility that certain depth zones in the Cambay Basin largely contribute groundwater rich in fluoride, could not be substantiated further in the present study.

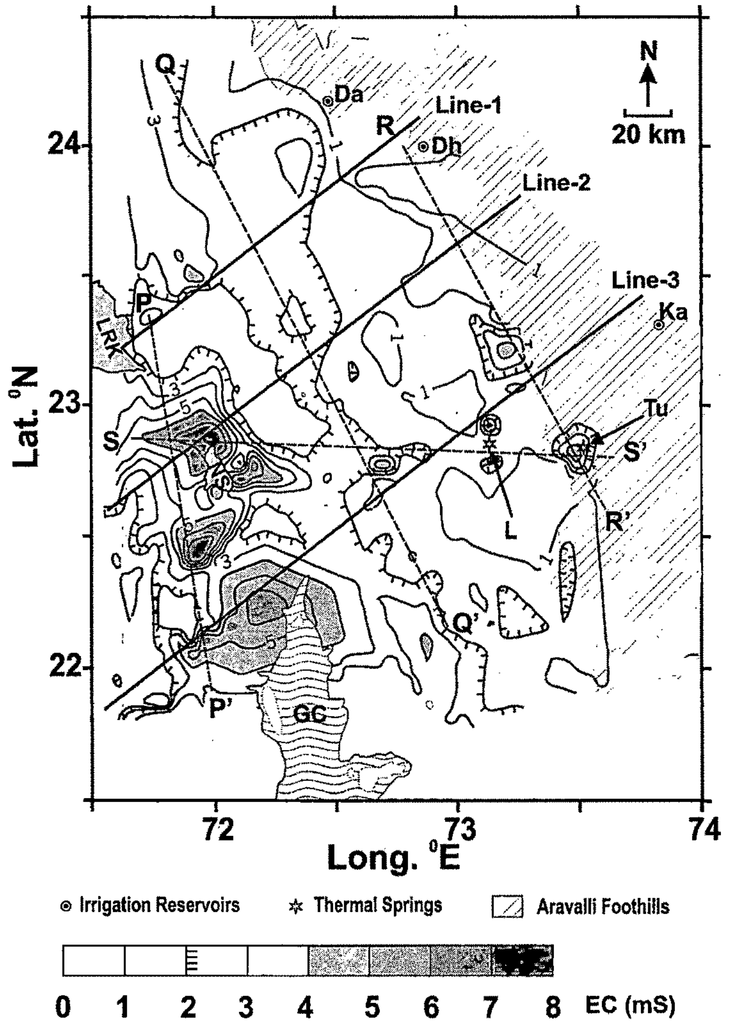

Figure 4.8 Isoline map of EC of groundwater from study area. Areas of high EC overlap in general with areas of high fluoride shown in Fig. 4.5. Acronyms for the locations are: Da –Dantiwada; Dh –Dharoi; Ka –Kadana; L –Lasundra; T –Tuwa. The geographical co-variation of EC and fluoride along Lines 1-3 and SS' is shown in Figure 4.9

4.1.3 Groundwater Electrical Conductivity

An isoline map of Electrical Conductivity (EC) of groundwater samples from the NGC region is shown in Figure 4.8 . Details of sampling locations and values of EC are given in Table 4.2. The EC values range from 0.3 to 8 mS, with values >5 mS in the LRK-NS-GC belt and the lowest values in isolated pockets along the Aravalli foothills. In general, areas with high EC overlap with those having high fluoride concentration (Figure 4.5). However, a pocket of high EC (>3 mS) in the NW part of the study area has low fluoride concentration (<1.5 ppm). Another pocket of EC ~1 mS, around 24^0N in the Aravalli foothills, on the other hand, has high fluoride concentration (>1.5 ppm). In spite of these differences, it can be seen from Figure 4.8 that high EC regions are approximately aligned around the same lines PP', QQ', RR', SS' that show high fluoride concentrations around them. The central (QQ') belt of both high fluoride concentration and EC is flanked on either side by belts of relatively lower values.

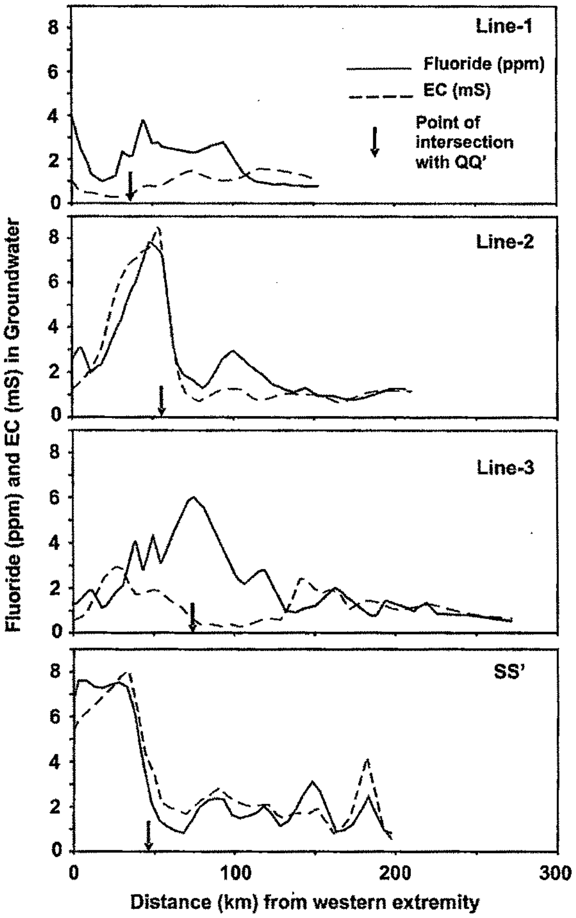

Figure 4.9 Geographical co-variation of fluoride and EC of groundwater along the four lines (1, 2, 3 and SS' in Figure 4.8) in NGC region. Distances are measured from the western end of each line and the arrow marks the point of intersection of each of these lines with QQ'. It is seen that the two parameters co-vary in the Cambay basin and the central belt of high fluoride – high EC is flanked by relatively lower values on either side.

With a view to observe the geographical co-variation of EC and fluoride concentration more clearly, their variation along four lines (Line-1, Line-2, Line-3 and the line SS' in Figure 4.8) is shown in Figure 4.9. The EC and fluoride concentrations at a particular point are plotted against the distance of that point from the western end of respective lines. Since these four lines intersect the line QQ', the point of intersection of these lines with QQ' is used as a reference point and marked in Figure 4.9 to compare the relative variation in EC and fluoride at a particular distance along these lines.

Whereas the two parameters appear to generally co-vary, a westward displacement of the high EC region relative to high fluoride region is seen along the Line-3.

Although geographical coincidence of areas having high fluoride concentrations with those having high EC in groundwater is visible from Figure 4.5 and Figure 4.8, no statistical correlation between these two is seen in the scatter plot (Figure 4.10) for the entire NGC region.

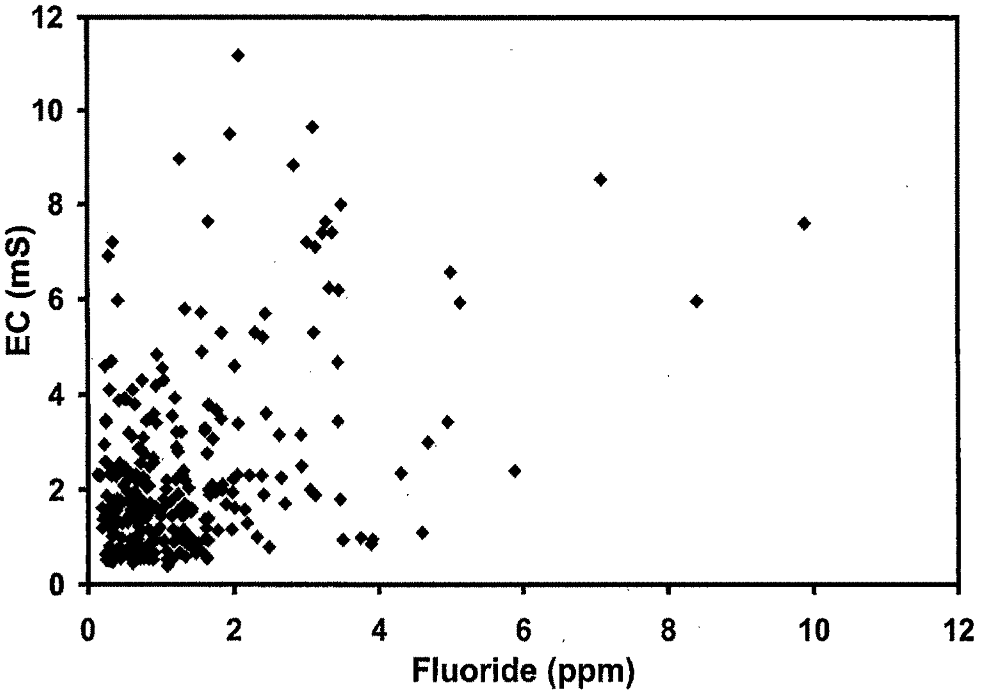

Figure 4.10 A scatter plot of fluoride concentration vs. EC in groundwater from the NGC region, showing absence of correlation between the two.

4.1.4 Fluoride and EC in Modern Precipitation

With a view to have an idea about ionic concentration in modern precipitation, dissolved fluoride and EC were measured in fortnightly accumulated precipitation samples collected at six dam sites (Dantiwada, Dharoi, Kadana, Shetrunji, Bhadar and Ukai; see Figure 4.14) located in and around the NGC region. The variation in rainfall, fluoride and EC in each fortnightly accumulated precipitation samples is shown in Figure 4.11 (for Dantiwada, Dharoi and Kadana) and Figure 4.12 (for Bhadar, Shetrunji and Ukai). It is seen that variations in both fluoride concentration and EC of successive fortnightly accumulated precipitation samples are nearly proportional, except for Ukai. The slopes (Figure 4.13) and intercepts of the best fit lines are, however, location dependent. It is also seen from Figure 4.11 and Figure 4.12 that variations in fluoride and EC are not related to variation in the local rainfall amount. Samples with relatively higher fortnightly rainfall do not necessarily have relatively lower fluoride and EC and vice versa. Precipitation samples from Dantiwada and Dharoi, located in the semi- arid parts of NGC region, have a distinctly higher range of fluoride and EC compared to other locations which are relatively less arid.

The highest and the average fluoride content at these stations as well as their relative latitudinal positions with reference to NGC region are shown in Figure 4.14. It is seen that Dantiwada, with highest aridity amongst these stations, has the highest fluoride levels in precipitation. The range, the highest value and the seasonal average of both fluoride and EC in precipitation from NGC region decreases with decreasing aridity southwards (see Figure 4.11 and Figure 4.12).

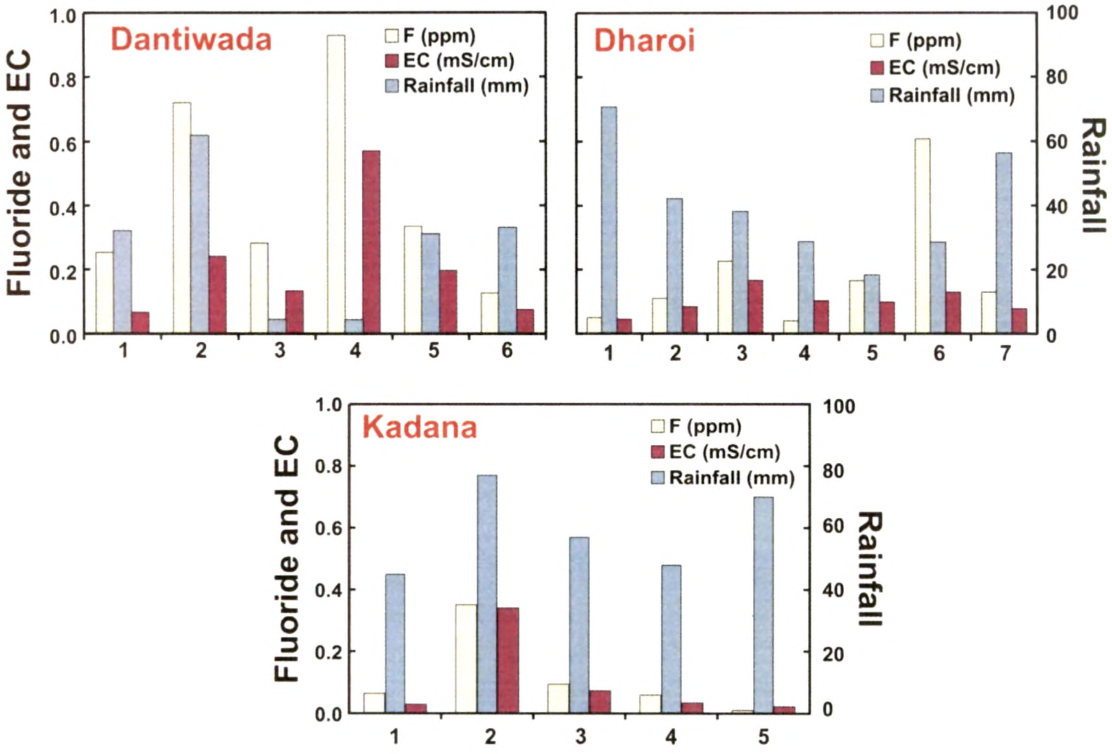

Figure 4.11 Variation in the amount of rainfall, dissolved fluoride and EC in the fortnightly accumulated precipitation samples at the dam sites of Dantiwada, Dharoi and Kadana. The locations of these dam sites within NGC region are shown in Figure 4.8.

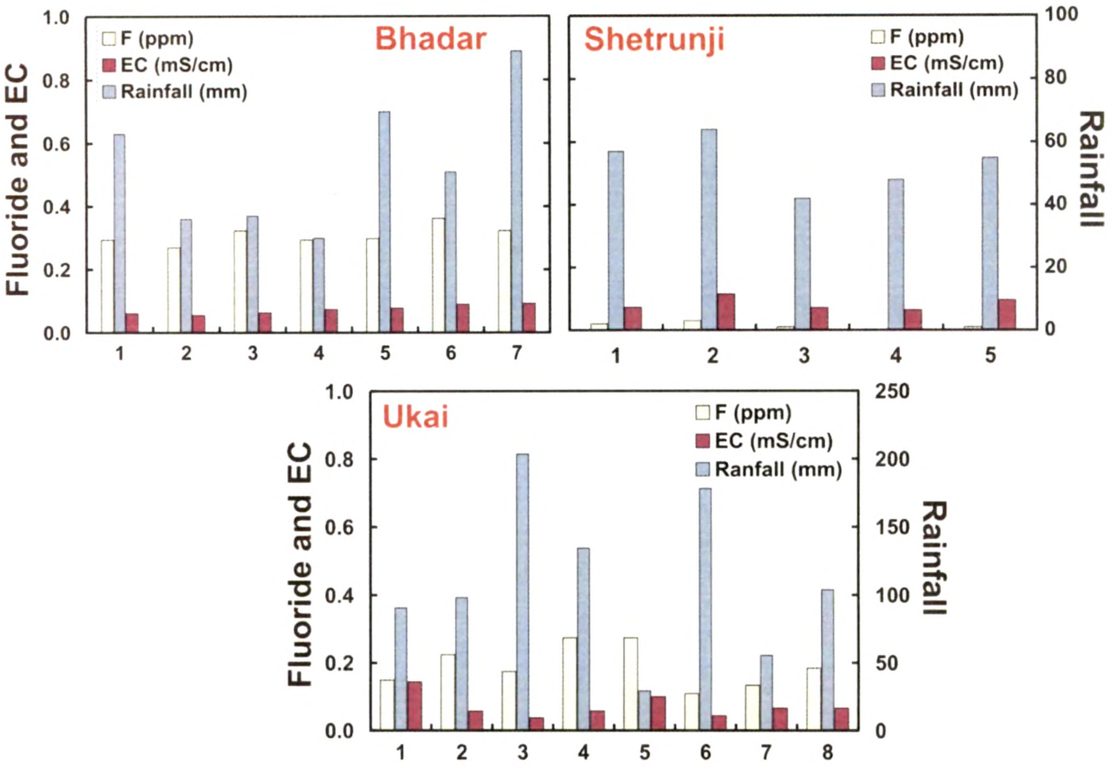

Figure 4.12 Variation in the amount of rainfall, dissolved fluoride and EC in the fortnightly accumulated precipitation samples at the dam sites of Bhadar, Shetrunji and Ukai. The locations of these dam sites are shown in Figure 4.14.

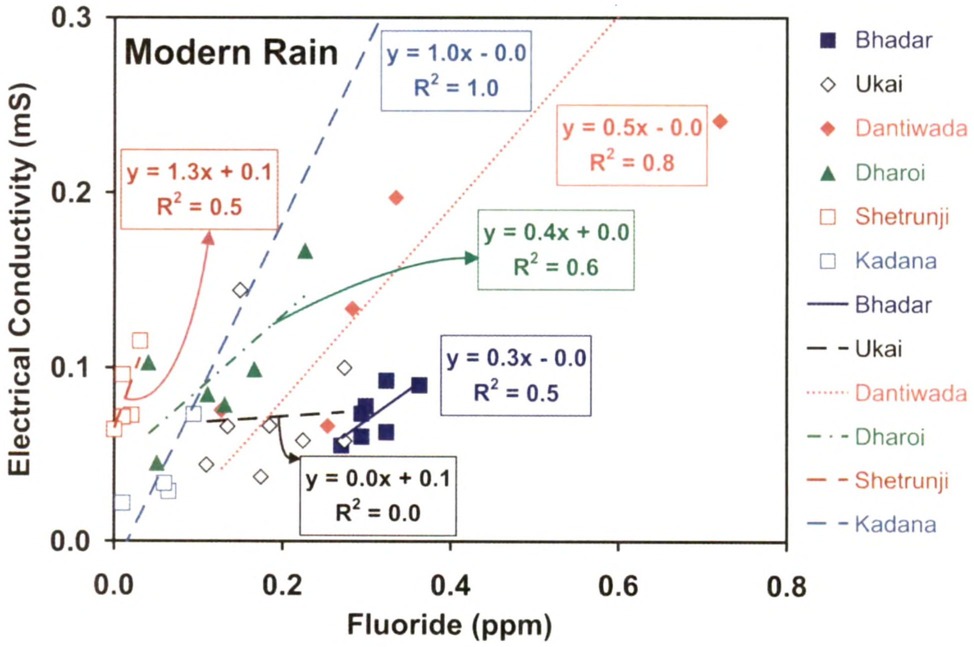

Figure 4.13 Relationship between dissolved fluoride and EC in modern rainwater collected at the six dam sites in and around NGC region.

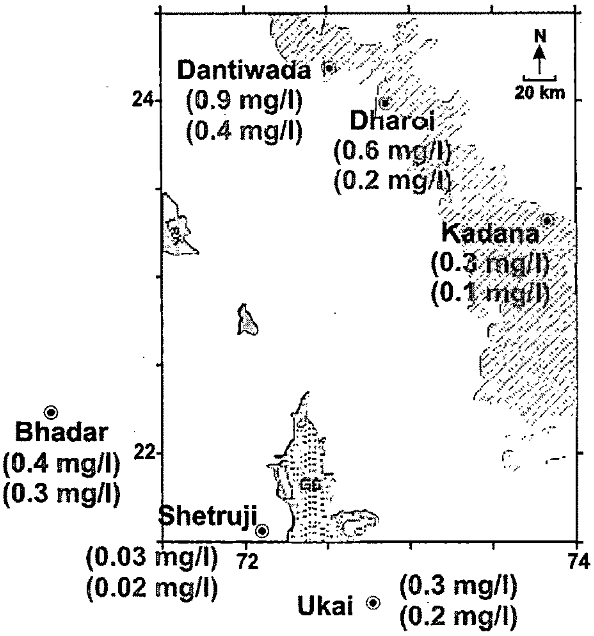

Figure 4.14 The highest and the average fluoride content at various dam sites and their relative latitudinal positions with reference to the NGC region.

4.1.5 Stable Isotopes of Oxygen and Hydrogen

Details of the (i) sampled well locations; (ii) location names; (iii) well type; (iv) measured values $\delta^{18}O$, δD; and the (v) calculated values of *d*-excess for groundwater from NGC region are given in Table 4.4. Similar details for precipitation samples are given in Table 4.5. Plots of $\delta^{18}O$ vs. δD, and $\delta^{18}O$ vs. *d*-excess for ground water and fortnightly precipitation samples from NGC region are shown in Figure 4.15.

Table 4.4 Details of groundwater sampling sites together with measured values of $\delta^{18}O$, δD and *d*-excess in the NGC region. (TW = tubewell; DCB= dug cum bore; DW = dug well; HP = hand pump; TA = thermal artesian; TS = thermal spring; bgl = below ground level; CBGW = Cambay Basin Ground Water)

CBGW Sample No.	Location name	Well type	Lat. (°N)	Long. (°E)	Depth bgl (m)	$\delta^{18}O$ (‰)	δD (‰)	*d*-excess (‰)
9	Lasundra	DW	22.91	73.14	6.1	-1.08	-17.5	-8.9
15	Lasundra	TW	22.92	73.15	85.3	-1.80	-18.3	-3.9
32	Adalaj	TW	23.17	72.58	228.6	-2.96	-26.4	-2.7
40	Kalak	DCB	22.02	72.76	21.3	-1.67	-15.0	-1.7
43	Manglej	TW	22.09	73.17	76.2	-1.68	-13.0	0.5
45	Dholera	TA	22.25	72.19	167.6	-1.96	-26.8	-11.1

Table 4.4 continues

CBGW Sample No.	Location name	Well type	Lat. (°N)	Long. (°E)	Depth bgl (m)	δ^{18}O (‰)	δD (‰)	*d*-excess (‰)
53	Bagodra	TA	22.64	72.20	335.3	-0.77	-24.6	-18.4
55	Gundi	TA	22.55	72.23	289.6	-2.97	-26.1	-2.3
56	Batod	HP	22.16	71.66	36.6	-1.61	-19.6	-6.8
58	Vejalka	DCB	22.40	71.72	53.3	-1.35	-16.6	-5.8
65	Shiyala	TA	22.70	72.16	274.3	-1.97	-24.4	-8.6
66	Ruhika	TA	22.66	72.23	457.2	-2.36	-25.8	-6.9
67	Sarala	TA	22.67	72.20	274.3	-1.91	-25.6	-10.3
76	Sarkhej	TW	22.99	72.49	91.4	-3.08	-25.3	-0.7
89	Sachana	TW	23.08	72.16	213.4	-2.08	-23.9	-7.3
98	Dhanap	TW	23.26	72.75	213.4	-3.14	-26.8	-1.7
99	Majara	TW	23.36	72.80	121.9	-2.69	-23.9	-2.4
100	Talod	TW	23.35	72.93	45.7	-2.92	-24.1	-0.8
102	Vadagam	HP	23.33	73.17	9.1	-2.26	-23.0	-5.0
104	Dhamanya	HP	23.34	73.25	30.5	-2.34	-22.4	-3.7
109	Vasvelia	TW	23.00	72.04	167.6	-3.31	-26.2	0.2
112	Zainabad	TW	23.26	71.68	213.4	-3.52	-26.5	1.7
114	Zinzuvada	TW	23.35	71.65	198.1	-3.15	-16.7	8.5
115	Zinzuvada	HP	23.35	71.66	15.2	-0.45	-14.9	-11.3
120	Zinzawadar	TW	22.45	71.69	285.0	-3.06	-26.6	-2.2
122	Chuda	TW	22.49	71.69	182.9	-0.73	-20.0	-14.1
124	Fulgam Jn	HP	22.54	71.54	54.9	-2.35	-21.7	-2.9
125	Shekhpur	TW	22.70	71.56	54.9	-0.88	-20.7	-13.7
126	Vana	HP	22.87	71.71	12.2	-1.42	-19.6	-8.2
132	Paliyad	HP	22.25	71.56	45.7	-0.38	-13.0	-9.9
135	Tatam	TW	22.06	71.62	64.0	-1.66	-19.1	-5.8
141	Porda	DCB	22.92	73.00	67.1	-2.89	-23.1	0.0
147	Sarangpur	HP	22.16	71.77	61.0	-0.51	-11.2	-7.2
149	Panavi	TW	22.08	71.89	125.3	-2.38	-23.1	-4.0
151	Vaya	DW	22.20	71.87	30.5	-2.19	-18.4	-0.9
153	Devthal	TW	22.76	72.12	274.3	-2.59	-26.0	-5.3
155	Sokhada	TW	22.74	72.68	97.5	-2.68	-21.6	-0.1
159	Bharel	TW	22.41	72.83	61.0	-1.65	-18.3	-5.1
161	Anand	TW	22.53	72.96	45.7	-2.44	-21.6	-2.1
179	Karjan	TW	22.05	73.12	106.7	-1.50	-15.5	-3.5
185	Mandwa	TW	22.01	73.43	45.7	-2.00	-13.5	2.5
186	Chandod	TW	22.99	73.46	121.9	-2.10	-16.3	0.5
208	Maniyor	TW	23.82	72.96	73.9	-3.25	-21.6	4.4
209	Dharewada	TW	23.98	72.39	212.3	-3.94	-27.9	3.7
210	Ganguva	TW	24.16	72.73	85.5	-3.42	-28.9	-1.5
211	Chadotar	TW	24.21	72.39	63.4	-1.99	-29.9	-14.1
213	Kuwarva	TW	24.04	71.90	186.6	-4.08	-30.1	2.5
214	Kuwarva	TW	24.05	71.90	121.9	-2.84	-30.1	-7.3
215	Tharad	TW	24.41	71.64	299.1	-2.72	-28.2	-6.5

Table 4.4 continues

CBGW Sample No.	**Location name**	**Well type**	**Lat. (°N)**	**Long. (°E)**	**Depth bgl (m)**	**$\delta^{18}O$ (‰)**	**δD (‰)**	***d*-excess (‰)**
216	Jitoda	TW	23.74	72.15	312.7	-1.38	-22.3	-11.3
218	Sami	TW	23.70	71.78	298.7	-3.16	-26.2	-1.0
220	Pilwai	TW	23.53	72.69	235.4	-3.16	-23.7	1.6
223	Vaghpur	TW	23.68	73.42	85.8	-3.30	-25.9	0.5
224	Edla	TW	23.54	72.06	288.7	-2.10	-24.8	-8.0
312	Diyodar	TW	24.10	71.74	207.3	-3.60	-24.2	4.6
313	Diyodar	TW	24.10	71.74	207.3	-3.58	-25.3	3.4
314	Tharad	TW	24.41	71.64	201.2	-0.89	-24.9	-17.8
316	Agathala	TW	24.29	71.88	137.2	0.50	-33.3	-37.3
317	Sujanipur	TW	23.89	72.11	91.4	-1.72	-24.1	-10.3
318	Sujanipur	TW	23.90	72.12	326.1	-3.28	-23.9	2.3
319	Sujanipur	TW	23.91	72.12	39.6	-3.63	-29.2	-0.2
320	Kuwarva	TW	24.04	71.90	186.6	4.46	-28.2	-63.9
321	Kharia	TW	23.94	71.83	158.5	-3.28	-32.5	-6.3
322	Sami	TW	23.70	71.78	298.7	-3.34	-24.0	2.8
323	Hedva	TW	23.57	72.34	82.3	-3.14	-21.6	3.5
324	Kuder	TW	23.70	71.87	262.1	0.25	-23.1	-25.1
325	Patan	TW	23.84	72.11	198.1	-3.11	-23.0	1.9
326	Patan	TW	23.84	72.11	129.5	-2.90	-22.1	1.1
327	Patan	TW	23.84	72.11	60.0	-1.45	-23.5	-11.9
328	Jitoda	TW	23.74	72.15	312.7	-2.48	-20.5	-0.6
329	Jitoda	TW	23.74	72.15	448.1	-2.79	-13.6	8.8
330	Kamboi	TW	23.67	72.02	213.4	-2.97	-15.6	8.1
331	Muthia	TW	23.09	72.69	141.7	-3.08	-20.6	4.1
332	Paliya	TW	23.18	72.83	118.9	-2.82	-21.5	1.0
333	Punsari	TW	23.39	73.10	32.3	-3.58	-25.5	3.1
334	Dalani Muwadi	TW	23.36	72.88	91.4	-3.47	-24.6	3.1
335	Rojad	HP	23.35	73.09	28.7	-0.70	-22.1	-16.5
336	Vadrad	TW	23.42	72.89	57.9	-2.98	-25.2	-1.4
337	Tejpur	TW	23.39	72.81	160.0	0.12	-23.2	-24.2
338	Navalpur	TW	23.60	72.90	121.9	-2.81	-21.8	0.7
339	Dhanap	TW	23.26	72.75	167.6	-3.11	-23.3	1.5
340	Indroda Park	TW	23.19	72.65	106.7	-1.79	-23.0	-8.7
341	Rupawati	TW	23.00	72.30	213.4	3.21	-24.4	-50.1
342	Sokali	TW	23.10	72.11	93.0	-2.60	-24.2	-3.4
343	Dulapur	TW	23.02	71.58	61.0	-3.13	-23.0	2.0
355	Salajada	TW	22.80	72.39		-3.32	-23.2	3.4
356	Salajada	TW	22.79	72.39	198.4	-3.27	-22.9	3.3
357	Salajada	TW	22.79	72.39	93.0	-2.89	-19.9	3.2
358	Gundi	TA	22.55	72.23	289.6	-3.56	-25.2	3.3
359	Shiyal	TW	22.68	72.16	274.3	-3.45	-26.1	1.5
360	Padgol	TW	22.59	72.84	137.2	-3.07	-21.5	3.0

Table 4.4 continues

CBGW Sample No.	Location name	Well type	Lat. (°N)	Long. (°E)	Depth bgl (m)	$\delta^{18}O$ (‰)	δD (‰)	*d*-excess (‰)
361	Morad	TW	22.54	72.86	91.4	-2.76	-21.2	0.8
362	Gumadia	TW	22.76	73.23	48.8	-2.62	-21.0	-0.1
363	Tuwa	TS	22.80	73.46	1	-1.94	-14.8	0.7
364	Tuwa	TS	22.80	73.46	1	-1.34	-14.4	-3.7
365	Tuwa	TS	22.80	73.46	1	-1.45	-14.6	-3.0
366	Tuwa	TS	22.80	73.46	1	-0.86	-12.5	-5.6
367	Dholera	TA	22.25	72.19	168	-3.71	-27.4	2.3
Average of all groundwater samples						-1.2±1.3	-22± 5	-4.5 ± 11

Table 4.5 Details of rainwater sampling sites together with values of $\delta^{18}O$, δD and *d*-excess in the NGC region. (Da = Dantiwada; Dh = Dharoi; Un = Unjha).

Sample No.	Rain fall (mm)	$\delta^{18}O$ (‰)	δD (‰)	*d*-excess (‰)
Da-1	32.2	-4.04	-32.9	-0.6
Da-2	61.9	-0.45	-1.7	1.9
Da-3	4.5	-0.24	-1.1	0.8
Da-4	4.4	1.75	9.3	-4.7
Da-5	31.2	-4.02	-39.9	-7.7
Da-6	33.2	-9.49	-81.5	-5.6
Da-8	126.6	-3.59	-26.3	2.4
Da-9	11.1	0.06	3.0	2.5
Da-10	96.4	-3.92	-31.4	0.0
Da-11	6	0.97	2.2	-5.6
Da-14	15.1	-2.66	-54.8	-33.5
Da-15	203.1	-7.05	-46.9	9.5
Da-17	100.5	-4.02	-29.4	2.7
Dh-1	70.8	-2.72	-20.9	0.9
Dh-2	42.2	-1.10	-3.6	5.3
Dh-3	38.2	-0.81	-5.7	0.7
Dh-4	28.8	0.81	4.8	-1.7
Dh-5	18.4	1.08	7.5	-1.1
Dh-6	28.6	-6.04	-46.1	2.2
Dh-18	145	-7.36	-57.7	1.2
Dh-19	620	-4.10	-32.4	0.4
Dh-20	56	-5.36	-46.5	-3.6
Amount weighted average		-4.3 ± 2.1	-33 ± 16	1.2 ± 4.8
Un-1	---	-3.51	-23.7	4.4
Un-2	---	-2.08	-17.5	-0.8
Un-3	---	1.08	-5.6	-14.3

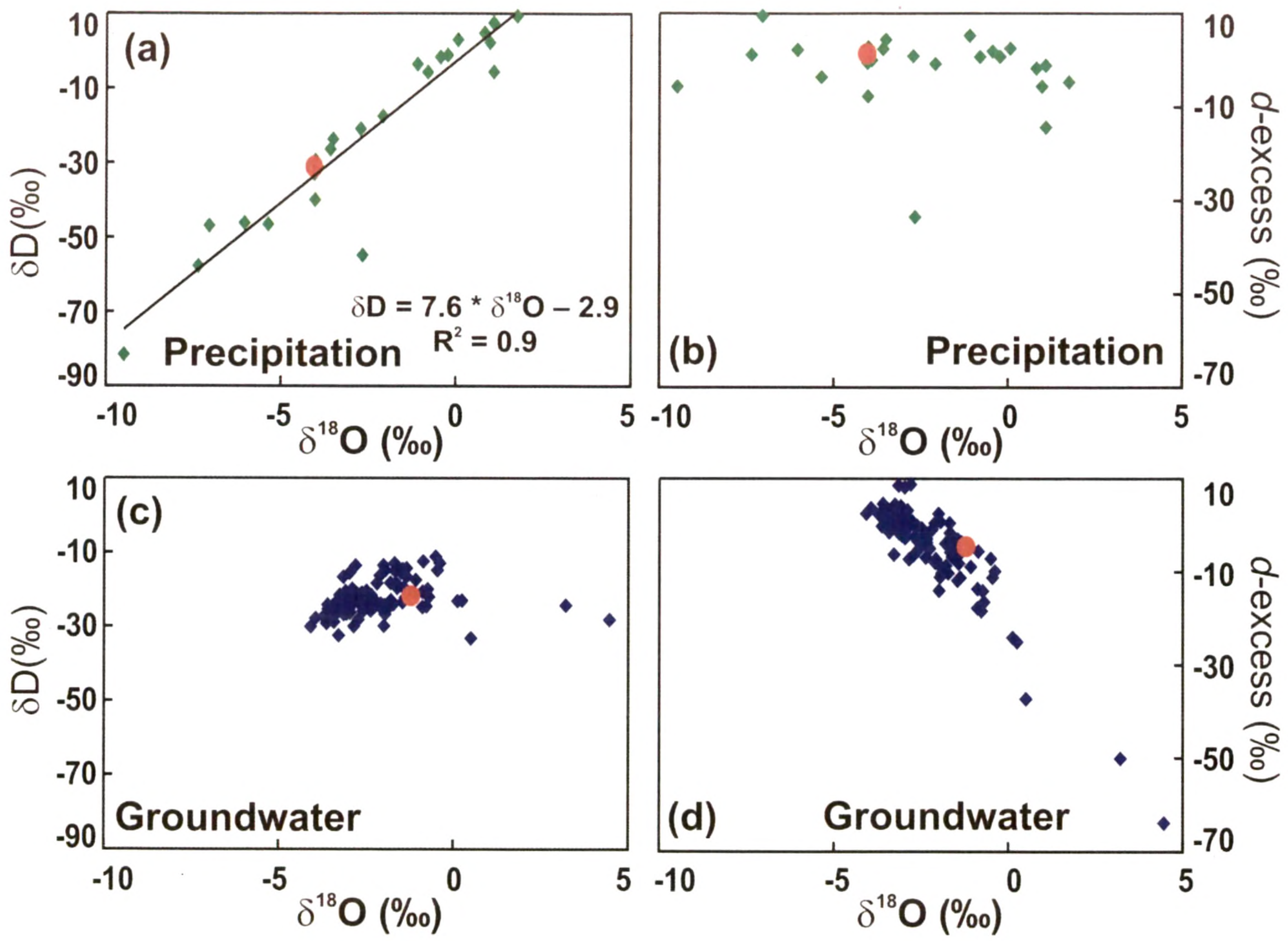

Figure 4.15 $\delta^{18}O$ vs. δD and $\delta^{18}O$ vs. *d*-excess for precipitation (a and b) and for groundwater samples (c and d). The average values for respective parameters in each figure are shown by big circle. In case of precipitation, the average value is amount weighted.

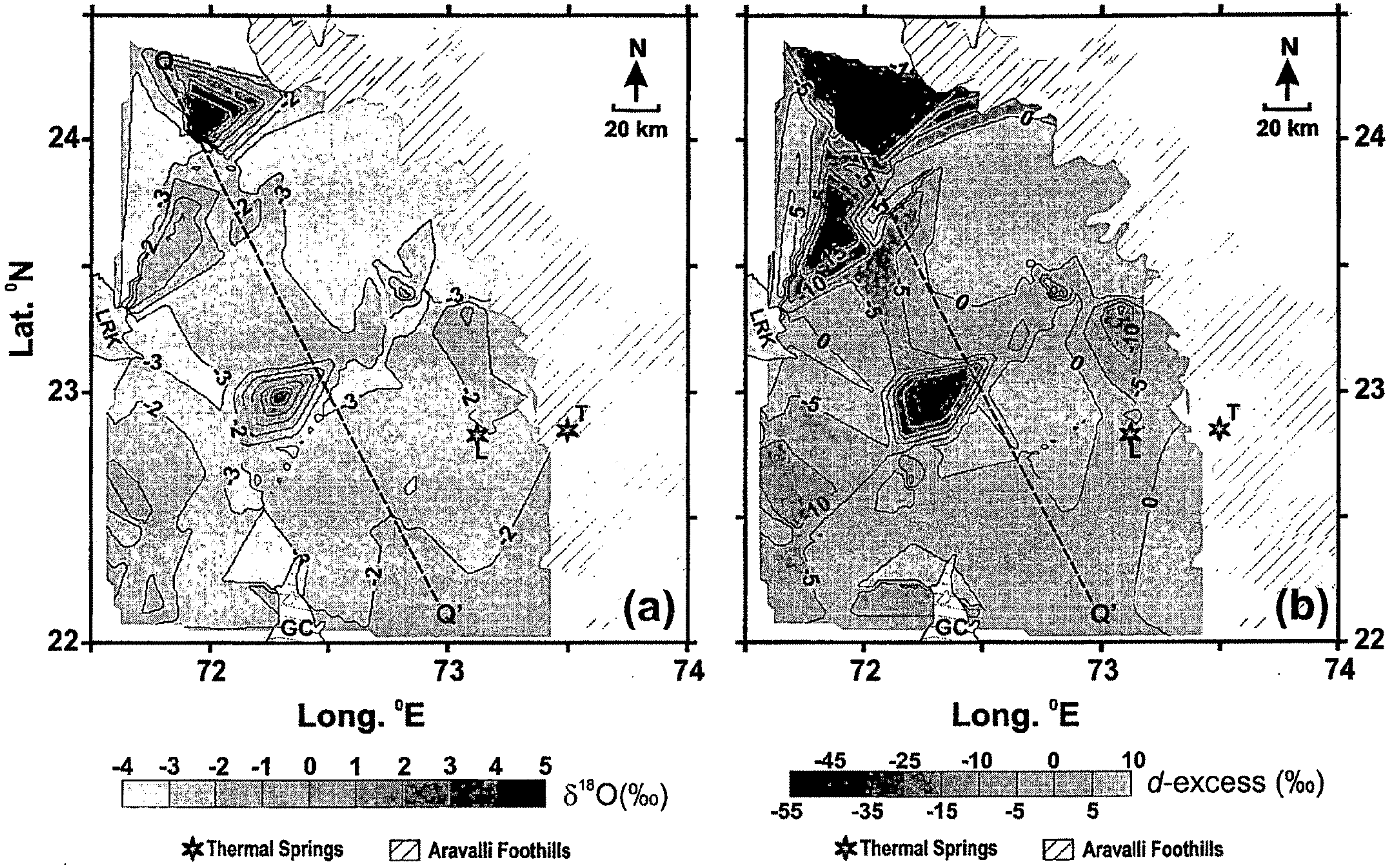

Figure 4.16 Isoline map of (a) δ^{18}O and (b) *d*-excess of groundwater from NGC region. Line QQ' representing the central linear belt of high fluoride (in Figure 4.5) and high EC (in Figure 4.8) is superposed for comparison.

The $\delta^{18}O$ and δD values of the fortnightly precipitation samples are linearly correlated (Figure 4.15a) and the regression line (LMWL) has a slope of (7.6 ± 0.6) with an intercept of (–2.9 ± 2.2‰). The amount weighted average values of $\delta^{18}O$ and δD for precipitation samples are –4.3 ± 2.1‰ and –33 ± 16‰ respectively. Using δ18O and δD values of each sample, d-excess values are calculated (= $\delta D - 8*\delta^{18}O$) and plotted against $\delta^{18}O$ in Figure 4.15b. The d-excess values of the precipitation samples lie between –10‰ and +10‰, except for two samples having d-excess value of –14‰ and –33‰. The amount weighted average d-excess value for precipitation samples is 1.2 ± 4.8‰.

A plot (Figure 4.15c) of $\delta^{18}O$ vs. δD for groundwater shows a cluster of data points and does not warrant further statistically meaningful analyses. Isotopic ratios of the groundwater samples have a narrow range of variation with average value of –1.2 ± 1.3‰ for $\delta^{18}O$ and –22 ± 5‰ for δD.

A plot of $\delta^{18}O$ vs. d-excess for groundwater samples (Figure 4.15d) shows a decrease in d-excess values with increase in $\delta^{18}O$. Unlike precipitation samples, several groundwater samples have d-excess values lower than –10‰. The average d-excess value of groundwater samples is –4.5 ± 11‰.

The geographical distributions of $\delta^{18}O$ and d-excess of groundwater in the NGC region are shown in Figure 4.16. It is seen from Figure 4.16a that in most part of the study area $\delta^{18}O$ values are < –3‰. There is, however, a prominent geographical belt with relatively higher $\delta^{18}O$ values (> –3‰). Several small regions with even higher values of $\delta^{18}O$ (>–2‰) are located within this belt. It is seen from Figure 4.16b that d-excess values of ground waters in large part of the NGC region are between 0 to 5‰. However, a prominent geographical belt with relatively lower d-excess (<0‰) is also seen. Several small regions with much lower d-excess values (<–15‰) are located within this broad belt. Line QQ' which marks the region of high fluoride (Figure 4.5) and high EC (Figure 4.8), is also superposed on Figure 4.16.

4.1.6 Groundwater Dating

Three different methods, namely ^{14}C, ^{4}He and $^{4}He/^{222}Rn$, were employed for estimating the age of ground waters in the study area. The estimated groundwater ages by each of these methods are described in the following.

Table 4.6 Details of the groundwater sampling sites together with measured values of $\delta^{13}C$, pmC, ^{14}C ages corrected for A_0 as well as un-corrected for A_0. (pmC = percentage modern carbon; TDIC = total dissolved inorganic carbon; bdl = below detection limit; A_0 = initial activity; CBGW = Cambay Basin Ground Water)

CBGW No.	**Location name**	**Lat. (°N)**	**Long. (°E)**	**$\delta^{13}C_{TDIC}$ (‰)**	**pmc**	**^{14}C ages (kaBP) [A_0 Uncorrected]**	**^{14}C ages (kaBP) [A_0 corrected]**
208	Maniyor	23.82	72.96	-10.78	115±1.1	modern	modern
209	Dharewada	23.98	72.39	-8.99	58±0.7	4.45±0.09	1.5±.0.14
210	Ganguva	24.16	72.73	-10.4	100±0.9	modern	modern
211	Chadotar	24.21	72.4	-8.62	99±0.9	modern	modern
212	Bhadath	24.34	72.2	-8.26	102±1.0	modern	modern
215	Tharad	24.41	71.64	-8.47	2.3±0.2	31.21±0.68	27.6±0.73
216	Jitoda	23.74	72.15	-7.26	35±0.5	8.63±0.12	3.9±0.16
218	Sami	23.7	71.78	-11.74	0.61±0.2	42.2±2.6	41.3±2.73
219	Wavadi	23.92	72.52	-9.56	90±1.0	0.92±0.09	modern
220	Pilwai	23.53	72.69	-11.56	22±0.4	12.53±0.14	11.5±0.17
222	Heduva	23.57	72.34	-9.17	37±0.5	8.19±0.1	5.3±0.14
223	Vaghpur	23.68	73.42	-11.34	81±0.8	1.73±0.08	0.6±0.11
224	Edla	23.54	72.06	-10.12	1.7±0.2	33.75±0.88	31.6±0.98
225	Sherisa	23.2	72.48	-9.47	50±0.6	5.75±0.1	3.1±0.13
320	Kuwarava	24.04	71.9	-8.81	2.8±0.3	29.64±0.97	26.3±0.90
331	Muthia	23.09	72.69	-8.6	68±0.8	3.15±0.1	modern
333	Punsari	23.39	73.1	-9.11	89±0.8	1.01±0.07	modern
336	Vadrad	23.42	72.89	-9.28	99±0.9	modern	modern
337	Tajpur	23.39	72.81	-11.6	68±0.7	3.25±0.08	2.2±0.11
341	Rupawati	23	72.3	-9.29	1.8±0.2	33.29±0.89	30.4±0.93
344	Gajanav	22.92	71.36	-9.75	80±0.7	1.82±0.08	modern
351	Navagam	22.62	71.18	-11.11	93±0.8	0.61±0.08	modern
355	Salajada	22.8	72.39	-8.23	9.5±0.2	19.5±0.21	15.7±0.20
358	Gundi	22.55	72.23	-21.36	b.d.l.	>45	>45
360	Padgol	22.59	72.84	-9.7	49±0.5	5.87±0.09	3.5±0.12
362	Gumadia	22.76	73.23	-8.94	84±0.8	1.47±0.08	modern
RC-1	PRL	23.04	72.54	-13	40±0.6	7.58±0.12	7.6±0.14

Initial activity A_0 (Un-corrected) = 100 % Modern;

Initial activity A_0 (corrected) $= \dfrac{\delta^{13}C_{TDIC}}{\delta^{13}C_{soil} - \varepsilon} 100$;

$\delta^{13}C_{soil} = -22‰$; $\varepsilon = -9‰$.

4.1.6.1 ^{14}C Dating

Details of the (i) sampled tubewell locations; and values of (ii) percentage modern carbon (pmC); (iii) $\delta^{13}C_{TDIC}$; (iv) ^{14}C ages un-corrected for initial activity (A_0) as well as (v) ^{14}C ages corrected for A_0, are given in Table 4.6 . The isoline map of radiocarbon ages is shown in Figure 4.17. It is seen that the groundwater ^{14}C ages progressively increase from <2 kaBP in the recharge area (foothills of Aravalli mountains) to a limiting value of >35 kaBP in the LRK-NS-GC tract. Within the Cambay Basin, ^{14}C age isolines are nearly parallel to each other and the horizontal distance between successive 5 kaBP isolines is nearly constant.

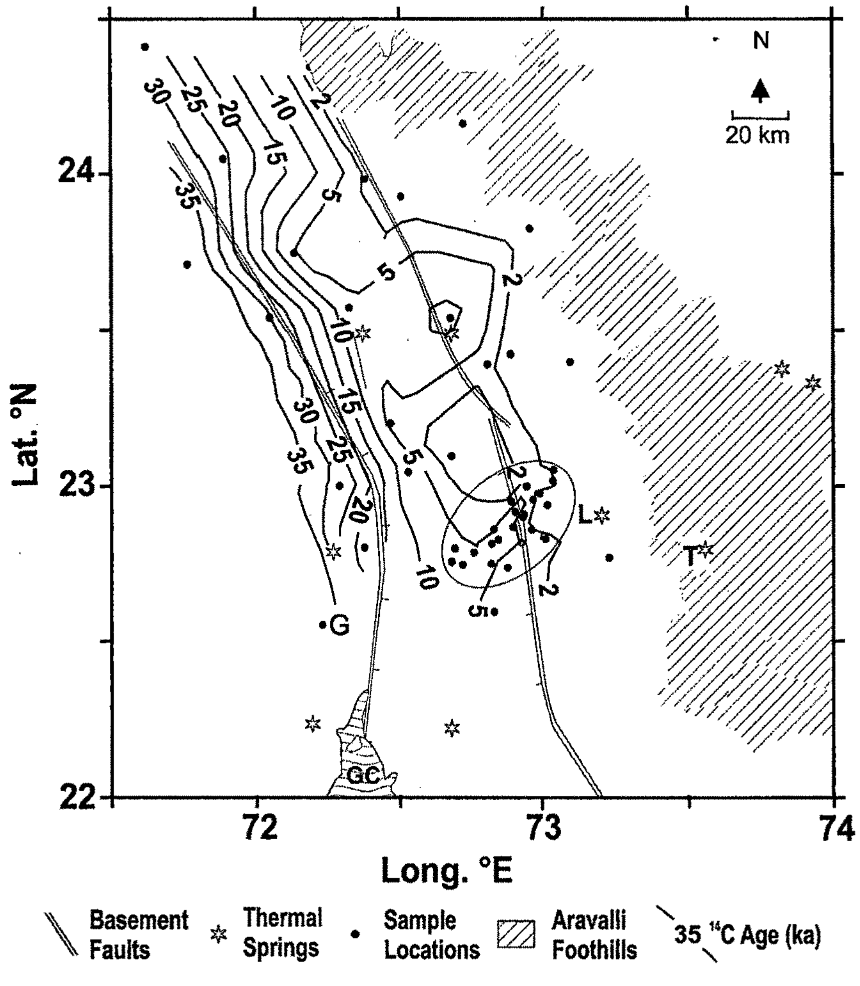

Figure 4.17 Isoline map of groundwater Radiocarbon ages, along with sampling locations. Sampling locations of an earlier study (Borole et al, 1979) are enclosed in an ellipse. Within the Cambay basin the groundwater ^{14}C ages increase progressively towards the WCBBF, beyond which a limiting ^{14}C age of >35 kaBP is observed. Dots indicate sampling locations. L, T and G respectively indicate the locations of thermal springs at Lasundra, Tuwa and a free flowing thermal artesian well at Gundi. The groundwater age gradient along BB' is shown in Figure 4.21.

4.1.6.2 ^{4}He Dating

The details of the (i) sampled well locations; and (ii) values of estimated ^{4}He ages for helium release factor (Λ_{He}) of 1 and 0.4 are given in Table 4.1. The isoline map of estimated ^{4}He ages of the groundwater in the NGC region is shown in Figure 4.18. The ^{4}He ages are calculated (see section 2.6.2) based on the measured concentration of Uranium (U = 1.07 ppm) and Thorium (Th = 7.54 ppm), and assuming the value of density (ρ) = 2.6 g cm^{-3}, porosity (n) = 20% and helium release factor (Λ_{He}) = 1. With these values, the 5 ppmAEU He$_{ex}$ (see Figure 4.1) corresponds to groundwater ^{4}He age of ~15 kaBP (Figure 4.18). If, however, the value of Λ_{He} is assumed to be 0.4, the 5 ppmAEU He$_{ex}$ would correspond to ^{4}He age of ~37 kaBP and would be in close agreement with the groundwater ^{14}C age isoline of >35 kaBP (Figure 4.17).

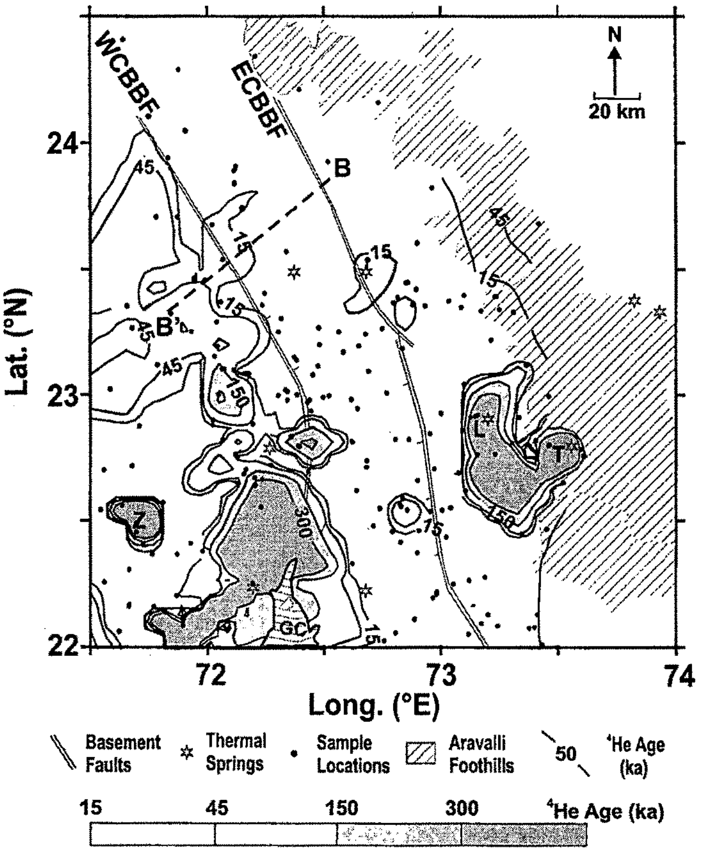

Figure 4.18 Isoline map of estimated ^{4}He ages of groundwater from the NGC region (for helium release factor; Λ_{He} = 1). Isoline of 15 kaBP runs almost along the WCBBF. This isoline will correspond to the ^{4}He age of ~37 kaBP for Λ_{He} = 0.4 (See Section 2.6.2). Dots indicate sampling locations. L, T and Z respectively indicate the locations of thermal springs at Lasundra, Tuwa, and the tubewell in Zinzawadar. The groundwater age gradient along BB' is shown in Figure 4.21.

Table 4.7 Results of $^{4}He/\ ^{222}Rn$ groundwater dating. Calculations are based on: Th/U = 7.1 ± 4.3; $\Lambda_{Rn}/\Lambda_{He} = 0.4$; ρ =2.6 g cm^{-3}; n = 20%.

CBGW Sample No.	**Location Name**	**Lat. (°N)**	**Long. (°E)**	**^{222}Rn activity (dpm/l)**	**He_{ex} (ppmAEU)**	**$^{4}He/^{222}Rn$ ages (kaBP)**
312	Diyodar	24.10	71.74	945±83	1.9	16
313	Diyodar	24.10	71.74	987±91	1.2	10
314	Tharad	24.41	71.64	810±65	33.7	330
316	Agathala	24.29	71.88	742±67	0.6	6
317	Sujnipur	23.89	72.11	1077±87	0.0	0
318	Sujnipur	23.90	72.12	1551±124	5.5	28
319	Sujnipur	23.90	72.12	629±57	0.0	0
320	Kuwarva	24.04	71.90	599±57	0.0	0
321	Kharia	23.94	71.83	916±83	0.0	0
322	Sami	23.70	71.78	137±30	44.1	2553
323	Hedwa	23.57	72.34	469±48	1.2	20
324	Kuder	23.73	72.19	462±58	1.2	20
325	Patan	23.84	72.11	822±72	0.0	0
326	Patan	23.84	72.11	673±63	0.3	3
327	Patan	23.84	72.11	261±36	0.0	0
328	Jitoda	23.74	72.15	1114±106	0.6	4
329	Jitoda	23.74	72.15	1871±144	9.9	42
330	Kamboi	23.67	72.02	1253±97	6.4	41
331	Muthia	23.09	72.69	481±24	0.0	0
332	Paliya	23.18	72.83	1262±52	0.0	0
333	Punsari	23.39	73.10	522±26	0.0	0
334	Dalani Muwadi	23.36	72.88	279±19	13.3	378
335	Rojad	23.35	73.09	281±19	0.0	0
336	Vadrad	23.42	72.89	923±41	1.7	15
337	Tajpur	23.39	72.81	721±36	0.0	0
338	Navalpur	23.60	72.90	245±17	0.0	0
339	Dhanap	23.26	72.75	643±34	0.0	0
340	Indroda Park	23.19	72.65	231±19	0.0	0
341	Rupawati	22.99	72.30	908±41	3.5	30
342	Sokali	23.10	72.11	657±31	0.7	8
343	Dudapur	23.02	71.58	2595±110	44.5	136
355	Salajada	22.80	72.39	480±28	0.9	15
356	Salajada	22.79	72.39	379±25	0.9	18

Table 4.7 continues

CBGW Sample No.	Location Name	Lat. (°N)	Long. (°E)	^{222}Rn activity (dpm/l)	He$_{ex}$ (ppmAEU)	^{4}He/^{222}Rn ages (kaBP)
357	Salajada	22.79	72.39	426±30	0.3	5
358	Gundi	22.55	72.23	301±18	175.3	4624
359	Shiyal	22.68	72.16	262±17	230.1	6958
360	Padgol	22.59	72.84	468±24	1.3	23
361	Morad	22.54	72.86	322±19	0.0	0
362	Gumadia	22.76	73.23	442±22	0.0	0
363	Tuwa	22.80	73.46	62571±2405	405.0	51
364	Tuwa	22.80	73.46	32538±1272	277.0	68
366	Tuwa	22.80	73.46	36394±1413	253.0	55
367	Dholera	22.25	72.19	362±17	465.0	10189

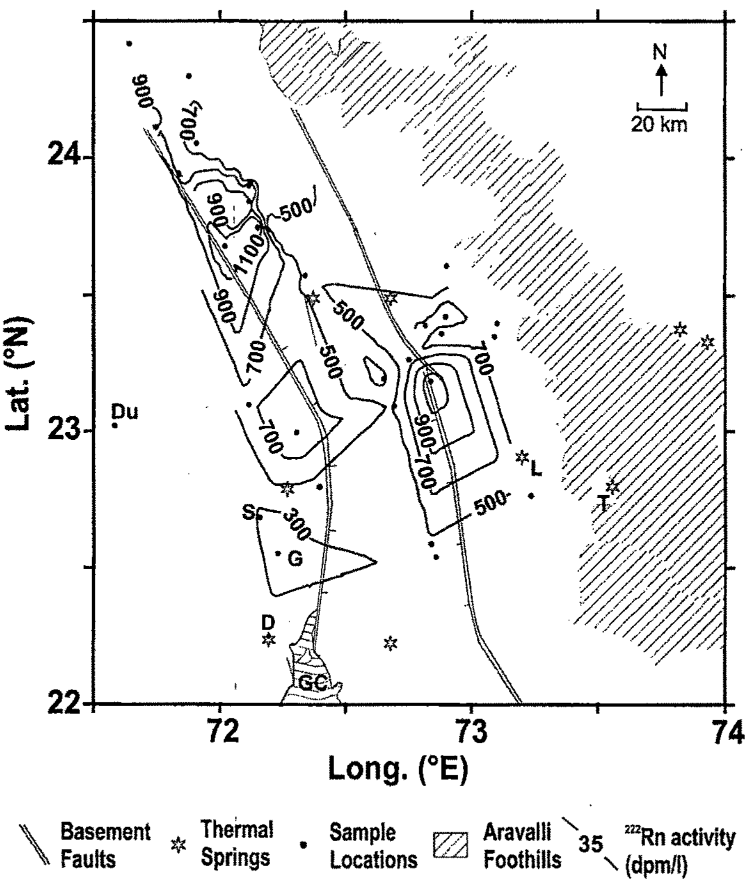

Figure 4.19 Iso-line map of groundwater ^{4}He/^{222}Rn ages in the NGC region for Th/U = 7.1; $\Lambda_{Rn}/\Lambda_{He}$ = 0.4; ρ =2.6 g cm^{-3} and n = 20%. Samples with >10ppmAEU ‘excess He’ and/or >2000 dpm/l ^{222}Rn were excluded during contouring. Dots indicate sampling locations. The groundwater age gradient along BB’ is shown in Figure 4.21.

4.1.6.3 ^{4}He /^{222}Rn Dating

Details of the (i) sampled well locations; and values of (ii) ^{222}Rn activity; (iii) He_{ex}; and (iv) estimated $^{222}Rn/^{4}He$ ages are given in Table 4.7. The isoline map of estimated $^{4}He/^{222}Rn$ ages of the groundwater in the NGC region is shown in Figure 4.19. The $^{4}He/^{222}Rn$ ages are calculated (see Section 2.6.3) based on Th/U concentration ratio = 7.1; ρ =2.6 g cm^{-3}; n = 20%; and release factor ratio ($\Lambda_{Rn}/\Lambda_{He}$) of 0.4. A gradual WSW progression of $^{4}He/^{222}Rn$ ages, away from the recharge area, is seen in Figure 4.19 similar to ^{14}C age progression (Figure 4.17). The $^{4}He/^{222}Rn$ ages were obtained using release factor ratio ($\Lambda_{Rn}/\Lambda_{He}$) of 0.4 which provided the best match with the ^{14}C age gradient.

4.2 Discussion

The salient points of the results from various geochemical and isotopic investigations are discussed in the following to understand respective roles of geohydrological, tectonic, topographic and palaeoclimatic factors in governing the observed geochemical and isotopic properties of groundwater in NGC region.

4.2.1 Groundwater Helium and Temperature

It is seen from Figure 4.1 and Figure 4.2 that areas of high He_{ex} (>15 ppm AEU) in groundwater are generally associated with areas of high groundwater temperatures (>35°C). Such areas are found to (i) lie along the major basement faults (ECBBF and WCBBF); (ii) overlie sympathetic faults both parallel and orthogonal to major faults; and (iii) overlie regions of thermal springs. Despite this geographical correlation between high He_{ex} and high temperature of groundwater, no quantitative correlation was seen between the two (Figure 4.3). This dichotomy is even more pronounced when comparing two samples – one with highest He_{ex} (CBGW-120; Figure 4.1; Table 4.1; 2843 ppmAEU; 34°C) from Zinzawadar and the other with highest groundwater temperature (CBGW-18; Table 4.1; Figure 4.1; 137 ppmAEU; 61°C).

It is also seen from Figure 4.18 that estimated ^{4}He ages of groundwater right in the recharge area, particularly around thermal springs of Tuwa and Lasundra, are >100 kaBP. This implies that these ground waters have been accumulating helium from *in-situ* sources alone (i.e. from aquifer/ rock volume that groundwater comes in contact with) for more than 100 kaBP. Such a long residence time, particularly in the recharge area is not compatible with the hydrogeology and the ^{14}C age (<2 kaBP; Figure 4.17) of groundwater in this region. Alternatively, local uranium mineralization can also cause high He_{ex}. However, unusually high ^{222}Rn activity is not observed (except for thermal springs at Tuwa; Table 4.7) in the region. No other evidence of near surface uranium mineralization has been reported from this region discounting the possibility of near surface uranium mineralization as a source for the observed He_{ex} in groundwater.

In case of groundwater far away from the recharge area, for example, at Zinzawadar (Figure 4.18), the required *in-situ* accumulation time for the observed He_{ex} (2843 ppmAEU), would be >8,000 kaBP. Groundwater inliers with such a high residence time surrounded by younger ground waters are hydro-geologically untenable even though the ^{14}C ages (Figure 4.17) of groundwater in this region are beyond the limiting age of >35 kaBP and the ^{4}He ages (Figure 4.18) are >45 kaBP little eastward of Zinzawadar. However, it is possible that observed high He_{ex} in certain groundwater inliers are due to injection from a deeper source that derives helium from much larger aquifer/ rock volume. This is also suggested by the geographical coincidence of areas with groundwater He_{ex} and high temperature and their position over the basement faults. In this scheme, deep subsurface faults provide routes for upward migration of deeper fluids having both very high concentration of helium and high temperature. Lack of any quantitative relationship between He_{ex} and groundwater temperature, however, indicates the possibility that many localized sources with their varying helium concentration and fluid temperature may be involved in transferring helium and/ or heat from deeper levels to shallower aquifers. This conceptual frame work is explained further in the following.

In the presence of concentration gradient, gaseous ^{4}He can physically diffuse out of rocks/minerals through the network of 100-200Å wide nano-pores present in the rock or grain body (Rama and Moore, 1984). If network of such diffusive pathways opens out into a bigger fault or fracture, gaseous helium can diffuse out through such preferential pathways and dissolve in the deep ground waters, considerably increasing its dissolved helium content. Plumes of such deep fluids can be injected (under hydrostatic pressure due to geothermal heat) into relatively shallow aquifers through underlying basement faults and fractures. This can result in localized pockets of very high He_{ex} and temperature in groundwater in such a way that these will be aligned around the basement fractures/ faults. It is, thus, possible for the groundwater overlying a fractured zone, to acquire the helium produced elsewhere (within or below the basement). There may be several such plumes in a large fractured terrain. The amount of helium and heat transferred to shallower layers would then depend on the concentration of helium and temperature of the fluid in a particular plume. If a single well-mixed fluid source was contributing helium and heat to shallower groundwater throughout the region, one could expect a relationship between observed helium concentration and the groundwater temperature. Absence of any such correlation is, therefore, a clear indication that several localized fluid injections are involved and deep fractures and faults provide pathways for upward migration of deeper fluids.

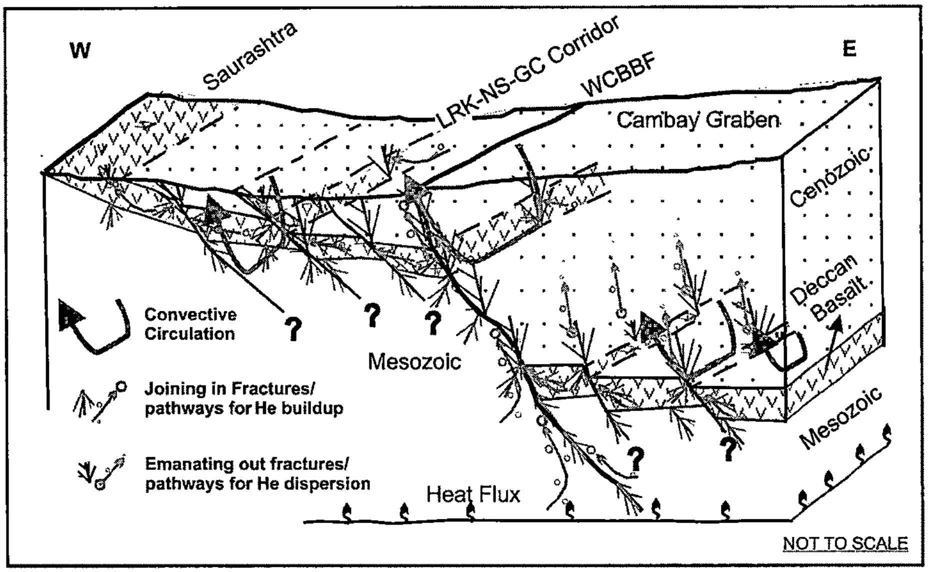

Figure 4.20 A conceptual tectono-hydrothermal model to explain the origin and observed geographical distribution of He_{ex} and high temperature of groundwater in NGC region. The set of braided fractures joining the major fault traces is indicative of migration of helium from micro-cracks into macro-fractures, eventually joining the conduits provided by the major fractures and faults. The joining-in fractures (indicated by an arrow with a circle at top) thus acts as the pathway for build-up of helium in deep groundwater. Another set of braided fractures emanating out of the major fault traces is indicative of pathway that the upward migrating helium follows through the overlying sedimentary cover leading to dispersion/diffusion. In both cases, the size of circles schematically depicts the changing helium concentration during upward migration of deeper fluids. The arrows leading to major faults depict the preferred pathways for migration of radiogenic helium derived from a large area. The thick arrows indicate the hydrothermal circulation along major faults, facilitated by high heat flux.

The above scheme can be presented in the form of a conceptual tectono-hydrothermal model for the NGC region depicted in Figure 4.20. The radiogenic helium produced in large volume of rocks within or below the basement migrates through micro-cracks into braided and interconnected fractures and dissolves in deep fluids/groundwater. Such deep fluids could even be of lower crust/ upper mantle origin but could also arise from downward migration of meteoric water from other locations through the pathways provided by deep fractures and fissures. This could result in setting up of a hydrothermal circulation along the deep seated fractures and fissures. The extent to which these deep fluids may have high concentration of helium is governed by interconnection of micro-cracks and fractures and the temperature is governed by the depth up to which a particular hydrothermal circulation cell penetrates. These factors will depend on the local geology affecting individual hydrothermal cells and, therefore, have local variation. The braided fractures emanating out from the major faults can also facilitate upward migration of helium through the overlying sedimentary cover. Sedimentary formations are characterized by uniform and high density pores that cause almost omni-directional migration of helium while crystalline formations have relatively small density of interconnected fractures and fissures governing the migration of helium. As a result, sedimentary formations cause large dispersion of the upward migratory helium plume whereas the crystalline formations tend to act as local source of helium plumes.

In addition to mixing of deep fluids with local groundwater and their dispersion in sedimentary formation, the helium can diffuse omni-directionally within the aquifer, be transported along with groundwater or diffuse out into atmosphere through the water-air interface. Similarly, heat is dissipated both through conduction and convection (along with groundwater flow). This is the reason why both helium and temperature anomalies are considerably subdued over the Cambay basin (between the ECBBF and the WCBBF) with ~3km thick sedimentary cover.

4.2.2 Fluoride and Electrical Conductivity

As seen from Figure 4.6, within the Cambay Basin certain sub-aquifer depth zones have high concentration (>1.5 ppm) of groundwater fluoride. As already mentioned, in view of the general topographic gradient, a particular depth (bgl) traces approximately the same sub-aquifer (see Figure 1.6) in different parts of the region. Based on the above arguments and investigation of 5 tubewells tapping various depth zones within a small region, it was further contended that if a particular tubewell taps the identified high fluoride depth zone (Table 4.3); its groundwater shows high concentration of fluoride (Figure 4.7). However, it was also mentioned that the above hypothesis could not be confirmed for the entire NGC regional aquifer system due to limited availability of tubewells providing suitable conditions (such as at Chadotar and Kuwarva). Further, it is also noticed that the entire NGC regional aquifer system comprises Quaternary sediments derived from fluvial transport of weathered, largely granitic, rocks from the Aravalli Mountains. Therefore, the bulk mineral assemblage of different sub-aquifer depth zones, though not expected to be significantly different from each other, may have some pockets at certain depths with accumulation of fluoride bearing minerals. But to expect such pockets forming regionally extensive sub-aquifer zones, contributing high fluoride to groundwater may be quite speculative.

Instead, the fluoride distribution in the NGC region is explained on the basis of a hydrological model comprising a recharge area in the Aravalli foothills, grading into the confined aquifer (Figure 1.6) towards LRK-NS-GC belt. The groundwater in this system moves through the confined aquifer with the dissolved chemical characteristics acquired from the recharge area but aging progressively as it moves away from the recharge area. In this model interaction with aquifer matrix after the zone of effective confinement is not considered to significantly alter the chemical properties of groundwater.

Geographical distribution of dissolved fluoride in groundwater of NGC region revealed that areas of high fluoride concentrations (>1.5 ppm) are aligned around four lines PP', QQ', RR' and SS' (Figure 4.5). Of these, three lines (PP', QQ' and RR') are trending NW-SE and are roughly parallel to the Aravalli foothills. These linear belts of high groundwater fluoride are distinctly separated by areas with relatively lower fluoride content. The fourth linear belt (SS') is trending nearly E-W and connects the regions of thermal springs of Tuwa and Lasundra to the low lying area around Nalsarovar. The groundwater pockets with high fluoride along these linear belts also geographically coincide with groundwater pockets of high salinity (EC >2 mS; Figure 4.8), excepting some pockets in the recharge area in the Aravalli foothills.

The mineral assemblage of the granites in the Aravalli foothills includes fluoride-rich minerals such as fluorite, apatite, biotite and amphiboles among several others. These granites are invaded by dykes of pegmatite that also contain xenoliths of amphibolites which are known for their high fluoride content. Since the sediments of the NGC region have been derived from the weathering of the Aravalli Mountains, it is possible that the aquifer matrix contains some fluoride rich minerals. Based on the fact that dissolved salt content of groundwater is to some extent related to leaching from the aquifer matrix, the high fluoride concentration in ground waters of NGC region was hitherto believed to be related to its residence time in the aquifer (Patel, 1986). However, comparison of isolines of fluoride (Figure 4.5) and isolines of ^{14}C ages (Figure 4.17) revealed that this may not be true.

The groundwater ^{14}C ages (Figure 4.17) progressively increase from <2 kaBP in the recharge area (Aravalli foothills) to >35 kaBP in the low lying belt linking LRK-NS-GC. If the residence time of groundwater indeed controlled its fluoride content, it should have progressively increased with the ^{14}C ages, as a function of distance from the recharge area. This, however, is not supported by Figure 4.5, which shows that three almost parallel linear geographical belts of high groundwater fluoride are clearly separated by areas with relatively lower fluoride content. The alternating high and low fluoride concentration in groundwater from confined aquifers suggest the possibility of an additional (other than progressive leaching from mineral grains) non-geological control on the fluoride concentration in groundwater of NGC region.

The enhanced aridity is generally associated with (i) increased evaporation; (ii) decreased rainfall; and (iii) increased dry deposition. Some imprints of evaporation and dry deposition in the present climate are seen in the ion concentration (Section 4.1.4) and stable isotope composition (Section 4.1.5) of modern rainfall. The significant control of dry deposition is seen in the variation of fluoride and EC of fortnightly accumulated rain water samples (Figure 4.11). It is seen that variation of fluoride and EC in rainwater are not related to the amount of rainfall. Therefore, the increased dry deposition seems to be the source of increased fluoride concentration and EC in certain fortnightly accumulated rainwater samples. It is also seen that variations in fluoride concentration and EC of rainwater are nearly proportional to each other (Figure 4.13). Therefore, the surface water, infiltrating to form the shallow groundwater can have both higher concentration of fluoride and higher EC due to enhanced dry deposition and higher evaporation during periods of increased aridity compared to preceding or succeeding periods of relatively wetter climate.

It is seen (Figure 4.5 and Figure 4.17) that the confined groundwater in the central high fluoride groundwater belt (QQ') within the Cambay Basin corresponds to groundwater ^{14}C age in the range 15-25 kaBP. The period around 20 kaBP, corresponding to the Last Glacial Maxima (LGM), is known to be a period of enhanced aridity in the NGC region (Prasad and Gupta, 1999; Pandarinath et al, 1999b; Wasson et al, 1983; Juyal et al, 2003). It is, therefore, inferred that groundwater recharged around LGM in the Aravalli foothills and subsequently migrated to its present position within Cambay Basin corresponds to the central (QQ') high fluoride groundwater belt. The groundwater, with relatively low fluoride concentration, on either side of QQ' suggests recharge during relatively less arid climatic regime. The first low fluoride zone between the eastern (RR') and central (QQ') high fluoride belts (^{14}C age 5 – 15 kaBP) is then an indication of groundwater recharged during climatic amelioration (higher precipitation and/or decreased dry deposition and/or reduced evaporation). The next low fluoride groundwater zone in between central (QQ') and western (PP') high fluoride belts is also an indication of groundwater recharged during ameliorated climatic condition prevalent during 25 – >35 kaBP, as indicated by ^{14}C age.

The eastern high fluoride belt (RR') located in the recharge area corresponds to the modern recharge which is an indication that even under the present geo-climatic conditions, groundwater recharged into the regional aquifer system is predisposed to a certain degree of high fluoride content. This is due to combination of (i) leaching; (ii) dry deposition and evaporation preceding the recharge; and (iii) increased rock-water interaction at higher temperatures during hydrothermal circulation (as evidenced in thermal springs).

The high fluoride-high EC belt (PP') in the western region, indicates the groundwater recharged during previous arid climate phase (^{14}C age >35 kaBP; ^{4}He age 45-110 kaBP, depending on helium release factor). However, sudden increase in fluoride concentration (from <2 ppm to >6 ppm) and EC (from <2 mS to >8 mS) in the shallow unconfined groundwater around PP' suggests a causal mechanism other than just increased aridity in the past and/ or progressive leaching. The line PP' overlies a low lying tract linking LRK-NS-GC which is a convergence zone for surface and subsurface drainage. The very high level of groundwater fluoride concentration in this belt is possibly due to evaporative enrichment of salts in the stagnant water accumulated in the topographically low lying convergence zone and its infiltration into the shallower aquifers.

The high fluoride and EC in the belt SS' linking the regions of thermal springs (Tuwa and Lasundra) to the low lying area around Nalsarovar can be explained as due to steady venting of hydrothermal fluids (with relatively high concentration of ions including fluoride) into the groundwater in the recharge area around Tuwa and Lasundra and the steady movement of the mixed groundwater in the regional aquifer system throughout the Late Quaternary period. The fluoride contribution by the hydrothermal fluids is so significant and steady that the imprints of arid excursions in climate are not identifiable prominently along SS'. Instead a continuous belt of higher fluoride concentration (>1.5 ppm) and high EC (>2 mS) is seen.

4.2.3 Oxygen and Hydrogen Isotopes in Groundwater and Precipitation

With a view to identify the possible signatures of the past aridity as well as source of thermal spring water, oxygen and hydrogen isotope ratios (δ^{18}O and δD) in thermal springs and ground waters of NGC region were measured. Isotopic analyses of modern precipitation were also carried out to provide reference for interpretation of the groundwater isotope data.

The amount weighted average values for the modern rainfall in the NGC region (Figure 4.15a and b; Table 4.5) are: $\delta^{18}O = -4.3 \pm 2.1‰$, $\delta D = -33 \pm 16‰$ and *d*-excess =1.2 ± 4.8‰. This *d*-excess value as well as the slope (7.6 ± 0.6) and the intercept (–2.9 ± 2.2‰) of the local meteoric water line (LMWL) are lower than the average values of global meteoric water line (GMWL). As discussed above (see Section 2.4), the evaporation of falling raindrops results in lower values of LMWL slope, its intercept and the *d*-excess, and higher values of δ^{18}O and δD in the residual water. Thus, the lower values of *d*-excess, the slope, and the intercept of LMWL in the NGC region are isotopic imprints of evaporation from falling raindrops under the present semi-arid climatic regime. Any further evaporation of the rain water, during infiltration and groundwater recharge, will further reduce the values of these isotopic parameters in the groundwater.

The $\delta^{18}O$ vs. δD plot (Figure 4.15c) of groundwater samples from the NGC region shows a cluster of data points having significantly narrower range of variation, than that for precipitation, with average values of both $\delta^{18}O$ (–1.2 ± 1.3‰) and δD (–22 ± 5‰) being higher than that for precipitation. The average value of d-excess of all groundwater samples is –4.5 ± 11‰, which is lower than that for precipitation samples. The lower value of *d*-excess, narrow range and relatively higher values of $\delta^{18}O$ and δD in groundwater, compared to that in precipitation, indicate mixing of rain water from different events in the soil zone and additional evaporation during its infiltration. The isotopic characteristics of both modern precipitation and groundwater indicate that the semi-arid NGC region is not only predisposed to significant evaporation during rainfall and recharge but its evidence is preserved in groundwater.

Since the NGC region has experienced more arid excursions in the palaeo-climatic history, as registered in sedimentary records (see Section 1.2.6; and 4.2.2 above), it is expected that the groundwater in this region, which is thousands of years old (see Section 4.1.6), may have recorded and preserved the imprints of past aridity. It is seen from the geographical distribution of $\delta^{18}O$ and *d*-excess of groundwater from NGC region that (Figure 4.16), groundwater around a linear belt (QQ') is characterized by relatively higher values of $\delta^{18}O$ and lower values of *d*-excess. In view of the expected isotopic modification of the evaporating water as discussed in section 2.4, the groundwater with relatively lower values of *d*-excess and higher values of $\delta^{18}O$ around QQ' indicate influence of relatively enhanced evaporation of infiltrating water during its recharge compared to the groundwater outside this belt. The ^{14}C age of the confined groundwater around QQ' within the Cambay Basin, representing the time when it was recharged in the identified recharge area, has been estimated (Section 4.2.2) as 15-25 kaBP. The period around 20 kaBP, corresponding to the Last Glacial Maxima (LGM), has also been identified as a period of enhanced aridity in the NGC region (Prasad and Gupta, 1999; Pandarinath et al, 1999b; Wasson et al, 1983; Juyal et al, 2003). Relatively lower *d*-excess and higher $\delta^{18}O$ values for groundwater around QQ', therefore, represent the signatures of relatively enhanced evaporation resulting from increased aridity in the region around LGM. Thus, the groundwater isotopic signatures corroborate enhanced aridity in the NGC region around period of LGM, as previously inferred from enhanced fluoride concentration and EC of groundwater around QQ'.

It has been shown that the geothermal waters in the NGC region have high fluoride as well as EC and enhanced concentrations of these geochemical parameters around the line SS' are due to continuous admixture of geothermal waters (around thermal springs of Tuwa and Lasundra) to the recharged groundwater (Section 4.2.2 above). The isotopic analyses of geothermal waters (samples marked TS for thermal springs and TA for thermal artesian wells in Table 4.4) and their comparison with other groundwater and modern precipitation samples offer an opportunity to study the possible interaction between the rock matrix and the infiltrating meteoric water. The $\delta^{18}O$ value of the crustal rocks range between 5–10 ‰ VSMOW (Figure 9.2 of Clark and Fritz, 1997) whereas most meteoric waters have $\delta^{18}O$ values <0 ‰. Although hydrogen has a much lower crustal abundance, it is present in several rock forming minerals. Unlike ^{18}O, the greatest enrichment of ^{2}H is observed in water, while mineral and rocks are preferentially depleted. This contrasting behavior of the two isotopes is important in the isotopic evolution of water in high temperature systems. In the case of the NGC region, the modern precipitation has average $\delta^{18}O = -4.3 \pm 2.1$‰; and the average of all groundwater samples, including geothermal waters, is $\delta^{18}O = -1.2 \pm 1.3$‰.

The thermal springs at Lasundra and Tuwa are seen to be slightly enriched (average $\delta^{18}O = -1.4 \pm 0.4$ ‰, for 6 samples) compared to ground waters in the surrounding region. On the other hand, $\delta^{18}O$ values of thermal artesian wells on the western flank do not show much difference (average $\delta^{18}O = -2.4 \pm 1.0$ ‰ for 8 samples) compared to the other groundwater samples in NGC region. With exchange induced enhancement of $\delta^{18}O$ and decrease of δD, one can expect a reduction in the *d*-excess values of thermal waters. The thermal springs from the eastern flank have *d*-excess = -4.1 ± 3.2 ‰ and thermal artesian wells on the western flank have *d*-excess = -6.5 ± 7.3‰. Statistically these averages are not distinguishable from the average groundwater values for the entire NGC region, but local enrichment of ^{18}O and lowering of *d*-excess in the areas with thermal waters is seen in Figure 4.16. Thus isotopic evidence of water-rock interaction in geothermal waters of the NGC region is indicated, but is not so unambiguous. The evidence is, however, clearer in case of thermal springs of Tuwa and Lasundra.

It may be noted that the $\delta^{18}O$ enrichment in groundwater around QQ', discussed earlier, is not related to any geothermal activity and also did not show any enhanced helium concentration. Whereas, the geothermal waters on both flanks have higher helium concentration (Section 4.1.1).

It is, therefore, inferred that the $\delta^{18}O$ in thermal springs at Tuwa and Lasundra show a trend towards isotopic equilibrium between ^{18}O depleted meteoric water and ^{18}O enriched rocks at higher temperatures. This also fits in with the conceptual tectono-hydrothermal model as described in Section 4.2.1.

4.2.4 Groundwater Ages

4.2.4.1 ^{14}C Ages

The estimated groundwater ^{14}C ages are seen (Figure 4.17) to increase progressively from <2 kaBP (along Aravalli foothills) to >35 kaBP in the low-lying tract linking LRK-NS-GC. Farther west, lower ^{14}C ages are found, but only in two groundwater samples (CBGW-344, -351; Table 4.6). The low lying LRK-NS-GC tract is the zone of convergence for the surface drainage (see Section 1.2.5; Figure 1.5). Presence of several free flowing artesian wells found in the LRK-NS-GC tract and continuity of the aquifers with those from the Cambay Basin confirm that their recharge area is in the foothills of Aravalli Mountains. It is seen (Figure 1.6) that succession of sand/ silty-clay layers is roughly inclined parallel to the ground surface and the sampled tube wells tap nearly the same water bearing formations across the NGC region. Since the tubewells tap all the water bearing horizons intercepted within their maximum depth, these are treated as pumping a single aquifer system for which the ^{14}C ages increase progressively in the flow direction. The above geo-hydrological model appears reasonable because, the unconfined aquifers in the region have almost completely dried up (as evident from several dried up and abandoned dug wells). Therefore, the groundwater in all the parallel layers of confined aquifers is recharged largely from the sediment-rock contact zone in the foot hills of Aravalli Mountains, and after the confinement becomes effective, moves with nearly the same velocity. The narrow range of $\delta^{13}C$ values of TDIC of groundwater (Table 4.6) indicates that the dead carbon dilution factor for the various samples is not significantly different from each other. As a result, the relative age difference between the samples can be relied upon. The only sample, with much lower $\delta^{13}C$ value (–21.4‰) is derived from a very deep aquifer from the Gundi village (CBGW-358; Table 4.6) and showed age beyond ^{14}C dating limit. The low redox potential (10 mV) of this sample suggested possible CO_2 contribution from its anaerobic oxidation.

From hydro-geological considerations (see Section 1.2; Figure 1.6), it seems that confinement of the regional aquifer in the NGC region becomes effective near the ECBBF around the ^{14}C age contour of ~2 kaBP. Within the Cambay Basin, the age isolines are nearly parallel to each other and the horizontal distance between the successive 5 kaBP isolines is nearly constant giving a regional flow velocity in the range

2.5 – 3.5 m a^{-1} for the prevailing hydrostatic gradient of 1 in 2000 (GWRDC, unpublished data), which is comparable to an earlier estimate of ~ 6 m a^{-1} (Borole et al, 1979) for a small part of the Vatrak-Shedhi sub-basin (marked by an ellipse in Figure 4.17). The Vatrak-Shedhi sub-basin is closer to the recharge area, therefore, both the permeability and the hydraulic gradient are expected to be relatively higher than that for the regional estimates of flow velocity (2.5 – 3.5 m a^{-1}) from this study.

4.2.4.2 ^{4}He Ages

As seen from Figure 4.1 and Figure 4.18, the 5 ppmAEU He_{ex} isoline runs along the WCBBF and corresponds to ^{4}He age of ~ 15 kaBP (for helium release factor; Λ_{He} = 1), and ~ 37 kaBP for $\Lambda_{He} = 0.4$. The ^{4}He ages (Figure 4.18) for $\Lambda_{He} = 0.4$ are in close agreement with the ^{14}C ages (Figure 4.17) when no crustal flux is considered, except for pockets of anomalous groundwater helium concentrations. This is supported by other studies, which indicate that relatively young ground waters are dominated by the *in-situ* production of ^{4}He. Torgersen and Clark (1985) found good concordance between ^{14}C and ^{4}He ages of groundwater in the Great Artesian Basin, Australia, up to ~ 50 kaBP. Kulongoski et al (2003) found a good correlation between ^{14}C and ^{4}He ages of groundwater up to ~25 kaBP in the Mojave River Basin, California. They explained the result by existence of wells in the basin at shallow depth and hence, above the influence of crustal ^{4}He flux. A similar situation also prevails in the NGC region up to the WCBBF. In the NGC region, the fluvial deposits grade from coarse grain sizes near the Aravalli foothills (recharge area) to fine grain sizes near the LRK-NS-GC region. This is also indicated by a rapid decrease in aquifer transmissivity from ~ 1000 m^2d^{-1} east of the ECBBF to < 200 m^2d^{-1} west of the WCBBF (GWRDC, unpublished data). Thus, greater transmissivity of the aquifers up to WCBBF of the NGC region may result in groundwater flow that entrains negligibly small basal crustal flux, thereby leaving groundwater ^{4}He ages virtually unaffected by the deep crustal ^{4}He flux.

As mentioned above (see Section 2.6.2), there is some uncertainty on the calculated He_{ex} that is dependent upon estimation of (i) excess air; and (ii) dissolved helium in solubility equilibrium with the atmosphere. Depending on the physical nature of capillary fringe zone just above the saturated zone, air bubbles can be entrapped and transported into the saturated zone by infiltrating water. The air bubbles can also be entrapped by rapid rise in the water table due to occasional heavy rainfall in semi arid regions. Dissolution of such air bubbles into the groundwater introduces excess-air and consequently all its components including helium ($^4He_{ea}$). The presence of 'excess air' in groundwater results in observed ^{4}He concentrations (^4He_s) to be higher than those expected from solubility equilibrium ($^4He_{eq}$) (Heaton and Vogel, 1981; Stute ad Schlosser, 1993; Aeschbach-Hertig et al, 2000). In the present study it was not possible to correct for the 'excess air' since neon concentrations were not measured. According to laboratory column experiments on the formation of 'excess air' in quasi saturated porous media (Holocher et al, 2002), the amount of 'excess air' can range from 1% to 16% of the equilibrium solubility concentration. However, in field studies higher Neon excesses have also been found (Heaton and Vogel, 1981; Aeschbach-Hertig et al, 2002).

Since the solubility of helium is relatively insensitive to temperature (Ozima and Podosek, 1983), variation in the temperature of recharge water has a small effect on ^4He dissolved in solubility equilibrium with atmosphere ($^4He_{eq}$), which can be estimated from the regional climate and groundwater temperature. The mean annual temperature of recently recharged groundwater in the Aravalli foothills is 30 ± 5 °C, as a result $^4He_{eq}$ can decrease by ~10% relative to the groundwater recharged in relatively colder climate.

Thus, both $^4He_{eq}$ and $^4He_{ea}$ would lead a systematic error of ~+10% and ~–20%, respectively on the atmospheric air equilibration value of 5.3 ppmAEU which is subtracted from the measured ^4He in groundwater samples to calculate $^4He_{ex}$ (see Section 2.6.2). While corrections due to recharge temperature and 'excess air' are important for precise groundwater age estimation, particularly in case of low ^4He concentration samples, the conclusion for high ^4He concentrations are not significantly affected by such corrections. Considering this, and the fact that accuracy of measurement for low helium concentrations is ~20%, the error on ^4He ages can be as high as 50% for groundwater samples which have <5 ppmAEU $^4He_{ex}$. Therefore, the isolines for $^4He_{ex}$ values <5 ppmAEU are not shown in Figure 4.1 and the conclusions are based only on samples with $^4He_{ex}$ ≥5 ppmAEU.

It is seen from Figure 4.1 that ^4He concentrations rapidly increase west of the 5 ppmAEU He_{ex} isoline that almost coincides with WCBBF. This could be due to (i) rapidly increasing residence time of groundwater resulting from decrease in the transmissivity as a result of a general decrease in grain size away from the sediment source; and/or (ii) increase in the influence of deep crustal flux of helium in the aquifer. The latter possibility is supported by very high (>50 ppmAEU) He_{ex} pockets on both eastern and west flanks of the Cambay Basin. The east flank is the major recharge area of aquifers in the Cambay Basin where groundwater pockets of very high helium are associated with the thermal springs of Tuwa and Lasundra. Considering the observed He_{ex} as *in-situ* produced will result in groundwater age >100 kaBP, which is not tenable hydrogeologically. The presence of extraneous ^4He in these pockets is also indicated by the overlapping of high groundwater temperature (>35°C) pockets suggesting hydrothermal venting of deep crustal fluids in such pockets. The ^{4}He method of dating is not applicable for groundwater in such pockets.

The deep crustal He flux may also affect the aquifer by diffusion from the underlying basement followed by entrainment and upward migration, particularly towards the discharge region of the aquifer (Bethke et al, 2000). Thus, higher amount of the crustal flux may be entrained with increasing distance along flow paths, resulting in a rapid increase in the helium concentration towards the discharge region. For the five samples west of the WCBBF for which ^{14}C groundwater ages (Figure 4.17) are also measured, a ^{4}He crustal flux of ~1.5 x 10^{-8} cm^3 STP He cm^{-2} y^{-1} produces an agreement between the two dating methods. This, however, ignores *in-situ* production. Considering finite *in-situ* production due to U and Th in the aquifer matrix, the ^{4}He crustal flux must <<1.5 x 10^{-8} cm^3 STP He cm^{-2} y^{-1}. However, for the Lasundra and Tuwa thermal springs in the East Flank and pockets of very high helium on the West flank of Cambay Basin a crustal flux >10^{-6} cm^3 STP He cm^{-2} y^{-1} is necessary for agreement between ^{4}He and ^{14}C ages. Takahata and Sano (2000) reported ^{4}He crustal flux of 3.0 x 10^{-8} cm^3 STP He cm^{-2} y^{-1} from a sedimentary basin in Japan. The typical continental ^{4}He flux is 3 x 10^{-6} cm^3 STP He cm^{-2} y^{-1} (O'Nions and Oxburgh, 1983). It is thus seen that the observed pattern of high helium concentrations in localized pockets can only be explained by invoking 2-3 orders of magnitude variation in crustal diffusion flux which is another way of saying that crustal diffusion occurs along preferred pathways formed by deep seated basement faults. The rising arm of the convective hydrothermal circulation, also formed along these faults, introduces this non *in-situ* component of ^{4}He in the form of a plume into groundwater where pockets of He_{ex} are observed. Thus, the possible role of the crustal flux also fits into the tectono-hydrothermal model described above (Section 4.2.1).

In case of groundwater out side the pockets of very high He_{ex}, the *in-situ* ^{4}He accumulation, even without crustal flux correction, produces a reasonable correspondence between ^{14}C and ^{4}He ages within the 50% uncertainty range. For samples from the west of the WCBBF, a low crustal flux value of <1.5x10^{-8} cm^3 STP He cm^{-2} y^{-1} can not be ruled out as invoking it produces a better agreement with the few definite ^{14}C groundwater ages. Farther west, ages must be >45 kaBP, possibly as old as 100 kaBP.

4.2.4.3 ^{4}He/ ^{222}Rn Ages

The measured ^{222}Rn activity in the NGC region (Table 4.7) showed a variation of ±50% around an average value of ~800 dpm/l (except the thermal spring water at Tuwa) suggesting a similar range of variation in the U concentration of the aquifer material. This range of U variation was also seen in the analyzed drill cutting samples and on shallow depth sediments from the NGC region (Srivastava et al, 2001; Agarwal et al, 2006).

As explained earlier (see Section 2.6.3), the ^{4}He/ ^{222}Rn ages (Table 4.7; Figure 4.19) are independent of porosity, density and U concentration but depend on Th/U of the aquifer material. Additionally, the ^{4}He/^{222}Rn ages also depend on the release factor ratio ($\Lambda_{Rn}/\Lambda_{He}$). As in the case of ^{14}C ages (Figure 4.17), a gradual ^{4}He/^{222}Rn age progression from the recharge area towards the WCBBF is observed in major part of the study area (Figure 4.19). These ^{4}He/^{222}Rn ages were obtained using $\Lambda_{Rn}/\Lambda_{He}$ = 0.4 to give the best match with the ^{14}C age gradient across the Cambay basin. This gradient matching approach was chosen because the inferred groundwater flow velocities in the confined aquifer by the two methods match only when age gradients match. This also ensures that various uncertainties in the age estimation related to (i) the initial activity of ^{14}C (A_0) in the recharge area; (ii) ^{4}He dissolved in solubility equilibrium at recharge temperature ($^{4}He_{eq}$); and (iii) dissolved ^{4}He due to 'excess air' have as little influence on matching as possible. A radon release factor (Λ_{Rn}) ranging from 0.01-0.2 has been indicated from laboratory experiments for granites and common rock forming minerals (Krishnaswami and Seidemann, 1988; Rama and Moore, 1984). Based on measured values of uranium concentration and ^{222}Rn activity, the value of Λ_{Rn} is estimated to be 0.15 ± 0.07 (using Eq. 2.31 and 2.32), which is consistent with the literature. On the other hand for ^{4}He, Torgersen and Clarke (1985), in agreement with numerous other authors have suggested $\Lambda_{He} \approx 1$. For Λ_{Rn}= 0.15 ± 0.07 and $\Lambda_{Rn}/\Lambda_{He}$ = 0.4, Λ_{He}= 0.4 ± 0.3 is obtained for best regional matching between ^{4}He/^{222}Rn (Figure 4.19) and ^{14}C ages (Figure 4.17). This is shown in Figure 4.21 where age progression along the line BB' (drawn in Figure 4.17, Figure 4.18 and Figure 4.19) is plotted. The arrow in the middle of each trapezoid shows the median value of the model age by the respective method. The progressively increasing width of the trapezoid depicts the estimated error at any given median age. The slopes of the respective median lines give the age gradients. It is seen that for Λ_{He} = 0.4, both ^{4}He and ^{4}He/^{222}Rn age gradients matches the ^{14}C age gradient. In view of the various uncertainties that affect the three methods, the ^{14}C method appears to be the most reliable one in the present case. Firstly, because the δ^{13}C values of TDIC show a very narrow range (–9.6 ± 1.2 ‰) and secondly, the ^{14}C age iso-lines show a nearly parallel distribution, approximately in agreement with the distribution of transmissivity of the aquifers obtained from the pumping test data, progressively decreasing from ~1000 m^{2} d^{-1} east of the ECBBF to <200 m^{2} d^{-1} west of the WCBBF (GWRDC, unpublished data). Therefore, considering ^{14}C age data as reference, the best match for both ^{4}He/^{222}Rn and ^{4}He ages is obtained for Λ_{He} = 0.4, so that the 5 ppmAEU

He_{ex} iso-line (Figure 4.18) corresponds to ^4He groundwater age of ~37 kaBP (instead of ~15 kaBP).

A value of $\Lambda_{He}<1$ in NGC region would appear contrary to the apparent $\Lambda_{He}>1$ due to release of geologically stored helium in young sediments derived from old protoliths (Solomon et al, 1996).

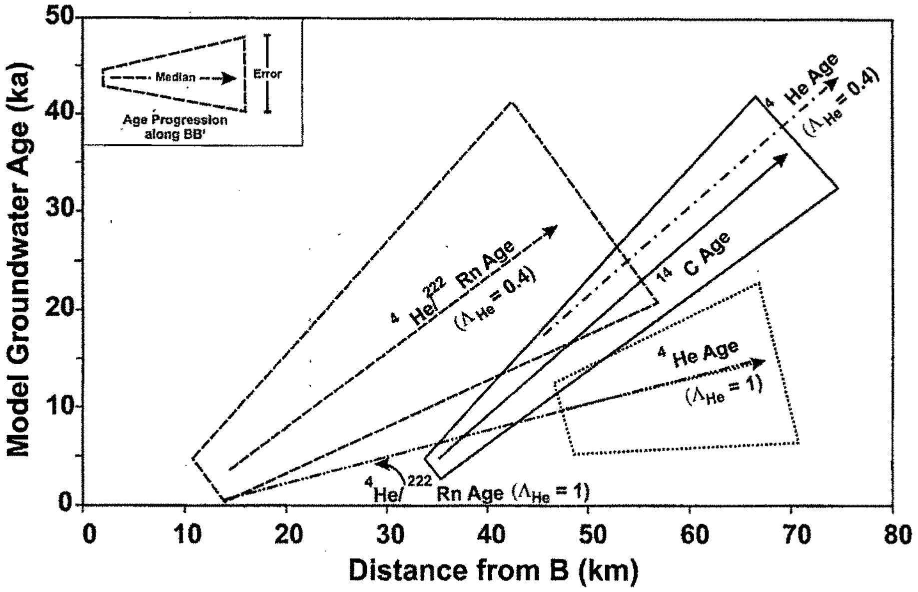

Figure 4.21 Plot of groundwater age progression along line BB' (shown in Figure 4.17, Figure 4.18 and Figure 4.19) for comparing the age gradients for model ^{14}C ages, ^4He ages for $\Lambda_{He} = 1$ and $^4He/^{222}Rn$ ages both for $\Lambda_{He} = 1$ and $\Lambda_{He} = 0.4$.

The comparatively low estimate of Λ_{He} can either be due to (i) loss of ^4He from the aquifer system, or (ii) incomplete release of radiogenic ^4He from the grains over time scales of ~100 kaBP. The former possibility is contrary to the basic assumptions of both ^4He and $^4He/^{222}Rn$ dating methods. The latter possibility may not be ruled out because the depositional age of aquifer material in the Cambay Basin is Late Quaternary (Pandarinath et al, 1999; Prasad and Gupta, 1999) and it is possible that all the helium produced in the aquifer material, since deposition, is only partially released to the interstitial water. Contrary to Solomon et al. (1996), this would require a mechanism that nearly releases all of the geologically stored helium in the grains due to mechanical/ thermal/ chemical stress during the process of weathering & transportation and subsequent build up within the grains with a partial release to interstitial water during the quiet post depositional period until a steady-state (for helium loss) is achieved within individual grains. The possibility of partial release of helium is justified since the grain size (> 0.5 mm) of aquifers forming horizons is considerably larger compared to the recoil path length (30–100 μm) for ^{4}He. Recoil of the decaying atom from the outer surface of the grain is one of the mechanism by which radioactive products in solids enter the pore fluid.(Torgersen, 1980; Gupta et al, 2002). Thus, the possibility of partial release of helium is justified; however, more definitive arguments concerning the involved mechanisms is not possible based on the present data. In fact, the use of groundwater helium for earthquake prediction (Sano et al, 1998) is based on the premise that in the normal course Λ_{He} may be <1.

In this Chapter results from various isotopic and geochemical investigations, and the discussion leading to specific conclusions were presented. In the Chapter 5 next, the summary and conclusions of this study are presented and the important contributions and advancements in the understanding of geohydrological processes operating in the NGC region are highlighted.

Chapter 5. Summary and Conclusions

In this chapter, results from various geochemical and isotopic investigations of groundwater in the North Gujarat Cambay (NGC) region of Gujarat State in Western India, undertaken as part of this study are summarized and major conclusions that have significantly improved understanding of the geo-hydrological processes in the NGC region and may also contribute to the science of hydrology are highlighted.

It may be recalled that the NGC region is characterized by a unique combination of geological, hydrological, tectonic and climatic features, namely (i) two major deep seated faults defining the Cambay Graben and several sympathetic faults parallel and orthogonal to these; (ii) more than 3 km thick sedimentary succession forming a regional aquifer system in the upper part; (iii) higher than average geothermal heat flow; (iv) intermittent seismicity; (v) emergence of thermal springs; (vi) arid climate with high rate of evapotranspiration; and (v) significant mining of groundwater over the past few decades.

As a result of the extensive groundwater mining, the piezometric levels have declined - by >3 m/yr during the last couple of decades. During the same period, progressive increase in groundwater fluoride concentrations with time and associated endemic fluorosis has been observed. In general, high fluoride in groundwater of the region has been associated with long residence time of the mined groundwater or subsurface injection of thermal waters. Very high amounts of dissolved helium and high groundwater temperatures from some parts of the NGC region were reported earlier (Datta et al, 1980) but, their inter-relationship as well as their possible relationship with basement faults in the region was not understood in terms of tectonic framework and geothermal regime of the NGC region. The Late Quaternary sedimentary record of the region is indicative of increased aridity around Last Glacial Maxima (LGM; ~20 kaBP) (Prasad and Gupta, 1999; Pandarinath et al, 1999b; Wasson et al, 1983; Juyal et al, 2003). However, no palaeoclimatic imprints were reported in hydrological studies.

Based on general topography, geology, lithologs of the drilled tubewells and the water level/ piezometric level data, the area of the foothills of the Aravalli Mountains in the NE was considered as the recharge area of the regional aquifer system with groundwater moving westwards towards the low lying tract linking Little Rann of Kachchh (LRK) – Nalsarovar (NS) – Gulf of Cambay (GC). However, this inference of groundwater recharge and movement, from conventional methods needed to be reinforced and substantiated by determining the age of groundwater by employing radiometric dating methods.

The objective of this study was to generate data for bridging the gap in the knowledge.

To achieve the above objectives, following methodology was adopted.

- Groundwater dating was undertaken employing ^{14}C decay, ^{4}He accumulation and $^{4}He/^{222}Rn$ ratio methods. Laboratory and field procedures for carbonate precipitation (for ^{14}C method) and water sample collection, storage and analyses for other groundwater dating methods were developed and standardized.
- A survey of dissolved helium and temperature of groundwater in the NGC region was undertaken. Simple procedures were developed and standardized for (i) sample collection and storage, and (ii) measurement of helium concentrations in soil-gas and groundwater using commercially available helium leak detector.
- A survey of dissolved groundwater fluoride and electrical conductivity (EC) was undertaken to identify areas of high concentration of fluoride, and to understand its origin. Dissolved fluoride and EC of modern rainfall were also measured to understand the role of dry deposition and/ or amount of rain in controlling the fluoride and EC of rainwater.
- Oxygen and hydrogen isotope ratios ($\delta^{18}O$ and δD) in thermal springs and groundwater samples were measured to identify the possible signatures of the past aridity and to identify the source of thermal spring water. Isotopic analyses of modern precipitation were also carried out to provide a reference for interpretation of the groundwater data.
- A groundwater CFC laboratory was set up as part of this study. Field and laboratory procedures for sample collection, storage, extraction of dissolved CFCs and injection for gas chromatographic analyses were standardized.

Important observations from the above investigations and conclusions drawn are summarized in the following.

5.1 Groundwater Helium and Temperature

Areas of high values of excess helium (He_{ex} >15 ppm AEU) in groundwater are generally associated with areas of high values of groundwater temperatures (>35 °C). Such areas are found to (i) lie along the major basement faults (ECBBF and WCBBF) on both flanks of the Cambay Graben; (ii) overlie sympathetic faults parallel or orthogonal to major faults; and (iii) overlie regions of thermal springs. Despite this geographical correlation between high He_{ex} (see Figure 4.1) and high temperature (see Figure 4.2) of groundwater, no quantitative correlation was seen between the two. Interpretation of such a high value of dissolved helium in groundwater pockets in terms of *in situ* accumulation would imply a long residence time (>100 kaBP) in aquifer. Such a long residence time of groundwater particularly in the recharge area and the observed inliers of old ground waters away from recharge area are not compatible with the hydrogeology and the ^{14}C age (see Figure 4.17). Evidence of near surface uranium mineralization was also not found from ^{222}Rn activity measurements and has also not been reported in any other study from this region ruling out the possibility of near surface uranium mineralization as the source for the observed He_{ex}. It is, therefore, inferred that observed high He_{ex} in certain groundwater pockets is due to injection from deeper sources that derive helium from much larger aquifer/rock volumes.

In this scheme of interpretation, deep subsurface faults provide pathways for upward migration of deeper fluids with high helium concentration and high temperature. Lack of quantitative relationship between He_{ex} and temperature, however, indicates that many localized sources with their varying helium concentration and fluid temperature may be involved in transferring helium and/ or heat from deeper levels to shallower aquifers.

This scheme of interpretation is also presented in the form of a conceptual tectono-hydrothermal model for the NGC region (see Figure 4.20). In this conceptual model, the radiogenic helium produced in a large volume of rocks within or below the basement migrates through micro-cracks into braided and interconnected fractures and dissolves in deep fluids/groundwater. Such deep fluids could either be of lower crust/ upper mantle origin or originate through downward migration of meteoric water from other locations using the pathways provided by deep fractures and fissures. This could result in setting up of a hydrothermal circulation along the deep seated fractures and fissures. The extent to which these deep fluids may have high concentration of helium is governed by interconnectedness of micro-cracks and fractures and the temperature is governed by the depth up to which any particular hydrothermal circulation cell penetrates.

5.2 Fluoride in Groundwater

Based on the understanding that dissolved salt content of groundwater is to some extent related to leaching from the aquifer matrix, the high fluoride concentration in ground waters of NGC region was earlier believed to be related (i) either to the relatively high concentration of fluoride bearing minerals in certain sub-aquifer zones or to the higher residence time (Patel, 1986). Geographical distribution of dissolved fluoride in groundwater of NGC region, however, reveals that areas of high fluoride concentrations (>1.5 ppm) are not related to residence time. Instead, it is observed that the areas of high fluoride and high EC (>2 mS) are aligned around four lines PP', QQ', RR' and SS' (see Figure 4.5 and Figure 4.8) with the central belt around QQ' having groundwater of higher residence time on the western side and lower residence time on its eastern side.

Within the Cambay Basin in the high fluoride belt around the QQ', certain sub-aquifer zones appeared to have high (>1.5 ppm) groundwater fluoride (see Figure 4.6). Based on investigation of 5 tube wells tapping these high fluoride depth zones within a small region, it appears that if a particular well taps the identified high fluoride depth zone, its water shows high concentration. However, this hypothesis could not be confirmed for other areas within this belt or in other parts of the NGC regional aquifer system due to limited availability of tube wells with suitable conditions for investigation. Instead, the fluoride distribution in the NGC region is explained based on a hydrological model comprising a recharge area in the foothills of the Aravalli Mountains, grading into the confined aquifer south westwards towards LRK-NS-GC belt and general disposition of this semi-arid region to enhanced groundwater fluoride concentration. The groundwater in this aquifer system moves through the confined aquifer with the chemical characteristics acquired in the recharge area but progressively aging as it moves away from the recharge area.

The groundwater ages (using ^{14}C, ^{4}He and $^{4}He/^{222}Rn$ methods) progressively increase away from recharge area but the dissolved fluoride concentration does not increase correspondingly. Instead, as mentioned earlier, alternating bands of high and low fluoride concentration in groundwater from confined aquifers are observed. This observation suggests the possibility of an additional control on fluoride concentration in groundwater of NGC region.

The confined groundwater in the central high fluoride groundwater belt (QQ') within the Cambay Basin corresponds to groundwater ^{14}C age in the range 15-25 kaBP (Figure 4.17). The period around 20 kaBP, corresponding to the Last Glacial Maxima (LGM) is known to be a period of enhanced aridity in the NGC region (Prasad and Gupta, 1999; Pandarinath et al, 1999b; Wasson et al, 1983; Juyal et al, 2003). The enhanced aridity is generally associated with (i) increased evaporation; (ii) decreased rainfall; and (iii) increased dry deposition. Some imprints of evaporation and dry deposition even in the present climate were seen in the ionic concentration (Section 4.1.4) and stable isotopic composition (Section 4.1.5) of modern rainfall. The significant control of dry deposition is seen in the variation of fluoride and EC of fortnightly accumulated rain water samples (Figure 4.11). It is, therefore, inferred that groundwater recharged around LGM in the Aravalli foothills during the period of enhanced aridity has since traveled to its present position within Cambay Basin and corresponds to the central (QQ') high fluoride groundwater belt. The groundwater, with relatively low fluoride concentration, on either side of QQ' suggests recharge during less arid climatic regime.

The eastern (RR') high fluoride belt (see Figure 4.5) located in the recharge area corresponds to the modern recharge. The existence of high fluoride groundwater pockets around RR' in the recharge area is an indication that even under the present geo-environmental conditions, groundwater recharged to the regional aquifer system is predisposed to a certain degree of high fluoride content due to combination of (i) leaching; (ii) dry deposition and evaporation prior to recharge; and (iii) increased rock-water interaction at higher temperatures during hydrothermal circulation (as evidenced in thermal springs).

The line PP' (see Figure 4.5) overlies a low lying LRK-NS-GC tract which is the convergence zone for surface and subsurface drainage. The very high level of groundwater fluoride concentration in this belt is possibly due to evaporative enrichment of salts in the stagnant water in the topographically low lying convergence zone and its infiltration into shallower aquifers. Deep groundwater in this low lying tract may have been recharged during a past arid climate phase (^{14}C age >35 kaBP; ^{4}He age 45-110 kaBP depending on helium release factor).

The high fluoride and EC in the E-W belt (SS'), linking the regions of thermal springs (Tuwa and Lasundra) to the low lying area around Nalsarovar, can be attributed to additional source (hydrothermal fluids with relatively high concentration of ions including fluoride) steadily venting into the groundwater in the recharge area of the confined aquifers around Tuwa and Lasundra throughout the Late Quaternary period and the steady movement of the mixed groundwater in the regional aquifer system. The fluoride contribution by the hydrothermal fluids is so prominent and steady that imprints of the wet/arid excursions in climate are not visible along SS'. Instead a continuous belt of higher fluoride (>1.5 ppm) and high EC (>2 mS) is seen.

It is, therefore, concluded that the high fluoride in groundwater of NGC region is not governed by its residence time in the aquifer but arises from a combination of (i) predisposition of this semi-arid region to high groundwater fluoride resulting from mineral assemblage in surface soils and aquifer matrix aided by general aridity, in particular the enhanced aridity around LGM; (ii) injection of hydrothermal fluids into groundwater; and

(iii) evaporative enrichment in the low lying convergence zone and infiltration into groundwater.

5.3 Isotopes of Oxygen and Hydrogen in Groundwater and Precipitation

The amount weighted average values for the modern rainfall in the NGC region are: $\delta^{18}O = -4.3 \pm 2.1‰$, $\delta D = -33 \pm 16‰$ and *d*-excess $=1.2 \pm 4.8‰$. This *d*-excess value and both the slope (7.6 ± 0.6) and the intercept ($-2.9 \pm 2.2‰$) of the local meteoric water line (LMWL) are lower than the average values of global meteoric water line (GMWL) and are interpreted as isotopic imprints of evaporation from falling raindrops under the present semi-arid climatic regime.

The groundwater samples from the NGC region exhibit a range of variation significantly narrower than that for precipitation and both $\delta^{18}O$ and δD are higher than that for modern precipitation (Figure 4.15). The average value of *d*-excess of all groundwater samples ($-4.5 \pm 11‰$) is also lower than that of precipitation samples. These isotopic characteristics for groundwater in the NGC region indicate mixing of rain water from different events in the soil and additional evaporation during the infiltration process confirming the predisposition of the region to evaporation, prior to groundwater recharge.

It is also seen (Figure 4.16) from the geographical distribution of $\delta^{18}O$ and *d*-excess that groundwater around a linear belt (QQ') is characterized by relatively lower values of *d*-excess and higher values of $\delta^{18}O$. Since evaporation of water results in low values of *d*-excess and higher $\delta^{18}O$ (see Section 2.4), the groundwater around QQ' represents relatively increased evaporation (indicative of enhanced aridity) either during rainfall or during groundwater recharge compared to that on either side of this belt. As mentioned earlier (see Section 5.2), the ^{14}C age of the confined groundwater around QQ' has been estimated to be in the range 15-25 kaBP corresponding to the known arid phase in the past. Taking a holistic view of the data, i.e., 15-25 kaBP groundwater age, its lowered *d*-excess and higher $\delta^{18}O$, it is concluded that groundwater recharged in the Aravalli foothills around LGM with signatures of enhanced aridity has since traveled to its present position. This corroborates enhanced aridity in the past as one of the important causes for the occurrence of enhanced fluoride and EC of groundwater around QQ'.

As mentioned above (see Section 5.2) , the geothermal waters in the NGC region too have high fluoride and EC, and higher values of these geochemical parameters around the line SS' were ascribed to continuous admixture of geothermal waters (in the region around Tuwa and Lasundra thermal springs) to the recharged groundwater. The isotopic exchange during interaction of geothermal waters and silicate rocks at elevated temperatures is known to impart a characteristic shift in the values of $\delta^{18}O$, δD and *d*-excess (see Section 4.2.3). The isotopic exchange with silicate rocks at elevated temperatures results in increase in $\delta^{18}O$, decrease of δD and a corresponding decrease in the *d*-excess values of thermal waters. In the NGC region two areas of significantly high groundwater temperature (>40°C) have been identified. These are: (i) the thermal springs at Lasundra and Tuwa on the eastern flank; and (ii) thermal artesian wells on the western flank of Cambay Basin. The thermal springs are seen to be slightly enriched in ^{18}O and lowered in *d*-excess (average $\delta^{18}O = -1.4 \pm 0.4$ ‰; *d*-excess = -4.1 ± 3.2‰ for 6 samples) compared to ground waters in the surrounding region. On the other hand, thermal artesian wells do not have much different isotopic composition (average $\delta^{18}O = -2.4 \pm 1.0$ ‰; *d*-excess = -6.5 ± 7.3‰ for 8 samples) compared to the other groundwater samples in NGC region. Statistically, these average values are indistinguishable from the average groundwater values for the entire NGC region, but local enrichment of ^{18}O and lowering of *d*-excess in the areas with thermal waters is seen in Figure 4.16.

The enrichment of ^{18}O in the thermal springs/ artesian wells is also associated with high concentration of dissolved helium. Similar enrichment of ^{18}O and lowering of *d*-excess around QQ', however, is not associated with high helium or high temperature and shows age corresponding to LGM and therefore, attributed to past climatic shift. The geothermal waters with enriched ^{18}O and low *d*-excess, on the other hand correspond to modern (on eastern flank) to >45 kaBP age (on western flank).

Thus, isotopic evidence of water-rock interaction in geothermal waters of the NGC region is indicated, though not very strong. It is, therefore, inferred that the $\delta^{18}O$ in thermal springs at Tuwa and Lasundra is perhaps a trend towards isotopic equilibrium between ^{18}O depleted meteoric water and ^{18}O enriched rocks at higher temperatures.

5.4 Groundwater Dating

5.4.1 ^{14}C Dating

It is observed that the succession of sand/ silty-clay layers forming multilayered aquifer system is nearly parallel to the regional inclination of ground surface and the sampled tube wells tap almost the same set of water bearing formations across the NGC region (Figure 1.6). The groundwater in these nearly parallel layers of confined aquifers is recharged largely from the sediment-rock contact zone in the foot hills of Aravalli Mountains, and after the confinement becomes effective, moves with approximately the same velocity. This geohydrological model of the regional aquifer system appears to be justified because, the unconfined aquifers in the regions of Cambay Basin and westwards are almost completely dried up (as evident from several dried up and abandoned dug wells). Since the tubewells tap all the water bearing horizons intercepted within their maximum depth, these are treated as pumping a single aquifer unit, within which the ^{14}C ages progressively increase in the flow direction. The estimated groundwater ^{14}C ages progressively increase from <2 kaBP in the ENE (along Aravalli foothills) to >35 kaBP in the WSW direction towards the low-lying tract linking LRK-NS-GC (Figure 4.17).

From hydro-geological considerations (see Section 1.2), it seems that the confinement of the regional aquifers in the NGC region becomes effective near the ECBBF. The ^{14}C age of the groundwater starts progressively increasing from ~2 kaBP westwards of ECBBF. Within the Cambay Basin, the age isolines are nearly parallel to each other and the horizontal distance between the successive 5 kaBP isolines is nearly constant giving a regional flow velocity in the range 2.5 – 3.5 m a^{-1} under the prevailing average hydraulic gradient of 1 in 2000 (GWRDC, unpublished data). West of WCBBF, the ^{14}C ages increase rapidly, roughly in agreement with the distribution of transmissivity of the aquifers obtained from the pump test data, progressively decreasing from ~1000 m^2 d^{-1} east of the ECBBF to <200 m^2 d^{-1} west of the WCBBF (GWRDC, unpublished data).

5.4.2 ^{4}He Dating

It is seen that the 5 ppmAEU He_{ex} isoline runs nearly along the WCBBF and corresponds to ^{4}He age of ~15 kaBP for helium release factor $\Lambda_{He} = 1$, and ~37 kaBP for $\Lambda_{He} = 0.4$ (Figure 4.1 and Figure 4.18). Except for pockets of anomalous groundwater helium concentrations, the ^{4}He ages (Figure 4.18) are in close agreement with the ^{14}C ages (Figure 4.17) for $\Lambda_{He} = 0.4$ when no crustal flux is considered. Ignoring the crustal flux is justified because the sampled wells up to the WCBBF in the in the NGC region tap shallow depth compared to total depth (~3 km) of the Cambay basin and hence are free from the crustal influence. For transmissivity values (~200 m^2d^{-1} – 1000 m^2d^{-1}) of the aquifers and crustal helium flux of 3.0 x 10^{-8} cm^3STPHe $cm^{-2}y^{-1}$ for sedimentary basin (Takahata and Sano, 2000), the groundwater flow entrains insignificant amount of helium and therefore, groundwater ^{4}He ages are almost unaffected by the deep crustal ^{4}He flux.

5.4.3 ^{4}He /^{222}Rn Dating

A gradual ^{4}He/^{222}Rn age progression from the recharge area towards the WCBBF is observed in the major part of the study area (Figure 4.19), similar to that for ^{14}C ages (Figure 4.17) and ^{4}He ages (Figure 4.18).

5.5 Important Contributions

In the forgoing, main inferences from various geochemical and isotopic investigations of this study were summarised. The major contributions of this study, are enumerated in the following.

5.5.1 A Geo-hydrological Model of Aquifer System in NGC Region

The regional aquifer system of NGC region comprises a sequence of unconfined and confined sub-aquifers. The recharge area of the confined aquifers lies in the foot hills of the Aravalli Mountains in the east. The confinement of aquifers becomes effective only towards west of the ECBBF. Beyond the region of effective confinement, the groundwater in the aquifer system preserves the geochemical and isotopic characteristics acquired at the time of recharge in the recharge area. The groundwater ages progressively increase in the general flow direction nearly along WSW up to the low lying tract of the LRK-NS-GC, which is also a zone of convergence with groundwater flow from its both the sides.

However, in certain pockets overlying the intersecting basement faults, deeper crustal fluids do get injected into the aquifer system and significantly alter some of the geochemical properties of the groundwater of the region.

5.5.2 A Conceptual Tectono-hydrothermal Model of NGC Region

Deeper crustal fluids injected into the groundwater of NGC region have been shown to affect temperature, dissolved helium, water isotopes, fluoride and EC of groundwater in certain pockets. The localization of these pockets along intersecting deep seated basement faults on the two flanks of the Cambay basin is conceptualised in the form of a tectono-hydrothermal model of the NGC region.

This tectono-hydrothermal model (Figure 4.20) involves hydrothermal circulation of water of meteoric origin into deeper crustal layers, its interaction with deeper fluids and its return flow back to shallow depths, either into groundwater or as thermal springs. The faults and fractures provide the pathways for (i) downward percolation of shallow groundwater (of meteoric origin) as also (ii) for the upward migration of return flow with changed geochemical properties due to interaction with deeper fluids. In this manner the hydrothermal circulation imprints its signatures on geochemical properties of groundwater localised over regions of deep seated faults and fractures on both flanks of the Cambay basin where the basement is at relatively shallow depth. The geochemical properties include enhanced helium (produced in large volume of rocks within or below the basement), enhanced temperature (resulting from geothermal gradient ~60°C km^{-1}

during hydrothermal circulation), and enhanced fluoride as also EC and some isotopic characters (acquired from rock-water interaction at elevated temperature). In this model the sedimentary cover overlying the basement rocks acts to diffuse the upward migrating plume of deeper fluids because of the primary porosity of the granular fabric. Whereas, the secondary porosity due to fractures and fissures in the crystalline basement restricts the location of upward migrating plumes. This explains the localization of various anomalies observed on both the flanks and their absence over the Cambay basin between the ECBBF and the WCBBF.

The temperature and geochemical as well as isotopic properties of injected plume depends on interconnectedness of micro-cracks and fractures and the depth of penetration of a hydrothermal circulation cell from where the deeper fluids rise. These factors will locally affect the temperature, geochemical and isotopic characteristic of individual hydrothermal cells. This explains absence of statistical correlation between anomalous helium and temperature of groundwater even while a significant geographical correlation exists between the two.

5.5.3 Origin of High Fluoride in Groundwater from NGC Region

The high fluoride concentration in groundwater of NGC region around the E-W line SS' (Figure 4.5) is explained by a continuous injection throughout Late Quaternary of hydrothermal fluids from around the thermal springs of Lasundra and Tuwa and the groundwater flow in the regional aquifer as governed by hydraulic gradient from the recharge area in the Aravalli foothills towards the Nalsarovar in low lying LRK-NS-GC tract. This mechanism, however, does not explain the observed distribution of enhanced groundwater fluoride around the three nearly NNW-SSE parallel lines PP', QQ' and RR'. This distribution is explained by: (i) predisposition of this semi-arid region to high groundwater fluoride arising from mineral assemblage in surface soils and in aquifer matrix, aided by general aridity particularly in the recharge area around RR'; (ii) enhanced aridity around the LGM leading to recharge of groundwater enriched in fluoride resulting from enhanced evaporation as well as dry deposition and flow of this groundwater to its present location around QQ' during the past 20 ± 5 kaBP; and (iii) evaporative enrichment of stagnant surface water in the low lying LRK-NS-GC convergence zone and infiltration of a part of it into groundwater.

5.5.4 Palaeo-climatic Imprints in Groundwater from NGC Region

As mentioned above, groundwater around the belt QQ' within Cambay Basin corresponds to ^{14}C ages around LGM (20 ± 5 kaBP) which is known to be a period of enhanced aridity in the palaeoclimatic history of the NGC region. The confined groundwater in this belt has characteristic geochemical (high fluoride and high EC) and isotopic (high $\delta^{18}O$ and low *d*-excess) signatures that are different from signatures of these parameters on either side. The alternating bands of groundwater with distinguishable geochemical and isotopic properties can only be explained as imprints of the past climate alternating between arid and humid phase, which modifies the geochemical and isotopic properties of the water infiltrating from the recharge area (Aravalli foothills) of the confined aquifer. The groundwater recharged during different climatic regime flows subsequently in the confined regional aquifer system giving rise to observed alternating bands of groundwater with distinctly different chemical properties. Thus, groundwater around the belt QQ' within Cambay Basin, indicate its recharge during enhanced aridity around LGM.

In addition to the important contributions, as mentioned above, it has also been possible, as a result of this study, to identify areas of future research that will reduce uncertainties in the present understanding of geohydrological processes. This is elaborated in Chapter 6.

Chapter 6. Future Scope

This study has enabled identification of important geohydrological processes and the controls that topographic, climatic, tectonic and geothermal factors exert on the quantity and quality of groundwater in the NGC region. While some of the conclusions may appear not fully substantiated at present, an effort is made to suggest future studies that will either confirm or reject the conclusions in favour of more viable models/ hypotheses leading to further improvement in understanding of the operating hydrologic processes.

6.1 Injection of Hydrothermal Fluids

The geographical coincidence of very high concentrations of dissolved ^{4}He in groundwater and high groundwater temperatures in certain pockets overlying the basement faults in the NGC region, has been ascribed to injection of deeper fluids (having high temperatures and high dissolved helium) in groundwater overlying the deep seated faults and fractures. This opens up the possibility that some of these fluids may be coming up from deep crustal/ upper mantle region. In the present study, it has not been possible to check if these hydrothermal fluids originated from the deep crustal region or else from the upper mantle. This can, however, be checked using $^{3}He/^{4}He$ isotopic ratio measurements in ground waters.

In addition to the atmospheric noble gases (He, Ne, Ar, Kr, Xe, Rn) dissolved in solubility equilibrium, groundwater can also have two other terrigenic components (Kipfer et al, 2002). These can be of: (i) crustal origin; and/ or (ii) mantle origin; each with characteristic $^{3}He/^{4}He$ ratios. The continental crust is dominated by the heavier isotope of helium (^{4}He) that is produced radiogenically in the crustal rocks and minerals. Therefore, crustal rocks and minerals have $^{3}He/^{4}He$ ratio ($<10^{-7}$; Mamyrin and Tolstikhin, 1984; Ballentine and Burnard, 2002). The earth's mantle, on the other hand, contains besides radiogenic ^{4}He relatively higher proportion of isotopically lighter helium (^{3}He) inherited during formation of the earth and has a distinct $^{3}He/^{4}He$ ratio ($>10^{-5}$; Mamyrin and Tolstikhin, 1984; Porcelli and Ballentine, 2002; Graham, 2002). This provides a means for identifying the deep crustal/ mantle fluids and has also been used to infer the possible signatures of mantle fluids in groundwaters and deep lake waters from different parts of the world (Imbach, 1997; Hoke et al, 2000; Kipfer et al 2002).

In India, helium isotopic investigations of several thermal springs in the Narmada-Son-Tapti rift zone do not indicate the presence of any appreciable amount of primordial ^3He (Minissale et al, 2000). However, such an investigation has not been carried out in the NGC region and may, therefore, be useful to check if there is an influx of fluids originating from the upper mantle. The present study can be advantageously used to identify suitable sites for collecting groundwater samples having high dissolved helium and high temperatures, in which $^3He/^4He$ ratio can be measured to identify the source region of the hydrothermal fluids and to ascertain if there is any significant contribution of mantle derived fluids in relatively shallower groundwater.

6.2 Estimation of Palaeo-recharge Temperature

This study has identified imprints of past aridity around the Last Glacial Maxima (LGM) in the NGC region in the form of higher values of fluoride concentration and EC, higher values of $\delta^{18}O$ and δD, and lower values of *d*-excess in groundwater recharged around 20 ± 5 ka BP (Section 4.2.2 and 4.2.3). This inference from chemical and isotopic proxies relates the observed signatures in groundwater to the possible effect of (i) increased evaporation, (ii) increased dry deposition and (iii) decreased rainfall, on groundwater recharged during relatively more arid climate that possibly prevailed in this region in the past (Prasad and Gupta, 1999; Pandarinath et al, 1999b; Wasson et al, 1983; Juyal et al, 2003). However, palaeo-recharge temperatures could not be investigated in this study. Estimation of which can provide a definite signature of past climatic fluctuations as recorded in groundwater.

Noble gases dissolved in groundwater provide a useful tool to estimate the palaeo-recharge temperature. The role that noble gases can play in climate studies was recognised way back in early seventies by Mazor (1972), who noted that the noble gas abundance patterns in ground waters reflect the air temperatures in the recharge area. He suggested that groundwater could be used as an archive of the past climate, because it appears to retain the dissolved gases over many thousands of years. It has been shown that progressively older groundwater down gradient in aquifers preserve record of past temperature variations (Porcelli et al, 2002).

6.3 Identifying the Modern Recharge

To overcome the general scarcity of water, a community and the State driven movement for groundwater recharge has been underway in the NGC region since past several years. Numerous groundwater recharge structures have been constructed but their usefulness and efficiency for artificial recharge has not been tested. The data on lowering of water levels in surface reservoirs and rise of water levels in nearby dug wells is interpreted as due to the groundwater recharge caused by the constructed structure. However, reduction in water levels in reservoirs may also be due to evaporation and consumptive use by human and cattle population. Rise in water levels in adjoining dug wells may partly arise from reduction in groundwater withdrawal due to surface availability of water in the vicinity. Therefore, variation in water levels in reservoirs and dug wells may not necessarily be related to the efficacy of the construction of recharge structures. Measuring dissolved CFCs in the groundwater in vicinity of the recharge structures may provide a more conclusive method to identify as well as quantify the modern recharge for assessing the efficacy of such structures.

Unrelated to any recharge structure, the CFC concentration in groundwater of unconfined aquifer can also be used to estimate the time since the water became isolated from the unsaturated zone during the past few decades. Presence of detectable CFC concentration in confined aquifer indicates mixing of modern water with groundwater recharged prior to 1945 after they were introduced into the atmosphere. Therefore, investigation of dissolved CFCs in groundwater can identify regions where modern waters have infiltrated into deeper layers.

The analytical capabilities for measuring CFC concentration, build during the present study can be readily employed for this purpose.

REFERENCES

Aeschbach-Hertig W, Peeters F, Beyerle U and Kipfer R. (2000). Palaeotemperature reconstruction from noble gases in ground water taking into account equilibration with entrapped air. Nature, 405, 1040–1044.

Aeschbach-Hertig W, Stute M, Clark JF, Reuter RF and Schlosser P. (2002). A palaeotemperature record derived from dissolved noble gases in groundwater of the Aquia aquifer (Maryland, USA). Geochim. Cosmochim. Acta, 66(5), 797–817.

AFEAS. (1997). Production, sales and atmospheric release of fluorocarbons through 1995. Alternative Fluorocarbons Environmental Acceptability Study (AFEAS). Program Office, The West Tower - Suite 400, 1333 H Street NW, Washington, DC 20005, U.S.A.

Agarwal M, Gupta SK, Deshpande RD and Yadava MG. (2006). Helium, radon and radiocarbon studies on a regional aquifer system of the North Gujarat–Cambay region, India. Chem. Geol., 228, 209–232.

Agrawal V, Vaish AK and Vaish P. (1997). Groundwater quality: Focus on fluoride and fluorosis in Rajasthan. Curr. Sci., 73(9), 743–746.

Allison GB, Barnes CJ, Hughes MW and Leaney FWJ. (1984). Effects of Climate and Vegetation on Oxygen-18 and Deuterium Profiles in Soils. In: Isotope Hydrology 1983, IAEA Symposium 270, September 1983, Vienna: 105–123.

Anderews JN, Goldbrunner JE, Darling WG, Hooker PJ, Wilson GB, Youngman MJ, Eichinger L, Rauert W and Stichler W. (1985). A radiochemical, hydrochemical and dissolved gas study of groundwater in the Molase basin of Upper Austria, Earth Planet. Sci. Lett., 73, 317–332.

Andrews JN and Fontes JCh. (1992). Importance of the in situ production of ^{36}Cl, ^{36}Ar and ^{14}C in hydrology and hydrogeochemistry. In Isotopes techniques in Water Resources Development, IAEA, Vienna, pp 245–269.

Andrews JN and Lee DJ. (1979). Inert gases in groundwater from the Bunter Sandstone of England as indicators of age and paleoclimatic trends. J. Hydrol., 41, 233–252.

Andrews JN, Davis SN, Fabryka-Martin J, Fontes JCh, Lehmann BE, Loosli HH, Michelot JL, Moser H, Smith B and Wolf M. (1989). The in situ production of radioisotopes in rock matrices with particular reference to the Stripa granite. Geochim. Cosmochim. Acta 53,1803–1815.

Araguas-Araguas L, Froehlich K and Rozanski K. (1998). Stable isotope composition of precipitation over Southeast Asia. J. Geophys. Res., 103(D22), 28,721–28,742.

Arora BR and Reddy CD. (1991). Magnetovariational study over a seismically active area in the Deccan trap province of western India. Phys. Earth Planet. Inter. 17, 21–28.

Barsukov VL, Varshal GM and Zamokina NS. (1984). Recent results of hydrogeochemical studies for earthquake prediction in the USSR. PAGEOPH, 122, 143–156.

BEIR. (1999). The Health Effects of Exposure to Indoor Radon. Biological Effects of Ionizing Radiation (BEIR) VI Report. National academy of sciences, USA, 1–500.

Bellentine CJ and Burnard PG. (2002). Production, release and transport of Noble gases in the continental crust. In Porcelli, D, Ballentine, CJ and Wieler R. (Eds.) Noble gases in geochemistry and cosmochemistry. Rev. Mineral. Geochem., 47, 481–538.

Bewers JM. (1971). North Atlantic fluoride profiles. Deep Sea Res., 18, 237.

Bhandari LL and Kumar S. (1970). Palaeocurrent analysis of Dhrangadhra Formation, Gujarat, India. Bull. Oil Nat. Gas. Comm., India, 7(2), 101–108.

Bhattacharya SK, Froehlich K, Aggrawal PK and Kulkarni KM. (2003). Isotope variation in Indian monsoon precipitation: records from Bombay and New Delhi. J. Geophys. Res., 30, doi:10.1029/2003GLO18453.

Bhattacharya SK, Gupta SK and Krishnamurthy RV. (1985). Oxygen and hydrogen isotopic ratios in groundwaters and river waters from India. Proc. Indian Acad. Sci.(Earth and Planet. Sci.), 94(3), 283 – 295.

BIS. (1990). Drinking water specifications, IS:10500, Bureau of Indian Standards, New Delhi.

Biswas SK. (1982). Rift Basins in Western margin of India and their hydrocarbon prospects with special reference to Kutch basin. American Assoc. Pet. Geol. Bull., 66 (10), 1497–1513.

Biswas SK. (1987). Regional tectonic framework, structure and evolution of the western marginal basins of India. Tectonophysics, 135, 307–327.

Borole DV, Gupta SK, Krishnaswami S, Datta PS and Desai BI. (1979). Uranium Isotopic investigations and Radiocarbon Measurement of River-Groundwater Systems, Sabarmati Basin, Gujarat, India. Isotopic Hydrology, vol. 1, IAEA, Vienna, pp. 181–201.

Bowen HJM. (1966). Trace elements in biochemistry. Academic Press, London-New York.

Brown JD. (1980). Evolution of Fluorocarbon Compounds as Ground Water Tracers–Soil Column Studies. M.S. Thesis. Department of Hydrology Water Resources, University Arizona, Tuscon, 97p.

Bu X and Warner MJ. (1995). Solubility of chlorofluorocarbon 113 in water and seawater. Deep Sea Res., 42(7), 1151–1161.

Bullister JL and Weiss RF. (1988). Determination of CCl3F and CClF2 in seawater and air. Deep Sea Res. 35(5), 839–854.

Bullister JL. (1984). Atmospheric chlorofluromethanes as tracers of ocean circulation and mixing: Studies in the Greenland and Norwegian seas. Ph.D. Dissertation, University of Califorina, San Diego, La Jolla, 172p.

Burke K and Dewey JF. (1973). Plume generated triple junctions: key indicators in applying plate tectonics to old rocks. J. Geol. 81, 406–433.

Busenberg E and Plummer LN. (1992). Use of chlorofluorocarbons (CCl3F and CCl2F2) as hydrologic tracers and age-dating tools: The alluvium and terrace system of Central Oklahoma. Water Resour. Res., 28(9), 2257–2283.

Carpenter R. (1966). Factor controlling the marine geochemistry of fluorine. Geochem. Cosmochim. Acta, 33, 1153.

Castro MC, Stute M and Schlosser P. (2000). Comparison of ^{4}He ages and ^{14}C ages in simple aquifer systems: implications for groundwater flow and chronologies. Appl. Geochem. 15, 1137–1167.

Chandrasekharam D and Antu MC. (1995). Geochemistry of Tattapani thermal springs, Madhyapradesh, India - Field and experimental investigations. Geothermics 24(4):553–559.

Chandrasekharan H, Sunandra Sarma KS, Das DK, Datta D, Mookerjee P and Navada SV. (1992). Stable isotope contents of perched water under different land use and salinization conditions in the canal command of Arid western Rajasthan. J. Arid Environ., 23, 365–378.

Clark I and Fritz P. (1997). Environmental Isotopes in Hydrogeology, Lewis Publishers, Boca Raton and New York, 328 p.

Clark JF, Davisson ML, Hudson GB and Macfarlane PA. (1998). Noble gases, stable isotopes, and radiocarbon as traces of flow in the Dakota aquifer, Colorado and Kansas. J. Hydrol. 211, 151–167.

Clark JF, Stute M, Schlosser P, Drenkard S and Bonani G. (1997). A tracer study of the Floridan aquifer in southeastern Georgia: Implications for groundwater flow and paleoclilmate. Water Resour. Res., 33, 281–289.

Cook PG and Solomon DK. (1995). The transport of atmospheric trace gases to the water table: Implications for groundwater dating with chlorofluorocarbons and Krypton-85. Water Resour. Res., 31(2), 263–270.

Cook PG and Solomon DK. (1997). Recent advances in dating young groundwater: chlorofluorocarbons, 3H/3He, and 85Kr. J. Hydrol., 191, 245–265.

Cook PG, Solomon DK, Plummer LN, Busenberg E, and Schiff SL. (1995). Chlorofluoricarbons as gracers of groundwater transport processes in a shallow, silty sand aquifer. Water Resources Research, 31(3), 425–434.

Cook PG, Solomon DK, Sanford WE, Busenberg E, Plummer LN, and Poreda RJ. (1996). Inferring shallow groundwater flow in saprolite and fractured rock using environmental tracers. Water Resources Research, 32(6), 1501–1509.

Craig H and Lupton JE. (1976). Primordial neon, helium and hydrogen in oceanic basalts. Earth & Planet. Sci. Lett. 31, 369–385.

Craig H. (1961a). Standard for Reporting Concentrations of Deuterium and Oxygen -18 in Natural Water. Science, 133, 1833–1834.

Craig, H. (1961b). Isotope Variations in Meteoric Waters. Science, 133, 1702–1703.

CRC (1980). CRC handbook of chemistry and physics. 60th Edition. CRC Press, Inc. Boca Raton, Florida.

Cserepes L and Lenkey L. (1999). Modelling of helium transport in groundwater along a section in the Pannonian basin. J. Hydrol, 225, 185–195.

Dansgaard W. (1964). Stable Isotopes in Precipitation. Tellus, 16, 436–438.

Das BK, Kakar YP, Moser H and Stichler W. (1988). Deuterium and oxygen-18 studies in groundwater of the Delhi area, India. J. Hydrol., 1988, 98, 133–146.

Datta PS, Bhattacharya SK and Tyagi SK. (1996). ^{18}O Studies on recharge of phreatic aquifers and groundwater flow-paths of mixing. J. Hydrol., 176, 25–36.

Datta PS, Bhattacharya SK, Mookerjee P and Tyagi SK. (1994). Study of groundwater occurrence and mixing in Pushkar (Ajmer) valley, Rajsthan, with δ^{18}O and hydrochemical data. J. Geol. Soc. Ind., 43, 449–456.

Datta PS, Deb DL and Tyagi SK. (1996). Stable isotope (^{18}O) investigations on the processes controlling fluoride contamination of groundwater. J. Cont. Hydrol., 24(1), 85–96.

Datta PS, Deb DL and Tyagi SK. (1996). Stable isotope (^{18}O) investigations on the proceses controlling fluoride contamination of groundwater. J. Contaminant Hydrol., 24, 85–96.

Datta PS, Gupta SK, Jaisurya A, Nizampurkar VN, Sharma P and Plusnin MI. (1980). A survey of helium in groundwater in parts of Sabarmati basin in Gujarat state and in Jaisalmer district, Rajasthan. Hydrol. Sci. Bull. 26, 183–193.

Datta PS, Tyagi SK and Chandrasekharan H. (1991). Factors controlling stable isotopic composition of rainfall in New Delhi, India. J. Hydrol, 128, 223–236.

Deshmukh AN, Gajbhiye RD and Ganveer JB. (1993). Hydrochemical impact of natural recharge on groundwater quality of fluorosis endemic Dongargaon village, Thsil Warora, District Chandrapur, Maharashtra. Gondwana. Geol. Mag., 6, 16–26.

Deshmukh AN, Shah KC and Sriram A. (1995b). Coal ash: A source of fluoride pollution, A case study of Koradi Thermal Power Station.

Deshmukh AN, Wadaskar PM and Malpe DB. (1995a). Fluorine in Environment: A review. Gondwana Geol. Mag., 9, 1–20.

Deshpande RD, Bhattacharya SK, Jani RA and Gupta SK. (2003). Distribution of Oxygen and Hydrogen Isotopes in Shallow Groundwaters from Southern India: Influence of a Dual Monsoon System. J. Hydrol., 271, 226–239.

Dev Burman GK, Singh B and Khatri P. (1995). Hydrogeochemical studies of groundwater having high fluoride content in Chandrapur district of Vidarbha region, Maharashra. Gondwana Geol. Mag., 9, 71–80.

Dikum AV, Korobeynik VM and Yanitskiy IN. (1975). Some indications of existence of transcrustal gas flow. Geochem. Int., 12(6), 73–78.

Dincer T, Al-Mugrin A and Zimmermann U. (1974). Study of the Infiltration and Recharge through the Sand Dunes in Arid Zones with Special Reference to the Stable Isotopes and Thermonuclear Tritium. J. Hydrol. 23, 79–109.

Dinçer T, Al-Mugrin A and Zimmermann U. (1974). Study of the infiltration and recharge through the sand dunes in arid zones with special reference to stable isotopes and thermonuclear tritium. J. Hydrol., 23, 79–109.

Douglas M. (1997). Mixing and Temporal Variation of Ground Water Inflow at the Con Mine, Yellowknife, Canada: An Analogue for a Radioactive Waste Repository. Unpublished M.Sc. Thesis, Department of Geology, Univ. of Ottawa, Canada.

Drever JI. (1997). The geochemistry of natural waters (surface and groundwater environments) 3rd Edition, Prentice Hall, Upper Saddle River, NJ 07458, pp. 436.

Dunkle SA, Plummer LN, Busenberg E, Phillips PJ, Denver JM, Hamilton PA, Michel RL and Coplen TB. (1993). Chlorofluorocarbons (CCl_3F and CCl_2F_2) as dating tools and hydrologic tracers in shallow ground water of the Delmarva Peninsula, Atlantic coastal plain, United States. Water Resour. Res., 29(12), 3837–3860.

Edmunds WM. (2001). Integrated geochemical and isotopic evaluation of regional aquifer systems in arid regions. In Proceedings: Regional Aquifer Systems In Arid Zones - Managing Non-Renewable Resources. Ihp-Vi Technical Documents in Hydrology, 42, 107-118.

Elkins JW, Thompson TM, Swanson TH, Butler JH, Hall BD, Cummings SO, Fisher DA and Raffo AG. (1993). Decrease in the growth rates of atmospheric chlorofluorocarbons 11 and 12. Nature, 364, 780–783.

Filippo MD, Lombardi S, Nappi G and Reimer GM. (1999). Vocano-tectonic structures, gravity and helium in geothermal areas of Tuscany and Latium (Vulsini volcanic district), Italy. Geothermics, 28(3), 377–393.

Fitts CR. (2002). Groundwater Science. Acedemic Press. 450p.

Fleischer M and Robinson WO. (1963). Some problems of the geochemistry of fluorine. *In* Studies in analytical geochemistry Shaw DM. (Ed). Toronto, University of Toronto Press.

Fontes JC and Garnier JM. (1979). Determination of the initial ^{14}C activity of the total dissolved carbon: A review of the existing models and new approach. Water Resour. Res., 15(2), 399–413.

Forstel H. (1982). $^{18}O/^{16}O$ Ratio of Water in Plants and Their Environment. *In* Stable Isotopes, (eds Schmidt, H. L., Forstel, H. and Heinzinger, K.) Elsevier, pp. 503–516.

Friedman I and Denton EH. (1975). A portable helium sniffer. US Geological Survey, Open File Report 75–532.

Fröhlich K and Gellermann R. (1987). On the potential use of uranium isotopes for groundwater dating. Chem. Geol., 65, 67–77.

Fry VA, Istok JD, Semprini L, O'Reilly LT and Buscheak TE. (1995). Retardation of dissolved oxygen due to a trapped gas phase in porous media. Groundwater, 333, 391–398.

Gamlen PH, Lane BC, Midgley PM and Steed JM. (1986). The production and release to the atmosphere of CCl_3F and CCl_2F_2 (chlorofluorocarbons CFC 11 and CFC 12). Atmos. Environ. 20, 1077–1085.

Gat JR and Matsui E. (1991). Atmospheric water balance in the Amazon basin: an isotopic evapotranspiration model. J. Geophys. Res., 96 (D7), 13179–13188.

Geyh MA. (1990). Absolute age determination: Physical and Chemical dating methods and their applications. Springer Verlag, Germany, 503 pp.

Gmelin L. (1959). Handbuch der anorganischen Chemie. Fluor Erganzungsband, 8, Auflage. Weinheim, VerlagChemie, GmbH.

Golubev VS, Yeremeyev AN and Yanitskiy IN. (1975). Analysis of some models of helium migration in the lithosphere. Geochem. Int., 11(4) 734–742.

Gombos AM, Powel WG and Norton IO. (1995). The tectonic evolution of western India and its impact on hydrocarbon occurrences: an overview. Sedimentary Geology, 96, 119–129.

Gonfiantini R. (1978). Standards for Stable Isotope Measurements in Natural Compounds. Nature, 271, 534–536.

Gonfiantini R. (1986). Environmental isotopes in lake studies. *In* Handbook of Environmental Isotope Geochemistry (eds. Fritz, P. and Fontes, J.-Ch.), vol. 2, The Terrestrial Environment. B. Elsevier, Amsterdam, The Netherlands, pp. 113–168.

Graham DW. (2002). Noble gas isotope geochemistry of mid-oceanic ridge island basalts: characterization of mantle source reservoir. In Porcelli, D, Ballentine, CJ and Wieler R. (Eds.) Noble gases in geochemistry and cosmochemistry. Rev. Mineral. Geochem., 47, 247–318.

GSI. (2000). Seismotectonic Atlas of India and its environs. Geological Survey of India, Calcutta, India. 87pp.

Gulec N, Hilton DR and Mutlu H. (2002). Heliumisotope variations in Turkey: relationship to tectonics, volcanism and recent seismic activities. Chemical Geology, 187, 129–142.

Gupta ML, Verma RK, Hamza VM, Rao GV and Rao RUM. (1970). Terrestrial heat flow and tectonics of the Cambay basin, Gujarat State (India). Tectonophysics, 10, 147–163.

Gupta ML. (1981). Surface heat flow and igneous intrusion in the Cambay basin, India. J. Volc. Geother. Res. 10, 279–292.

Gupta SK and Deshpande RD. (1998). Depleting Groundwater Levels and Increasing Fluoride Concentration in Villages of Mehsana District, Gujarat, India: Cost to Economy and Health. Water Resources Research Foundation (WRRF), PRL, Ahmedabad 74pp

Gupta SK and Deshpande RD. (2003a). Origin of groundwater helium and temperature anomalies in the Cambay region of Gujarat, India. Chem. Geol., 198, 33–46.

Gupta SK and Deshpande RD. (2003b). Dissolved helium and TDS in groundwater from Bhavnagar in Gujarat: Unrelated to seismic events between August 2000 and January 2001. Proc. Indian Acad. Sci. (Earth Planet. Sci.), 112(1), 51–60.

Gupta SK and Deshpande RD. (2003c). Synoptic hydrology of India from the data of isotopes in precipitation. Curr. Sci., 85(11), 1591–1595.

Gupta SK and Deshpande RD. (2005a). Groundwater Isotopic Investigations in India: What has been learned? Curr. Sci., 89(5), 825–835.

Gupta SK and Deshpande RD. (2005b). Isotopes for Water Resource Management in India. Himalayan Geology, 26(1), 211–222.

Gupta SK and Deshpande RD. (2005c). The Need and Potential Applications of a Network for Monitoring of Isotopes in Waters of India. Curr. Sci., 88(1), 107–118.

Gupta SK and Polach HA. (1985). Radiocarbon Dating Practices at ANU., Handbook, Radiocarbon Laboratory, Research School of Pacific Studies, ANU, Canberra, 173p.

Gupta SK and Sharma P. (1984). Soil Moisture Transport Through Unsaturated Zone: Tritium Tagging Studies in Sabarmati Basin, Western India., Hydrol. Sci. J., 29(2), 177-189.

Gupta SK, Bhandari N, Thakkar PS and Rengarajan R. (2002). On the Origin of the Artesian Groundwater and Escaping Gas at Narveri After the Bhuj Earthquake in 2001. Curr. Sci., 82(4), 463–468.

Gupta SK, Deshpande RD, Agarwal M and Raval BR. (2005a). Origin of high fluoride in groundwater in the North Gujarat-Cambay region, India. Hydrogeol. J., 13, 596–605.

Gupta SK, Deshpande RD, Bhattacharya SK and Jani RA. (2005b). Groundwater $\delta^{18}O$ and δD from Central Indian Peninsula: Influence of Arabian Sea and the Bay of Bengal Branches of Summer Monsoon. J. Hydrol., 303(1-4), 38-55.

Gupta SK, Lal D and Sharma P. (1981). An approach to determining pathways and residence time of groundwaters: Dual radiotracer dating. J. Geophys. Res., 86 (C6), 5292–5300.

Gupta SK, Lau LS, Moravcik PS and El-Kadi A. (1990). Injected helium: a new hydrological tracer. Special Report 06.01:90, Water Resources Research Center, University of Hawaii at Manoa, Honolulu.

Gupta SK. (2001). Modelling advection –dispersion process for dual radiotracer dating of groundwater with an example of application to a ^{14}C nd ^{36}Cl data set from Central Australia. In Modelling in hydrogeology (Eds. Elango L and Jayakumar R.) pp. 169–190.

Guymon GL. (1972). Notes on the finite element solution of diffusion advection equation. Water Resources Res., 8, 1357–1360.

Hamid S, Dray M, Fehri A, Dorioz JM, Normand M and Fontes J Ch. (1989). Etude des transfers d'eau a l'interieur d'une formation morainique dans le Bassin du Leman-transfer d'eau dans la zone non-saturee, J. Hydrol., 109, 369–385.

Handa BK. (1975). Geochemistry and genesis of fluoride containing groundwaters in India. Ground water, 13, 275–281.

Handa BK. (1977). Presentation and interpretation of fluorine ion concentrations in natural waters. Proc. Sym. on fluorosis, Hyderabad, 317–347.

Hardas MG. (1980). Textural parameters and depositional processes of the sub-surface Serau Formation, Cambay Basin. J. Palaeontol. Soc. India, 25, 106–109.

Heaton THE and Vogel JC. (1981). "Excess air" in groundwater. J. Hydrol., 50, 201–216.

Heaton THE. (1981). Dissolved gases: Some applications to groundwater research. Trans. Geol. Surv. Soc. S. Afr., 84, 91–97.

Heaton THE. (1986). Dissolved gas palaeotemperatures and ^{18}O variations derived from the groundwater near Uitenhage, South Africa. Quat. Res., 25, 79–88.

Hofer M and Imboden DM. (1998). Simultaneous determination of CFC-11, CFC-12, N2 and Ar in water. Anal. Chem. 70, 724–729.

Hoke L, Lamb S, Hilton DR and Poreda RJ. (2000). Southern limit of mantle derived geothermal helium emissions in Tibet: implications for lithospheric structure. Earth and Planet. Sci. Lett., 180, 297308.

Holocher J, Peeters F, Aeschbach-Hertig W, Hofer M, Brennwald M, Kinzelbach W and Kipfer R. (2002). Experimental investigations on the formation of excess air in quasi-saturated porous media. Geochem. Cosmochim. Acta, 66 (23), 4103–4117.

Hubner M. (1969a). Untersuchung der F/OH Austauscha-dsorption an Mineralen der Illitgruppe und an Kaolinit. Freiberger Forschungsheft c 244 Mineralogie-Lagerstattenlehre.

Hubner M. (1969b). Geochemische Interpretation von Fluorid/Hydroxid-Austauschversuchen an Tonmineralen Ber. Deutsch. Ges. Geol. Wiss. B. Miner. Lagerstattenforsch, 14, 5.

Imbach T. (1997). Deep groundwater circulation in the tectonically active area of Bursa, Northwest Anatolia, Turkey. Geothermics, 26(2), 251–278.

Ivanovich M. (1992). Uranium series disequilibrium: Applications to earth marine and environmental sciences. Claderon Press, Oxford, pp 910.

Jacks G, Rajagopalan K, Alveteg T and Jonsson M. (1993). Genesis of high F groundwaters, southern India. Applied Geochemistry Suppl Issue 2, 241–244.

Jean-Baptiste P, Messias MJ, Alba C, Charlou JL and Bougault H. (1994). A simple copper-tube sampler for collecting and storing seawater for post-cruise CFC measurements. Deep Sea Res., 41(9), 1361–1372.

Jones VT and Drozd RJ. (1983). Predictions of oil and gas potential by near-surface geochemistry. Amer. Asso. Petrol. Geol. Bull., 67(6), 932–952.

Juyal N, Chamyal LS, Bhandari S, Bhushan R and Singhvi AK. (2006). Continental records of the southwest monsoon during the last 130ka: evidence from the southern margin of the Thar Desert, India. Quat. Sci. Rev., 2632–2650.

Juyal N, Kar A, Rajaguru SN and Singhvi AK. (2003). Luminescence chronology of aeolian deposition during the Late Quaternary on the southern margin of Thar Desert, India. Quat. Inter., 104, 87–98.

Kaila KL and Krishna VG. (1992). Deep seismic sounding studies in India and major discoveries. Curr. Sci., 62, 117–154.

Kaila KL, Krishna VG and Mall DM. (1981). Crustal structure along Mehmadabad-Billimora profile in the Cambay Basin, India, from deep seismic soundings. Tectonophysics, 76, 99–133.

Kaila KL, Rao IBP, Rao PK, Rao NM, Krishna VG and Sridhar AR. (1989). D.S.S. studies over Deccan traps along the Thuadara-Sendhawa-Sindad profile, across Narmada-Son lineament, India. In: Properties and Processes of Earth's Lower Crust. Mereu R.F., Mueller, S., Fauntain, D.M. (Eds.), pp.127–141, AGU Geophy. Mono. 51, IUGG6.

Kaila KL. (1988). Mapping the thickness of Deccan Trap flows in India from DSS studies and inferences about hidden Mesozoic basin in the Narmda-Tapti region. Mem. Geol. Soc. India., 10, 91–116.

Kendall C and McDonnell JF. (1998). Isotope tracers in catchment hydrology. Elsevier Sciences, BV., Amsterdam, The Netherlands, p. 839.

Khalil MAK and Rasmussen RA. (1989). The potential of soils as a sink of chlorofluorocarbons and other man-made chlorofluorocarbons. Geophys. Res. Lett., 16, 679–682.

Kipfer R, Werner Aeschbach-Hertig, Peeters F and Stute M. (2002). Noble gases in lakes and ground waters. In Porcelli, D, Ballentine, CJ and Wieler R. (Eds.) Noble gases in geochemistry and cosmochemistry. Rev. Mineral. Geochem., 47, 615–700.

Koritnig S. (1951). Ein Beitrag zur Geochemie des Fluor. (A contribution to the geochemisty of fluorine) Geochem Cosmochim Acta, 1, 89.

Krishnamurthy RV and Bhattacharya SK. (1991). Stable Oxygen and Hydrogen Isotope Ratios in Shallow Groundwaters from India and a Study of the Role of Evapotranspiration in the Indian Monsoon. The Geochemical Society, Spl. Publ. 3, 187–193.

Krishnaswami S and Seidemann DE. (1988). Comparative study of ^{222}Rn, ^{40}Ar, ^{39}Ar and ^{37}Ar leakage from rocks and minerals: Implications to the role of nanopores in gas transport through natural silicates. Geochim. Cosmochim. Acta, 52, 655–658.

Krishnaswami S, Bhushan R and Baskaran M. (1991). Radium isotoes and ^{222}Rn in shallow brines, Kharaghoda (India). Chemical Geology, 87, 125–136.

Kulongoski JT, Hilton DR and Izbicki JA. (2003). Helium isotope studies in the Mojave Desert, California: implications for groundwater chronology and regional seismicity. Chem. Geol., 202, 95–113.

Kulongoski JT, Hilton DR and Izbicki JA. (2005). Source and movement of helium in the eastern Morongo groundwater basin: The influence of regional tectonics on crustal and mantle helium fluxes. Geochemica et Cosmochemica Acta, 69 (15), 3857–3872.

Kumar B, Athavale RN and Sahay KSN. (1982). Stable isotope geohydrology of the Lower Maner Basin, Andhra Pradesh, India. J. Hydrol, 59, 315–330.

Lehmann BE, Loosli HH, Rauber D, Thonnard N and Willis RD. (1991). ^{81}Kr and ^{85}Kr in groundwater, Milk River Aquifer, Alberta, Canada. Appl. Geochem., 6, 419–424.

List RJ. (1949). Smithsonian Meteorological Tables. Sixth ed., Smithsonian Institution Press, Washington, D.C. 527p.

Luke J. (1997). The Effect of Fluoride on the Physiology of the Pineal Gland. Ph.D. Thesis. University of Surrey, Guildford.

Lupton JE, Weiss RF and Craig H. (1977). Mantle helium in the Red Sea. Nature. 266, 244–246.

Mamyrin BA and Tolstikhin LN. (1984). Developments in geochemistry (3), Helium isotopes in Nature. Elsevier, pp. 273.

Maurya DM, Chamyal LS and Merh SS. (1995). Tectonic evolution of the Central Gujarat plain, western India. Curr. Sci., 69(7), 610–613.

Maurya DM, Malik JN, Raj R and Chamyal LS. (1997). Soft sediment deformation in the Quaternary sediments of the Lower Mahi river basin, Western India. Curr. Sci., 72 (7), 519–522.

Mazor E and Bosch A. (1992). Helium as semi-quantitative tool for groundwater dating in the range of 104-108 years. In Isotopes of noble gases as tracers in environmental studies, IAEA, Vienna, pp 163–178.

Mazor E. (1972). Palaeotemperatures and the other hydrological parameters deduced from noble gases dissolved in groundwaters; Jordan Rift Valley, Israel, Geochim Cosmochim Acta, 36, 1321–1336.

McFarland M and Kaye J. (1992). Chlorofluorocarbons and ozone. Photochemistry and Photobiology, 55, 911–29.

Merh SS and Chamyal LS. (1993). The Quaternary sediments in Gujarat. Curr. Sci. 64, 823–827.

Merh SS. (1993). Neogene-Quaternary sequence in Gujarat: A review. J. Geol. Soc. Ind., 41, 256–276.

Merh SS. (1995). Geology of Gujarat. Geological Society of India, Bangalore, 222 p.

Midgley PM and Fisher DA. (1993). Production and release to the atmosphere of chlorodifluoromethane (HCFC-22). Atmos. Environ., 27A, 2215–2223.

Minissale A, Vaselli O, Chandrasekharam D, Magro G, Tassi F and Casiglia A. (2000). Origin and evolution of 'intracratonic' thermal fluids from central-western peninsular India. Earth Planet. Sci. Lett., 181, 377–397.

Misra KS. (1981). The tectonic setting of Deccan volcanism in southern Saurashtra and northern Gujarat. Deccan volcanism and related basalts provinces in other pars of the world. Geol. Surv. Ind. Memoir, 3, 81–86.

Misra KS. (2001). Lineament fabric and its relation to the eruption of Deccan volcanics and seismicity of west-central India. Geol. Surv. Ind., Spl. Publ., 64, 209–221.

Mook WG. (1976). The dissolution-exchange model for dating groundwater with ^{14}C. In Interpretation of environmental isotopes and hydrochemical data in groundwater hydrology. IAEA, Vienna, pp 213–225.

Münnich KO. (1957). Messung des ^{14}C – Gehaltes von hartem Grundwasser. Naturwissenschaften, 34, 32–33.

Münnich KO. (1968). Isotopen-Datierung von Grundwasser, Naturwissenschaften, 55, 158–163.

Navada SV and Rao SM. (1991). Study of Ganga River – groundwater interaction using environmental ^{18}O. Isotopenpraxis, 27(8), 380–384.

Navada SV, Nair AR, Rao SM, Paliwall BL and Dashy CS. (1993). Groundwater Recharge Studies in Arid Region of Jalore, Rajasthan Using Isotope Techniques. J. Arid Environ., 24, 125–133.

Nazaroff WW, Moed BA, Sextro RG. (1988). Soil as a source of Indoor Radon: Generation, Migration and Entry. In: Nazaroff, W.W. and Nero, A.V. Jr.,(Eds.),Radon and its decay Products in Indoor Air, John Wiley & Sons, NY.

Negi JG, Agrawal PK, Singh AP and Pandey OP. (1992). Bombay gravity high and eruption of Deccan flood basalts India from a shallow secondary plume. Tectonophysics 206, 341–350.

Oelschläger W. (1965). Die Verunreinigung der atmosphere durch fluor. Z.Staub, 12, 528.

Panda PK. (1985). Geothermal maps of India and their significance in resources assessments. Petrol. Asia J. VIII 2, 202–210.

Pandarinath K, Prasad S and Gupta SK. (1999a). A 75 ka record of Palaeoclimatic changes inferred from crystallinity of Illite from Nal Sarovar, Western India. J. Geol. Soc. India, 54, 515–522.

Pandarinath K, Prasad S, Deshpande RD and Gupta SK. (1999b). Late Quaternary sediments from Nal Sarovar, Gujarat, India: Distribution and Provenance. Proc Indian Acad Sci (Earth Planet Sci), 108(2), 107–116.

Pandey OP and Agrawal PK. (2000). Thermal regime, hydrocarbon maturation and geodynamic events along the western margin of India since late Cretaceous. J. Geodyn. 30, 439–459.

Patel PP. (1986). A Note On Drinking Water Problem In The Patan-Chanasma Area Of Mehsana District. Dept. of Geology, M.S. Univ. of Baroda, Vadodara-390 002, India.

Perel'man AI. (1977). Geochemistry of elements in the supergene zone. Keter Publishing House, Jerusalem Ltd. pp 266.

Perry JH. (1984). Chemical Engineers' Handbook. McGraw-Hill Book Company, New York.

Plummer LN and Busenberg E. (1999). Chlorofluorcarbons. In Environmental tracers in subsurface hydrology. Cook PG and Herczeg AL. (Eds.), Kluwer Academic Publishers, Boston-Dordrecht-London, 441–478.

Porcelli D and Ballentine CJ. (2002). Models of the distribution of terrestrial noble gases and evolution of the atmosphere. In Porcelli, D, Ballentine, CJ and Wieler R.

(Eds.) Noble gases in geochemistry and cosmochemistry. Rev. Mineral. Geochem., 47, 411–480.

Porcelli D, Ballentine CJ and Wieler R. (2002). An overview of noble gas geochemistry and comochemistry. In Porcelli, D, Ballentine, CJ and Wieler R. (Eds.) Noble gases in geochemistry and cosmochemistry. Rev. Mineral. Geochem., 47, 1–19.

Prasad S and Gupta SK. (1999). Role of eustasy, climate and tectonics in late Quaternary evolution of Nal-Cambay region, NW India. Z Geomorph N F, 43, 483–504.

Prasad S, Kusumgar S and Gupta SK. (1997). A mid-late Holocene record of palaeoclimatic changes from Nal Sarovar: A palaeo-desert margin lake in western India. J Quat Sci 12:153–159

Prasad S, Pandarinath K and Gupta SK. (1998). Geomorphology, tectonism and sedimentation in the Nal region, western India. Geomorphology, 25, 207–223.

Raju ATR. (1968). Tertiary basins of India. Am. Assoc. Pet. Geol. Bull., 52, 2422–2437.

Rama and Moore WS. (1984). Mechanism of transport of U-Th series radioisotopes from solids into groundwater. Geochim. Cosmochim. Acta, 48, 395–399.

Ramakrishnan S. (1998). Groundwater. Published by S. Ramakrishnan, Chennai 761pp

Randall JH and Schultz TR. (1976). Chlorofluorocarbons as hydrologic tracers: A new technology. Hydrology Water Resources Arizona Southwest 6, 189–195.

Rank D, Volkl G, Maloszewski P and Stichler W. (1992). Flow Dynamics in an Alpine Karst Massif Studied by Means of Environmental Isotopes. In Isotope techniques in Water Resources Development, Proc. IAEA Symposium 319, Vienna, 1991, pp 327–343.

Rao GV, Reddy GK, Rao RUM and Gopalan K. (1994). Extraordinary helium anomaly over surface rupture of September 1993 Killari earthquake, India.

Ravi Shankar. (1988). Heat flow map of India and discussions on its geological and economic significance. Ind. Min. 42, 89–110.

Raynolds GW, Hoff JT and Gillham RW. (1990). Sampling bias caused by materials used to monitor halocarbons in groundwater. Environ. Sci. Technol., 24, 135–142.

Reddy DV, Sukhija BS, Nagabhushanam P, Reddy GK, Devender Kumar and Lachassagne P. (2006). Soil gas radon emanometry: A tool for delineation of fractures for groundwater in granitic terrains. J. Hydrology, 329(1-2), 186–195.

Reimer GM. (1976). Design and Assembly of a portable helium leak detector for evaluation as a uranium exploration instrument. US Geol. Sur. Open-File Rep., 18, 76–398.

Reimer GM. (1984). Prediction of central California earthquakes from soil-gas helium, PAGEOPH 122, 369–375.

Riley JP. (1965). The occurrence of anomalously high fluoride concentrations in the North Atlantic. Deep Sea Res., 12, 219.

Rozanski K, Araguas-Araguas L and Gonfiantini R. (1993). Isotopic Patterns in Modern Global Precipitation. In: Climate Change in Continental Isotopic Records. American Geophysical Union Monograph, 78, 1–36.

Salati E, Dall'olio A, Matusi E and Gat JR. (1979). Recycling of water in Amazon Basin: an Isotopic Study. Water Resour. Res.,15, 1250–1258.

Sareen BK, Tandon SK and Bhola AM. (1993). Slope deviatory alignment, stream network and lineament orientation of Sabarmati river system. Neotectonic activity in the Mid-Late Quaternary. Curr. Sci., 64, 827–836.

Scheidegger AE. (1961). General theory of dispersion in porous media. J. Geophy. Res., 66,3273–3278.

Schlosser P, Stute M, Sonntag C and Munnich KO. (1989). Tritiogenic ^{3}He in shallow groundwater. Earth Planet. Sci. Lett., 94, 245–256.

Schultz TR, Randall JH, Wilson LG and Davis SN. (1976). Tracing sewage effluent recharge- Tucson, Arizona. Ground Water, 14, 463–470.

Semprini L, Hopkins GD, Roberts PV and McCarty PL. (1990). In-situ biotransformation of carbon tetrachloride, 1,1,1,-trichloroethane, Freon-11, and Freon-12 under anoxic conditions. Eos, Trans. Am. Geophys. Union, 71, 1324.

Shapiro MH. (1981). Relationship of the 1979 southern California radon anomaly to a possible regional strain event. J. Geophy. Res., 86, 1725–1730.

Shivanna K, Kulkarni UP, Joseph TB and Navada SV. (2004). Contribution of storm to groundwater in semi-arid regions of Karnataka, India, Hydrological Processes, 18(3), 473–485.

Singh AP and Meissner R. (1995). Crustal configuration of the Narmada-Tapti region India from gravity studies. J. Geodyn. 20, 111–127.

Singh AP. (1998). 3-D structure and geodynamics evolution of accreted igneous layer in the Narmada-Tapti region. J. of Geodyn. 252, 129–141.

Solomon DK, Hunt A and Poreda RJ. (1996). Source of radiogenic helium-4 in shallow aquifers: Implications for dating young groundwater. Water Resour. Res., 32, 1805–1813.

Solomon DK, Schiff SL, Poroda RJ and Clark WB. (1993). A validation of the 3H/3He method for determining groundwater recharge. Water Resources Research, 29(9), 2951–2962.

Sridhar V, Chamyal LS and Merh SS. (1994). North Gujarat rivers: remnants of super fluvial system. J. Geol. Soc. Ind. 44, 427–434.

Srivastava P, Juyal N, Singhvi, AK, Wasson RJ and Bateman MD. (2001). Luminescence chronology of river adjustment and incision of Quaternary sediments in the alluvial plain of the Sabarmati River, North Gujarat, India. Geomorphology, 36, 217–229.

Srivastava, BN, Deshmukh AN and Kodate JK. (1995). The impact of groundwater composition of fluorite solubility product: A case study of selected Indian aquifers. Gondwana Geol. Mag., 9, 31–44.

Strunz H. (1970). Mineralogische Tabellen, 5. Aufl. Leipzig, Geest und Portig.

Stute M, Schlosser P and Clark JF. (1992a). Palaeotemperatures in Southwestern United States derived from the noble gases in groundwater. Science, 256, 1000–1003.

Stute M, Sonntag C, Deak J and Schlosser P. (1992b). Helium in deep circulating groundwater in the Great Hungarian Plain: Flow dynamics and crustal and mantle helium fluxes. Geochim. Cosmochim. Acta, 56, 2051–2067.

Sugawara K. (1967). Migration of elements through phases of the hydrosphere and atmosphere. In AP Vinogradov (ed) Chemistry of the Earth's Crust, Vol 2, Jerusalem: Israel Program for Scientific Translations 501pp.

Sukhija BS, Reddy DV and Nagabhushanam P. (1998). Isotopic fingerprint of palaeoclimates during the last 30,000 years in deep confined groundwaters of Southern India. Quat. Res., 50, 252–260.

Tandon SK, Sareen, BK, Someshwararao M and Sighvi AK. (1997). Aggradation history and luminescence chronology of Late Quaternary semi-arid sequenfces of the Sabarmati basin, Gujarat, western India. Palaeogeogr. Palaeoclimatol. Palaeoecol. 128, 339–357.

Thompson GM, Hayes JM and Davis SN. (1974). Fluorocarbon tracers in hydrology. Geophys. Res. Lett., 1, 177–180.

Torgensen T and Ivey GN. (1985). Helium accumulation in groundwaters, II. A model for the accumulation of the crustal 4He degassing flux. Geochim. Cosmochim. Acta, 49, 2445–2452.

Torgersen T and Clarke WB. (1985). Helium accumulation in groundwater, I: An evaluation of sources and the continental flux of crustal 4He in the Great Artesian Basin, Australia. Geochim. Cosmochim. Acta, 49, 1211–1218.

Torgersen T. (1980). Controls on pore-fluid concentration of ^{4}He and ^{222}Rn and the calculation of ^{4}He/^{222}Rn ages. J. Geochem. Explor. 13, 57–75.

Torgersen T. (1992). Helium-4 model ages for pore fluids from fractured lithologies, Discussion and application. In Isotopes of Noble Gases as Tracers in Environmental Studies. IAEA, Vienna, pp 179–201.

Vasavada BJ. (1998). Excessive fluoride in Gujarat. A perspective plan of solution. J. Indian Water Works Assoc., 1998, 191–198.

Virk HS, Walia V and Kumar N. (2001). Helium/radon precursory anomalies of Chamoli earthquake, Garhwal Himalaya, India. Journal of Geodynamics, 31, 201–210.

Vogel JC. (1967). Investigation of groundwater flow with radiocarbon. *In* Isotopes in hydrology, IAEA, Vienna, pp 355–368.

Vogel JC. (1970). Carbon-14 dating of groundwater. *In* Isotope hydrology. IAEA, Vienna, pp 225–237.

Volk CM, Elkins JW, Fahey DW, Dutton GS, Gilligan JM, Loewenstein M, Podolske JR, Chan KR and Gunson MR. (1997). Evaluation of source gas lifetimes from stratospheric observations. J. Geophys. Res. – Atmos., 102(D21), 25543–25564.

Warner MJ and Weiss RF. (1985). Solubilities of chlorofluorocarbons 11 and 12 in water and seawater. Deep Sea Res. 32, 1485–1497.

Wasson RJ, Rajguru SN, Misra VN, Agrawal DP, Dhir RP and Singhvi AK. (1983). Geomorphology, Late Quaternary stratigraphy and palaeoclimatology of the Thar dune field. Z Geomorph NF, 45,117–151.

Wedepohl KH. (1974). Hand-book of Geochemistry. Vol. II-4, Springer-Verlage, Berlin, Heidelberg, New York, pp 9K-1.

Weeks EP, Earp DE and Thompson GM. (1982). Use of atmospheric fluorocarbons F-11 and F-12 to determine the diffusion parameters of the unsaturated zone in the southern high plains of Texas. Water Resources Research, 15, 1365–1378.

Weismann TJ. (1980). Developments in geochemistry and their contribution to hydrocarbon exploration. *In* Proceedings of the 10th World Petroleum Congress, Bucharest, Romania, Vol. 2, 369–386.

Weiss RF and Price BA. (1980). Nitrous oxide solubility in water and seawater. Mar. Chem. 8, 347–359.

Weiss RF. (1971). Solubility of helium and neon in seawater. J. Chem. Eng. Data, 167, 235–241.

WHO. (1970). Fluorides and human health. World Health Organisation, Geneva

WHO. (1984). Fluorine and fluorides. Environmental health Criteria 36, World Health Organisation, Geneva

Wilkowske CD and Solomon DK. (1997). Evaluation of a simple copper tube sampler for dating ground water with chlorofluorocarbons (CFCs). Geological Society of America, 1997 Annual Meeting, GSA Abstracts with Programs, 29(6), A–77.

Yadav DN. (1997). Oxygen isotope study of evaporating brines in Sambar lake, Rajasthan (India). Chem. Geol., 138, 109–118.

Yong L and Hua ZW. (1991). Environmental characteristics of regional groundwater in relation to fluoride poisoning in North China. Environ. Geol. Water Sci., 18:3–10.

Zero DT, Raubertas RF, Pedersen AM, Fu J, Hayes AL and Featherstone JD. (1992). Studies of fluoride retention by oral soft tissues after the application of home-use topical fluorides. J. Dental Res. 71, 1546–1552.

Zeuner FE. (1950). Stone age Pleistocene chronology of Gujarat. Deccan College Monograph, 6, 46 pp.

Zimmermann U, Munnich KO and Roether W. (1967). Downward Movement of the Soil Moisture Traced By Means of Hydrogen Isotopes. In: Isotope Techniques in the Hydrologic Cycle. Geophysical Monograph Series 11, American Geophysical Union.

Publications

1. Agarwal M, Gupta SK, **Deshpande RD** and Yadava MG. (2006). Helium, radon and radiocarbon studies on a regional aquifer system of the North Gujarat–Cambay region, India. Chem. Geol., 228, 209–232.
2. Gupta SK and **Deshpande RD**, Agarwal M and Raval BR. (2005). Origin of high fluoride in groundwater in the North Gujarat-Cambay region, India. Hydrogeol. J., 13, 596–605.
3. Gupta SK and **Deshpande RD.** (2003). Origin of groundwater helium and temperature anomalies in the Cambay region of Gujarat, India. Chem. Geol., 198, 33–46.
4. Gupta SK and **Deshpande RD.** (2003). Dissolved helium and TDS in groundwater from Bhavnagar in Gujarat: Unrelated to seismic events between August 2000 and January 2001. Proc. Indian Acad. Sci. (Earth Planet. Sci.), 112(1), 51–60.
5. Gupta SK and **Deshpande RD.** (2003). High Fluoride in Groundwater of North Gujarat – Cambay Region: Origin, Community Perception and Remediation. *In* Proc. Int. Conf. on Water and Environment Vol. Ground Water Pollution (Eds. V.P. Singh & R.N. Yadav). Allied Publishers Pvt. Ltd. New Delhi. 368–388.

Chemical Geology 228 (2006) 209–232

CHEMICAL GEOLOGY
INCLUDING
ISOTOPE GEOSCIENCE

www.elsevier.com/locate/chemgeo

Helium, radon and radiocarbon studies on a regional aquifer system of the North Gujarat–Cambay region, India

Meetu Agarwal, S.K. Gupta *, R.D. Deshpande, M.G. Yadava

Planetary and Geosciences Division, Physical Research Laboratory, Navrangpura, Ahmedabad 380 009, Gujarat, India

Received 22 July 2003; accepted 31 October 2005

Abstract

The study reports the age evolution of groundwater as it flows from the recharge area through a regional alluvial aquifer system in North Gujarat–Cambay region in western India. Radiocarbon (^{14}C), ^{4}He and $^{4}He/^{222}Rn$ dating methods have been employed. Sediments from a drill core in the Cambay Basin were also analysed for uranium (U) and thorium (Th) concentrations and the measured values have been used to estimate the ^{4}He and ^{222}Rn production rate for groundwater age calculations. Additionally, factors controlling the distribution of ^{222}Rn, ^{4}He and temperature anomalies in groundwater, vis-à-vis their relation to the tectonic framework and lithology of the study area, have also been examined.

The multi-isotope study indicated a reasonable correspondence in groundwater age estimates by the three methods employed. The groundwater ^{14}C ages increased, progressively, in the groundwater flow direction: from the foothills of Aravalli Mountains in the east, and reached a value of ~35 ka towards the region of lowest elevation, linking Little Rann of Kachchh (LRK)–Nalsarovar (NS)–Gulf of Khambhat (GK) in the western part of the study area. In this region, groundwater ages obtained for free flowing thermal wells and springs employing ^{4}He and $^{4}He/^{222}Rn$ systematics are in the order of million years. Such anomalous ages are possibly due to enhanced mobilisation and migration of 'excess helium' from hydrothermal circulation vents along deep-seated faults. Excluding such anomalous cases and considering all uncertainties, presently estimated ^{4}He and $^{4}He/^{222}Rn$ groundwater ages are in reasonable agreement with ^{14}C age estimates in the Cambay Basin for helium release factor (Λ_{He}) value of 0.4 ± 0.3. The ^{4}He method also indicated west-southwards progression of groundwater ages up to ~100 ka beyond the Cambay Basin.

Large 'excess helium' concentrations are also seen to be generally associated with anomalous groundwater temperatures (>35 °C) and found to overlie some of the basement faults in the study area, particularly along the east and the west flanks of the Cambay Basin. Groundwater ^{222}Rn activities in most of the study area are 800 ± 400 dpm/l. But, a thermal spring at Tuwa on the east flank of the Cambay Basin, having granitic basement at shallow depth, recorded the highest ^{222}Rn activity (~63,000 dpm/l).

Keywords: Helium; Radon; Radiocarbon; Groundwater age; Tectonics

1. Introduction

Determining the age evolution of groundwater as it moves in an aquifer from the recharge area to a distant discharge location is still a challenging task for hydrogeochemists. Sampling locations are often randomly scattered over an area where water from an aquifer is pumped from various depths or where springs bring

---

* Corresponding author. Tel.: +91 79 26314259; fax: +91 79 26301502.

E-mail addresses: meetu_agarwal20@yahoo.com (M. Agarwal), skgupta@prl.res.in (S.K. Gupta), deshpand@prl.res.in (R.D. Deshpande), myadava@prl.res.in (M.G. Yadava).

0009-2541/$ - see front matter © 2005 Elsevier B.V. All rights reserved.
doi:10.1016/j.chemgeo.2005.10.007

water to the surface. Several environmental tracers (including radio nuclides) find important and wide applications in determining direction and flow of groundwater, hydro-geological parameters of the aquifer and age of groundwater (Andrews et al., 1989; Cserepes and Lenkey, 1999).

In regional aquifer systems, groundwater ages may range up to 10^3 ka and beyond. Radiocarbon, with a half-life ($t_{1/2}$) of 5.73 ka can be used for groundwater dating up to ~35 ka (Geyh, 1990). The other available radionuclides such as ^{36}Cl ($t_{1/2}=3.01 \times 10^2$ ka; Andrews and Fontes, 1992), ^{81}Kr ($t_{1/2}=2.1 \times 10^3$ ka; Lehmann et al., 1991) and ^{234}U ($t_{1/2}=2.45 \times 10^2$ ka; Fröhlich and Gellermann, 1987) provide groundwater ages well beyond the radiocarbon dating range. On the other hand, the range of groundwater age estimation by radiogenic ^{4}He is 10^0 to 10^2 ka (Torgersen, 1980, 1992; Mazor and Bosch, 1992; Clark et al., 1998; Castro et al., 2000). When combined with ^{222}Rn activity measurements, the ^{4}He/^{222}Rn systematics also provide groundwater age estimation from 10^0 to 10^3 ka (Torgersen, 1980; Gupta et al., 2002). Another advantage of both ^{4}He and ^{4}He/^{222}Rn methods is that measurements of ^{4}He and ^{222}Rn are relatively simple. However, some complications also exist. (i) Recent studies (Stute et al., 1992; Imbach, 1997; Minissale et al., 2000; Gupta and Deshpande, 2003a,b) indicate that ^{4}He in deep groundwater often exceeds the accumulated in situ production by several orders of magnitude, particularly in regions of active tectonism and/or deep hydrothermal circulation. (ii) The possibility of a steady state whole crustal helium degassing flux affecting the dissolved helium in groundwater has been suggested (Torgersen and Clarke, 1985; Torgensen and Ivey, 1985). (iii) The possibility of enhanced release of geologically stored radiogenic helium in relatively young fine grained sediments derived from old protoliths was shown by Solomon et al. (1996). (iv) Ground waters carry small excesses of helium and radon along with dissolved air acquired during the recharge process, both in solubility equilibrium and as a supersaturation component of atmospheric air (Heaton and Vogel, 1981; Aeschbach-Hertig et al., 2000, 2002). Thus from a practical point, He in groundwater comprises, in addition to in situ radiogenic production, a mixture of atmospheric and terrigenic He. Use of ^{4}He for dating requires that components other than radiogenic production be small and /or accountable.

As part of a larger study aimed at understanding the recharge and flow in regional alluvial aquifer systems in arid environments and under exploitation stress, the applicability of ^{14}C, ^{4}He and ^{4}He/^{222}Rn groundwater dating methods was investigated in the regional aquifer system of the North Gujarat–Cambay region. The region is characterised by well defined recharge and discharge areas, presence of a few thermal springs (GSI, 2000) and neo-tectonic activity along major basement faults (Merh, 1995; Maurya et al., 1997; Srivastava et al., 2001).

The objectives of this investigation were to study (i) groundwater age progression from the recharge area towards the discharge area employing ^{14}C, ^{4}He and ^{4}He/^{222}Rn dating methods, and (ii) factors controlling the distribution of ^{4}He, ^{222}Rn and temperature in groundwater vis-à-vis their relation to the tectonic framework and hydrothermal venting in the North Gujarat–Cambay region.

2. Hydro-geological setting of the study area

The study area in the North Gujarat Cambay region (71.5–74°E and 22–24.5°N) has been divided into three main geographical units (i) the Cambay Basin (ii) West Flank, i.e., the region to the west of the West Cambay Basin Boundary Fault (WCBBF), and (iii) East Flank, i.e., the region to the east of the East Cambay Basin Boundary Fault (ECBBF); (Fig. 1).

The Cambay Basin, is a 'Graben' characterised by a NNW–SSE trending major fault system and successive down faulting along sympathetic faults that run parallel to the major trend line and many orthogonal faults cutting across (Merh, 1995). Geomorphologic studies have indicated recent movements along many faults in this region (Maurya et al., 1997; Srivastava et al., 2001). Several thermal springs also lie along some faults and fissures in this region (GSI, 2000) suggesting active hydrothermal circulation. The Deccan basalt of Late Cretaceous age forms the basement in most of the study area excepting the East Flank where Proterozoic granitic rocks are also exposed on the surface. Within the Cambay Basin, the Quaternary alluvial deposits are underlain by a succession of Tertiary sedimentary formations with productive oil and gas reservoirs. The thickness of the sedimentary cover varies from a few metres on the east and west flanks to >3 km towards the centre of Cambay Basin. Quaternary alluvial sediments with alternating sand and silty-clay layers constitute the regional aquifer system having its recharge area in the foothills of Aravalli Mountains and discharge area in the Little Rann of Kachchh–Nalsarovar–Gulf of Khambhat region (LRK–NS–GK). Deccan traps and Mesozoic sediments are exposed on the West Flank (Fig. 1). Parts of the East Flank lying along the foothills of Aravalli Mountains are mainly granitic.

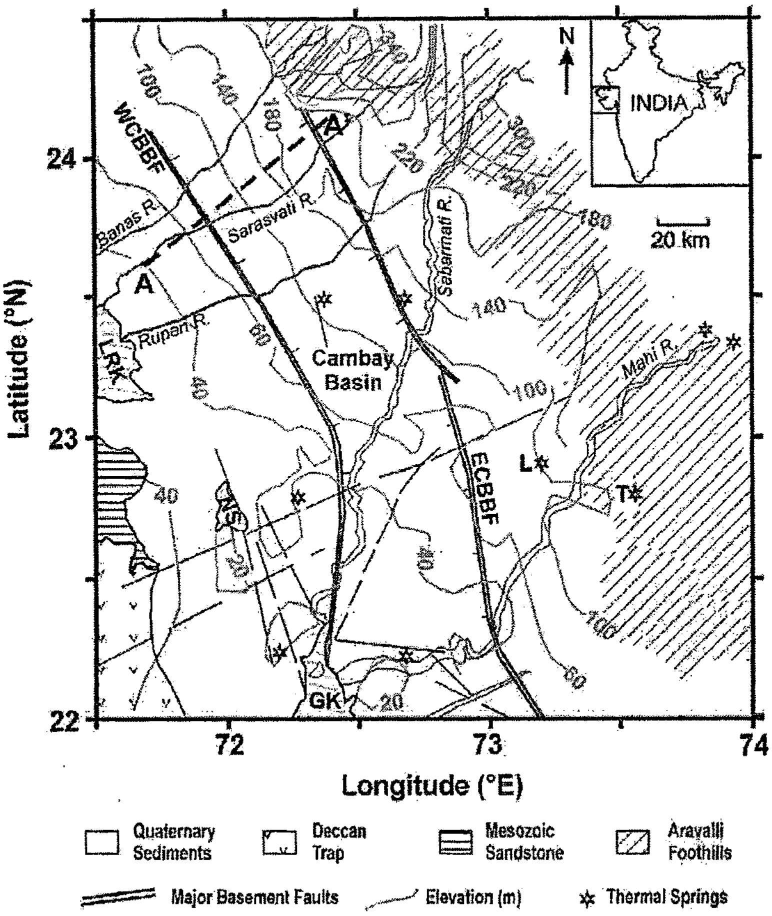

Fig. 1. Map of the North Gujarat–Cambay (NGC) region showing major geological formations, faults, surface elevations, major streams and locations of thermal springs. The Cambay basin (CB) is a Graben with a >3 km thick sedimentary succession. Several sympathetic faults, parallel and orthogonal to the two bounding faults, are also shown. A Quaternary regional aquifer system lies in the area between the Aravallis and the low lying track linking LRK–NS–GK. The foothills of the Aravallis act as the recharge zone. A section along AA' is shown in Fig. 2.

A subsurface section along AA' (Fig. 1), based on drilling logs obtained from Gujarat Water Resources Development Corporation Ltd (GWRDC) is shown in Fig. 2. It is seen that sand layers forming the major aquifer horizons are laterally continuous though vertically interspersed with silty-clay layers that may not have extensive lateral continuity. Approximate piezometric levels for two periods (1978–1983 and 1998–2003) recorded at the time of construction of new tubewells in the vicinity of the selected locations and obtained from the files of GWRDC are also shown in this diagram. The general groundwater flow direction is from the foothills of the Aravalli Mountains (elevations>300 m), towards the LRK–NS–GK region having the lowest ground elevations (~20 m). The ground elevation increases further west of LRK–NS–GK region. The deep tubewells in this part are free flowing artesian wells with their aquifer continuity in the east. In view of the very high artesian pressures recorded in the sixties (Exploratory Tubewells Organisation, Govt. of India, Unpublished data) and the continuity of deep aquifers with those in the Cambay Basin, it is considered that any significant recharge to the regional aquifer system from the west is not feasible. Farther west, only a thin cover of sediments cap the basaltic rocks exposed. The elevation gradient governs the surface drainage and major rivers, namely, the Banas, the Saraswati, the Rupen and the Sabarmati originate in the Aravalli hills and flow towards the south-west.

The rainfall in the study area is highly seasonal with >90% during south west monsoon in the months of June to September and decreases from ~90 cm a^{-1} in the east to ~65 cm a^{-1} in the region of the Cambay basin, further decreasing to <60 cm a^{-1} on the west flank (Gazetteer, 1975).

3. Theory

The theoretical background concerning the three groundwater dating methods employed in this study is summarised below.

3.1. ^{14}C dating

The method is based on measuring the residual activity of ^{14}C in the total dissolved inorganic carbon (TDIC) of a given groundwater sample. Two key assumptions made are: (i) the initial activity (A_0) in the TDIC in the recharge area is known and has remained constant in time; (ii) the system is closed to subsequent gain or loss of ^{14}C, except through the radioactive decay. In the case of radiocarbon dating of vegetal remains, A_0 can be taken as equal to 100% modern carbon (pmc) since the only source of ^{14}C is atmospheric CO_2. However, in case of ground waters A_0 in TDIC depends on the contribution from soil CO_2 and from soil carbonate which can have any value of ^{14}C activity between nil (dead carbon) to 100 pmc. Depending on the contribution from soil carbonate, A_0 can have any value between 50–100 pmc. This is because, of the two carbons in TDIC $[CaCO_3+H_2O+CO_2 \leftrightarrow Ca(HCO_3)_2]$, one is derived from soil CO_2 and the other from soil carbonate. There is a further complication due to isotopic exchange between TDIC and the soil CO_2 and carbonate material. Various correction models exist, which principally attempt to estimate the contribution of soil carbonate to the TDIC and estimate the applicable value of A_0. This is done either through a

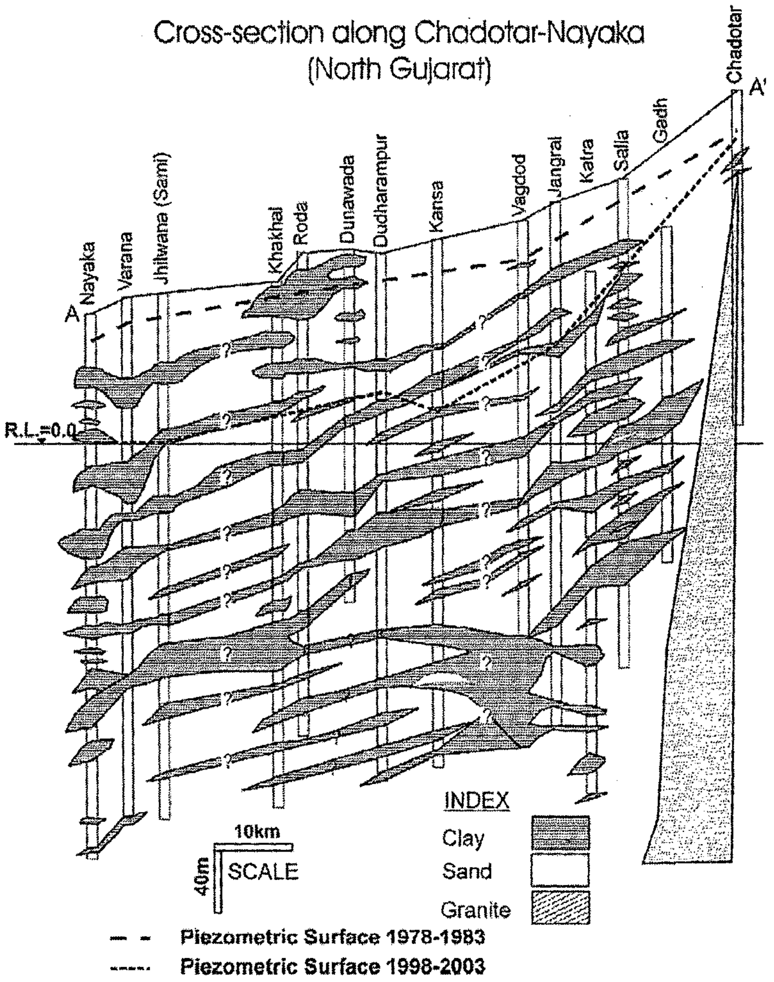

Fig. 2. Cross-section (along AA' in Fig. 1) depicting the lateral continuity of the major aquifer formed by sand layers interspersed by relatively thin silty-clay layers that may not have large lateral continuity. The uncertainty of continuity in view of large separation is indicated by question mark (?). Tubewells tap all water bearing horizons up to their maximum depth. The approximate positions of piezometric surfaces during 1978–1983 and 1998–2003 are also shown.

stoichiometry approach for the various chemical reactions involving carbon or by estimating dilution of active carbon using an isotope mixing approach based on the ^{13}C content of each species involved or a combination of the two approaches. Various methods for estimating A_0 can be found in Mook (1976) and Fontes and Garnier (1979). The error due to inappropriate estimation of A_0, however, is $<t_{1/2}$ of ^{14}C, except in some special cases of carbonate aquifers where continuous exchange between TDIC and the aquifer matrix may reduce A_0 to <50 pmc. Since most chemical and isotope exchanges occur in the unsaturated soil zone during the recharge process, and between TDIC and soil CO_2, the A_0 in several ground waters has been found to approach 85 ± 5 pmc (Vogel, 1967, 1970). However, in regional aquifers, the difference in groundwater ages between any two locations, after the confinement has become effective, depends little on the applicable value of A_0. Therefore, in the present investigation, the theoretical value of A_0 after equilibrium between soil CO_2, soil carbonate (at $^{14}C=0$ pmc; $\delta^{13}C=0‰$) and infiltrating water has been achieved, is estimated using the following equation (Münnich, 1957, 1968):

$$A_0 = \frac{\delta^{13}C_{TDIC}}{\delta^{13}C_{soil} - \varepsilon} 100 \qquad (1)$$

where, $\delta^{13}C_{TDIC}$ is the $\delta^{13}C$ value of the groundwater TDIC, $\delta^{13}C_{soil}$ is the $\delta^{13}C$ of soil CO_2 ($\sim -22‰$) and ε is the equilibrium fractionation between the soil CO_2 and the TDIC of groundwater ($\sim -9‰$). This is done with the knowledge that application of any other model would give radiocarbon ages differing by $< \pm 2$ ka, that is much smaller than the errors inherent in the age estimation by ^4He and $^4He/^{222}Rn$ dating methods used in this investigation as discussed below.

3.2. ^{4}He dating

The method is based on estimating the amount and rate of accumulation of in situ produced radiogenic ^4He in groundwater (Andrews and Lee, 1979; Stute et al., 1992). If secular equilibrium and release of all the produced ^4He atoms into the interstitial water is assumed, the groundwater ages can be calculated as outlined in the following (Torgersen, 1980). The ^4He production rate in cm^3 STP g^{-1} rock a^{-1} is given by:

$$J'_{He} = 0.2355 \times 10^{-12}\, U^* \qquad (2)$$

$$\text{where, } U^* = [U]\{1 + 0.123([Th]/[U] - 4)\} \qquad (3)$$

[U] and [Th] are concentrations (ppm) of U and Th, respectively, in rock/sediment.

The accumulation rate of ^4He in cm^3 STP cm^{-3} water a^{-1} is therefore given by:

$$A'_{He} = J'_{He}\rho \cdot \Lambda_{He} \cdot (1 - n)/n \qquad (4)$$

where, Λ_{He} = helium release factor; ρ = rock density (g cm^{-3}); n = rock porosity.

In the present study, the dissolved helium concentration is not given in cm^3 STP cm^{-3} water but is given in Air Equilibration Unit (AEU), which expresses the dissolved helium in terms of the corresponding equilibrium dry gas phase mixing ratio at 1 atm and 25 °C. As a result, water in equilibrium with air containing 5.3 ppmv helium is assigned a dissolved He concentration of 5.3 ppm AEU. Using a dimensionless Henry Coefficient (H_x) of 105.7 for helium at 25 °C (calculated from Weiss, 1971), this corresponds to a moist air equilibrium concentration of $4.45 \cdot 10^{-8}$ cm^3 STP He cm^{-3} water. Therefore,

$$A_{He} = A'_{He} 10^6 \cdot H_x \cdot (T/T_0) \cdot P_0/(P_0 - e) \qquad (5)$$

where, A_{He} = accumulation rate of ^4He in ppm AEU a^{-1}; T_0 = 273.15 K; P_0 = 1 atm and e = saturation water vapour pressure (0.031 atm) at 25 °C, H_x = 105.7.

For an average [U] = 1 ppm for alluvial sedimentary formations and [Th]/[U] = 4 (Ivanovich, 1992), n = 20%; Λ_{He} = 1; ρ = 2.6 g cm^{-3}, an in situ ^4He accumulation rate (A_{He}) of 2.59×10^{-4} ppm AEU a^{-1} is obtained. Therefore, from the measured helium concentration of the sample (^4He_s), the age of groundwater can be obtained by using:

$$\text{Age (a)} = {}^4He_{ex}/A_{He} \qquad (6)$$

where $^4He_{ex}$ is the 'excess He' (ppm AEU) and is obtained by subtracting dissolved helium in solubility equilibrium between water and atmosphere ($^4He_{eq}$ = 5.3 ppm AEU at 25 °C and 1 atm pressure) from the measured concentration in the groundwater sample (^4He_s).

The above formulation, however, ignores 'excess air' helium ($^4He_{ea}$) due to supersaturation of atmospheric air as the groundwater infiltrates through the unsaturated zone. Various models have been proposed for estimating this component in groundwater studies (Aeschbach-Hertig et al., 2000; Kulongoski et al., 2003) based on measurement of other dissolved noble gases. Since measurements of dissolved noble gases have not been made in this study, it has not been possible to correct for this effect. However, from other studies (Holocher et al., 2002) it appears that $^4He_{ea}$ can

Table 1

Calculated ^{4}He ages along with geographical coordinates, well type and temperature, EC, pH and ^{4}He concentration of groundwater samples from the North Gujarat–Cambay Region, India

CBGW sample no.	Location name	Well type	Latitude (°N)	Longitude (°E)	Temp. (°C)	EC (mS)	pH	'Excess ^{4}He' ppm AEU	^{4}He ages (ka) (Λ_{He}=1)	^{4}He ages (ka) (Λ_{He}=0.4)
1	Gandhinagar	TW	23.24	72.68	–	0.5	–	0	0	0
2	Prantij	DCB	23.44	72.85	–	0.5	–	0	0	0
3	Prantij	TW	23.45	72.86	–	0.5	–	0	0	0
4	Shikha	DCB	23.39	73.23	–	0.6	–	0	0	0
5	Bayad	TW	23.22	73.21	–	4.8	–	0	0	0
6	Gundela	DW	23.12	73.36	–	0.8	–	0	0	0
7	Rojawa	TW	22.91	73.33	–	2.0	–	0	0	0
8	Lasundra	DW	22.91	73.14	52	7.4	–	186	547	1368
9	Lasundra	DW	22.91	73.14	–	7.6	–	55	162	404
10	Sinhuj	DCB	22.82	72.86	–	2.3	–	0	0	0
11	Dakore	TW	22.76	73.16	–	2.4	–	0	0	0
12	Ladvel	HP	22.91	73.12	–	0.7	–	0.2	1	1
13	Kapadvanj	DCB	23.04	73.10	–	0.9	–	0	0	0
14	Kunha	TW	23.01	72.77	–	1.0	–	0	0	0
15	Lasundra	TW	22.92	73.15	–	2.0	–	221	650	1625
16	Anghadi	DCB	22.81	73.30	–	0.7	–	0	0	0
17	Timba	HP	22.82	73.40	–	1.9	–	0	0	0
18	Tuwa	DW	22.80	73.46	61	3.4	–	137	403	1007
19	Tuwa	DW	22.80	73.46	47	6.2	–	96	282	706
20	Tuwa	DW	22.80	73.46	28	6.2	–	475	1397	3493
21	Tuwa	HP	22.80	73.46	51	4.7	–	1163	3421	8551
22	Tuwa	DW	22.80	73.46	–	0.7	–	0	0	0
23	Godhara	DW	22.78	73.60	–	0.8	–	0	0	0
24	Godhara	TW	22.76	73.61	–	0.5	–	0	0	0
25	Baska	HP	22.47	73.45	–	2.3	–	0	0	0
26	Baroda	TW	22.27	73.19	–	2.3	–	0	0	0
27	Jarod	HP	22.44	73.35	–	0.5	–	0	0	0
28	Khadki	HP	22.65	73.52	–	1.1	–	0	0	0
29	Dabhoi	HP	22.13	73.41	–	2.0	–	0	0	0
30	Sathod	TW	22.07	73.38	–	1.2	–	0	0	0
32	Adalaj	TW	23.17	72.58	–	2.1	–	0.1	0	1
33	Kalol	TW	23.26	72.47	–	2.3	–	0.1	0	1
34	Malharpur	HP	22.81	72.62	–	2.7	–	0.1	0	1
35	Marala	DCB	22.62	72.64	–	0.8	–	0.1	0	1
36	Khambhat	TW	22.33	72.62	–	2.8	–	0.8	2	6
37	Nadiad	TW	22.56	72.82	–	1.9	–	0.1	0	1
38	Bhadran	TW	22.37	72.90	–	2.2	–	0.4	1	3
39	Masar Rd.	TW	22.11	72.89	–	4.2	–	5.2	15	38
40	Kalak	DCB	22.02	72.76	–	2.2	–	0.1	0	1
43	Manglej	TW	22.09	73.17	–	1.6	–	0.1	0	1
44	Dholka	TW	22.69	72.43	–	3.1	–	0.5	1	4
45	Dholera	TA	22.25	72.19	43	6.9	–	109	321	801
50	Rampara	TW	22.11	71.89	–	1.3	–	2.7	8	20
51	Dhandhuka	DCB	22.38	71.98	–	3.1	–	0.2	1	1
52	Bawala	TW	22.83	72.36	33	1.6	–	6.3	19	46
53	Bagodra	TA	22.64	72.20	41	1.9	–	88	259	647
54	Bagodra	TA	22.64	72.20	41	1.4	–	190	559	1397
55	Gundi	TA	22.55	72.23	40	1.5	–	234	688	1721
56	Batod	HP	22.16	71.66	–	1.0	–	0.1	0	1
58	Vejalka	DCB	22.40	71.72	–	0.9	–	6.3	19	46
59	Wadhwan	TW	22.72	71.68	35	1.9	–	0.2	1	1
60	Bajana	TW	23.12	71.78	–	1.6	–	16	47	118
61	Dashada	TW	23.32	71.84	–	1.2	–	49	144	360
62	Sachana	TW	23.08	72.17	34	1.1	–	2.7	8	20
63	Vithalpur	TW	23.37	72.05	–	1.5	–	1	3	7

Table 1 (*continued*)

CBGW sample no.	Location name	Well type	Latitude (°N)	Longitude (°E)	Temp. (°C)	EC (mS)	pH	'Excess ^{4}He' ppm AEU	^{4}He ages (ka) ($\Lambda_{He}=1$)	^{4}He ages (ka) ($\Lambda_{He}=0.4$)
64	Umerkhaya	DW	22.90	72.02	–	7.6	–	0.2	1	1
65	Shiyala	TA	22.70	72.16	38	3.4	–	73	215	537
66	Ruhika	TA	22.66	72.23	41	3.0	–	157	462	1154
67	Sarala	TA	22.67	72.20	40	2.6	–	89	262	654
68	Vithalgadh	DW	22.99	71.97	–	5.9	–	0.2	1	1
69	Nardipur	TW	23.25	72.56	29	1.2	–	0	0	0
70	Santej	TW	23.11	72.47	29	1.2	–	0	0	0
71	Rancharda	TW	23.08	72.45	–	1.1	–	0	0	0
72	Nardipur	TW	23.25	72.56	29	1.2	–	0	0	0
73	Santej	TW	23.11	72.47	29	1.2	–	0	0	0
74	Rancharda	TW	23.08	72.45	–	1.1	–	0	0	0
75	Ananddham	TW	22.99	72.52	–	2.1	–	0	0	0
76	Sarkhej	TW	22.99	72.49	–	1.9	–	0	0	0
77	Sarkhej	TW	22.99	72.49	–	2.2	–	0	0	0
78	Collet	TW	22.97	72.43	33	1.6	–	1	3	7
79	Collet	TW	22.98	72.44	30	3.6	–	0	0	0
80	Sanand	TW	23.00	72.38	29	3.2	–	0.4	1	3
81	Thol	TW	23.13	72.38	32	3.2	–	0	0	0
82	Thol	HP	23.15	72.37	31	3.2	–	0	0	0
83	Rangpurda	TW	23.25	72.30	31	2.3	–	0.5	1	4
84	Kadi	TW	23.30	72.31	31	1.6	–	0	0	0
85	Bhoyani	TW	23.36	72.23	32	2.4	–	0.4	1	3
86	Katosan Road	TW	23.40	72.24	32	2.9	–	0.4	1	3
87	Navdeep Ind.	TW	23.01	72.34	30	2.4	–	0.8	2	6
88	Vansa	DCB	23.02	72.33	28	1.4	–	0.1	0	1
89	Sachana	TW	23.08	72.16	39	1.7	–	34	100	250
90	Hansalpur	TW	23.10	72.07	33	2.3	–	22	65	162
91	Viramgam	TW	23.10	72.06	34	1.8	–	66	194	485
92	Juna Padhar	TW	23.19	72.04	40	1.6	–	62	182	456
93	Endla	TW	23.29	72.04	38	1.6	–	23	68	169
94	Sitapur	TW	23.45	71.99	34	1.8	–	16	47	118
95	Sitapur	TW	23.44	71.98	38	1.5	–	21	62	154
96	Valevda	TW	23.46	71.94	32	4.3	–	2.8	8	21
97	Valevda	TW	23.45	71.94	40	1.8	–	17	50	125
98	Dhanap	TW	23.26	72.75	31	1.0	–	0.2	1	1
99	Majara	TW	23.36	72.80	29	1.2	–	0.1	0	1
100	Talod	TW	23.35	72.93	28	1.3	–	0	0	0
101	Tajpur Camp	HP	23.37	73.03	29	1.6	–	0.2	1	1
102	Vadagam	HP	23.33	73.17	29	0.5	–	0.2	1	1
103	Ramnagar	HP	23.39	73.23	28	0.6	–	0	0	0
104	Dhamanya	HP	23.34	73.25	29	0.7	–	0	0	0
105	Kamaliya	HP	23.33	73.31	28	1.5	–	0	0	0
106	Ranmalgadh	TW	22.98	72.34	33	1.5	–	0.7	2	5
107	Rethal	TW	22.88	72.19	34	1.5	–	12	35	87
108	Shahpur	HP	22.88	72.02	29	8.5	–	2	6	15
109	Vasvelia	TW	23.00	72.04	37	2.3	–	131	385	963
110	Bhojva	TW	23.15	72.03	31	3.0	–	2.3	7	17
111	Malanpur	TW	23.25	71.93	35	2.0	–	56	165	412
112	Zainabad	TW	23.26	71.68	34	2.3	–	112	329	824
113	Zainabad	HP	23.26	71.68	29	0.9	–	0	0	0
114	Zinzuvada	TW	23.35	71.65	35	2.6	–	31	91	228
115	Zinzuvada	HP	23.35	71.66	28	0.7	–	0	0	0
116	Changodar	HP	22.93	72.44	29	1.7	–	0.3	1	2
117	Kalayangdh	TW	22.72	72.27	27	5.2	–	1.4	4	10
118	Limbdi	HP	22.57	71.81	28	3.4	–	0	0	0
119	Vadod	TW	22.56	71.63	29	1.5	–	1.6	5	12
120	Zinzawadar	TW	22.45	71.69	34	3.5	–	2843	8362	20,904

(*continued on next page*)

Table 1 (*continued*)

CBGW sample no.	Location name	Well type	Latitude (°N)	Longitude (°E)	Temp. (°C)	EC (mS)	pH	'Excess ^{4}He' ppm AEU	^{4}He ages (ka) ($\Lambda_{\mathrm{He}}=1$)	^{4}He ages (ka) ($\Lambda_{\mathrm{He}}=0.4$)
121	Zinzawadar	HP	22.45	71.69	29	1.3	–	0	0	0
122	Chuda	TW	22.49	71.69	31	3.9	–	1290	3794	9485
123	Vekaria	HP	22.82	72.06	29	6.6	–	0.4	1	3
124	Fulgam	HP	22.54	71.54	31	1.1	–	0.2	1	1
125	Shekhpur–Rd.	TW	22.70	71.56	31	5.3	–	0.2	1	1
126	Vana	HP	22.87	71.71	–	6.0	–	0	0	0
127	Rangpur	DW	22.41	71.93	27	9.0	–	0.6	2	4
128	Vagad	DW	22.36	71.87	29	3.7	–	0	0	0
129	Nagnesh	TW	22.36	71.76	31	2.2	–	2	6	15
130	Nagnesh	HP	22.36	71.76	31	2.3	–	1.1	3	8
131	Alampur	DW	22.30	71.66	28	0.6	–	0	0	0
132	Paliyad	HP	22.25	71.56	30	2.3	–	0	0	0
133	Paliyad	TW	22.25	71.56	32	1.4	–	0.7	2	5
134	Botad	HP	22.17	71.66	–	0.9	–	0	0	0
135	Tatam	TW	22.06	71.62	31	1.1	–	0.8	2	6
137	Ahmedabad	TW	22.98	72.62	35	1.5	–	0	0	0
138	Hathijan	TW	22.94	72.64	35	1.1	–	0.5	1	4
139	Onthwari	DCB	22.82	72.80	35	2.0	–	0	0	0
140	Ran Na Muvada	DCB	22.84	72.95	35	1.5	–	3.6	11	26
141	Porda	DCB	22.92	73.00	33	0.8	–	0.2	1	1
147	Sarangpur	HP	22.16	71.77	34	2.2	–	0	0	0
149	Panavi	TW	22.08	71.89	41	6.0	–	1624	4776	11,941
150	Keriya Dhal	TW	22.11	71.89	35	0.8	–	0	0	0
151	Vaya	DW	22.20	71.87	30	1.0	–	0	0	0
152	Devthal	DCB	22.75	72.13	35	9.6	–	4.4	13	32
153	Devthal	TW	22.76	72.12	35	2.6	–	116	341	853
154	Kanera	TW	22.81	72.62	33	3.2	–	1.4	4	10
155	Sokhada	TW	22.74	72.68	34	5.7	–	0.3	1	2
156	Matar	TW	22.71	72.68	35	0.9	–	0.1	0	1
157	Nar	TW	22.48	72.71	35	2.5	–	0.7	2	5
158	Jogan	DCB	22.45	72.79	32	0.9	–	0.1	0	1
159	Bharel	TW	22.41	72.83	34	0.9	–	0.1	0	1
160	Dededa	DW	22.46	72.91	32	1.4	–	0.3	1	2
161	Anand	TW	22.53	72.96	32	0.8	–	0	0	0
162	Uttarsanda	TW	22.66	72.90	32	1.2	–	0	0	0
163	Sojitra	TW	22.55	72.74	35	1.5	–	1.8	5	13
164	Jedwapura	TW	22.55	72.83	34	2.3	–	0	0	0
165	Bedva	DCB	22.55	73.04	–	0.8	–	0	0	0
166	Ode	TW	22.62	73.11	32	0.8	–	0.7	2	5
167	Lingda	HP	22.69	73.08	31	0.7	–	0.5	1	4
168	Alindra	HP	22.70	72.97	34	0.6	–	0.5	1	4
169	Vaghasi	TW	22.54	73.00	–	0.9	–	0	0	0
170	Bhetasi	TW	22.43	73.02	33	1.2	–	0	0	0
171	Samiala	TW	22.26	73.12	33	0.9	–	0.1	0	1
172	Dabhasa	TW	22.25	73.05	34	1.0	–	0	0	0
173	Vadu	DCB	22.21	72.98	33	1.4	–	0.2	1	1
174	Vadu	TW	22.22	72.98	37	2.1	–	3.5	10	26
175	Gavasad	TW	22.19	72.97	35	0.9	–	0.1	0	1
176	Jambusar	TW	22.05	72.81	34	3.4	–	1	3	7
179	Karjan	TW	22.05	73.12	34	2.1	–	0	0	0
184	Kanara	TW	22.08	73.40	34	1.0	–	0	0	0
185	Mandwa	TW	22.01	73.43	35	0.7	–	0.1	0	1
186	Chandod	TW	22.99	73.46	34	0.8	–	0	0	0
187	Ankhi	TW	22.13	73.20	33	2.4	–	4.6	14	34
188	Kayvarohan	TW	22.08	73.24	33	1.2	–	0	0	0
189	Dantiwada	HP	24.17	72.48	34	0.5	–	0	0	0
190	Dantiwada	TW	24.16	72.48	31.5	0.6	–	0.4	1	3

Table 1 (*continued*)

CBGW sample no.	Location name	Well type	Latitude (°N)	Longitude (°E)	Temp. (°C)	EC (mS)	pH	'Excess ^{4}He' ppm AEU	^{4}He ages (ka) ($\Lambda_{He}=1$)	^{4}He ages (ka) ($\Lambda_{He}=0.4$)
191	Gola	DCB	24.19	72.78	28	0.7	–	0.2	1	1
192	Dharoi	HP	24.00	72.85	29	0.6	–	0.1	0	0
193	Mumanvas	DW	24.04	72.83	27	0.9	–	0.4	1	3
194	Mathasur	HP	23.80	73.01	30	1.2	–	0.2	1	1
195	Himmatnagar	HP	23.72	72.96	29	0.9	–	0.3	1	3
196	Dalpur	DCB	23.51	72.95	29	0.6	–	0	0	0
202	Math	HP	23.43	73.82	28	0.4	–	0.2	1	1
203	Aritha	HP	23.14	73.65	29	0.5	–	0.1	0	1
204	Limbodra	HP	23.19	73.60	29	0.7	–	0.3	1	2
205	Ghaliya Danti	HP	23.36	73.51	29	0.8	–	0.1	0	1
206	Shehra	HP	22.95	73.63	29	0.5	–	0.1	0	1
207	Popatpura	HP	22.79	73.45	29.5	0.6	–	0.2	1	1
208	Maniyor	TW	23.82	72.96	35	1.9	–	0.1	0	1
209	Dharewada	TW	23.98	72.39	35	3.5	–	2.0	6	15
210	Ganguva	TW	24.16	72.73	33	0.5	–	0	0	0
211	Chadotar	TW	24.21	72.39	32	1.0	–	0	0	0
212	Bhadath	TW	24.34	72.20	32	0.4	–	0.3	1	2
213	Kuwarava	TW	24.04	71.90	35	1.7	–	0.3	1	2
214	Kuwarava	TW	24.05	71.90	33	1.7	–	0.3	1	2
215	Tharad	TW	24.41	71.64	42	3.4	–	30	88	221
216	Jitoda	TW	23.74	72.15	35	2.3	–	0.6	2	4
217	Jitoda	TW	23.74	72.15	42	2.3	–	9.7	29	71
218	Sami	TW	23.70	71.78	44	3.9	–	64	188	471
219	Wavadi	TW	23.92	72.52	34	1.0	–	0	0	0
220	Pilwai	TW	23.53	72.69	39	1.6	–	17	50	125
221	Pilwai	TW	23.54	72.68	37	1.3	–	0.5	1	4
222	Hedwa	TW	23.57	72.34	37	2.3	–	1.8	5	13
223	Vaghpur	TW	23.68	73.42	33	1.4	–	23	68	169
224	Edla	TW	23.54	72.06	40	2.6	–	11	32	81
225	Sherisa	TW	23.20	72.48	35	1.7	–	0.3	1	2
312	Diyodar	TW	24.10	71.75	33	1.8	7.5	1.9	6	14
313	Diyodar	TW	24.10	71.75	33	4.1	7.2	1.2	4	9
314	Tharad	TW	24.41	71.64	39	2.3	7.4	30	88	221
316	Agathala	TW	24.29	71.88	31	1.8	7.6	0	0	0
317	Sujanipur	TW	23.89	72.11	31	9.5	7.1	0	0	0
318	Sujanipur	TW	23.90	72.12	37	3.6	7.1	16	47	118
319	Sujanipur	TW	23.91	72.12	29	5.3	7.6	0	0	0
320	Kuwarva	TW	24.04	71.90	32	1.9	7.6	0	0	0
321	Kharia	TW	23.94	71.83	30	1.0	7.8	0	0	0
322	Sami	TW	23.70	71.78	41	4.7	7.4	45	132	331
323	Hedwa	TW	23.57	72.34	33	3.1	7.1	1.5	4	11
324	Kuder	TW	23.70	71.87	34	2.5	7.3	1.5	4	11
325	Patan	TW	23.84	72.11	31	2.0	7.6	0	0	0
326	Patan	TW	23.84	72.11	32	1.8	7.8	0	0	0
327	Patan	TW	23.84	72.11	29	3.4	7.1	0	0	0
328	Jitoda	TW	23.74	72.15	33	3.3	7.1	0.3	1	2
329	Jitoda	TW	23.74	72.15	39	4.3	7.0	10	29	74
330	Kamboi	TW	23.67	72.02	32	2.8	7.1	6.4	19	47
331	Muthia	TW	23.09	72.69	31	1.4	7.5	0.3	1	2
332	Paliya	TW	23.18	72.83	31	1.6	7.1	0.3	1	2
333	Punsari	TW	23.39	73.10	30	0.7	7.4	0	0	0
334	Dalani Muwadi	TW	23.36	72.88	31	1.6	7.2	12	35	88
335	Rojad	HP	23.35	73.09	29	1.7	7.6	0	0	0
336	Vadrad	TW	23.42	72.89	31	1.6	7.1	0	0	0
337	Tejpur	TW	23.39	72.81	30	1.7	7.1	0	0	0
338	Navalpur	TW	23.60	72.90	32	1.5	6.9	0.6	2	4
339	Dhanap	TW	23.26	72.75	32	1.7	7.2	0	0	0

(*continued on next page*)

Table 1 (*continued*)

CBGW sample no.	Location name	Well type	Latitude (°N)	Longitude (°E)	Temp. (°C)	EC (mS)	pH	'Excess ^{4}He' ppm AEU	^{4}He ages (ka) (A_{He}=1)	^{4}He ages (ka) (A_{He}=0.4)
340	Indroda Park	TW	23.19	72.65	31	1.2	7.3	0.3	1	2
341	Rupawati	TW	23.00	72.30	37	2.1	7.8	0	0	0
342	Sokali	TW	23.10	72.11	32	4.6	7.4	0.6	2	4
343	Dudapur	TW	23.02	71.58	32	3.5	7.0	44	129	324
355	Salajada	TW	22.80	72.39	35	2.3	7.7	0.9	3	7
356	Salajada	TW	22.79	72.39	35	2.3	7.6	0.9	3	7
357	Salajada	TW	22.79	72.39	31	4.9	7.5	0	0	0
358	Gundi	TA	22.55	72.23	42	4.1	8.2	178	524	1309
359	Shiyal	TA	22.68	72.16	42	4.6	8.2	230	676	1691
360	Padgol	TW	22.59	72.84	32	1.8	7.6	1.4	4	10
361	Morad	TW	22.54	72.86	31	1.2	7.6	0	0	0
362	Gumadia	TW	22.76	73.23	31	1.3	7.7	0.3	1	2
363	Tuwa	HS	22.80	73.46	50	7.2	7.2	405	1191	2978
364	Tuwa	HS	22.80	73.46	43	7.4	7.5	229	674	1684
365	Tuwa	HS	22.80	73.46	36	7.1	7.4	265	779	1949
366	Tuwa	HS	22.80	73.46	33	8.0	7.6	253	744	1860
367	Dholera	TA	22.25	72.19	45	7.2	7.9	443	1303	3257

TW: tubewell; DCB: dug cum bore; DW: dug well; HP: handpump; TA: thermal artesian; HS: hot spring; 'Excess He' = measured − 5.3 ppm AEU; A_{He} = helium release factor; calculations of ^{4}He ages are based on Th = 7.54 ± 3.5; U = 1.07 ± 0.41; ρ = 2.6 g cm^{-3}; n = 20%.

be up to 10–30% of $^4He_{eq}$ resulting in a possible overestimation of groundwater age of up to ~6 ka.

Further, (^4He_s) can contain other terrigenic helium components (Stute et al., 1992) that can cause overestimation of groundwater age. These terrigenic components are: (1) flux from an external source, e.g., deep mantle or crust, adjacent aquifers etc. (Torgersen and Clarke, 1985); and (2) release of geologically stored ^{4}He from young sediments (Solomon et al., 1996). Depending upon the geological setting, particularly in regions of active tectonism and/or hydrothermal circulation, the contribution of these sources may exceed the in situ production by several orders of magnitude (Stute et al., 1992; Minissale et al., 2000; Gupta and Deshpande, 2003a,b). For recent reviews on terrigenic helium, reference is made to Ballentine and Burnard (2002) and Castro et al. (2000). Additional measurements/data (e.g., $^3He/^4He$, other noble gases) are required to resolve these components. However, in many cases it seems possible to rule out major contribution from terrigenic He sources since the helium flux may be shielded by underlying aquifers that flush the Helium out of the system before it migrates across them (Torgensen and Ivey, 1985; Castro et al., 2000). According to Andrews and Lee (1979), with the exception of a few localised sites and for very old ground waters, 'excess He' in groundwater is due to in situ production only and is often used for quantitative age estimation within the aquifer if the U and Th concentrations of the aquifer material are known. But, in case there is evidence of deep crustal ^{4}He flux (J_0) entering the aquifer, Eq. (6) modifies to (Kulongoski et al., 2003):

$$\text{Age (a)} = {}^4\text{He}_{\text{Ex}}/[(J_0/nZ_0\rho_w) + A_{\text{He}}]/8.39 \times 10^{-9} \quad (7)$$

where, Z_0 is the depth (m) at which the ^{4}He flux enters the aquifer and ρ_w is the density of water (1 g cm^{-3}). In Eq. (7), the factor 8.39×10^{-9} results from expressing $^4He_{ex}$ in ppm AEU and A_{He} and J_0 terms in cm^3 STP/g.

3.3. $^4He/^{222}Rn$ dating

Since both ^{4}He and ^{222}Rn have a common origin in groundwater, being produced by the α decay of U and/or Th in the aquifer material, their simultaneous measurements in groundwater can also be utilized for calculating its age (Torgersen, 1980).

As in case of ^{4}He, the ^{222}Rn accumulation rate (cm^3 STP cm^{-3} water a^{-1}) is given by:

$$A_{\text{Rn}} = J'_{\text{Rn}}\rho \cdot A_{\text{Rn}} \cdot (1-n)/n \quad (8)$$

$$\text{where, } J'_{\text{Rn}} = 1.45 \times 10^{-14}[\text{U}] \quad (9)$$

and J'_{Rn} = production rate of ^{222}Rn in cm^3 STP g^{-1} rock a^{-1} and [U] = concentration (ppm) of U in rock/sediment.

Thus, computing the accumulation rate ratio of ^{4}He and ^{222}Rn (= A_{He}/A_{Rn}), the age of groundwater can be calculated as follows:

$$\text{Age (a)} = (A_{\text{Rn}}/A_{\text{He}})(A_{\text{Rn}}/A_{\text{He}})(C_4/A_{222}) \quad (10)$$

where, A_{Rn}/A_{He} is the release factor ratio for radon and helium from the aquifer material to groundwater; C_4 is concentration (atoms l^{-1}) of ^{4}He and A_{222} is activity (disintegration l^{-1} a^{-1}) of ^{222}Rn in groundwater. From Eqs. (2)–(4) and (8)–(10), it is seen that ^{4}He/^{222}Rn ages are independent of porosity, density and U concentration, but do require a measure of [Th]/[U] in the aquifer material. The ratio A_{Rn}/A_{He} depends upon grain size and recoil path length of both ^{222}Rn (~0.05 μm) and ^{4}He (30–100 μm) (Andrews, 1977). Release of ^{222}Rn by α-recoil from the outer surface (~0.05 μm) of a grain (~2–3 mm) has been estimated to ~0.005% (Krishnaswami and Seidemann, 1988). Apart from α-recoil, both ^{222}Rn and ^{4}He can diffuse out of rocks/minerals through a network of 100–200 Å wide nanopores throughout the rock or grain body (Rama and Moore, 1984). Radon release factors (A_{Rn}) ranging from 0.01–0.2 have been indicated from laboratory experiments for granites and common rock forming minerals (Krishnaswami and Seidemann, 1988; Rama and Moore, 1984). On the other hand, Torgersen and Clarke (1985), in agreement with numerous other authors have shown that the most likely value of A_{He} is ≈ 1. Converting C_4 (atoms l^{-1}) to ppm AEU units and A_{222} (disintegration $^{-1}$ a^{-1}) to dpm l^{-1} units, Eq. (10) can be rewritten as:

$$\text{Age (a)} = 4.3 \times 10^8 \cdot (A_{Rn}/A_{He}) \cdot (A_{Rn}/A_{He}) \cdot C_{He}(\text{ppmAEU})/A_{222}(\text{dpm } l^{-1}). \quad (11)$$

Here, 1 ppm AEU ^{4}He concentration corresponds to 2.26×10^{14} atoms of ^{4}He l^{-1} of water. Another inherent assumption of the ^{4}He/^{222}Rn dating method is that both ^{4}He and ^{222}Rn have originated from the same set of parent grains/rocks and their mobilization in groundwater is similarly affected.

Table 2
Results of groundwater radiocarbon dating from the North Gujarat–Cambay region, India

CBGW sample no.	Location name	Latitude (°N)	Longitude (°E)	$\delta^{13}C_{TDIC}$ (‰)	Percent modern carbon	^{14}C ages* (ka)	^{14}C ages**
208	Maniyor	23.82	72.96	−10.78	115 ± 1.1	Modern	Modern
209	Dharewada	23.98	72.39	−8.99	58 ± 0.7	4.45 ± 0.09	1.5 ± 0.14
210	Ganguva	24.16	72.73	−10.40	100 ± 0.9	Modern	Modern
211	Chadotar	24.21	72.40	−8.62	99 ± 0.9	Modern	Modern
212	Bhadath	24.34	72.20	−8.26	102 ± 1.0	Modern	Modern
215	Tharad	24.41	71.64	−8.47	2.3 ± 0.2	31.21 ± 0.68	27.6 ± 0.73
216	Jitoda	23.74	72.15	−7.26	35 ± 0.5	8.63 ± 0.12	3.9 ± 0.16
218	Sami	23.70	71.78	−11.74	0.61 ± 0.2	42.2 ± 2.6	41.3 ± 2.73
219	Wavadi	23.92	72.52	−9.56	90 ± 1.0	0.92 ± 0.09	Modern
220	Pilwai	23.53	72.69	−11.56	22 ± 0.4	12.53 ± 0.14	11.5 ± 0.17
222	Hedwa	23.57	72.34	−9.17	37 ± 0.5	8.19 ± 0.1	5.3 ± 0.14
223	Vaghpur	23.68	73.42	−11.34	81 ± 0.8	1.73 ± 0.08	0.6 ± 0.11
224	Edla	23.54	72.06	−10.12	1.7 ± 0.2	33.75 ± 0.88	31.6 ± 0.98
225	Sherisa	23.20	72.48	−9.47	50 ± 0.6	5.75 ± 0.1	3.1 ± 0.13
320	Kuwarava	24.04	71.90	−8.81	2.8 ± 0.3	29.64 ± 0.97	26.3 ± 0.90
331	Muthia	23.09	72.69	−8.60	68 ± 0.8	3.15 ± 0.1	Modern
333	Punsari	23.39	73.10	−9.11	89 ± 0.8	1.01 ± 0.07	Modern
336	Vadrad	23.42	72.89	−9.28	99 ± 0.9	Modern	Modern
337	Tajpur	23.39	72.81	−11.60	68 ± 0.7	3.25 ± 0.08	2.2 ± 0.11
341	Rupawati	23.00	72.30	−9.29	1.8 ± 0.2	33.29 ± 0.89	30.4 ± 0.93
344	Gajanav	22.92	71.36	−9.75	80 ± 0.7	1.82 ± 0.08	Modern
351	Navagam	22.62	71.18	−11.11	93 ± 0.8	0.61 ± 0.08	Modern
355	Salajada	22.80	72.39	−8.23	9.5 ± 0.2	19.5 ± 0.21	15.7 ± 0.20
358	Gundi	22.55	72.23	−21.36	b.d.l.	>45	>45
360	Padgol	22.59	72.84	−9.70	49 ± 0.5	5.87 ± 0.09	3.5 ± 0.12
362	Gumadia	22.76	73.23	−8.94	84 ± 0.8	1.47 ± 0.08	Modern
RC-1	PRL	23.04	72.54	−13.00	40 ± 0.6	7.58 ± 0.12	7.6 ± 0.14

b.d.l.: below detection limit; ^{14}C half life = 5730 ± 40 a.

* $A_0 = 100\%$ modern.

** $A_0(\text{corrected}) = \dfrac{\delta^{13}C_{TDIC}}{\delta^{13}C_{soil} - \varepsilon} 100$; $\delta^{13}C_{soil} = -22‰$ and $\varepsilon = -9‰$.

Andrews et al. (1982) used the following one-dimensional equation for calculating diffusive transport of ^{222}Rn in granites:

$$C_x = C_0 \exp\left(-\sqrt{\lambda/D}\cdot X\right) \qquad (12)$$

where, C_0 and C_x are the concentrations of ^{222}Rn at the point $x=0$ and $x=X$; D is the diffusion coefficient in water (~10^{-5} cm^2 s^{-1}); and λ is the decay constant for ^{222}Rn. They calculated that $C_x/C_0=0.35$ at a distance equal to one diffusion length ($X=[D/\lambda]^{1/2}$, i.e., 2.18 cm). Therefore, even at high ^{222}Rn activity its diffusion beyond a few metres distance is not possible. The average radon diffusion coefficient in soils with low moisture content and composed of silty and clayey sand is even lower ~2×10^{-6} cm^2 s^{-1} (Nazaroff et al., 1988). Therefore, ^{222}Rn measurements of groundwater depend essentially on U in the pumped aquifer horizons in the vicinity of the sampled tubewell. Further, measured ^{222}Rn because of

Table 3
Results of ^{4}He/^{222}Rn groundwater dating from the North Gujarat–Cambay region, India

CBGW sample no.	Location name	Latitude (°N)	Longitude (°E)	^{222}Rn activity (dpm/l)	'Excess ^{4}He' (ppm AEU)	^{4}He/^{222}Rn ages (ka)
312	Diyodar	24.10	71.74	945 ± 83	1.9	16
313	Diyodar	24.10	71.74	987 ± 91	1.2	10
314	Tharad	24.41	71.64	810 ± 65	33.7	330
316	Agathala	24.29	71.88	742 ± 67	0.6	6
317	Sujnipur	23.89	72.11	1077 ± 87	0.0	0
318	Sujnipur	23.90	72.12	1551 ± 124	5.5	28
319	Sujnipur	23.90	72.12	629 ± 57	0.0	0
320	Kuwarva	24.04	71.90	599 ± 57	0.0	0
321	Kharia	23.94	71.83	916 ± 83	0.0	0
322	Sami	23.70	71.78	137 ± 30	44.1	2553
323	Hedwa	23.57	72.34	469 ± 48	1.2	20
324	Kuder	23.73	72.19	462 ± 58	1.2	20
325	Patan	23.84	72.11	822 ± 72	0.0	0
326	Patan	23.84	72.11	673 ± 63	0.3	3
327	Patan	23.84	72.11	261 ± 36	0.0	0
328	Jitoda	23.74	72.15	1114 ± 106	0.6	4
329	Jitoda	23.74	72.15	1871 ± 144	9.9	42
330	Kamboi	23.67	72.02	1253 ± 97	6.4	41
331	Muthia	23.09	72.69	481 ± 24	0.0	0
332	Paliya	23.18	72.83	1262 ± 52	0.0	0
333	Punsari	23.39	73.10	522 ± 26	0.0	0
334	Dalani Muwadi	23.36	72.88	279 ± 19	13.3	378
335	Rojad	23.35	73.09	281 ± 19	0.0	0
336	Vadrad	23.42	72.89	923 ± 41	1.7	15
337	Tajpur	23.39	72.81	721 ± 36	0.0	0
338	Navalpur	23.60	72.90	245 ± 17	0.0	0
339	Dhanap	23.26	72.75	643 ± 34	0.0	0
340	Indroda Park	23.19	72.65	231 ± 19	0.0	0
341	Rupawati	22.99	72.30	908 ± 41	3.5	30
342	Sokali	23.10	72.11	657 ± 31	0.7	8
343	Dudapur	23.02	71.58	2595 ± 110	44.5	136
355	Salajada	22.80	72.39	480 ± 28	0.9	15
356	Salajada	22.79	72.39	379 ± 25	0.9	18
357	Salajada	22.79	72.39	426 ± 30	0.3	5
358	Gundi	22.55	72.23	301 ± 18	175.3	4624
359	Shiyal	22.68	72.16	262 ± 17	230.1	6958
360	Padgol	22.59	72.84	468 ± 24	1.3	23
361	Morad	22.54	72.86	322 ± 19	0.0	0
362	Gumadia	22.76	73.23	442 ± 22	0.0	0
363	Tuwa	22.80	73.46	62,571 ± 2405	405.0	51
364	Tuwa	22.80	73.46	32,538 ± 1272	277.0	68
366	Tuwa	22.80	73.46	36,394 ± 1413	253.0	55
367	Dholera	22.25	72.19	362 ± 17	465.0	10,189

Calculations are based on: Th/U=7.1 ± 4.3; $\Lambda_{Rn}/\Lambda_{He}=0.4$; $\rho=2.6$ g cm^{-3}; $n=20\%$.

its short half-life ($t_{1/2}=3.825$ d) is indicative of local mobilisation only whereas ^{4}He, being stable, might have been mobilized from the entire flow-path. For ground waters having high 'excess He' from sources external to the aquifer, the resulting ^{4}He/^{222}Rn ages might be over estimated.

4. Experimental

Groundwater samples used in this study were collected from tubewells/hand pumps/dug wells and thermal springs ranging in depth from 3 to 350 m. The sampling locations and other relevant details are given in Tables 1–3 and Figs. 3–6. Prior to sampling, the tubewells were purged long enough (>3 well volumes) to flush out stagnant water. Temperature, pH and electrical conductivity (EC) were measured in the field during sampling.

For ^{14}C dating, ~100 l of groundwater samples from 27 locations spread across the study area as shown in Fig. 3 were collected. The groundwater at each location was piped directly into a collapsible high density PVC bag through a narrow opening. A few pellets of NaOH (~10 g) were added to the PVC bag before piping the groundwater to raise the solution pH>10 for immobilising the dissolved CO_2. Depending upon the alkalinity and sulphate concentration of groundwater samples (measured in the field), a calculated amount of barium chloride ($BaCl_2$) was then added to the 'groundwater–NaOH' solution to ensure complete precipitation of dissolved carbonates (Clark and Fritz, 1997). Following vigorous stirring, the mixture was left undisturbed for precipitates to settle in the conical base of the PVC bag. After discarding the supernatant liquid, precipitates were transferred to glass bottles and sealed by capping the bottle with a bromobutyl synthetic rubber stopper

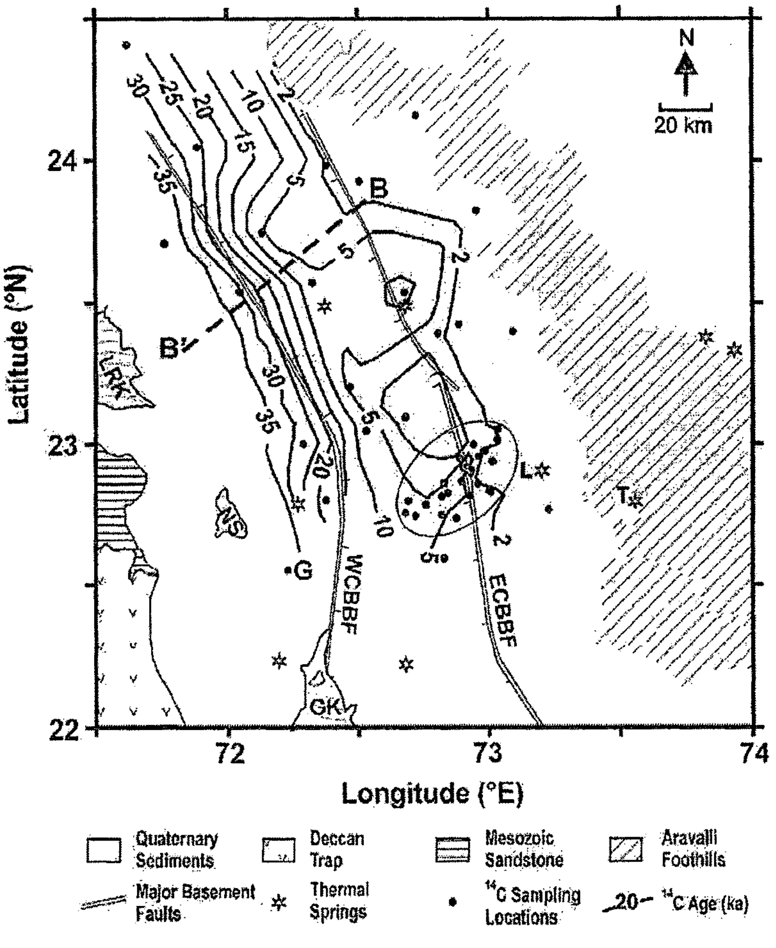

Fig. 3. Radiocarbon groundwater ages (ka) along with sampling locations. Sampling locations of an earlier study (Borole et al., 1979) are enclosed by an ellipse. Within the CB the groundwater ^{14}C ages increase progressively towards the WCBBF, beyond which a limiting age of >40 ka is reached. Dots indicate sampling locations. L, T and G respectively indicate the locations of thermal springs at Lasundra, Tuwa and the free flowing thermal artesian well at Gundi. The groundwater age gradient along BB' is shown in Fig. 9.

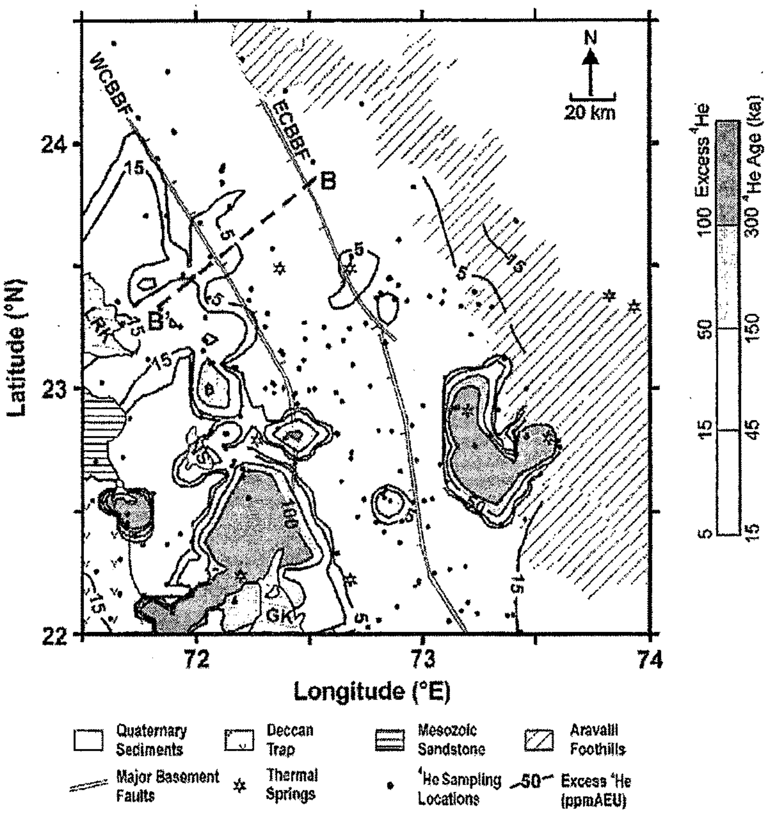

Fig. 4. Iso-distribution map of 'excess He' concentration in groundwater of the North Gujarat–Cambay region. The contour line of 5 ppm AEU runs almost along the WCBBF. For U = 1.07 ppm, Th = 7.54 ppm, ρ = 2.6 g cm^{-3} and n = 20%, 5 ppm AEU 'excess He' corresponds to a ^{4}He groundwater age of ~15 ka for a helium release factor, Λ_{He} = 1. In contrast, for Λ_{He} = 0.4, it corresponds to ~37 ka. Pockets of 'excess He' > 50 ppm AEU overlap pockets of high (>40 °C) temperature. Dots indicate sampling locations. The groundwater age gradient along BB' is shown in Fig. 9.

and triple aluminium protective cover using a hand held crimping tool. Care was taken to prevent/minimise sample exchange with atmospheric CO_2 during the entire field procedure. The ^{14}C analyses were made on the CO_2 liberated from the precipitated barium carbonate by reaction with ortho-phosphoric acid. The liberated CO_2 was first converted to acetylene and then trimerised into benzene and counted by liquid scintillation spectroscopy (Gupta and Polach, 1985). A small aliquot of the sample CO_2 was sealed in glass ampoules for δ^{13}C measurement (PDZ Europa Model GEO 20-20).

For ^{4}He measurements, water samples from 243 locations (Table 1, Fig. 4) were filled in 3 mm thick, 1.2-l capacity soda-lime glass bottles using standardized procedures reported by Gupta and Deshpande (2003a,b). The water samples were analysed for dissolved ^{4}He within 48 h after collection using a helium sniffer probe (ALCATEL Model ASM 100 HDS). The helium probe is a leak detector consisting of a mass spectrometer tuned for ^{4}He ions (m/e = 4). ^{4}He concentration results are expressed in air equilibration units (AEU). Total uncertainty of helium measurements is estimated to be <5%. Reference is made to Gupta and Deshpande (2003a,b) for details of sample collection and helium analysis procedures.

For ^{222}Rn measurements, water samples from 43 locations were drawn directly in 630-ml PVC bottles (Brand Tarson) filled completely after overflowing >3 bottle volumes and sealed to prevent escape of gases. ^{222}Rn was measured, within 5 d of sample collection, by counting 609 keV gamma rays produced by the decay of its short-lived daughter ^{214}Bi using a high purity germanium (HPGe) gamma ray spectrometer. The background in the ^{214}Bi peak was 0.062 ± 0.001 cpm. The counting efficiency of ^{214}Bi determined using a ^{226}Ra source of known activity (107.4 ± 0.4 dpm) in the same configuration as the sample bottle was 0.31 ± 0.01%. Repeated counting for some samples after more than three weeks confirmed that ^{222}Rn was unsupported by ^{226}Ra in the groundwater. Activity values were decay corrected to the time of collection, with quoted errors as one standard deviation based on counting statistics. Total uncertainty of ^{222}Rn measure-

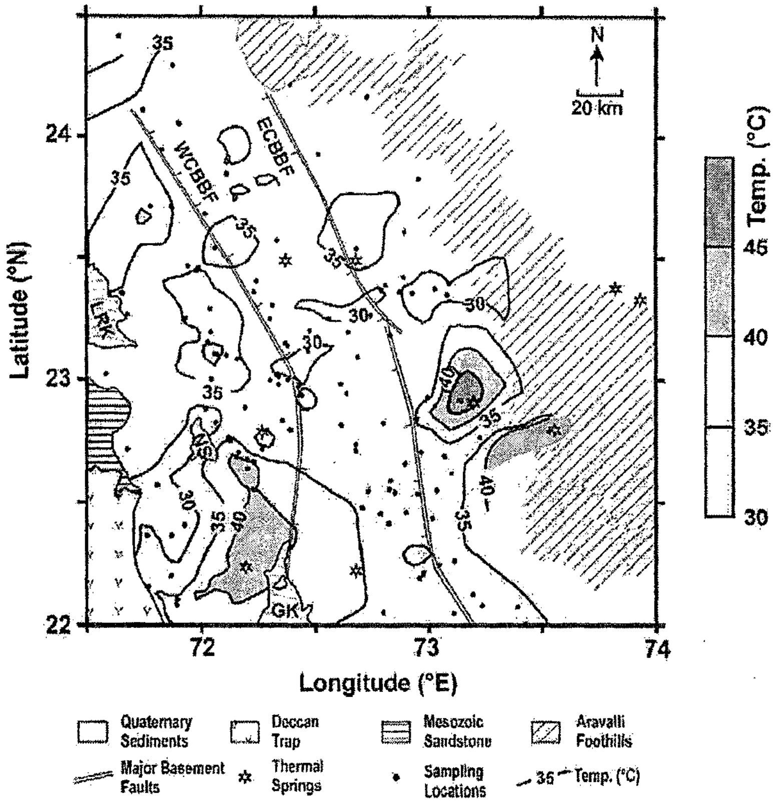

Fig. 5. Contours of groundwater temperature in the North Gujarat–Cambay region. Large areas on both east and west flanks of the CB show temperatures >35 °C, whereas within the CB the temperatures are lower. Temperatures >40 °C are seen around thermal springs. Dots indicate sampling locations.

ments, based on repeat analyses and counting statistics, is <10%.

In addition to groundwater samples, sediments from drill cuttings of a tubewell from Dela village (23.61°N; 72.42°E) in the Cambay Basin were also analysed by γ-spectrometry for uranium and thorium. For this, 22 sediment samples were taken from all the litho-layers encountered in the tubewell between 0–302 m. The samples were dried at 110 °C for 24 h after which they were crushed and packed in pre-weighed plastic containers and then sealed with epoxy resin to prevent escape of gases. Equilibration time of >15 d was given to the sediments in the containers to allow growth of daughter nuclides for steady state achievement. The concentration of U and Th was measured by counting 609 and 583 keV gamma rays using the HPGe gamma ray spectrometer and a common standard sediment sample of known concentration (i.e., 5.69 ppm U and 14.5 ppm Th) with the same configuration as the other samples. Measured U and Th concentrations in the sediments were used to estimate the production of ^{4}He and ^{222}Rn in the groundwater for the subsequent groundwater age determination using Eqs. (8)–(11).

5. Results

The geographical coordinates of well locations, measured values of basic water quality parameters, 'excess He' concentrations and calculated groundwater ^{4}He ages are given in Table 1. The δ^{13}C of TDIC, ^{14}C pmc and calculated radiocarbon groundwater ages are given in Table 2. The contours of radiocarbon dates are shown in Fig. 3. The groundwater sampling locations for ^{4}He measurements and the contours of 'excess He' are shown in Fig. 4. The contours of groundwater temperature are plotted in Fig. 5. The ^{4}He/^{222}Rn ages of the selected samples for which both ^{4}He concentration and ^{222}Rn activity was measured, are given in Table 3. The contours of ^{222}Rn activity in groundwater are given in Fig. 6. The results are summarised as follows:

1. The average groundwater pH for the samples analysed was 7.3 ± 0.4. Only for free flowing artesian thermal wells at Gundi (G), Shiyal (S) and Dholera (D) on the West Flank (see Fig. 6 for locations), pH was >7.9. The redox potential of

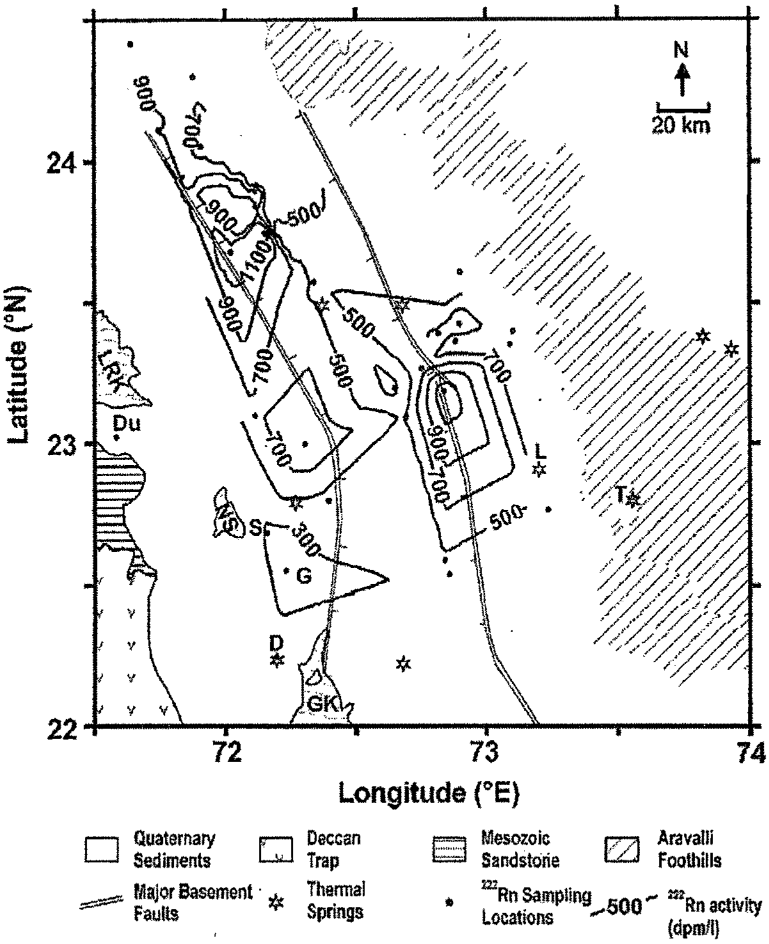

Fig. 6. Iso-distribution map of groundwater ^{222}Rn (dpm/l) in the North Gujarat–Cambay region. Low ^{222}Rn activity was seen in the free flowing artesian wells of Gundi (G), Shiyal (S) and Dholera (D). These wells, however, showed high temperature and helium concentrations (Figs. 4 and 5). Two sampling locations, namely, Tuwa (T) and Dudapur (Du) having very high ^{222}Rn activity (>2500 dpm/l) were excluded during contouring. Dots indicate sampling locations.

groundwater from these wells suggested reducing conditions.

2. The $\delta^{13}C$ of TDIC for all groundwater samples varied within a narrow range, with an average of -9.6 ± 1.2 ‰ except for one sample from an artesian thermal well at Gundi with $\delta^{13}C = -21.4$‰ (Table 2).
3. The ^{14}C age contours are nearly parallel to each other and to the WCBBF. The ages increase progressively in the general groundwater flow direction away from the Aravalli foothills (Fig. 3) and reach a value of >35 ka beyond WCBBF (Table 2).
4. The EC of groundwater was lowest (<1 mS) in the foothills of the Aravallis and increased gradually towards the WCBBF running parallel to the Aravalli foothills. Highest EC values were encountered in the south-western part of the study area. A detailed discussion on EC variation in the study area has been presented by Gupta and Deshpande (2003a,b).
5. The groundwater temperatures ranged from 28 to 61 °C (Fig. 5). Within the Cambay Basin which has a thick sedimentary cover, the average groundwater temperature was ~30 °C. Along the WCBBF and on the West Flank a large area showed high groundwater temperatures (≥35 °C). On the East Flank, high groundwater temperatures were observed in and around the thermal springs tapping the Precambrian granitic basement. The highest groundwater temperature (61 °C) was measured in one of the eight sampled vents of the thermal springs at Tuwa (T).
6. Different vents of the Tuwa thermal springs showed different temperature (28–61 °C) and ^{4}He concentrations (137–475 ppm AEU), with

no apparent correlation between these two parameters.

7. Areas of high 'excess He' (>15 ppm AEU; Fig. 4) are generally associated with areas of high temperature (>35 °C), and such samples are mostly found to lie along the major basement faults (i.e., East and West Cambay Basin Boundary Faults) and several criss-cross faults (Fig. 4). On the East Flank, the highest value of 'excess He' (~1100 ppm AEU) was obtained from a hand pump near the thermal spring at Tuwa very close to the Aravalli foothills. On the West Flank, the highest value was from a tubewell in the Zinzawadar village (>2000 ppm AEU).
8. In all samples, except for the thermal springs at Tuwa, the measured ^{222}Rn activity was found unsupported by ^{226}Ra in groundwater. The average ^{222}Rn activity of groundwater within the Cambay Basin was 820 ± 400 dpm/l with lower values in the southern part of the Cambay Basin (Fig. 6). On the East Flank, except for the thermal springs at Tuwa (^{222}Rn ~63,000 dpm/l; ^{226}Ra ~300 dpm/l) the average ^{222}Rn activity of groundwater was 600 ± 300 dpm/l. On the West Flank, samples showed low ^{222}Rn activities (300 ± 100 dpm/l), except for a shallow depth sample at Dudapur (~2600 dpm/l; Table 3; location Du in Fig. 6).
9. High temperatures and high ^{4}He were not necessarily associated with high ^{222}Rn activities. This was particularly apparent from the lowest ^{222}Rn activities (~300 dpm/l) observed at three free flowing thermal wells at Dholka (D), Shiyal (S) and Gundi (G) on the West Flank (Fig. 6). Contrary to this, thermal springs at Tuwa (~50 °C) on the East Flank located in the granitic substrate with ^{4}He concentrations of ~400 ppm AEU showed the highest ^{222}Rn activity (~63,000 dpm/l). In another case, a sample at Dudapur on West Flank exhibited low temperature (~31 °C), high ^{4}He (~50 ppm AEU) and high ^{222}Rn (~2600 dpm/l; Table 3).
10. The average U and Th concentrations of drill cut sediment samples collected from the Dela village (23.61°N; 72.42°E) in the study area were 1.07 ± 0.41 and 7.54 ± 3.5 ppm, respectively, with Th (ppm)/U (ppm) = 7.1 ± 4.3 (Fig. 7). Ten surface sediment samples up to 8.4 m depth from

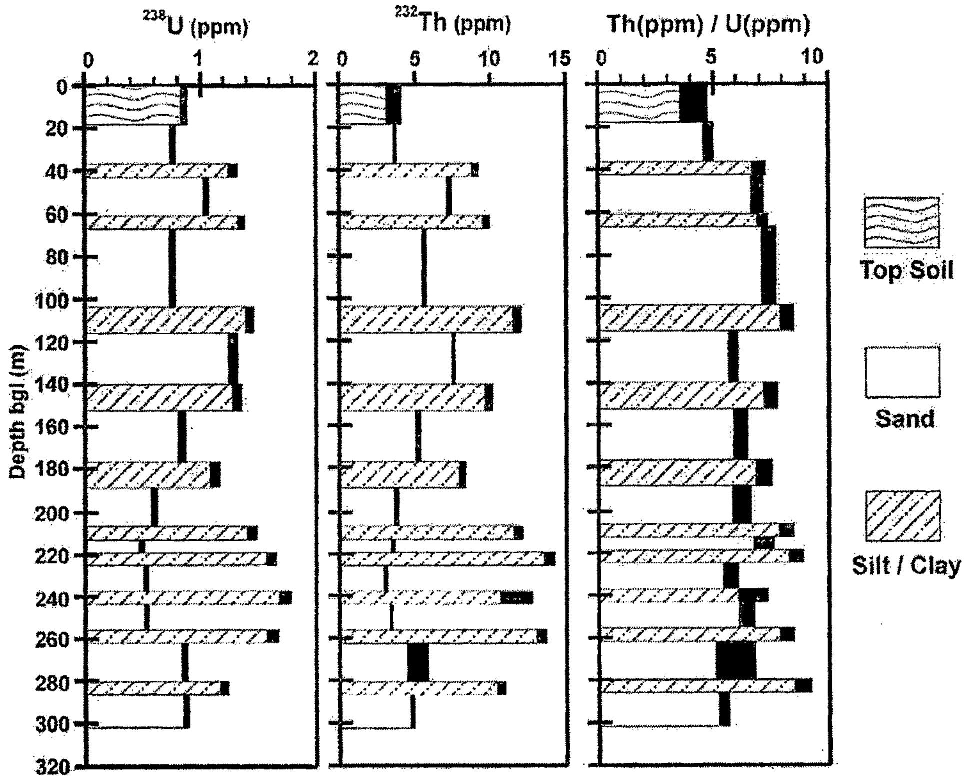

Fig. 7. Plot of U, Th concentration and Th/U ratio in the sediment of drill core samples from Dela village (23.61°N; 72.42°E) in CB. Width of the black vertical bars represents standard counting errors.

the Cambay Basin yielded an average value of U=1.7 ± 0.7 ppm and Th=8.0 ± 3.7 ppm (Srivastava et al., 2001) with Th/U=4.85 ± 2.2.

6. Discussion

6.1. Groundwater radiocarbon age

The estimated groundwater radiocarbon ages are seen to increase roughly westwards from the Aravalli foothills up to the LRK–NS–GK corridor. Further west, lower groundwater ^{14}C ages are encountered (CBGW-344, -351; Table 2). The LRK–NS–GK corridor with the lowest elevation (Fig. 1) in the study area is the zone of convergence for surface drainage (Prasad et al., 1998). Existence of free flowing artesian wells found in the LRK–NS–GK region, and the continuity of their aquifers with those of the Cambay Basin region confirm their recharge area in the foothill region of the Aravalli Mountains. It may also be noted from the subsurface cross-section (Fig. 2) that layers of sand/ silty-clay are roughly inclined parallel to the ground surface and the sampled tubewells tap nearly the same set of water bearing formations across the Cambay Basin. Because the available tubewells tap all the horizons that yield water up to their maximum depth, these are treated as pumping a single aquifer unit, within which the radiocarbon ages progressively increase in the flow direction. The very narrow range of $\delta^{13}C$ values of the TDIC of groundwater (Table 2) indicates that the dead carbon dilution factor for the various samples is not significantly different. As a result the relative age differences between the samples can be relied upon. The only sample (from Gundi) with much depleted $\delta^{13}C$ (−21.4 ‰) is derived from a very deep (>400 m) aquifer and gave an age beyond the ^{14}C dating limit. The low redox potential value (10 mV) of this sample suggested possible CO_2 contribution from anaerobic oxidation.

Further, based on hydro-geological considerations (Fig. 2) the confinement of the regional aquifer in the Cambay Basin appears to become effective near the ECBBF around the ^{14}C age contour of ~2 ka. Within the Cambay Basin, age contours are nearly parallel to each other and the horizontal distance between successive 5 ka contours is nearly constant giving a regional flow velocity in the range 2.5–3.5 m a^{-1} for a natural hydrostatic gradient of 1 in 2000 (GWRDC, Unpublished data), which is comparable to an earlier estimate of ~6 m a^{-1} (Borole et al., 1979) for the small part of the Vatrak–Shedi sub-basin marked in Fig. 3. The Vatrak–Shedi sub-basin (enclosed by an ellipse in Fig. 3) is closer to the recharge area, so both permeability and hydraulic gradient are expected to be relatively higher than the regional estimates of flow velocity (2.5–3.5 m a^{-1}) as given above.

6.2. Groundwater helium ages

It is seen from Fig. 4 that the contour of 5 ppm AEU 'excess He' runs close to the WCBBF. Considering [U] (1.07 ± 0.41 ppm), [Th] (7.5 ± 3.5 ppm), porosity (n)=20%; helium release factor (Λ_{He})=1 and grain density (ρ)=2.6 g cm^{-3} the accumulation time for 'excess He' of 5 ppm AEU will be ~15 ka (Eq. (6)). These ^4He ages are in close agreement with the ^{14}C ages, (Fig. 3), when no crustal flux is considered. This is supported by the findings of other workers that relatively young groundwater are dominated by in situ production. Torgersen and Clarke (1985) found good concordance between ^{14}C and ^4He ages in the Great Artesian Basin up to ~50 ka. Kulongoski et al. (2003) have found a good match between ^{14}C and ^4He ages up to ~25 ka in the Mojave River Basin, California. They have explained the phenomenon by the existence of wells in the basins at shallow depth and hence, above crustal influence. This probably might be the case in the North Gujarat Cambay Basin Region up to the WCBBF. In the Cambay Basin, the fluvial deposits grade from coarse grain sizes near the Aravalli foothills (major recharge region) to fine grain sizes near the LRK–NS–GK (discharge) region. This is indicated by a rapid decrease in aquifer transmissivity from ~1000 m^2 d^{-1} east of the ECBBF to <200 m^2 d^{-1} west of the WCBBF (GWRDC, Unpublished data). Thus, greater transmissivity of the aquifer up to WCBBF of the North Gujarat Region, may result in groundwater flow that entrains insignificant or no basal crustal flux, thereby leaving groundwater ^4He ages almost unaffected by the deep crustal ^4He flux.

Further, as mentioned earlier, there is some uncertainty on the calculated 'excess ^4He' that depends upon (1) 'excess air', and (2) dissolved helium at solubility equilibrium with the atmosphere. It is a common knowledge that the presence of 'excess air' in groundwater leads to ^4He concentrations higher than expected from solubility equilibrium (Heaton and Vogel, 1981; Stute and Schlosser, 1993; Aeschbach-Hertig et al., 2000). In this study we are unable to correct for the 'excess air' contribution, as neon concentrations have not been measured. According to laboratory column experiments on the formation of 'excess air' in quasi saturated porous media (Holocher et al., 2002), the amount of 'excess air' can range between 1% to 16%

of the equilibrium solubility concentration. In field studies, higher Ne excesses have also been found (e.g., Heaton and Vogel, 1981; Aeschbach-Hertig et al., 2002).

Since the solubility of He is relatively insensitive to temperature (Ozima and Podosek, 1983); the recharge temperature has a small effect on $^4He_{eq}$, which can be estimated from the regional climate and groundwater temperature measurements. In this study, the mean annual temperature of recently recharged groundwater at the Aravalli foothills was 30 ± 5 °C, as a result $^4He_{eq}$ can decrease by ~10% relative to the groundwater recharged in relatively colder climate.

Thus, both $^4He_{eq}$ and $^4He_{ea}$ would lead a systematic error of ~+10% and ~−20%, respectively on the atmospheric air equilibration value of 5.3 ppm AEU which is subtracted from the measured ^{4}He in groundwater samples to calculate $^4He_{ex}$ (Section 3.2). While we recognize that such corrections are very important for precise groundwater age estimation, particularly in case of low ^{4}He concentration samples, the interpretation and conclusion at high ^{4}He concentrations are not significantly influenced by their absence. Considering this and the accuracy of measurement for low helium concentrations being ~20%, the error on ^{4}He ages can be as high as 50% for groundwater samples which have <5 ppm AEU 'excess He'. Therefore, only those samples that showed ≥ 5 ppm AEU 'excess He' are included in the discussion.

It is further seen from Fig. 4 that ^{4}He concentrations rapidly increase farther west of the 5 ppm AEU 'excess He' contour that almost coincides with WCBBF. This could be due to (i) rapidly increasing residence time of groundwater in response to decreasing transmissivity as a result of a general decrease in grain size away from the sediment source; and/or (ii) increasing effect of the deep crustal flux of helium in the aquifer. The latter possibility is supported by existence of very high helium pockets (>50 ppm AEU) on both East and West Flanks. The East Flank is the major recharge area of aquifers in the Cambay Basin where very high helium pockets are associated with the thermal springs of Lasundra (L) and Tuwa (T). On this flank another small patch of high helium concentration is seen across the ECBBF along the Sabarmati River. Pockets of very high ^{4}He (>50 ppm AEU) lie outside the Cambay Basin on both flanks (shaded areas in Fig. 4) and considering this helium as in situ production will yield groundwater age $>10^3$ ka, which is not tenable hydro-geologically. The presence of non in situ produced ^{4}He in these pockets is also indicated by the overlapping pockets of high groundwater temperature (>35 °C) suggesting hydrothermal venting of deep crustal fluids in such pockets. The ^{4}He method of dating groundwater is not applicable to such pockets.

The deep crustal He flux may also enter the aquifer by diffusion from underlying basement followed by entrainment and upward migration, particularly in the discharge region (Bethke et al., 2000). Thus, more crustal flux may be entrained with increasing distance along flow paths and hence, resulting in a rapid increase in the helium concentration towards the discharge region. For the five samples west of the WCBBF for which ^{14}C groundwater ages were also measured, a ^{4}He crustal flux of $>1.5 \times 10^{-8}$ cm^3 STP He cm^{-2} y^{-1} produces a good match between the two dating methods. However, for the Lasundra and Tuwa thermal springs in the East Flank and pockets of very high helium on the West flank (shaded areas in Fig. 4) a crustal flux$>10^{-6}$ cm^3 STP He cm^{-2} y^{-1} is necessary for agreement between ^{4}He and ^{14}C ages. Takahata and Sano (2000) have reported ^{4}He crustal flux of 3.0×10^{-8} cm^3 STP He cm^{-2} y^{-1} from a sedimentary basin in Japan. The typical continental ^{4}He flux is 3×10^{-6} cm^3 STP He cm^{-2} y^{-1} (O'nions and Oxburgh, 1983). It is thus seen that the observed pattern of high helium concentrations in localised pockets can only be explained by invoking 2–3 orders of magnitude variation in crustal diffusion flux which is another way of saying that crustal diffusion occurs along preferred pathways that open where high helium pockets are located.

In the present case, outside the anomalous pockets of helium, the in situ ^{4}He accumulation (i.e., without crustal flux correction) produces a reasonable correspondence between ^{14}C and ^{4}He ages within the 50% uncertainty range. For samples to the west of the WCBBF, a low crustal flux of $\sim 1.5 \times 10^{-8}$ cm^3 STP He cm^{-2} y^{-1} cannot be ruled out as invoking it does produce a better match with the few definite ^{14}C groundwater ages. Farther west, ages must be >45 ka, possibly as old as 100 ka.

In the foregoing, the value of Λ_{He} was taken as 1. It is clear from Eqs. (3)–(6) that for lower values of Λ_{He}, the estimate of groundwater ^{4}He age for the 5 ppm AEU contour (roughly along the WCBBF; Fig. 4) will increase correspondingly. This will result in a better match with the ^{14}C ages (Fig. 3).

6.3. Groundwater helium/radon ages

The measured ^{222}Rn activity within the Cambay Basin and in other parts of the study area (Table 3 and Fig. 6) showed a variation of ± 50% around an average value of ~800 dpm/l (except the thermal spring water at Tuwa) suggesting a similar range of variation in the U concentration of the aquifer material. This range of U variation was also seen in the analysed drill cutting samples (Fig. 7) and on shallow depth sediments from the Cambay Basin (Srivastava et al., 2001).

The distribution of estimated groundwater $^4He/^{222}Rn$ ages using Eq. (11) with measured values of ^{222}Rn activity, ^4He concentrations and the concentration ratio of $[Th]/[U]=7.1\pm4.3$ are shown in Fig. 8. As explained earlier, these ages are independent of porosity, density and U concentration but depend on Th/U of the aquifer material. Additionally, the $^4He/^{222}Rn$ ages also depend on the release factor ratio ($\Lambda_{Rn}/\Lambda_{He}$) and accumulation rate ratio ($\Lambda_{Rn}/\Lambda_{He}$) of ^4He and ^{222}Rn. As in the case of ^{14}C ages, a gradual age progression from the recharge area towards the WCBBF is observed in the major part of the study area. These ages (Fig. 8) were obtained using $\Lambda_{Rn}/\Lambda_{He}=0.4$ to give the best match with the ^{14}C age gradient (Fig. 3) across the Cambay basin. This gradient matching approach was chosen because the inferred groundwater flow velocities in the confined aquifer by the two methods match when age gradients match. This also ensures that the uncertainties related to, for example the initial activity of ^{14}C in the recharge area or the 'excess He', have as little influence on matching as possible. A Radon release factor (Λ_{Rn}) ranging from 0.01–0.2 has been indicated from laboratory experiments for granites and common rock forming minerals (Krishnaswami and Seidemann, 1988; Rama and Moore, 1984). If measured values of $[U]=1.07\pm0.41$ ppm and ^{222}Rn are substituted in Eqs. (9) and (10), Λ_{Rn} is estimated to be 0.15 ± 0.07, which is consistent with the literature. On the other hand for ^4He, Torgersen and Clarke (1985), in agreement with numerous other authors have suggested $\Lambda_{He}\approx1$. For $\Lambda_{Rn}=0.15\pm0.07$ and $\Lambda_{Rn}/\Lambda_{He}=0.4$, $\Lambda_{He}=0.4\pm0.3$ is obtained for best regional matching

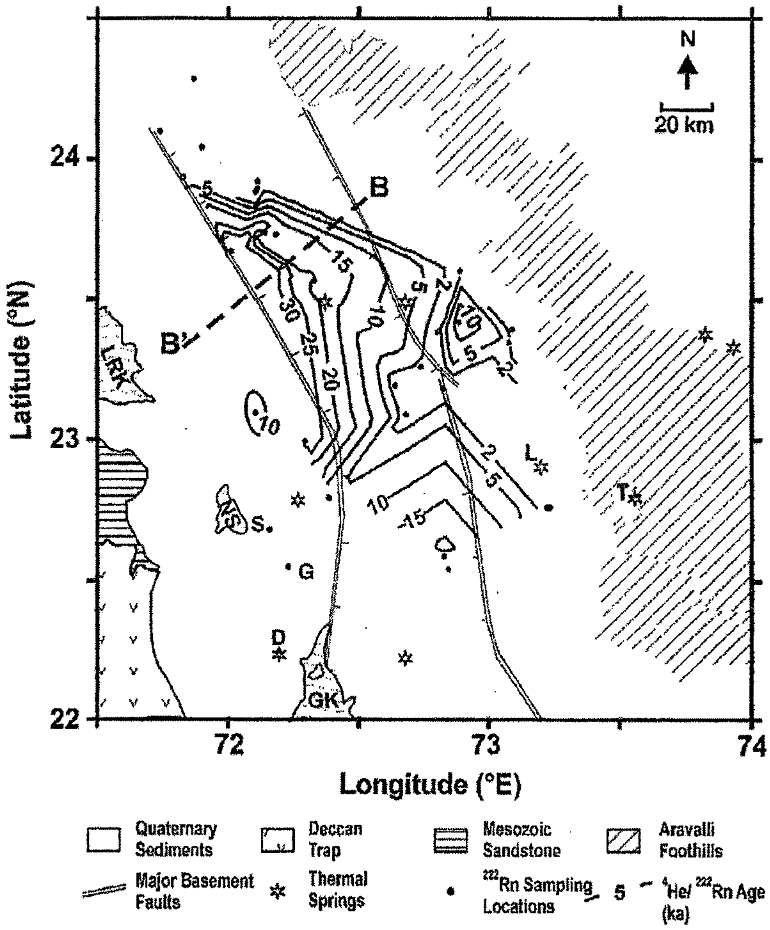

Fig. 8. Iso-distribution map of $^4He/^{222}Rn$ groundwater ages in the NGC region for Th/U=7.1; $\Lambda_{Rn}/\Lambda_{He}=0.4$; $\rho=2.6$ g cm^{-3} and $n=20\%$. Samples with >10 ppm AEU 'excess He' and/or >2000 dpm/l ^{222}Rn were excluded during contouring. Dots indicate sampling locations. The groundwater age gradient along BB' is shown in Fig. 9.

between $^4He/^{222}Rn$ and ^{14}C ages, i.e., between Figs. 8 and 3. This is shown in Fig. 9 where age progression along the line BB′ (drawn in Figs. 3, 4 and 8) is plotted. The arrow in the middle of each trapezoid shows the median value of the model age by the respective method. The progressively increasing width of the trapezoid depicts the error at any given median age. The slopes of the respective medians give the age gradients. It is seen that for $\Lambda_{He}=0.4$, the $^4He/^{222}Rn$ age gradient matches the ^{14}C age gradient and, for $\Lambda_{He}=1$, the $^4He/^{222}Rn$ age gradient matches the ^4He age gradient. In view of the various uncertainties that affect the three methods, the ^{14}C method appears most reliable in the present case. Firstly, because the $\delta^{13}C$ values of TDIC show a very narrow range (-9.6 ± 1.2 ‰) and secondly, the ^{14}C age iso-lines show a nearly parallel distribution, approximately in agreement with the distribution of transmissivity of the aquifers obtained from the pumping test data, progressively decreasing from ~1000 $m^2\ d^{-1}$ east of the ECBBF to <200 $m^2\ d^{-1}$ west of the WCBBF (GWRDC, unpublished data). Therefore, taking ^{14}C age data as reference, the best match for both $^4He/^{222}Rn$ and ^4He ages is obtained for $\Lambda_{He}=0.4$, with the ^4He groundwater age of ~37 ka (instead of ~15 ka) corresponding to the 5 ppm AEU 'excess He' iso-line (Fig. 4). A value of $\Lambda_{He}<1$ in North Gujarat–Cambay region would appear contrary to the apparent $\Lambda_{He}>1$ due to release of geologically stored helium in young sediments derived from old protoliths (Solomon et al., 1996).

The comparatively low estimate of Λ_{He} can either be due to (i) loss of ^4He from the aquifer system, or (ii) incomplete release of radiogenic ^4He from the grains over time scales of ~100 ka. The former possibility is contrary to the basic assumptions of both ^4He and $^4He/^{222}Rn$ dating methods. The latter possibility may not be ruled out because the depositional age of aquifer material in the Cambay Basin is Late Quaternary (Pandarinath et al., 1999; Prasad and Gupta, 1999) and it is possible that all the produced helium has not been released to the interstitial water since deposition. Contrary to Solomon et al. (1996), this would require a mechanism that nearly releases all of the geologically stored helium in the grains due to mechanical/thermal/chemical stress during the process of weathering and transportation and subsequent build up within the grains with a partial release to interstitial water during the quiet post depositional period until steady-state for helium loss is achieved within individual grains. The large grain size (>0.5 mm) of aquifers forming horizons may be a contributory factor to partial helium release in the post depositional period. The present data does not permit giving more definitive arguments concerning the involved mechanisms.

It is interesting to note that the use of groundwater helium for earthquake prediction (Sano et al., 1998) is

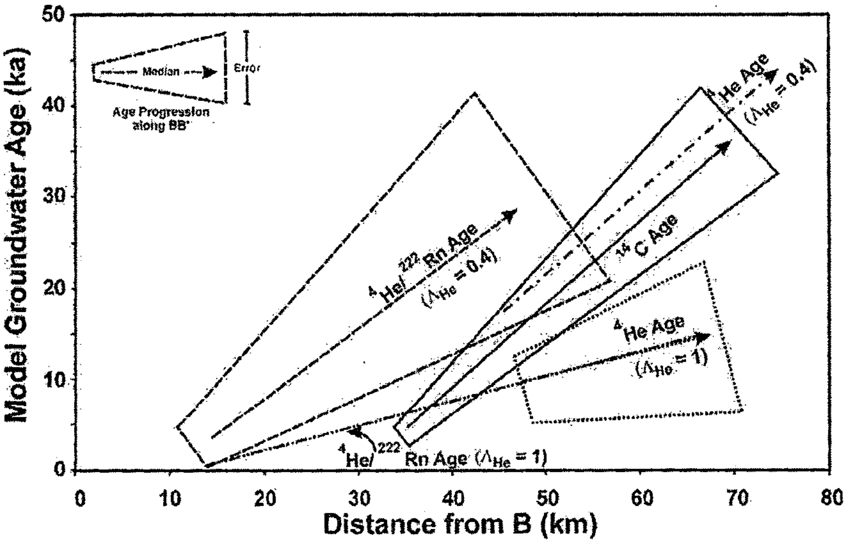

Fig. 9. Plot of groundwater age progression along line BB' (shown in Figs. 3, 4 and 8) for comparing the age gradients for model ^{14}C ages, ^4He ages for $\Lambda_{He}=1$ and $^4He/^{222}Rn$ ages. It is seen that the gradient of $^4He/^{222}Rn$ ages for $\Lambda_{He}=0.4$ matches the gradient for ^{14}C ages. But, the gradient of ^4He ages for $\Lambda_{He}=1$ though matching with the gradient of $^4He/^{222}Rn$ ages for $\Lambda_{He}=1$ is discordant with the ^{14}C age gradient along BB'. Yet for $\Lambda_{He}=0.4$, the gradients of both $^4He/^{222}Rn$ ages and ^4He ages match the ^{14}C age gradient. Only the median values of the age distributions for ^4He ages ($\Lambda_{He}=0.4$) and $^4He/^{222}Rn$ ages ($\Lambda_{He}=1$) are shown.

based on the premise that in the normal course Λ_{He} may be <1.

6.4. Tectonic effects on groundwater helium, radon and temperature

Whatever the Λ_{He} value, high (>50 ppm AEU) ^{4}He concentrations observed in pockets on East Flank (Fig. 4) require residence time >100 ka which is not compatible with the hydrogeology of the region, as this flank forms the recharge area of the regional aquifer system. Association of these high ^{4}He patches with geothermal springs and anomalous (>35 °C) groundwater temperature suggests a role of deep hydrothermal circulation (Gupta and Deshpande, 2003a,b). On this flank, ^{222}Rn measurements do not indicate any unusually high activity suggesting absence of near surface uranium mineralization, except for the thermal water from Tuwa (T). A similar association of helium, geothermal springs and groundwater temperature was observed in the SW part of the study area around 22.5°N and 72.3°E. This region had the highest ^{4}He in groundwater along with the lowest ^{222}Rn activity; clearly suggesting that local near surface uranium mineralization cannot be invoked to explain high groundwater helium. This indicates that, besides the radiogenic component, there is an additional ^{4}He crustal flux with or without physical mixing of groundwater. This area also has a series of criss-cross basement faults and at least two reported thermal springs (Fig. 1) suggesting active deep hydrothermal circulation along these faults. In the majority of groundwater samples, high temperatures (>35 °C) along with very high 'excess He' concentrations (>50 ppm AEU) suggest the possibility of physical mixing of deeper (>500 m) thermal fluids with shallow groundwater. Minissale et al. (2000) have shown, based on ^{3}He/^{4}He ratio and stable isotopic studies on thermal fluids from central-western peninsular India including Tuwa that no signature of mantle derived fluids exists in the thermal waters.

Thus, a few pockets of high helium concentrations overlapping with high temperature pockets located along major basement faults indicate intrusion of deeper crustal fluids to shallow groundwater and adjoining areas. Excluding such pockets, in situ radiogenic production of ^{4}He and ^{222}Rn is able to account for their observed concentrations.

7. Summary and conclusions

A regional aquifer system in the North Gujarat–Cambay region in western India has been investigated for ascertaining the groundwater age evolution from the recharge to the discharge area. A suite of natural tracers, namely ^{14}C, ^{4}He and ^{222}Rn has been employed in addition to temperature and electrical conductivity. The field and laboratory measurements indicated the range of variation for the different parameters as follows: temperature: 28 to 61 °C; EC: 0.5 to 7.6 mS; pH: 6.9 to 8.2; ^{14}C: 0 to 115 pmc; δ^{13}C: −7.26‰ to −21.36‰; ^{4}He: 5.3 to 2850 ppm AEU; and ^{222}Rn: 260 to 62600 dpm/l. The anomalous values of the various parameters were found generally in association with thermal groundwater.

The groundwater age estimates by the three methods (^{14}C, ^{4}He and ^{4}He/^{222}Rn) indicated present to <2 ka ages in the recharge area along the Aravalli foothills. The ages progressively increased in the general flow direction of groundwater, approximately westward in the Cambay Basin, reaching a limiting value of ~35 ka for ^{14}C near the West Cambay Basin Boundary Fault. The ^{4}He method also indicated further west-southwards progression of groundwater ages up to ~100 ka. In the entire study area, there was correspondence in age estimates by the three dating methods within ~50% uncertainty for both ^{4}He and ^{4}He/^{222}Rn methods. In spite of such a large uncertainty in age estimates, the best match of groundwater age distributions by the three methods is obtained for a helium release factor (Λ_{He}) value of 0.4 ± 0.3, significantly less than the conventionally used value of 1. These investigations have validated the hydrological model of the study area as comprising of a regional confined aquifer system with recharge area in the Aravalli foothills and subsurface discharge area in the Gulf of Khambhat.

In addition to the progressive increase of groundwater age in the flow direction, some pockets of anomalously high ^{4}He concentrations, not accompanied by high ^{222}Rn activities (except at Tuwa thermal spring) have been observed along some deep-seated faults in the study area. These anomalously high ^{4}He concentrations were geographically associated with anomalously high groundwater temperatures (Figs. 4 and 5). Considering the positive geographic correlation between ^{4}He and temperature, an active hydrothermal circulation involving deep crustal layers, as suggested earlier (Gupta and Deshpande, 2003a,b), is reaffirmed.

This multi-parameter groundwater study also indicated that release of radiogenic radon from the solid to the liquid phase in the study area was $15 \pm 7\%$ for alluvial sedimentary formations in agreement with previous estimates. Radiogenic helium release from the solid to the liquid phase was, however, estimated as only ($40 \pm 30\%$) instead of literature value of ~100%.

The lower helium release over long time scale (~100 ka) is probably consistent with several known instances of anomalous ^{4}He release during rock dilation and fracturing in association with earthquakes and enhanced release of geologically stored radiogenic helium in relatively young fine grained sediments derived from old protoliths.

Acknowledgements

This study forms part of a research project entitled "Estimation of Natural and Artificial Groundwater Recharge Using Environmental, Chemical and Isotopic Tracers and Development of Mathematical Models of Regional Aquifer Systems in North Gujarat". We thank the Gujarat Water Resources Development Corporation Ltd., Gandhinagar (GWRDC) for sponsoring this project and for sharing the unpublished hydrogeology data from the study area. We are grateful to Prof. N. Bhandari for providing us the HPGe detector for U, Th and ^{222}Rn activity measurements using gamma spectrometry. Help of Mr. M.H. Patel and Mr. N.B Vaghela is gratefully acknowledged for ^{14}C and δ^{13}C analyses. Shri B.R. Raval is thanked for help in fieldwork. We also thank the two referees (Drs. A. Minissale and W. Aeschbach-Hertig) for their valuable suggestions towards improving the manuscript. [SG]

References

Aeschbach-Hertig, W., Peeters, F., Beyerle, U., Kipfer, R., 2000. Palaeotemperature reconstruction from noble gases in ground water taking into account equilibration with entrapped air. Nature 405, 1040–1044.

Aeschbach-Hertig, W., Stute, M., Clark, J.F., Reuter, R.F., Schlosser, P., 2002. A palaeotemperature record derived from dissolved noble gases in groundwater of the Aquia aquifer (Maryland, USA). Geochim. Cosmochim. Acta 66 (5), 797–817.

Andrews, J.N., 1977. Radiogenic and inert gases in groundwater. In: Paquet, H., Tardy, Y. (Eds.), Proc. of the Sec. Int. Symp. On Water–Rock Interaction, Strassbourg, pp. 334–342.

Andrews, J.N., Lee, D.J., 1979. Inert gases in groundwater from the Bunter Sandstone of England as indicators of age and paleoclimatic trends. J. Hydrol. 41, 233–252.

Andrews, J.N., Fontes, J. Ch., 1992. Importance of the in situ production of ^{36}Cl, ^{36}Ar and ^{14}C in hydrology and hydrogeochemistry. Isotopes Techniques in Water Resources Development. IAEA, Vienna, pp. 245–269.

Andrews, J.N., Giles, I.S., Kay, R.L.F., Lee, D.J., Osmond, J.K., Cowart, J.B., Fritz, P., Barker, J.F., Gale, J., 1982. Radioelements, radiogenic helium and age relationships for groundwaters from the granites at Stripa, Sweden. Geochim. Cosmochim. Acta 46, 1533–1543.

Andrews, J.N., Davis, S.N., Fabryka-Martin, J., Fontes, J.Ch., Lehmann, B.E., Loosli, H.H., Michelot, J.L., Moser, H., Smith, B., Wolf, M., 1989. The in situ production of radioisotopes in rock matrices with particular reference to the Stripa granite. Geochim. Cosmochim. Acta 53, 1803–1815.

Ballentine, C.J., Burnard, P.G., 2002. Production, release and transport of noble gases in the continental crust. In: Porcelli, D., Ballentine, C.J., Wieler, R. (Eds.), Noble Gases in Geochemistry and Cosmochemistry, Rev. Mineral. Geochem., vol. 47. pp. 481–538.

Bethke, C.M., Torgersen, T., Park, J., 2000. The "age" of very old groundwater: insights from reactive transport models. J. Geochem. Explor. 69–70, 1–4.

Borole, D.V., Gupta, S.K., Krishnaswami, S., Datta, P.S., Desai, B.I., 1979. Uranium isotopic investigations and radiocarbon measurement of river–groundwater systems, Sabarmati Basin, Gujarat, India. Isotopic Hydrology, vol. 1. IAEA, Vienna, pp. 181–201.

Castro, M.C., Stute, M., Schlosser, P., 2000. Comparison of ^{4}He ages and ^{14}C ages in simple aquifer systems: implications for groundwater flow and chronologies. Appl. Geochem. 15, 1137–1167.

Clark, I.D., Fritz, P., 1997. Environmental Isotopes in Hydrogeology, Lewis Publisher, CRC Press. 328 pp.

Clark, J.F., Davisson, M.L., Hudson, G.B., Macfarlane, P.A., 1998. Noble gases, stable isotopes, and radiocarbon as traces of flow in the Dakota aquifer, Colorado and Kansas. J. Hydrol. 211, 151–167.

Cserepes, L., Lenkey, L., 1999. Modelling of helium transport in groundwater along a section in the Pannonian basin. J. Hydrol. 225, 185–195.

Fontes, J.C., Garnier, J.M., 1979. Determination of the initial ^{14}C activity of the total dissolved carbon: a review of the existing models and new approach. Water Resour. Res. 15 (2), 399–413.

Fröhlich, K., Gellermann, R., 1987. On the potential use of uranium isotopes for groundwater dating. Chem. Geol. 65, 67–77.

Gazetteer, 1975. In: Rajyagor, S.B. (Ed.), Gujarat State Gazetteers. 862 pp.

Geyh, M.A., 1990. Absolute Age Determination: Physical and Chemical Dating Methods and their Applications. Springer Verlag, Germany. 503 pp.

GSI, 2000. Seismotectonic atlas of India and its environs. Geological Survey of India, Calcutta, India. 87 pp.

Gupta, S.K., Polach, H.A., 1985. Radiocarbon Practices at ANU, Handbook, Radiocarbon Laboratory, Research School of Pacific Studies, ANU, Canberra. 173 pp.

Gupta, S.K., Deshpande, R.D., 2003a. Origin of groundwater helium and temperature anomalies in the Cambay region of Gujarat, India. Chem. Geol. 198, 33–46.

Gupta, S.K., Deshpande, R.D., 2003b. High fluoride in groundwater of North Gujarat–Cambay region: origin, community perception and remediation. In: Singh, V.P., Yadava, R.N. (Eds.), Proc. Int. Conf. on Water and Environment 2003, Ground Water Pollution. pp. 368–388.

Gupta, S.K., Bhandari, N., Thakkar, P.S., Rengarajan, R., 2002. On the origin of the artesian groundwater and escaping gas at Narveri after the 2001 Bhuj earthquake. Curr. Sci. 82 (4), 463–468.

Heaton, T.H.E., Vogel, J.C., 1981. "Excess air" in groundwater. J. Hydrol. 50, 201–216.

Holocher, J., Peeters, F., Aeschbach-Hertig, W., Hofer, M., Brennwald, M., Kinzelbach, W., Kipfer, R., 2002. Experimental investigations on the formation of excess air in quasi-saturated porous media. Geochim. Cosmochim. Acta 66 (23), 4103–4117.

Imbach, T., 1997. Deep groundwater circulation in the tectonically active area of Bursa, northwest Anatolia, Turkey. Geothermics 26 (2), 251–278.

Ivanovich, M., 1992. Uranium Series Disequilibrium: Applications to Earth Marine and Environmental Sciences. Claderon Press, Oxford. 910 pp.

Krishnaswami, S., Seidemann, D.E., 1988. Comparative study of ^{222}Rn, ^{40}Ar, ^{39}Ar and ^{37}Ar leakage from rocks and minerals: implications to the role of nanopores in gas transport through natural silicates. Geochim. Cosmochim. Acta 52, 655–658.

Kulongoski, J.T., Hilton, D.R., Izbicki, J.A., 2003. Helium isotope studies in the Mojave Desert, California: implications for groundwater chronology and regional seismicity. Chem. Geol. 202, 95–113.

Lehmann, B.E., Loosli, H.H., Rauber, D., Thonnard, N., Willis, R.D., 1991. ^{81}Kr and ^{85}Kr in groundwater, Milk River Aquifer, Alberta, Canada. Appl. Geochem. 6, 419–424.

Maurya, D.M., Malik, J.N., Raj, R., Chamyal, L.S., 1997. Soft sediment deformation in the Quaternary sediments of the Lower Mahi river basin, Western India. Curr. Sci. 72 (7), 519–522.

Mazor, E., Bosch, A., 1992. Helium as semi-quantitative tool for groundwater dating in the range of 104–108 years. Isotopes of Noble Gases as Tracers in Environmental Studies. IAEA, Vienna, pp. 163–178.

Merh, S.S., 1995. Geology of Gujarat. Geological Society of India. 222 pp.

Minissale, A., Vaselli, O., Chandrasekharan, D., Magro, G., Tassi, F., Casiglia, A., 2000. Origin and evolution of 'intracratonic' thermal fluids from central-western peninsular India. Earth Planet. Sci. Lett. 181, 377–397.

Mook, W.G., 1976. The dissolution-exchange model for dating groundwater with ^{14}C. Interpretation of Environmental Isotopes and Hydrochemical Data in Groundwater Hydrology. IAEA, Vienna, pp. 213–225.

Münnich, K.O., 1957. Messung des ^{14}C—Gehaltes von hartem Grundwasser. Naturwissenschaften 34, 32–33.

Münnich, K.O., 1968. Isotopen-Datierung von Grundwasser. Naturwissenschaften 55, 158–163.

Nazaroff, W.W., Moed, B.A., Sextro, R.G., 1988. Soil as a source of indoor radon: generation, migration and entry. In: Nazaroff, W.W., Nero Jr., A.V. (Eds.), Radon and its Decay Products in Indoor Air. John Wiley and Sons, NY.

O'nions, R.K., Oxburgh, E.R., 1983. Heat and helium in the earth. Nature 306, 429–431.

Ozima, M., Podosek, F.A., 1983. Noble Gas Geochemistry. Cambridge University Press, NY.

Pandarinath, K., Prasad, S., Deshpande, R.D., Gupta, S.K., 1999. Late Quaternary sediments from Nal Sarovar, Gujarat, India: distribution and provenance. Proc. Indian Acad. Sci. (Earth Planet. Sci.) 108 (2), 107–116.

Prasad, S., Gupta, S.K., 1999. Role of eustasy, climate and tectonics in Late Quaternary evolution of Nal–Cambay region, NW India. Z. Geomorph. N.F. 43, 483–504.

Prasad, S., Pandarinath, K., Gupta, S.K., 1998. Geomorphology, tectonism and sedimentation in the Nal Region, western India. Z. Geomorph. N.F. 25, 207–223.

Rama, Moore, W.S., 1984. Mechanism of transport of U–Th series radioisotopes from solids into groundwater. Geochim. Cosmochim. Acta 48, 395–399.

Sano, Y., Takahata, N., Igarashi, G., Koizumi, N., Sturchio, N.C., 1998. Helium degassing related to the Kobe earthquake. Chem. Geol. 150, 171–179.

Solomon, D.K., Hunt, A., Poreda, R.J., 1996. Source of radiogenic helium-4 in shallow aquifers: implications for dating young groundwater. Water Resour. Res. 32, 1805–1813.

Srivastava, P., Juyal, N., Singhvi, A.K., Wasson, R.J., Bateman, M.D., 2001. Luminescence chronology of river adjustment and incision of Quaternary sediments in the alluvial plain of the Sabarmati River, North Gujarat, India. Geomorphology 36, 217–229.

Stute, M., Schlosser, P., 1993. Principles and applications of the noble gas palaeothermometer. In: Swart, P.K., Lohmann, K.C., McKenzie, J., Savin, S. (Eds.), Climate Change in Continental Isotopic Records, Geophysical Monograph Series, vol. 78. American Geophysical Union, Washington, DC, pp. 89–100.

Stute, M., Sonntag, C., Deak, J., Schlosser, P., 1992. Helium in deep circulating groundwater in the Great Hungarian Plain: flow dynamics and crustal and mantle helium fluxes. Geochim. Cosmochim. Acta 56, 2051–2067.

Takahata, N., Sano, Y., 2000. Helium flux from a sedimentary basin. Appl. Radiat. Isotopes 52, 985–992.

Torgersen, T., 1980. Controls on pore-fluid concentration of ^{4}He and ^{222}Rn and the calculation of ^{4}He/^{222}Rn ages. J. Geochem. Explor. 13, 57–75.

Torgersen, T., 1992. Helium-4 model ages for pore fluids from fractured lithologies, discussion and application. Isotopes of Noble Gases as Tracers in Environmental Studies. IAEA, Vienna, pp. 179–201.

Torgersen, T., Clarke, W.B., 1985. Helium accumulation in groundwater. I. An evaluation of sources and the continental flux of crustal ^{4}He in the Great Artesian Basin, Australia. Geochim. Cosmochim. Acta 49, 1211–1218.

Torgensen, T., Ivey, G.N., 1985. Helium accumulation in groundwaters: II. A model for the accumulation of the crustal ^{4}He degassing flux. Geochim. Cosmochim. Acta 49, 2445–2452.

Vogel, J.C., 1967. Investigation of groundwater flow with radiocarbon. Isotopes in Hydrology. IAEA, Vienna, pp. 355–368.

Vogel, J.C., 1970. Carbon-14 dating of groundwater. Isotope Hydrology. IAEA, Vienna, pp. 225–237.

Weiss, R.F., 1971. Solubility of helium and neon in water and seawater. J. Chem. Eng. Data 16, 235–241.

Origin of high fluoride in groundwater in the North Gujarat-Cambay region, India

S. K. Gupta · R. D. Deshpande · Meetu Agarwal · B. R. Raval

Abstract This paper reports on the origin of high fluoride in a regional alluvial aquifer system under water stress in the North Gujarat-Cambay (NGC) region in western India. This region is severely affected by endemic fluorosis due to ingestion of groundwater containing excessive fluoride. With an objective to understand factors controlling high fluoride concentration in groundwater of this region, 225 groundwater samples have been analysed for various chemical parameters. Samples were collected from different depth zones tapping shallow dug wells, geothermal springs, hand-pumps and tubewells, including free flowing artesian wells up to 450 m depth from the aquifers in the Quaternary alluvial formation covering most of the study area. No relation was found between fluoride concentration and depth of sampled groundwater. However, certain sub-aquifer zones have been identified within the Cambay Basin where groundwater contains relatively high fluoride concentration. In general, areas of high fluoride overlap areas with high electrical conductivity (EC). On the west flank of the Cambay Basin in the low lying belt linking Little Rann of Kachchh-Nalsarovar-Gulf of Khambhat (LRK-NS-GK), high fluoride and EC in shallow aquifers originate from evaporative enrichment. On the east flank of Cambay Basin, some high fluoride pockets are observed which are probably due to preferential dissolution of high fluoride bearing minerals. On this flank high fluoride is also associated with thermal springs. Within the Cambay Basin, alternating belts of low and high fluoride concentrations are ascribed to groundwater recharge during the past wet and arid climatic phases, respectively. This is based on groundwater radiocarbon age contours of ~20 ka overlapping the high fluoride belt.

Résumé Cet article étudie l'origine des teneurs élevées en Fluorure dans un système aquifère alluvial régional, soumis à un stress hydrique dans le Nord Gujarat–région Cambay (NGC) à l'Ouest de l'Inde. Cette région est sévèrement affectée par une fluorose endémique, due à l'ingestion d'eau souterraine très riche en fluor. Avec pour objectif de comprendre les paramètres contrôlant les fortes teneurs en fluor, 225 échantillons d'eau souterraine ont été analysés sur différents paramètres. Les échantillons ont été pris à différentes profondeurs : puits de surface, sources géothermiques, pompes à main, forages artésiens jaillissant dont la profondeur avoisine les 450 m dans les formations alluviales quaternaire recouvrant la plus grande partie de la région étudiée. Il n'y a pas de relation entre la profondeur et les teneurs en fluorure. Néanmoins, certaines zones sub-aquifères ont été identifiées dans le Basin de Cambay où l'eau souterraine présentait des concentrations relativement élevées en fluorure. En général les zones de hautes concentrations en fluorure recouvrent les zones à fortes conductivité électrique (abréviation en anglais: EC). Sur le flanc Ouest du bassin de Cambay dans le mince lit reliant Little Ran de Kachchh-Nalsarovar au golfe de Khambhat (LRK-NS-GK), les fortes teneurs en fluorure et les EC dans la nappe phréatique proviennent de l'enrichissement par les évaporites. Sur le flanc Est du bassin, des poches de teneurs élevées en fluorures ont été observées, probablement dues à des dissolutions préférentielles de minéraux fluorés. Sur ce flanc des teneurs sont également associées à la présence de sources géothermales. Dans le bassin de Cambay, les alternances de couches lits à fortes teneurs et de lits à faibles teneurs sont expliquées par la recharge durant les périodes climatiques humides et les périodes climatiques plus sèches. Ceci est corroboré par les datations au radiocarbone (environ 20.000 an) au dessus du lit riche en fluorure.

Resumen Este artículo reporta sobre el origen de altas concentraciones de flúor en un sistema regional de acuíferos bajo presión hídrica en la región del norte de Gujarat-Cambay (NGC) del occidente de India. Esta región está afectada severamente por fluorosis endémica debido a la ingestión de agua subterránea que contiene exceso de flúor. Se tomaron 225 muestras de agua subterránea las cuales fueron analizadas por varios parámetros químicos con el objetivo de entender los factores que controlan las elevadas concentraciones de flúor en esta región. Las muestras se colectaron a diferentes profun-

Received: 8 May 2003 / Accepted: 18 August 2004

S. K. Gupta (✉) · R. D. Deshpande · M. Agarwal · B. R. Raval
Physical Research Laboratory (PRL),
PO Box 4218, 380 009 Navrangpura, Ahmedabad, India
e-mail: skgupta@prl.ernet.in

Hydrogeology Journal (2005) 13:596–605

DOI 10.1007/s10040-004-0389-2

didades en pozos someros, manantiales geotermales, pozos con bom-bas de mano, y pozos entubados incluyendo pozos artesianos de flujo libre de hasta 450 m de profundidad emplazados en los acuíferos de la formación aluvial Cuaternaria que cubre la mayor parte del área de estudio. No se encontró ninguna relación entre la concentración de flúor y la profundidad de las muestras de agua subterránea. Sin embargo, se identificaron dentro de la cuenca Cambay algunas zonas sub-acuíferas donde el agua subterránea contiene concentraciones relativamente altas de flúor. En general, las áreas con elevada concentración de flúor están sobrepuestas a áreas de alta conductividad eléctrica (CE). Sobre el flanco occidental de la cuenca Cambay, en la faja baja que une Little Rann con Kachchh-Nalsarovar-Golfo de Khamhat (LRK-NS-GK), las altas concentraciones de flúor y altas CE en acuíferos someros se derivan de enriquecimiento por evaporitas. Sobre el flanco orien-tal de la cuenca Cambay se observaron algunos cuerpos con alta concentración de flúor los cuales se deben probablemente a la disolución preferencial de minerales con alto contenido de flúor. En este flanco el alto contenido de flúor también se asocia con manantiales termales. Dentro de la cuenca Cambay existen fajas alternantes, con concentraciones altas y bajas de flúor, las cuales se atribuyen a recarga de agua subterránea durante las fases climáticas pasadas, húmedas y áridas, respectivamente. Este planteamiento se basa en contornos de edades de ~20 ka de radiocarbono que están sobrepuestos a la faja alta en flúor.

Keywords Groundwater · Fluoride · North Gujarat · Cambay Basin

Introduction

The effects of fluoride on human health have been extensively studied (WHO 1970, 1984). The occurrence and development of endemic fluorosis has its roots in the high fluoride content in water, air and soil, of which water is perhaps the major contributor. Bureau of Indian Standards (BIS 1990) has suggested the permissible limit of fluoride in drinking water to be 1 ppm, which is lower then the WHO (1984) drinking water limit of 1.5 ppm.

Almost the entire population of the NGC region in western India uses groundwater for drinking and other purposes. Evidences of dental and skeletal fluorosis in many areas of this region have been noticed (Gupta and Deshpande 1998). Although knowledge concerning fluoride-affected parts of Gujarat is available (Vasavada 1998; Gujarat Water Supply and Sewerage Board, 1997, unpubl. data), very little is understood about the origin of high fluoride in affected areas. It is only during the last 3–4 decades that high concentrations of fluoride in groundwater have been noticed in North Gujarat and assigned to health problems. During this period, areas irrigated by groundwater increased three times and the water table declined by as much as 100–150 m, particularly in the Mehsana district. This has lead to a general belief that excessive exploitation of groundwater is in some way responsible for the increase of fluoride in groundwater. The most common hypothesis suggests that deep groundwater in the area contains high concentrations of fluoride (Patel, 1986, personal communication). This could be due to its high residence time in the aquifer system thereby having longer contact time for dissolution of fluoride bearing minerals present (Ramakrishnan 1998). Another hypothesis suggests higher concentrations of fluoride bearing minerals in the deeper aquifers. Handa (1975) has linked high fluoride to high evapo-transpiration in arid regions of India.

Since clays are known to be generally rich in fluoride concentration (Agrawal et al. 1997), it is possible that pore water in clay-rich aquitards has relatively higher fluoride concentrations. As a result of decline in piezometric level during the last few decades, increase in flow across the aquitards could provide increased fluoride to the aquifers and be pumped with the groundwater. However, these hypotheses are essentially conjectures, not based on any detailed investigation of the distribution of fluoride and its association with other hydro-geological parameters in the NGC region.

The objective of this study was to understand factors controlling the high fluoride concentration in groundwater of the NGC region. In addition to purely academic inquiry, the understanding of the origin and distribution of fluoride may be useful in devising water exploitation and management strategies.

Various groundwater quality parameters have been measured in samples from various depth zones ranging from shallow dug wells, geothermal springs, hand-pumps and tubewells to artesian wells up to 450 m depth.

Geohydrology of the North Gujarat-Cambay region

North Gujarat—Cambay region (Fig. 1) comprise ~500-m thick multilayered sedimentary sequence of fluvially transported Quaternary alluvium deposited in the Cambay Graben and on its flanks (Merh 1995). This forms the regional aquifer system of NGC region with several sub-aquifers at different depths (Fig. 2).

A geological cross-section from Chadotar to Nayaka across the Cambay Basin (along the line AA' in Fig. 1) is shown in Fig. 2. The sandy layers forming aquifer horizons are seen to be laterally continuous and vertically interspersed with thin semi-permeable clay/silt layers that may not have lateral continuity over a large area. Since the tubewells tap all the horizons that yield water up to their maximum depth, all the pumped horizons have been treated as a single regional aquifer unit and the individual sand layers as sub-aquifers. It is also seen that various sub-aquifers are roughly inclined parallel to the ground surface; so that at different locations, a given depth below ground level (bgl) reaches approximately the same sub-aquifer within the Cambay Basin.

Major rivers traversing the region, namely, Banas, Rupen, Saraswati, Sabarmati and Mahi have eroded the igneous and metamorphic rocks associated with the Delhi

DOI 10.1007/s10040-004-0389-2

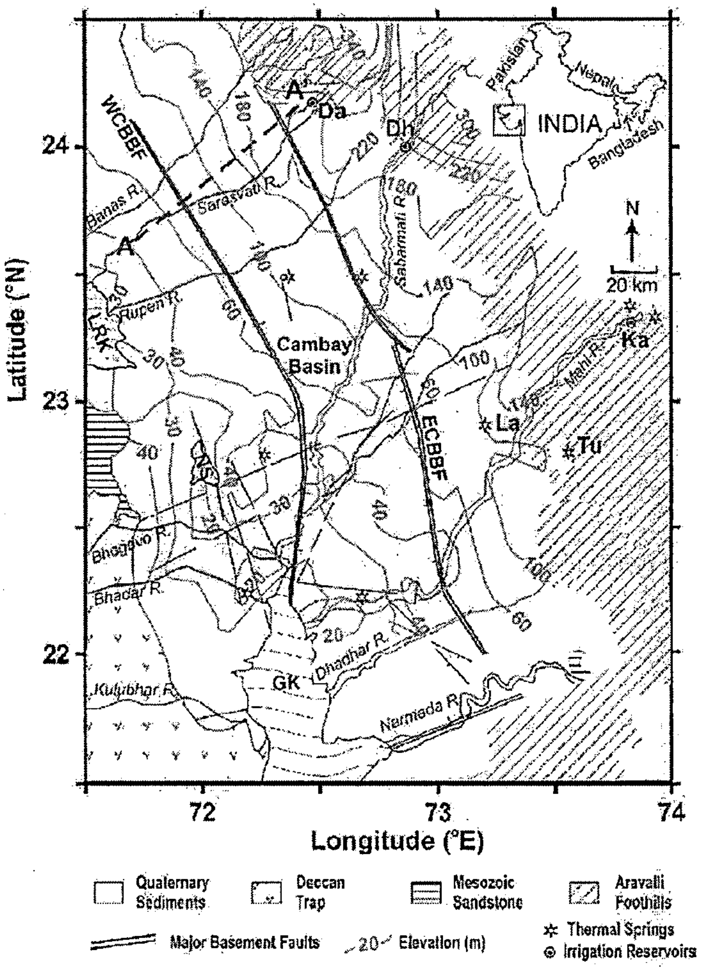

Fig. 1 Map of NGC region showing geological formations, surface elevation (m), drainage pattern and tectonic features. Proterozoic rocks of Delhi super group are exposed in the Aravalli foothills, which is the highest elevation in the study area. The lowest elevations are seen in the tract linking Little Rann of Kachchh, NS and GK. This is also the zone of convergence of rivers originating from Aravallis in the east and Saurashtra in the west. The major faults bounding Cambay Basin, namely, East and West Cambay Basin Boundary Faults (ECBBF and WCBBF) along with sympathetic faults parallel or orthogonal are also shown. A lithological cross section along line AA' is shown in Fig. 2. Acronyms for locations are: *Da* Dantiwada; *Dh* Dharoi; *Ka* Kadana; *La* Lasundra; *Tu* Tuwa

super group from the Aravalli hills in the northeastern part of the study area (Fig. 1). Of these, Banas, Saraswati and Rupen originate from granitic terrain associated with Erinpura and Ambaji granite. In their upper reaches, Sabarmati and its major tributaries traverse across quartzites, phyllites, slates and schists associated with Kumbalgarh, Gogunda, Jharol and Lunawada group of rocks (Merh 1995).

On the west flank of the Cambay Basin, fluvial sediments were also deposited by minor rivers, namely, Bhogavo and Bhadar that traverse the basaltic terrain of the Deccan Trap. Shallow marine sediments were also deposited in the low-lying tract between the Gulf of Khambhat and Little Rann of Kachchh during Late Quaternary. A model of late quaternary deposition related to westward migration of a depositional front caused by marine regression and/or tectonic uplift of the east flank was presented by Prasad et al. (1997), Prasad and Gupta (1999) and Pandarinath et al. (1999a).

From the contours of surface elevation in Fig. 1, it is seen that the low-lying tract linking Gulf of Khambhat and Little Rann of Kachchh has the lowest elevation and forms a zone of convergence wherein both east and west flowing rivers tend to reach.

Due to scanty rainfall (<600 mm a^{-1}), and an ephemeral river system, the entire study area depends heavily on groundwater for its domestic, agriculture and industrial requirements. An acute shortage of water is exacerbated by the inferior water quality in terms of salinity and excessive fluoride.

Experimental

Tubewells and handpumps were purged long enough to flush out the stagnant residual water from the pipes and obtain groundwater samples with in situ chemical composition. In most cases, samples were collected from tubewells that were pumped for several hours prior to sampling. A total of 225 samples were collected and analysed for various parameters. Sample details, including geographical coordinates, groundwater source type, depth below ground level (bgl) along with results of fluoride and EC analyses can be downloaded from (http://www.prl.res.in/%7Ewebprl/web/announce/hydrogeol.pdf)

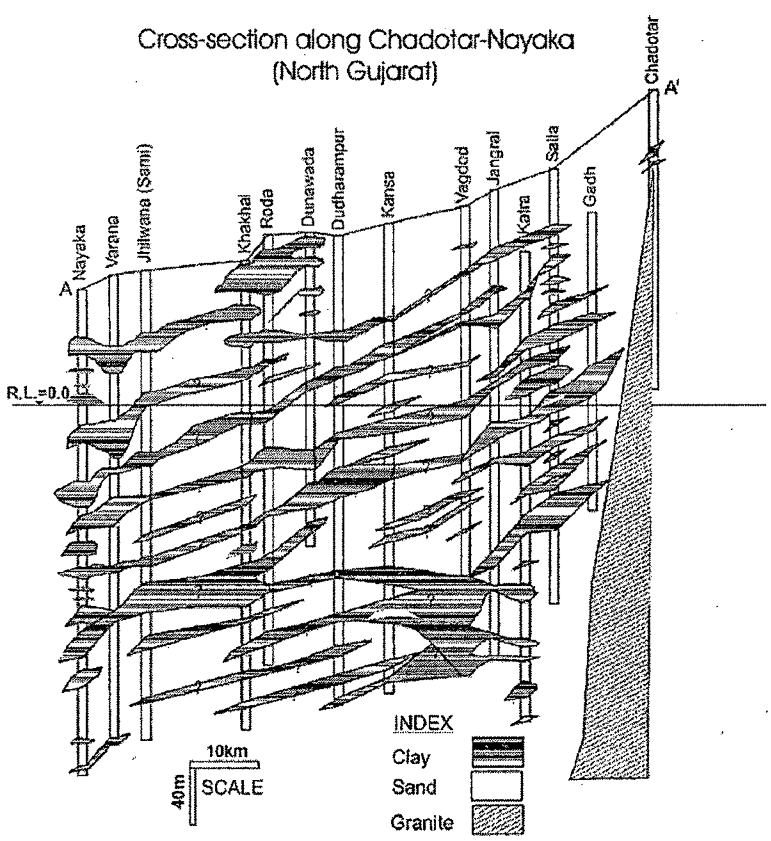

Fig. 2 A typical subsurface litho-section across Cambay Basin along line AA' of Fig. 1. The sandy layers forming sub-aquifers are seen laterally continuous and vertically interspersed with thin semi-permeable clay/silt layers that may not have lateral continuity over a large area. Since the tubewells tap all the horizons that yield water up to their maximum depth, the pumped horizons are treated as forming a single regional aquifer system

The groundwater samples were collected in soda-lime glass bottles after rinsing with the sample water. Sample bottles were immediately sealed using Bromobutyl rubber stoppers and triple aluminium protective caps crimped by a hand-held crimping device. To ensure the integrity of stored water for fluoride addition from the sampling bottles, de-ionised water was stored in several bottles over a period of one year. No measurable fluoride was detected in the stored water.

The standard parameters like temperature, pH, alkalinity, oxidation-reduction potential (ORP) and EC were measured in the field and fluoride concentrations were measured in the laboratory within a few days of the sample collection. Samples were also analysed for their dissolved helium concentration. The results of helium analyses have been separately published (Gupta and Deshpande 2003). Samples were also collected and analysed for radiocarbon dating from some selected wells. These results are being separately reported in detail (Agarwal et al. submitted).

The standard parameters were measured using the μ-processor based water analysis kit (Century: model CMK-731) and fluoride concentrations were measured colorimetrically using 580-nm-tuned colorimeter (Model: Hach) using SPADNS reagent method. The precision of fluoride measurements is <0.1 ppm.

Results

Spatial distribution of fluoride in groundwater from the Cambay Basin area is shown in Fig. 3. It is seen that starting from the 71.5°E, there is a major high fluoride concentration (4–8 ppm) belt (PP') linking LRK-NS-GK roughly in the north–south direction on the west flank of the Cambay Basin. Towards the east, another high fluoride (1.5–4 ppm) belt (QQ') within the Cambay Basin can also be seen. Farther east, there are several small patches with fluoride concentrations greater than 1.5 ppm aligned linearly in a belt (RR') roughly parallel to the Aravallis. Another belt of high fluoride concentration is in E–W direction linking Nalsarovar region to thermal springs of Lasundra (La) and Tuwa (Tu). The fluoride concentrations are high (4–8 ppm) in this belt also.

A plot of fluoride concentration in groundwater samples vs. depth (bgl) of the sampled wells in the NGC region is shown in Fig. 4a. It is seen that in the LRK-NS-GK low lying tract, groundwater at shallow depths indeed have very high fluoride concentrations. Elsewhere in the region, no apparent relationship between the fluoride concentration and depth (bgl) can be discerned. In several cases high fluoride concentrations are found in the shallow dug wells and low fluoride concentrations in deep tubewells and vice versa. This observation is contrary to the conventional understanding that deeper, confined groundwater has high fluoride due to longer residence

DOI 10.1007/s10040-004-0389-2

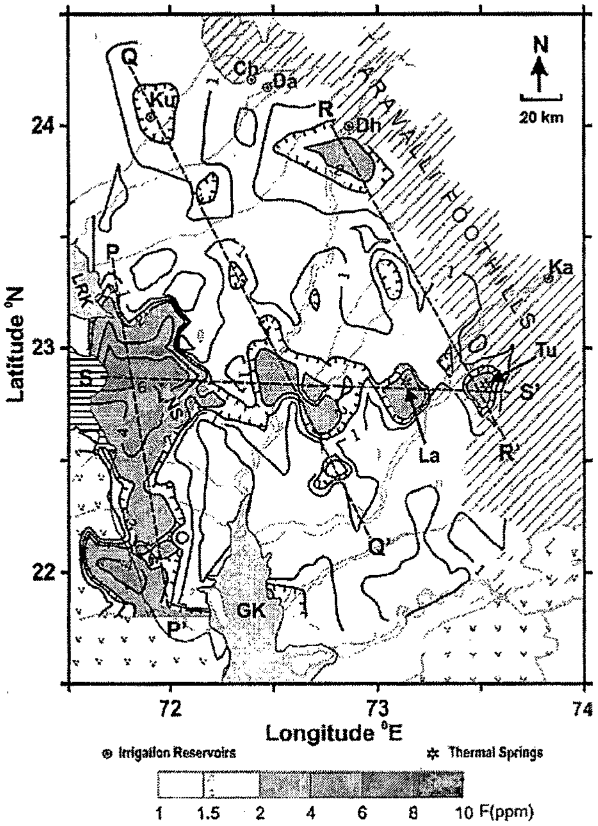

Fig. 3 Contour plot of fluoride concentration in groundwater from NGC region. Patches of high fluoride concentration (>1.5 ppm) appear aligned along four linear belts (PP', QQ', RR', SS') separated by low fluoride areas. Acronyms for locations are: *Ch* Chadotar; *Ku* Kuwarva; *Da* Dantiwada; *Dh* Dharoi; *Ka* Kadana; *La* Lasundra; *Tu* Tuwa

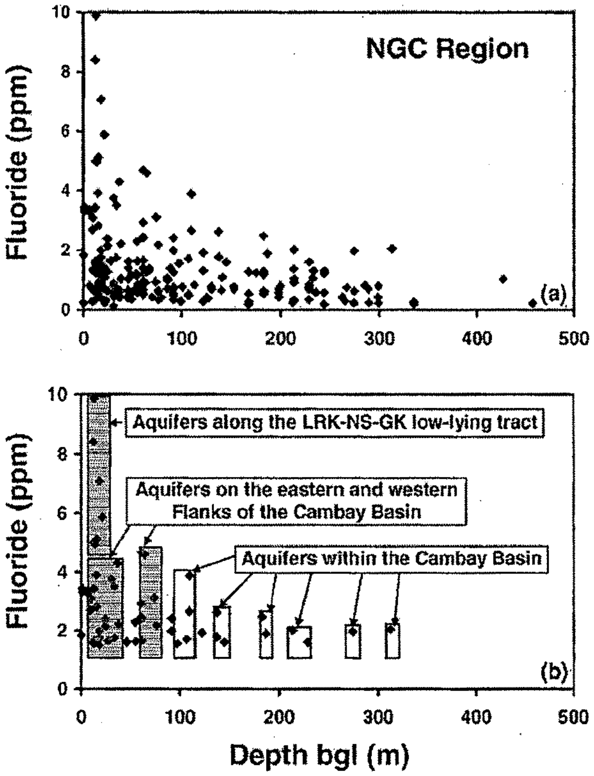

Fig. 4 a Groundwater fluoride concentration versus depth 'bgl' of tubewells in the NGC region. **b** Samples with fluoride concentration <1.5 ppm are filtered out from (*a*). Fluoride rich aquifers can be identified at certain depth zones within Cambay Basin

Table 1 Sub-aquifer zones with depth having excessive fluoride in the Cambay Basin

Zone	Depth range (m)	Zone	Depth range (m)
I	<40	V	180–190
II	50–75	VI	210–230
III	90–110	VII	~275
IV	135–145	VIII	~310

time, hence longer reaction time with the aquifer material to dissolve fluoride (Ramakrishnan 1998). A similar plot, but only for the samples with >1.5 ppm of fluoride from the same dataset, is shown in Fig. 4b. This leads to identification of fluoride rich sub-aquifers with certain depth zones (Table 1) in the Cambay Basin. This follows from Fig. 2, wherein it was shown that by measuring depths bgl, nearly the same sub-aquifer is encountered at different locations within the Cambay Basin.

Most fluoride rich handpumps and tubewells up to the depth of 40 m are located on the west flank of Cambay Basin where aquifers are comprised either of fluvio-marine sediments deposited in the low-lying tract linking LRK-NS-GK or further west in the Mesozoic sandstones. Tubewells shallower than ~40 m and with fluoride concentration <1.5 ppm are mainly located on the east flank of Cambay Basin. Tubewells tapping the depth zones of 53–76 m and yielding groundwater with >1.5 ppm fluoride are located on both east flank and west flank of the Cambay Basin.

All fluoride rich tubewells ranging in depth from 90–300 m are located within the Cambay Basin, limited only to certain depth zones as above. It is hypothesised that if these sub-aquifers are tapped by a particular tubewell, which also taps other sub-aquifers, the fluoride concentration in groundwater exploited from the tubewell is likely to be relatively higher.

To verify this hypothesis, a tubewell (A) in Chadotar village (Ch) and four other tubewells (B, C, D, E) in the vicinity of each other in Kuwarva village (Ku) ~50 km from the village of Chadotar (Fig. 3) were examined for their fluoride content and the depth (bgl) of aquifers tapped (Fig. 5). It is seen that the shallowest (63 m). tubewell-A with fluoride content of 0.9 ppm, taps the fluoride rich zone-II. Tubewell-B taps fluoride rich zones-III and -IV and has the highest fluoride concentration of 2.2 ppm. Tubewell-C taps only one fluoride rich zone-III and its fluoride content is 1.9 ppm. Tubewell-D taps three

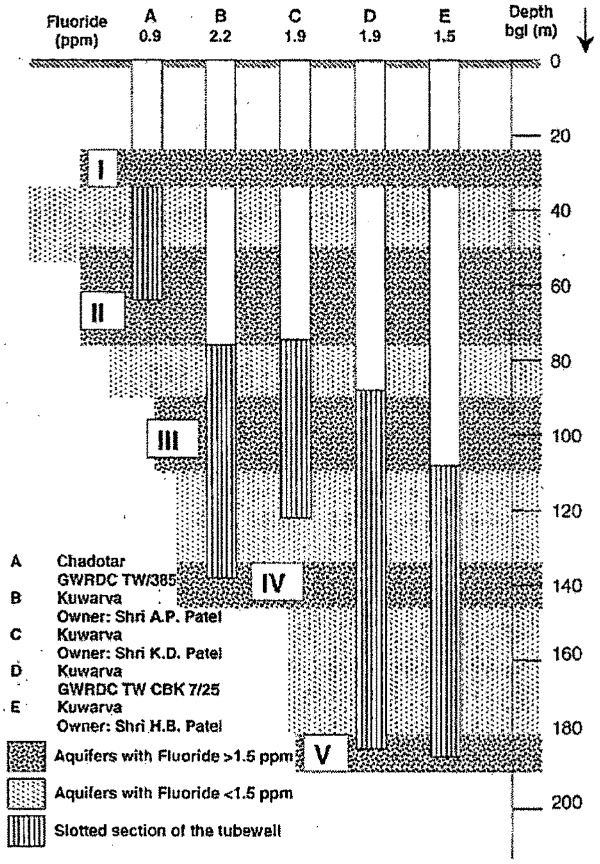

Fig. 5 A comparison of fluoride content of five tubewells with their tapped aquifers. The shallowest tubewell (*A*), taps the fluoride rich Zone II and has the lowest fluoride content. Tubewells *B*, *C* and *D* tap fluoride rich Zone III and have higher fluoride content of ~2 ppm. The deepest tubewell *E*, which taps aquifers from depth zones *IV* and *V*, has comparatively lower fluoride content of 1.5 ppm. It is seen that among these high fluoride zones highest fluoride is contributed by zone *III*

fluoride rich zones (III, IV and V) and fluoride concentration of groundwater from it is 1.9 ppm. Tubewell-E is the deepest tubewell (185 m) and taps only two fluoride rich zones (IV and V). Its fluoride content is 1.5 ppm. It is seen that depth zones-III and -IV provide maximum fluoride input to the water pumped from the concerned tubewells. Depth zone-V has relatively low fluoride content and acts as a diluter in case of tubewells-D and -E.

A contour map of EC of groundwater samples is shown in Fig. 6. The EC values range from 0.3–8 mS, with values >5 mS in the LRK-NS-GK belt and lowest values in isolated pockets along the Aravalli foothills. In general, the areas with high EC overlap with the areas having high fluoride concentrations (Fig. 2). However, a patch of >3 mS in the NW corner of the study area has lower fluoride concentration. Another patch of ~1 mS around 24°N along the Aravalli foothills on the other hand has high fluoride concentration. In spite of these differences, it can be seen from Fig. 6 that high EC regions are approximately aligned along the same linear belts PP', QQ', RR', SS' showing high fluoride concentrations. The central (QQ') belt of both high fluoride concentration and EC is flanked on either side by belts of relatively low values. This is also seen in Fig. 7 that shows variation in both EC and Fluoride concentrations along four lines (lines 1–3 approximately NE–SW and SS' approximately E–W). Some westward displacement of the high EC region along line-3 is also noticed.

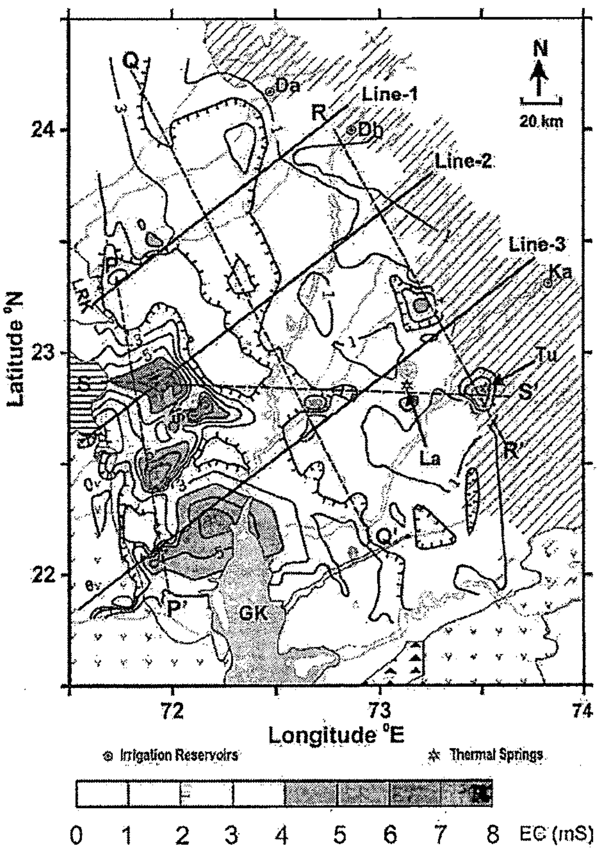

Fig. 6 Contour plot of EC of groundwater from NGC region. Areas of high EC overlap in general with areas of high fluoride shown in Fig. 3. Acronyms for locations are: *Da* Dantiwada; *Dh* Dharoi; *Ka* Kadana; *La* Lasundra; *Tu* Tuwa

A contour plot of radiocarbon ages from Agarwal et al. (personal communication) is reproduced in Fig. 8. The radiocarbon ages are based on total dissolved carbonate precipitated from groundwater pumped from all the sub-aquifers tapped by the sampled tubewells. These, therefore represent the composite ages of groundwater in the regional aquifer system. The groundwater ages are seen to progressively increase in a W-SW direction from a recharge zone in the Aravalli foothills. This implies that the composite residence time of groundwater increases progressively in a W-SW direction.

DOI 10.1007/s10040-004-0389-2

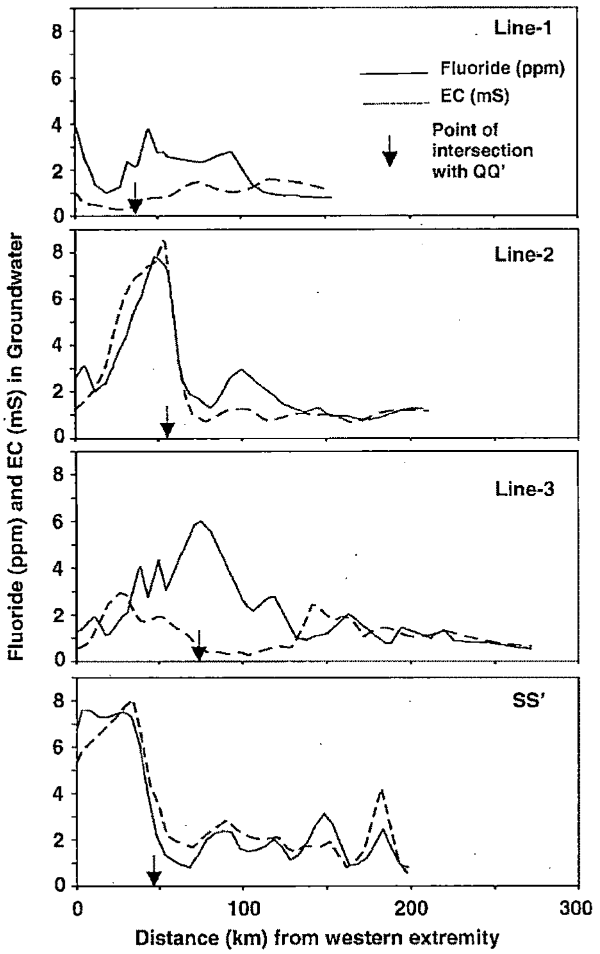

Fig. 7 Variation of fluoride and EC of groundwater along four lines shown in Fig. 6. The distances are from the western extremity of each line and the position of intersection with QQ' is marked by an *arrow*

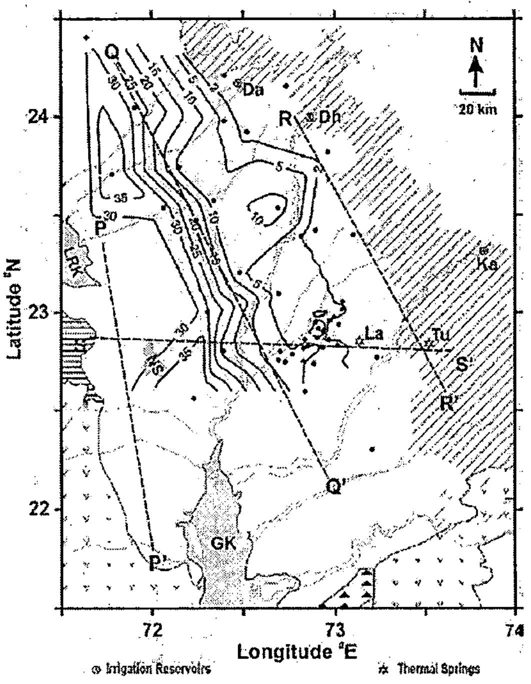

Fig. 8 Contour plot of radiocarbon ages of groundwater in the regional aquifer system from NGC region (reproduced from Agarwal et al., personal communication). The ages are seen to progressively increase away from the recharge zone in Aravalli foothills. The age of the high Fluoride, high EC groundwater belt QQ' is ~20 ka, i.e., around LGM. This is identified as the arid climatic phase in the study area. Acronyms for locations are: *Da* Dantiwada; *Dh* Dharoi; *Ka* Kadana; *La* Lasundra; *Tu* Tuwa

Discussion

From the global map of endemic fluorosis available at UNICEF website (http://www.unicef.org/programme/wes/info/fl_map.gif) it is seen that most of the affected regions have an arid to semiarid climate. Within India, fluoride rich groundwaters are found in the dry parts, especially Rajasthan, Gujarat and interior parts of the southern peninsula characterised by episodic rainfall separated by extended dry periods (Agrawal et al. 1997; Vasavada 1998; Jacks et al. 1993). Fluoride poisoning is also reported from the dry climatic regime (Yong and Hua 1991) in North China.

Although aridity of climate in general seems to be the primary reason for the origin of high fluoride globally, several processes, namely, dissolution of fluoride bearing minerals, ion exchange and evaporative concentration can locally account for high fluoride concentration in groundwater. With this in mind, occurrence of high fluoride in the following three sub-regions of the study area was examined.

1. West flank of Cambay Basin in the low-lying tract
2. East flank of Cambay Basin
3. The Cambay Basin

Groundwaters in the low-lying LRK-NS-GK tract have >5 ppm fluoride (Fig. 3) at a shallow depth of up to 15 m. This area is relatively flat, receives low rainfall (~500 mm a^{-1}) and is the zone of convergence of surface gradients wherein surface flow both from Aravallis (in the NE) and Saurashtra (in the West) accumulates. These factors lead to evaporative enrichment of fluoride and other salts along this tract. The deeper confined aquifers in this belt are at the farthest end of the regional aquifer system of Late Quaternary origin (Prasad and Gupta 1999) and do not necessarily have high fluoride or EC. In terms of fluoride distribution these exhibit similar characteristics as sub-aquifers in the Cambay Basin as described later.

Groundwaters on the east flank of Cambay Basin, in general, have lower fluoride concentrations. However, there are patches of fluoride concentration >1.5 ppm located along the rock-alluvium contact zone (RR') in the Aravalli foothills (Fig. 3). This sub-region, forming a recharge area of the regional aquifer system in the NGC, receives fresh rainwater annually. The presence of high fluoride (with low EC) patches in this sub-region, therefore, suggests preferential dissolution of fluoride bearing minerals. The proterozoic rocks of the Kumbhalgarh group, Ambaji Granites and Gneisses of Delhi super group, Lunawada group and Godhra granite are exposed in the vicinity of the high fluoride-bearing groundwater patches. These rocks are characterized by mineralogical assemblages of quartz, K-feldspar, plagioclase, biotite, amphiboles, fluorite and apatite (Choudhary 1984). These granites are invaded by dykes of pegmatite and also xenoliths of amphibolite. Both pegmatites and amphibolites have high concentrations of fluoride. It is likely that these rocks could be providing higher fluoride to groundwater during weathering. Koritnig (1951) suggested that fluoride is leached in the initial stages of weathering of granite massifs. Deshmukh et al. (1995) suggested that fluoride is particularly leached out rapidly from micas. Preferential dissolution of fluoride can, however, explain high fluoride patches only in the Aravalli foothills and not within the Cambay Basin wherein sediments eroded from diverse rock types in Aravalli have been transported and deposited by several rivers (Prasad et al. 1997).

With the general understanding that groundwater in deeper aquifers contains relatively long resident water; confinement of high fluoride concentrations to certain sub-aquifer zones (Figs. 3, 4b and 5) within the Cambay Basin implies that the contact time of groundwater with the aquifer material is not the principal factor governing the origin of high fluoride in the Cambay Basin. This is also supported by the results of radiocarbon dating of groundwater samples from this region. As seen in Fig. 8, groundwater radiocarbon ages increase progressively in the W-SW direction away from the recharge area in the Aravalli foothills. If the fluoride dissolution were proportional to groundwater residence time, the alternation of high and low fluoride concentration belts as seen in Fig. 3 can not be explained.

Another hypothesis involved leakage of fluoride rich pore water from the intervening clay rich aquitard layers induced by excessive exploitation of groundwater and a resultant decrease in piezometric level. This was examined by comparing the geographical distribution of high fluoride regions with regions of high groundwater withdrawal. It was found that the two do not overlap. The high groundwater withdrawal areas were actually found to overlap the low fluoride concentration areas, i.e., between PP' and QQ', and QQ' and RR'. Roughly, these are also areas of the highest decline in piezometric level during the last few decades. This ruled out leakage of fluoride rich pore-fluid from clay rich horizons as a primary source of high fluoride concentration in the Cambay Basin.

It is thus seen that the various hypothesis on the origin of fluoride—long residence time of groundwater, sediments containing fluoride bearing minerals in the aquifer material and leakage of fluoride from clay rich aquitard horizons in response to excessive pumping—cannot explain the observed geographical distribution of fluoride in the Cambay Basin.

It can be seen by comparing Figs. 3 and 8 that the central belt of high fluoride concentration within Cambay Basin corresponds to a groundwater age of ~20 ka which is globally know to be the maxima of the last glacial period and an arid period in the climatic history of the study area. Prasad and Gupta (1999) have reported the presence of a thick gypsum layer dated by interpolation in luminescence ages to be ~20–30 ka in the Nalsarovar core, which represents periods of extreme aridity. Based on the crystallinity index of illite, Pandarinath et al. (1999b) have also indicated aridity for this layer. Regional evidences of aridity have also been reported in the form of dune building activity which began ~20 ka in N. Gujarat (Wasson et al. 1983). The evidence of increased aridity ~20 ka and the dating of the high fluoride/high EC belt QQ' to this period suggest that the dated groundwater was recharged during a relatively arid climatic phase and has since moved to its present location through subsurface transport.

In the following, combining the explanations given for the three sub regions of the study area, a general hydrologic model to explain the high fluoride concentration (>1.5 ppm) in groundwater of the NGC region is presented. In this model general aridity of the region together with presence of granitic rocks with pegmatites, amphibolites and other minerals susceptible to preferential dissolution of fluoride in the Aravalli Hill ranges and/or sediments derived there from make the region naturally prone to increased fluoride concentration in groundwater. Superposed on to this general hydrologic model, local imprints of increased/decreased aridity and/or other applicable factors can be seen.

During the arid regime, the dry deposition of dust is also expected to increase. The normal fluoride content in the atmospheric air is reported between 0.01–0.4 $\mu g/m^3$ (Bowen 1966). Average fluoride content of precipitation varies from almost nil to 0.089 mg/L (Sugawara 1967). However, fortnightly accumulated precipitation samples from selected irrigation reservoirs (Fig. 3) during the early part (June) of the 1999 rainy season, showed a fluoride content of 0.90 ppm at Dantiwada (Da), 0.60 ppm at Dharoi (Dh) in North Gujarat, 0.34 ppm at Kadana (Ka) in East Gujarat, 0.35 ppm at Bhadar (21.08^{0}N; 70.77^{0}E) in Saurashtra, and 0.26 ppm at Ukai (21.29^{0}N; 72.65^{0}E) in South Gujarat. The latter two locations are just outside the study area shown in Fig. 3. These values of fluoride in local precipitation matched the general trend of decreasing aridity from Dantiwada to Ukai. Although average fluoride concentration in seasonal precipitation at these locations was ~ 0.1 ppm, high values in June precipitation suggest significant input of fluoride along with the dust. This further suggests that during an arid climate with an intense wind regime, dry precipitation can be a significant source of salts including fluoride. Coupled with high evaporation, both fluoride and EC will tend to be high in the groundwater recharged in the naturally fluoride prone region such as the NGC. This is manifested in the form of a high fluoride and EC in the LRK-NS-GK belt on the west flank of the Cambay Basin, where not only is the rainfall lowest (~500 mm a^{-1}), but due to it's being a regional depression, the runoff from surrounding regions accumulates, evaporates and contributes to shallow groundwater. Corollary to this is that relatively lower aridity on the east flank (rainfall ~900 mm a^{-1}) together with low surface retention time due to high ground slope results in lower EC and fluoride in groundwater except where pockets of fluoride rich rocks exist locally and/or thermal waters are vented. In such regions there will be little correspondence between EC and fluoride concentrations. The aquifers in the main Cambay Basin are largely confined with recharge area in the foothills of Aravallies. These aquifers receive little direct recharge locally except in the recharge area. But, groundwater in these aquifers will reflect the fluoride and EC in the recharged groundwater of the past at different distances from the recharge area. Relatively high EC and fluoride concentrations will be seen in groundwater recharged in relatively arid climatic phases and low EC and fluoride in relatively wet phases. This is actually observed in the Cambay Basin where groundwater recharged in an arid phase ~ 20 ka shows high EC and fluoride concentration (along QQ'). The low fluoride and EC areas on either side represent groundwater recharged during preceding and succeeding wetter phases.

The east–west belt SS' approximately linking the Nalsarovar on west flank with thermal springs (~60 °C) of Lasundra (La) and Tuwa (Tu) on the east flank also showed both high fluoride and EC (Figs. 3, 4). This is possibly due to increased rock-water interaction at elevated temperature (Chandrasekharam and Antu 1995) and/or scavenging from the larger volume during hydrothermal circulation (Minissale et al. 2000; Gupta and Deshpande 2003). Since Nalsarovar is the lowest elevation, it is possible that a constant venting of thermal fluids with high EC and fluoride have always been contributed to the groundwater flow streams linking Lasundra and Tuwa in the recharge area to Nalsarovar. This continuous venting of thermal fluids is superposed on the palaeocilmatic effects to give the SS' belt of high fluoride and EC.

The observation that in Cambay Basin, only certain sub-aquifer zones have high fluoride concentrations still must be explained (Figs. 4b and 5). It is possible to speculate that these layers represent small variations in the sediment mineralogy deposited at different times during the Late Quaternary during which the entire region was receiving sediments from the east and evolving (Prasad and Gupta 1999).

Summary and conclusions

Geographical distribution of fluoride in groundwaters of the Cambay region is presented. Areas with high fluoride have been identified and possible causes of excessive fluoride have been investigated. From the contour map of fluoride (Fig. 3), it is seen that patches of fluoride concentration (>1.5 ppm) are aligned along certain linear belts (PP', QQ', RR', SS'). The areas with high fluoride content in groundwater in general overlap areas of high EC (Fig. 6), although all patches of high fluoride along the Aravalli foothills (RR') are not overlapped by high EC. These are explained by preferential dissolution of fluoride bearing minerals from certain rocks in the Aravallis.

The low lying LRK-NS-GK belt has the highest fluoride concentrations in the study area due to high evaporation of stagnant water converging from both the Saurashtra in the west and Aravallis in the east. Within the Cambay Basin, there are certain depth zones where sub-aquifers contain groundwater with high fluoride (Fig. 4). It is shown that tapping of such aquifers results in groundwater with higher fluoride content (Fig. 5).

It is shown that low fluoride and EC areas separate the high fluoride and EC belts running parallel to the Aravalli foothills. A groundwater radiocarbon age of (~20 ka) for the central (QQ') high fluoride and EC belt is indicated. This suggests the groundwater corresponding to this belt may have been recharged during the global climatic phase of last glacial maxima (LGM). Earlier studies have indicated that this was an arid phase (compared to the present) in this part of the world. Taking a cue from the present day distribution of high fluoride in the arid regions, the high fluoride and EC of water in the Cambay Basin have been hypothesised to have originated during the past climatically arid phases.

In this model, the general aridity of the region together with presence of granitic rocks with pegmatites, amphibolites and other fluoride bearing minerals, susceptible to preferential dissolution (and their sedimentary derivatives), make the region naturally prone to increased fluoride concentrations in groundwater. As a result, enhanced groundwater fluoride concentrations are seen in shallow, relatively young ground waters, in more arid parts and/or those parts of the region where specific local factors such as accumulation and evaporative enrichment of runoff, presence of fluoride bearing minerals and hydrothermal influx operate. In deeper confined aquifers enhanced fluoride is observed where ground waters recharged during past periods of enhanced aridity ~20 ka (last glacial maxima) are being exploited. There may have been other minor periods of aridity but their signatures appear to have been obliterated by dispersion and mixing during regional groundwater flow.

The westward flowing groundwater acquired its fluoride content from the prevailing fluoride content in the recharge area in the past and the model shows the influence of varying past aridity/wet conditions at the time of recharge. The confinement of high fluoride concentrations in specific sub-aquifer intervals within Cambay Basin as shown in Figs. 4b and 5, though apparently convincing, has been verified only in a small area around Chadotar and Kuwarva (Fig. 5). Given the uncertainty in regionally correlating the sub-aquifer zones and the fact that the entire region has evolved during Late Quaternary through sediments from the east, the observed confinement is explained within the above general hydrologic model as due to variations in the sediment mineralogy (including clay content) deposited at different times during Late Quaternary.

The enhanced EC and fluoride concentrations in the groundwater flow streams linking thermal springs of Lasundra and Tuwa in the recharge area to the Nalsarovar along the SS' belt, are explained as due to superposition on the above general hydrologic model of the constant venting of thermal fluids into the groundwater of the flow stream.

This study has indicated that exploitation of deeper groundwater per se is not responsible for origin of high fluoride concentration in groundwater of the NGC region. Although, the problem of high fluoride cropped up within the last few decades, its origin involved prevalence of a more arid climate approximately 20 ka before present, a period globally known as the last glacial maxima. Apparently recent appearance of high fluoride in groundwater in parts of the study area is linked to recent exploitation of groundwater recharged during the past arid climatic phases. This study has helped in identifying certain fluoride rich sub-aquifer zones and the geographical area where they exist, indicating thereby that if during construction of tubewells, these zones are sealed, it should be possible to avoid high fluoride groundwater.

Acknowledgement This study forms a part of a research project entitled "Estimation of Natural and Artificial Groundwater Recharge Using Environmental, Chemical and Isotopic Tracers and Development of Mathematical Models of Regional Aquifer Systems in North Gujarat". We thank Gujarat Water Resources Development Corporation Ltd., Gandhinagar (GWRDC) for sponsoring this project and sharing important dataset of elevation and groundwater withdrawal for NGC region. Several colleagues from PRL have helped us in this study. Dr. M. G. Yadava provided the radiocarbon ages for groundwater samples. Mrs. Vasanti Somayajulu analysed the fluoride concentration and EC of groundwater samples. Their contribution is acknowledged with thanks. Mr. M.H Patel helped in field and various laboratory operations.

References

Agrawal V, Vaish AK, Vaish P (1997) Groundwater quality: focus on fluoride and fluorosis in Rajasthan. Curr Sci 73(9):743–746

BIS (1990) Drinking water specifications, IS:10500. Bureau of Indian Standards, New Delhi

Bowen HJM (1966) Trace elements in biochemistry. Academic Press, New York

Chandrasekharam D, Antu MC (1995) Geochemistry of Tattapani thermal springs, Madhyapradesh, India: field and experimental investigations. Geothermics 24(4):553–559

Choudhary AK (1984) Pre-Cambrian geochronology of Rajasthan, western India. PhD Thesis, Physical Research Laboratory, Ahmedabad, India

Deshmukh AN, Wadaskar PM, Malpe DB (1995) Fluorine in environment: a review. Gondwana Geol Mag 9:1–20

Gupta SK, Deshpande, RD (1998) Depleting groundwater levels and increasing fluoride concentration in villages of Mehsana District, Gujarat, India: cost to economy and health. Water Resources Research Foundation (WRRF), PRL, Ahmedabad, 74 pp

Gupta SK, Deshpande RD (2003) Origin of groundwater helium and temperature anomalies in the Cambay region of Gujarat, India. Chem Geol 198:33–46

Handa BK (1975) Geochemistry and genesis of fluoride containing groundwaters in India. Ground Water 13:275–281

Jacks G, Rajagopalan K, Alveteg T, Jonsson M (1993) Genesis of high F groundwaters, southern India. Appl Geochem 2:241–244

Koritnig S (1951) Ein Beitrag zur Geochemie des Fluor (A contribution to the geochemisty of fluorine). Geochim Cosmochim Acta 1:89

Merh SS (1995) Geology of Gujarat. Geol Soc India, Bangaore, 220 pp

Minissale A, Vaselli O, Chandrasekharam D, Magro G, Tassi F, Casiglia A (2000) Origin and evolution of 'intracratonic' thermal fluids from central-western peninsular India. Earth Planet Sci Lett 181:377–397

Pandarinath K, Prasad S, Deshpande RD, Gupta SK (1999a) Late Quaternary sediments from Nal Sarovar, Gujarat, India: distribution and provenance. Earth Planet Sci 108(2):107–116

Pandarinath K, Prasad S, Gupta SK (1999b) A 75 ka record of Palaeoclimatic changes inferred from crystallinity of Illite from Nal Sarovar, western India. J Geol Soc India 54:515–522

Prasad S, Kusumgar S, Gupta SK (1997) A mid-late Holocene record of palaeoclimatic changes from Nal Sarovar: a palaeodesert margin lake in western India. J Quat Sci 12:153–159

Prasad S, Gupta SK (1999) Role of eustasy, climate and tectonics in late Quaternary evolution of Nal-Cambay region, NW India. Z Geomorph N F 43:483–504

Ramakrishnan S (1998) Groundwater. Ramakrishnan, Chennai 761 pp

Sugawara K (1967) Migration of elements through phases of the hydrosphere and atmosphere. In: AP Vinogradov (ed) Chemistry of the earth's crust, vol 2, Israel Program for Scientific Translations, Jerusalem, 501 pp

Vasavada BJ (1998) Excessive fluoride in Gujarat. a perspective plan of solution. J Indian Water Works Assoc 1998:191–198

Wasson RJ, Rajguru SN, Misra VN, Agrawal DP, Dhir RP, Singhvi AK (1983) Geomorphology, Late Quaternary stratigraphy and palaeoclimatology of the Thar dune field. Z Geomorph NF 45:117–151

WHO (1970) Fluorides and human health. World Health Organisation, Geneva

WHO (1984) Fluorine and fluorides. Environmental health Criteria 36, World Health Organisation, Geneva

Yong L, Hua ZW (1991) Environmental characteristics of regional groundwater in relation to fluoride poisoning in North China. Environ Geol Water Sci 18:3–10

DOI 10.1007/s10040-004-0389-2

ELSEVIER

Chemical Geology 198 (2003) 33–46

CHEMICAL
GEOLOGY
INCLUDING
ISOTOPE GEOSCIENCE

www.elsevier.com/locate/chemgeo

Origin of groundwater helium and temperature anomalies in the Cambay region of Gujarat, India

S.K. Gupta*, R.D. Deshpande

Earth Science Division, Physical Research Laboratory, Post Box No. 4218, Navrangpura, Ahmedabad 380 009, India

Received 12 March 2002; accepted 13 November 2002

Abstract

A survey of natural helium in soil-gas and groundwater was undertaken in the Cambay region of Gujarat, India. The Cambay basin, known for high heat flow, is a graben characterised by NNW–SSE trending major fault system and successive down faulting along sympathetic faults parallel to major trendline and orthogonal faults cutting across. Several wells indicated higher than atmospheric equilibration concentration of helium, referred to as anomalous helium concentration. These wells generally had high groundwater temperature and appear to be located along basement faults in the study area, particularly on both eastern and western flanks of the Cambay basin.

Groundwater helium anomalies are explained through a conceptual model as originating largely from within the crystalline basement, through radioactive decay in the form of plumes localised by the major faults and fractures. Groundwater temperature anomalies originate due to setting up of a shallow (~ 1–2 km) depth convective circulation, again along major faults and fractures, which facilitate both upward and downward migration of groundwater. The sedimentary cover acts as a dispersive medium. Therefore, no significant helium anomalies are seen within the Cambay graben that has more than 3-km-thick sedimentary cover. It is thus seen that even though helium and groundwater have different origins, the faults and fractures in the crust can associate anomalous concentrations of helium and groundwater temperatures along themselves in a longitudinally distributed manner by providing preferred pathways for migration of helium and by facilitating establishment of convective hydrothermal circulation of groundwater.

Keywords: Groundwater; Soil-gas; Helium anomalies; Groundwater temperature; Hydrothermal circulation; Cambay basin; Gujarat; India

1. Introduction

Following the Bhuj earthquake of January 26, 2001, there has been a renewed interest in identifying active faults in western India. Most of the recent work in this direction is based on re-evaluation of seismic data combined with remote sensing and geomorphological investigations of a few selected localities. These studies in the state of Gujarat have delineated four major linear tectonic structures (Fig. 1) that converge in this region: the 'Kachchh rift zone', the 'Cambay tectonic zone', the 'Narmada Tapti tectonic zone' and the 'Kukdi–Ghod lineament zone' (Misra, 2001). Earlier, Burke and Dewey (1973) had identified the region of this convergence as a 'triple junction' comprising of the 'Cambay graben' (CG),

---

* Corresponding author. Tel.: +91-79-6302129; fax: +91-79-6301502.

E-mail address: skgupta@prl.ernet.in (S.K. Gupta).

doi:10.1016/S0009-2541(02)00422-9

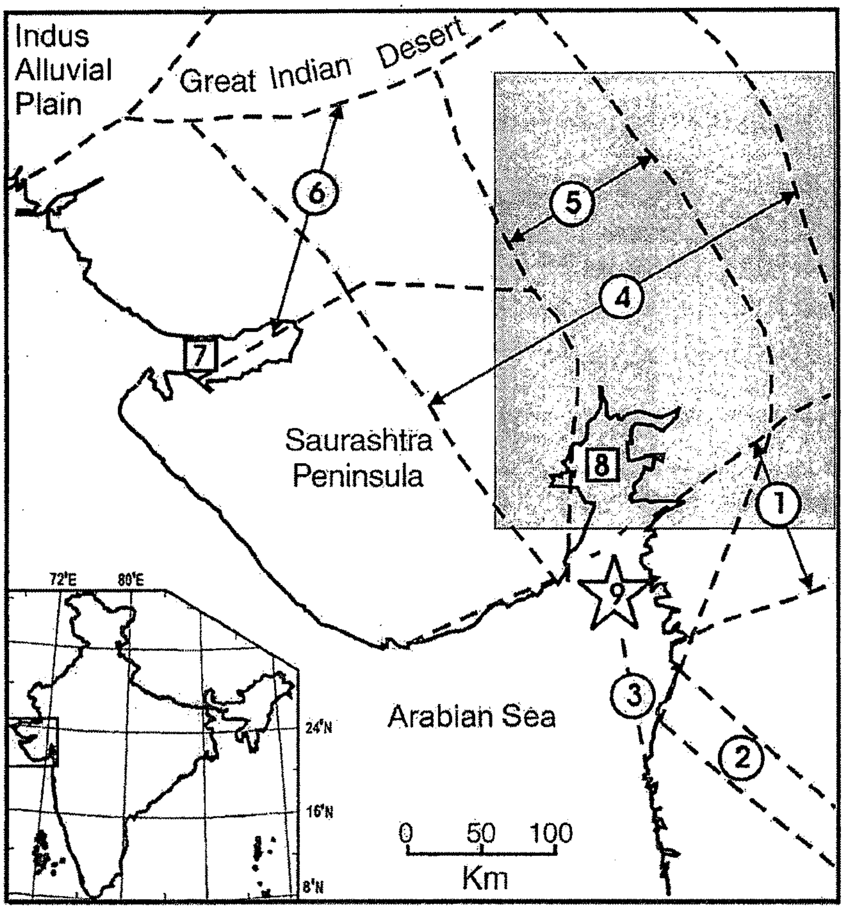

Fig. 1. Tectonic framework of the Gujarat State in western India showing major linear tectonic structures based on Burke and Dewey (1973), Biswas (1987) and Misra (1981, 2001). The names of various structural elements are as follows: (1) Narmada Tapti tectonic zone; (2) Kukdi–Ghod lineament zone; (3) West Coast fault; (4) Cambay structure; (5) Cambay graben; (6) Kachchh rift; (7) Gulf of Kachchh; (8) Gulf of Khambhat; and (9) triple junction of 1, 2 and 5. The study area is marked in grey shade.

the 'Narmada Tapti (NT) rift system' and the 'West Coast (WC) fault' in the Gulf of Cambay (also known as Gulf of Khambhat). Repeated block faulting along these tectonic structures has broken the lithosphere into several blocks separated by major or minor faults running parallel and orthogonal to each other. The intersecting network of faults has given rise to such a tectonic configuration that movement of any lithospheric block along a particular fault is propagated along other faults. Many of these faults and fissures within these major structures seem to extend to the lower lithosphere (Ravi Shankar, 1991; 1995) and several hot springs lie along them indicating hydrothermal circulation. It has long been recognised (Golubev et al., 1975; Dikum et al., 1975) that helium and radon produced by radioactive decay of U and Th in rocks and minerals get liberated during convective circulation, rock dilation and fracturing. Since the Cambay region is known to be tectonically active, anomalously high amounts of these gases may be escaping the crust from above the active faults.

The gases, before escaping to the atmosphere, must pass through the omnipresent groundwater zone. Hence, a survey of helium and radon in groundwater can potentially help to identify regions of active fault zones, hydrothermal circulation and fluid transfer through the crust, in addition to zones of radioactive mineral accumulation. Because of its short half-life (3.84 days), radon may not be so useful in identifying deep structures. Helium, on the other hand, through its characteristic of having higher isotopic ratio of $^3He/^4He$ in mantle fluids ($\sim 10^{-6}$) in comparison to $< 10^{-7}$ in crust, can also help to identify regions of mantle fluid transfer.

With the above perspective, a programme of groundwater and soil-gas helium survey in parts of the Cambay basin was initiated. Results of this investigation are presented in this paper.

As part of the investigations, a simple standardised procedure was also developed for sample collection, storage and measurement of helium concentrations in soil-gas and groundwater samples using commercially available helium leak detector.

2. Sample collection procedure

2.1. Soil-gas samples

Soil-gas samples are collected from 1 m below the ground level. A 1.2-m-long copper tube ($\Phi = 5$ mm) with 15-cm-long perforated wall at its lower end is inserted into the soil. The ground near the upper end of the copper tube is then hammered and watered to effectively seal the hole from direct contact with atmosphere. The upper end of the copper tube is connected to a hand-operated suction pump by a Tygon tube. The pump is operated sufficiently long to ensure removal of atmosphere/soil-gas mixture from the copper tube and the surrounding soil-gas. The upper end of Tygon tube is then closed using a three-way stopcock for accumulating soil-gas inside the tubes. After about 12 h, the hypodermic needle fitted to the third end of the stopcock is made to pierce the rubber stopper of a 1.2-l pre-evacuated soda-lime glass bottle for soil-gas sample collection. Withdrawal of the hypodermic needle from rubber stopper effectively seals the soil-gas sample.

2.2. Groundwater samples

Groundwater samples are collected directly from the pump outlet (that has been pumping for some time prior to sampling) using PVC tubing ($\Phi = 8$ mm) to divert the water flow and to transfer the same to the bottom of a 1.2-l soda-lime glass sample bottle. After allowing the sample bottle to overflow for a while and when no bubbles are visually seen, the PVC tube is withdrawn and the sample volume is reduced to a premarked position leaving 98 ml of air in the bottle above water surface. The bottle is then sealed within few seconds with rubber stopper and triple aluminium protection cap using hand-operated crimping tool. Wherever pumping facility does not exist (e.g. a dug well), the sample is collected by immersing an inverted (mouth at lower end) empty 2-l glass bottle inside the water with the help of a rope and weight attached to it. After the bottle reaches the required sampling depth, it is reverted for water sampling. The collected sample is then transferred to a 1.2-l soda-lime bottle and sealed as above. The bottles with water sample are stored in inverted position to minimise any loss of helium from the stopper. The air in the bottle is equilibrated with water by shaking for sometime before measurement of helium concentration following the procedure outlined subsequently.

3. Sample storage

Helium permeates readily through many materials, and for this reason, it is important to carefully choose the containers in which the soil-gas and groundwater samples intended for later helium analysis are to be stored. The optimal material for such containers is oxygen-free high conductivity (OFHC) copper tubing in which samples for helium analyses are sealed by crimping at either ends (Craig and Lupton, 1976; Lupton et al., 1977). Gupta et al. (1990) showed that loss of dissolved helium from thick-walled soda-lime glass bottles with conventional laboratory rubber stopper was less than 3% during a storage period of 24 h. This storage method, however, is not suited for soil-gas and for equilibration measurement techniques of helium. Therefore, thick (3 mm)-walled soda-lime glass bottles with bromobutyl synthetic rubber stopper manufactured according to guidelines of U.S. Pharmacopoeia standard II (USP Std-II) and secured by additional triple aluminium cap fixed by hand-held crimping tool in the field are used for sample collection and storage. The synthetic rubber stopper is easily pierced by hypodermic needle and seals effectively when the needle is withdrawn. Each bottle used for sampling is pre-checked for vacuum retention by evacuating the same and measuring air pressure inside after 10 days. Bottles showing pressure >2 Torr are

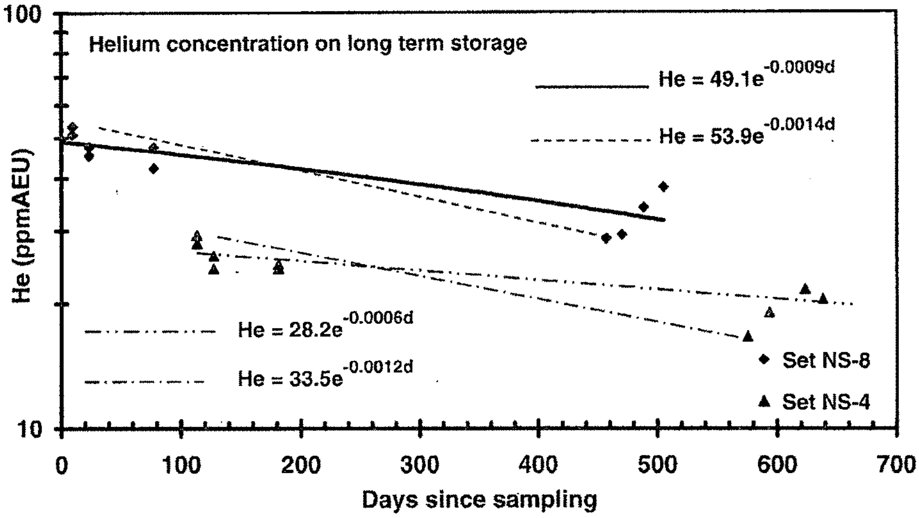

Fig. 2. Residual helium concentrations on long-term storage in soda-lime glass sampling bottles with bromobutyl rubber stopper and triple aluminium protection seal. Two separate sets of multiple samples were collected from two different sources. Individual samples were analysed subsequently at different times up to 20 months after the collection. The maximum observed loss of helium is given by the steepest line on this log-linear plot which corresponds to a loss of $<0.15\%$ per day. The average loss obtained by averaging the rates from the two best-fit lines is, however, 0.075% per day.

rejected. To test the preservation of samples against leakage and diffusion of helium, two sets of 10 water samples each were simultaneously collected from the same source following the procedure described previously. Helium concentrations in these sets of sample bottles were measured over a period of 20 months. The measured concentrations are then plotted on a log-linear plot (Fig. 2). It is assumed that the loss during storage is a first-order process, like radioactive decay, depending on the concentration. The slope of the steepest line through any particular set of data points corresponds to the highest loss rate and the best-fit line corresponds to the average loss rate. It is seen from Fig. 2 that the maximum loss of helium during storage is given by the line ($\mathrm{He}=53.94\mathrm{e}^{-0.0014\ \mathrm{day}}$ for NS-8). Applying the concept of half life; a value of 495 days is obtained corresponding to 50% loss using this equation. This corresponds to a loss of $<0.15\%$ per day.

4. Measurement procedure

A helium leak detector (ALCATEL Model ASM 100 HDS) comprising of a tuned mass spectrometer for helium ions ($m/e=4$) was used for helium measurements by connecting an inlet port to its sniffer probe. This system is in many ways similar to the one used by Friedman and Denton (1975) and Reimer (1984). Equilibrated air samples (Fig. 3a) are drawn from the head space of the bottles by piercing their rubber seal using a 20-ml syringe (Syringe-1). As the sample is drawn, an equal amount of air from another syringe (Syringe-2) enters the bottle and mixes with the sample gas. Test sample drawn in Syringe-1 is injected first into a pre-evacuated Syringe-3 by piercing the rubber septum on the inlet port and then allowed to be sucked into the leak detector through a moisture trap connected to sniffer probe (Fig. 3b). The system response, directly proportional to the helium partial pressure in the air/gas flowing through the analyser, is recorded as voltage output on a data logger and chart recorder. The measured helium concentrations are corrected for (i) volume of headspace, (ii) water volume, (iii) volume of air drawn in during analysis and (iv) duration of storage (obtained by averaging the values given by the two solid lines in Fig. 2).

Since the helium measurements were actually made on equilibrated headspace air samples, the

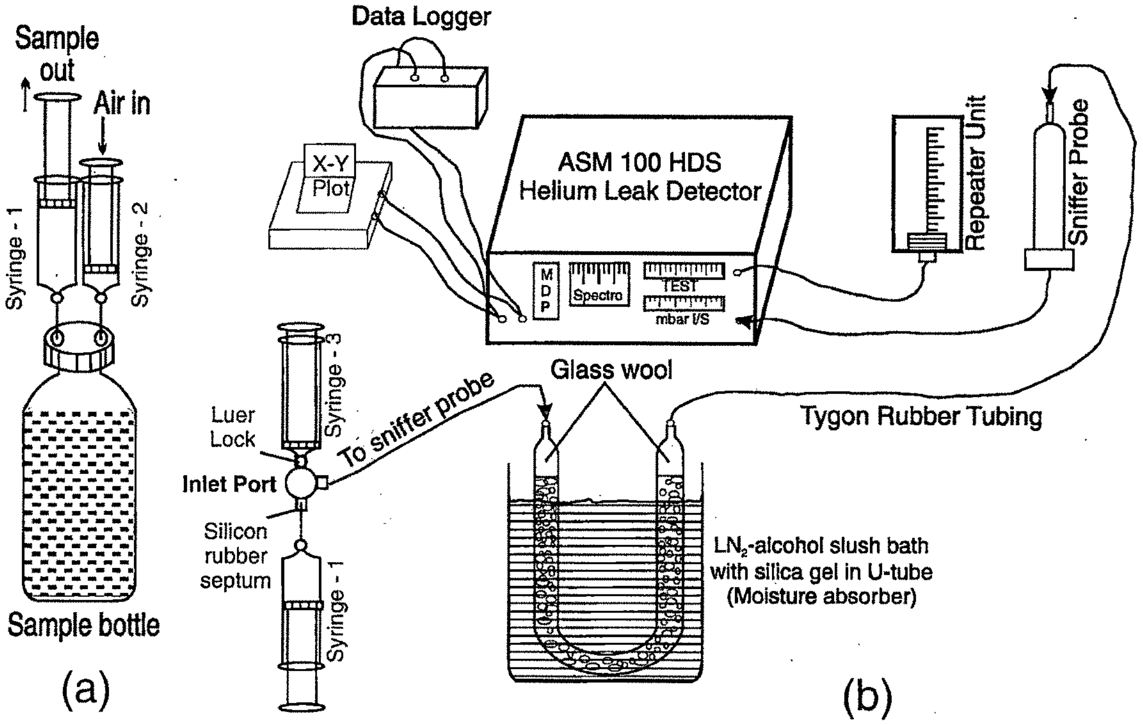

Fig. 3. Schematic diagram showing layout of (a) drawing of equilibrated air sample and (b) helium measurement through helium leak detector for water/air/gas samples.

groundwater helium concentrations can be calculated using Henry's law and the respective volumes of water and air in the sampling bottles. Dimensionless Henry's Law constant is defined as [H_x=(mass of helium in gas phase/gas phase volume)/(mass of dissolved helium/water volume), i.e. $=C_g/C_w$]. Using $H_x=94.5$ at 25 °C (Fry et al., 1995), the concentration of dissolved helium in equilibrium with air containing 5.3 ppmv helium is given by (5.6×10^{-2} ppmv). For the sake of convenience, dissolved helium concentrations are expressed in terms of Air Equilibration Units (AEU). This unit expresses helium concentration in air in equilibrium with water sample at 1 atm. Thus dissolved helium concentration of 5.6×10^{-2} ppmv is equal to 5.3 ppm AEU.

5. Calibration

The helium leak detector is calibrated using atmospheric air with He concentration of 5.3 ppmv. The standard calibration curve for the chart recorder reading (set at 10 V range) is given by the mathematical expression:

$$\mathrm{He} = \mathrm{Const}_1 \times \exp(\mathrm{Const}_2 \times D_s) \qquad (1)$$

where D_s is the number of chart recorder divisions at the 10-V full-scale setting and He is the concentration of helium in ppmv.

If the chart recorder divisions are measured as deviation/difference from the atmospheric background reading, the calibration equation can be rewritten as;

$$\mathrm{He} = 5.3\exp(\mathrm{Const}_2 \times (D_s - D_{bkg})) \qquad (2)$$

where $D_s - D_{bkg}$ is the difference in the chart recorder reading between the sample and the atmospheric background.

The calibration checks carried out in the study were designed to verify the combination of factory calibration and modification made in the input port and to verify the robustness of procedure specified in the previous section for helium assay in air/gas

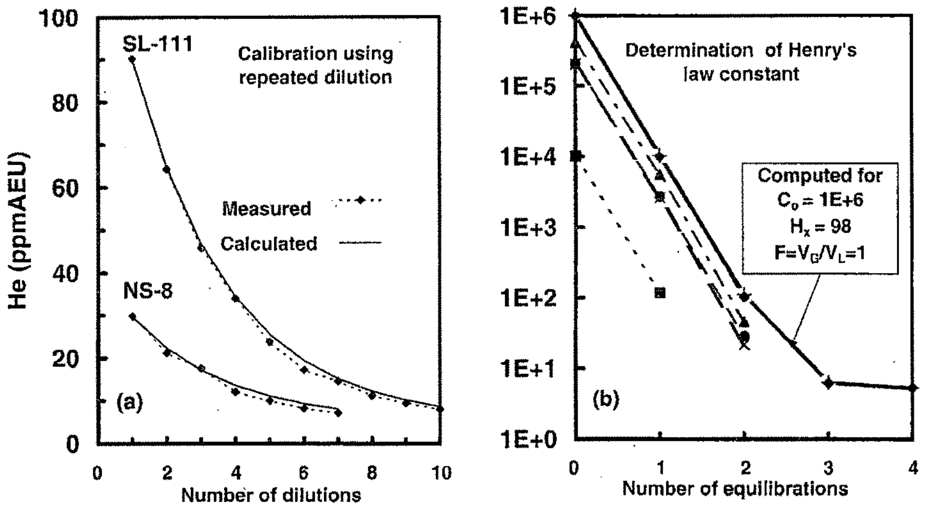

Fig. 4. (a) Comparison of measured and calculated dilution curves); (b) the results of a set of six experiments undertaken for estimation of Henry's law constant for water–helium system. The experimental values are similar to the known value of 94.5 at 20 °C (Fry et al., 1995). These experiments verify the calibration of the helium measurements and the robustness of the analytical procedure.

samples. For this purpose, we used (i) repeated dilution of an arbitrary helium concentration sample with fixed volume of atmospheric air and (ii) determination of Henry's law constant for helium.

5.1. Repeated dilution by atmospheric air

A fixed volume ($=V_A$) is drawn from the head space (volume $=V_0$) of storage bottle using a hypodermic syringe. As the sample is drawn, equal volume of atmospheric air is allowed to enter the sampling bottle through another hypodermic syringe (Fig. 3a). As a result, helium concentration in the sample being drawn varies continuously in response to dilution by atmospheric air and mixing with remaining 'mixed' sample in the bottle. If drawing of sample and dilution is repeated several times, a recursive equation as below can be obtained:

$$C_{Mn} = \frac{C_0 e^{-(n-1)f}}{f}(1-e^{-f}) - \frac{C_A e^{-(n-1)f}}{f}(1-e^{-f}) + C_A$$

where C_{Mn} is the measured helium concentration drawn by the hypodermic syringe after nth dilution, C_0 is the original helium concentration in volume V_0, and C_A is the helium concentration of incoming atmospheric air; $f=V_A/V_0$.

For $C_A \ll C_0$, $C_{Mn} = \frac{C_0 e^{-(n-1)f}}{f}(1-e^{-f})$

Therefore,

$$\frac{C_{Mn}}{C_{M(n-1)}} = e^{-f} \tag{3}$$

Thus, the measured concentration will decrease by a factor of e^{-f} after every dilution. In our standard experiments, $V_A=20$ ml, $V_0=56$ ml.

Eq. (3) can be used to experimentally check the calibration of the instrument and the entire analytical procedure, starting with air/gas sample with any arbitrary helium concentration. A graph of two separate experiments showing measured and calculated

Table 1
Reproducibility of measured helium concentration in groundwater samples

Sample location	Helium concentration (ppm AEU)		Variability (%)
	Sample-1	Sample-2	
Ranip	6.17	6.20	1
Bagodra	339.7	339.7	0
Roika	24.3	24.8	2
Tilaknagar	5.3	5.3	0

helium concentration variation involving repeated dilution with atmospheric air is given in Fig. 4a. The close matching between the measured and calculated values not only confirm the calibration of the instrument but also the correctness of the experimental procedures.

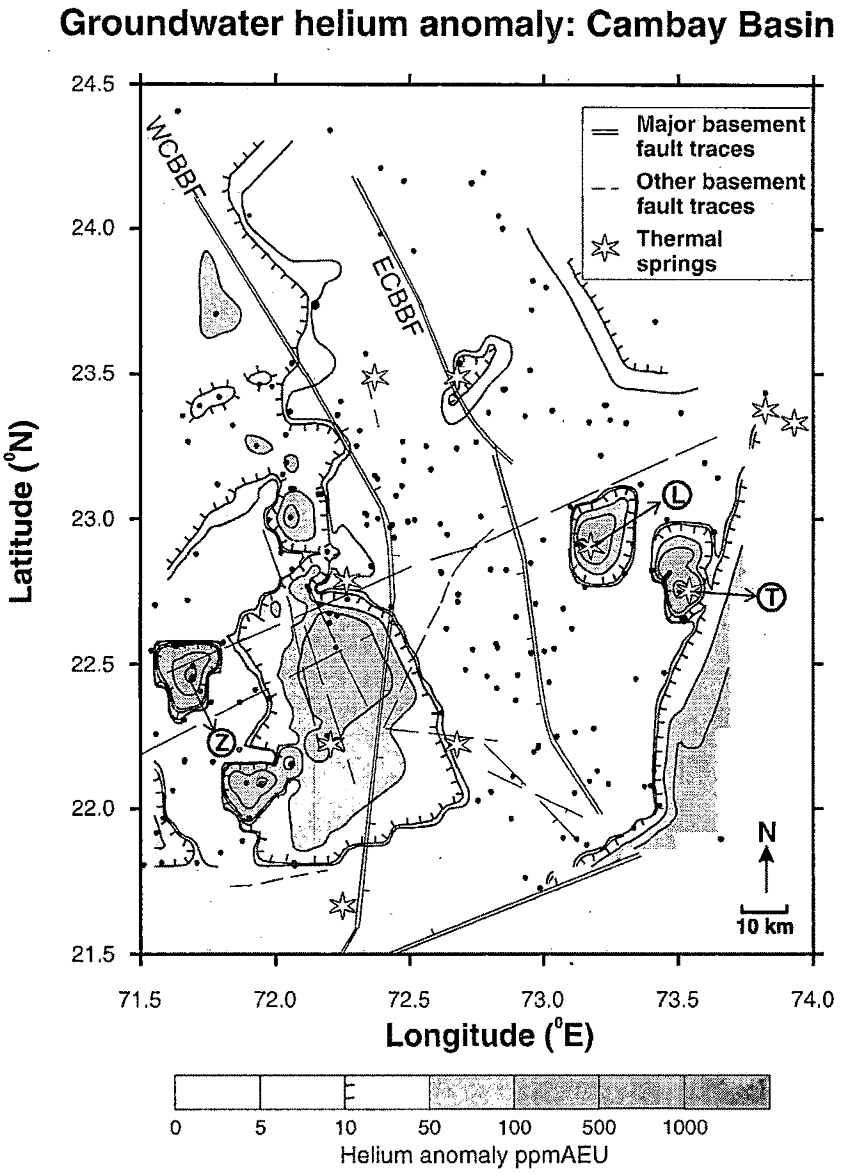

Fig. 5. The study area in the Cambay basin showing (i) contours of anomalous groundwater helium concentrations along with sampling locations; (ii) traces of major basement faults (after Mathur et al., 1968; Merh, 1995); and (iii) locations of thermal springs (after GSI, 2000). The helium anomaly contours of 510 ppm AEU run approximately along the WCBBF and almost equidistant from the groundwater recharge area along the Aravalli foothills in the NE (see Fig. 6). Very high groundwater helium anomalies are seen west of WCBBF in the SW corner where a set of intersecting orthogonal basement faults are located. These fault traces are shown by broken lines. The highest helium anomaly was observed at Zinzawadar (Z) located close to the western extremity of the longest orthogonal fault trace cutting across the Cambay basin. High groundwater helium anomalies are also seen at a few locations on the eastern flank of the Cambay basin, mostly in association with thermal springs of Lasundra (L) and Tuwa (T).

5.2. Estimation of Henry's law constant

The next step in calibration test was to estimate the Henry's law constant following the standardised measurement procedure. For *n*th equilibration, the relation derived for determination of Henry's law constant by repeated equilibration of atmospheric air with water containing dissolved helium is:

$$\log C_{Gn} = \log C_{G0} - n\log(1 + FH_x) \qquad (4)$$

where C_{Gn} = concentration of helium in gas phase after *n*th equilibration; C_{G0} = original concentration of helium in gas phase; $F = V_G/V_L$ = volume of gas phase/volume of liquid phase; and H_x = Henry's law constant.

Plot of log C_{Gn} vs. *n* (equilibration number) would be a straight line with intercept = log C_{G0} and slope = − log(1 + FH_x).

In our experiments, while the values of C_0 were arbitrarily varied, the values of V_G and V_L were 50 ml each. Fig. 4b is a plot showing measured helium concentration in equilibrated air against the number of equilibration in several experiments involving different initial helium concentrations. The estimated average value of Henry's law constant for six sets of similar experiments is 98 against the known value of 94.5 at 25 °C (Weiss, 1971; Perry, 1984). Close matching between the different experiments and between estimated and standard value once again confirm the calibration of the total set up and the robustness of the standardised procedure for helium concentration estimation in air/water sample.

Reproducibility of helium measurements was checked by repeated analyses on a set of four samples collected at the same time in two different bottles in the concentration range of 5.3–340 ppm AEU. The results of these experiments (Table 1) show that the analytical precision is better than 5%.

6. Results of field survey

A field survey of helium in groundwater and soil-gas was undertaken in the Cambay basin (Fig. 5). The geographical coordinates of the sampling locations were determined using hand-held Geographical Positioning System (GPS) receiver (Trimble Scout GPS). Temperature of water was also measured at the time of collection.

Of the 12 soil-gas samples analysed, only 1 sample, ~ 100 m away from the thermal springs of Tuwa, showed helium concentration (7.0 ppmv) higher than the atmospheric background (5.3 ppmv). All other soil-gas samples had helium concentrations close to atmospheric value. However, many groundwater samples from the 246 analysed from the study area showed dissolved helium concentrations significantly higher (up to >200 times) than the atmospheric equilibration concentration (5.3 ppm AEU). It may be noted that reproducibility of measurements of dissolved helium concentration is better than 5% (Table 1).

Table 2
Variation of groundwater temperature and anomalous helium concentration in different emergences of thermal springs at the locations of Lasundra and Tuwa on eastern flank and some free-flowing artesian wells on the western flank of the Cambay basin

Sample no.	Temperature (°C)	Depth below ground level of the spring/well (m)	Dissolved helium anomalous concentration (ppm AEU)
On eastern flank of Cambay basin			
Location: Lasundra (22.914°N; 73.145°E)			
CBDW/8/98	51.5	6.1	186
CBDW/9/98	33.0	6.1	55
Location: Lasundra (22.918°N; 73.153°E)			
CBT/15/98	33.0	85.4	221
Location: Tuwa (22.800°N; 73.461°E)			
CBDW/18/98	61.0	0.9	137
CBDW/19/98	46.5	0.9	96
CBDW/20/98	27.5	0.9	475
Location: Tuwa (22.798°N; 73.461°E)			
CBHP/21/98	51.0	12.2	1163
On western flank of Cambay basin			
Location: Dholera (22.249°N; 72.192°E)			
CBTA/45/98	42.5	167.6	109
Location: Gundi (22.553°N; 72.227°E)			
CBTA/55/98	40.0	289.6	235
Location: Shiyala (22.702°N; 72.164°E)			
CBTA/65/98	38	274.3	73
Location: Ruhika (22.663°N; 72.231°E)			
CBTA/66/98	41	457.2	157
Location: Sarala (22.671°N; 72.201°E)			
CBTA/67/98	40	274.3	90
Location: Zinzawadar (22.452°N; 71.694°E)[a]			
CBTW/120/99	34	285.0	2843

[a] This is not a free-flowing tubewell but is included in this table because the highest dissolved groundwater helium anomaly was observed at this location.

Interpretation of groundwater helium data on regional scale may, at times, be difficult because of local scale variability, as, for example, noticed at the location of the thermal springs of Tuwa and Lasundra. At both these locations, even within a distance of 20 m, springs show different temperature and helium concentrations (Table 2).

Fig. 5 shows the contour lines of anomalous helium concentration (i.e. in excess of 5.3 ppm AEU) in groundwater samples. Traces of major basement faults

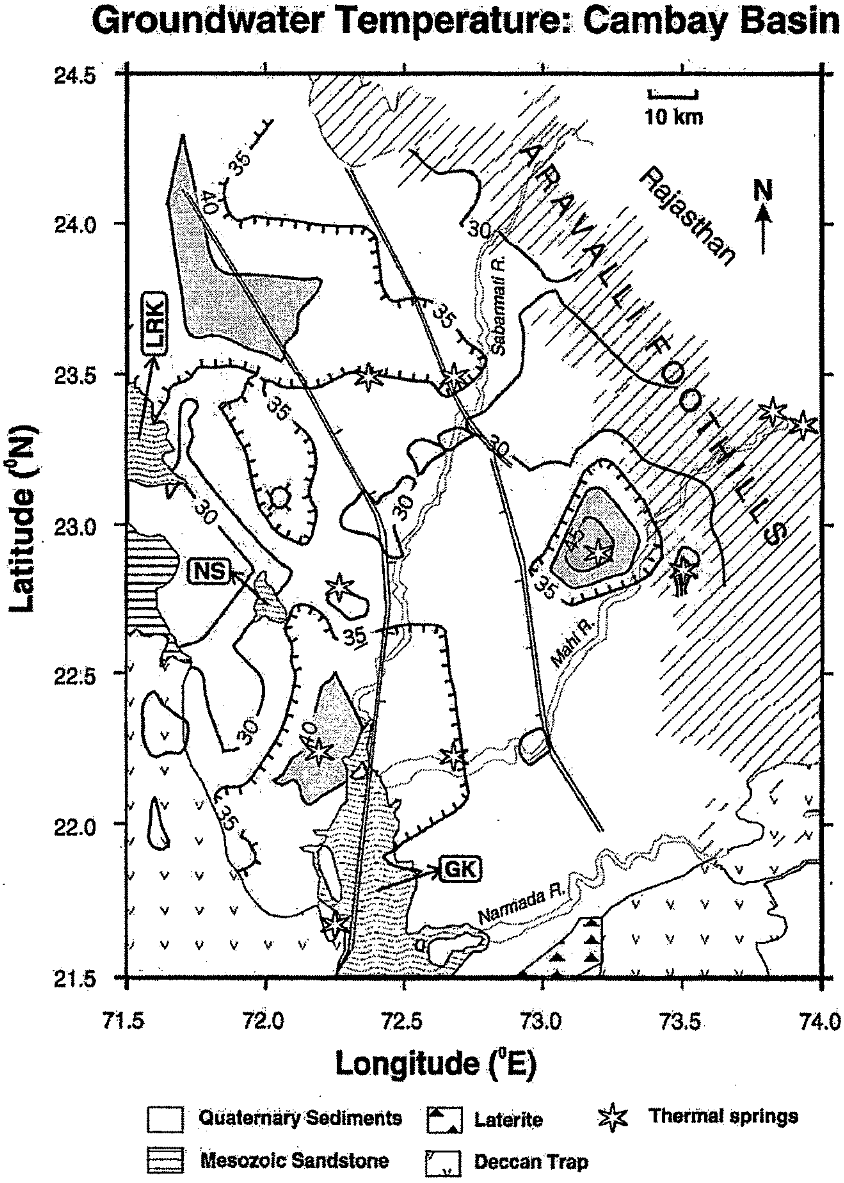

Fig. 6. Contours of groundwater temperature and locations of thermal springs (after GSI, 2000) superposed on geological map (after Merh, 1995) of the study area in the Cambay basin. The sampling locations are shown in Fig. 5. The areas with enhanced groundwater temperature (>35 °C) are associated with (a) locations of thermal springs, (b) enhanced groundwater helium (Fig. 5) except within the Cambay graben with >3 km thick sedimentary cover, and (c) the major basement faults. The region linking Little Rann of Kachchh (LRK)–Nalsarovar (NS)–Gulf of Khambhat (GK) forms the lowest elevation in the study area.

(Merh, 1995; Misra, 1981; Biswas, 1982, 1987) in the region are superposed on the contour map. As one moves eastwards from 71.5°E, a series of N–S trending step faults roughly parallel to West Cambay Basin Boundary Fault (WCBBF) have caused a progressive lowering of the Deccan Basalt, where the basaltic layer is abruptly downthrown by >3 km. The highest helium anomalies in this region are seen between 22° and 23°N (Fig. 5) on the faults running transverse to the fault traces linking the Little Rann of Kachchh–Nalsarovar–Gulf of Khambhat (LRK–NS–GK) corridor. Further north, several pockets of high helium concentration can be identified up to 24°N. Datta et al. (1980) had also noted that some artesian wells on the western flank of Cambay basin in the vicinity of the Nalsarovar (22°48′ N; 72°E) had enhanced groundwater temperature and helium. Within the CG, between WCBBF and the East Cambay Basin Boundary Fault (ECBBF), the thickness of Cenozoic sedimentary cover is >3 km (Mathur et al., 1968). The groundwater in this region is almost completely devoid of anomalous helium.

On the eastern flank of CG, highest helium anomalies are associated with the thermal springs of Lasundra and Tuwa. On this flank, another small patch of high helium concentration is seen across ECBBF along the Sabarmati River. Major concentration of anomalous helium is also seen in southern part at the extension of ECBBF along the Narmada-Son-Geofracture that confines the flow of Narmada River.

Fig. 6 shows the contours of groundwater temperature, superposed by traces of regional basement fault and geology (after Merh, 1995). Average groundwater temperature in the study area is about 30 °C. Temperatures >35 °C are generally seen associated with high helium anomalies particularly along the two flanks of the CG. Geographically, the areas with anomalous helium >5 ppm AEU tend to lie within the contours with groundwater temperature >35 °C. It is also noticed from Figs. 5 and 6 that areas of helium and temperature anomalies surround the locations of known thermal springs in this region. In fact, all three appear to be geographically related to the known positions of the basement faults in the study area. However, major areas of high groundwater temperature, not associated with groundwater helium anomalies, are seen across the CG between 23.5–24°N and 22–22.5°N. However, an association with geothermal springs is clearly seen.

7. Discussion

Minissale et al. (2000) have ascribed the high concentration of helium in the gas phase of thermal springs along the arms of the triple junction to long residence time. Within the Cambay basin, 10 samples of fluvial deposits gave average concentration of 1.7 ± 0.8 ppm for uranium and 8.0 ± 3.3 ppm for thorium (Srivastava et al., 2001). Since there are no known deposits of uranium/thorium mineralisation in the entire study area, we assume a uniform mineralogy with an average of the above reported concentrations and porosity $\approx 20\%$. A residence time of the order of $\sim 10^4$ years is required for growth of ~ 10 ppm AEU anomalous helium under the assumption of complete acquisition of radiogenic helium by groundwater. This is in conformity with the radiocarbon ages in the area having helium anomaly of the order of ~ 10 ppm AEU (PRL ^{14}C Laboratory, M.G. Yadav, personal communication). Further, the 10 ppm AEU contour is roughly parallel and equidistant from the trend of Aravalli foothills which is the recharge area of aquifers in this region (Fig. 5). It therefore seems that, for groundwater on the western flank of Cambay basin, a helium anomaly of the order of 10 ppm AEU may be attributable to the groundwater residence time. However, the high anomaly contours of 50–100 ppm AEU do not form a continuous patch parallel to Aravalli foothills but encircle the location of thermal springs on either flanks of Cambay basin. On the western flank, anomaly contours of 50–100 ppm AEU overlie the crisscrossing basement faults. The highest values of helium anomaly (~ 1000 ppm AEU) were obtained at Tuwa, on the eastern flank very close to foot hills and (>2000 ppm AEU) from the Zinzawadar village on the western flank. The residence time of $\sim 10^6$ years required to explain the high groundwater helium is not compatible with the hydrogeology of the region. Therefore, additional source for anomalous helium is required. Alternatively, in the absence of any report of high U–Th concentrations in the alluvial sediments of Cambay basin, the additional helium must be derived from a rock/sediment/soil volume many times larger than the one that groundwater comes in contact with.

As mentioned earlier, the study area of Cambay basin is part of a larger tectonic structure in the western part of India (Fig. 1). The Narmada Tapti (NT) rift system and the CG cross each other in the Gulf of Cambay (also known as Gulf of Khambhat). Together with West Coast (WC) fault, the area has been identified as a triple junction (Burke and Dewey, 1973). These structures are considered to reach the mantle in the NT and Cambay areas (~ 40 km in depth; Kaila et al., 1989). Based on deep seismic soundings (Kaila et al., 1981, 1989; Kaila and Krishna, 1992) and gravity surveys (Singh and Meissner, 1995; Singh, 1998), it has been hypothesised that a thick high density (3.02 g cm^{-3}) igneous layer lies at the base of the crust in this region. Underlying the accreted igneous layer, a low velocity zone of hot mantle and/or a zone of intense lower crust and upper mantle interaction has been identified beneath the area of triple junction (Arora and Reddy, 1991). This configuration is compatible with high geothermal regime (heat flow 55–90 mW m^{-2}; temperature gradient 36–58 °C km^{-1}) in the region (Gupta, 1981; Panda, 1985; Ravi Shankar, 1988; Negi et al., 1992). Therefore, the lithosphere beneath the triple junction and the three arms, namely the CG, NT rift zone and WC fault, is now much warmer, thinner relatively ductile and less viscous compared to the margins (Pandey and Agrawal, 2000).

A large number of thermal springs dot the three arms of the triple junction. From a tectonic perspective, these thermal springs along geologically, well-defined structures, with frequent earthquakes of moderate intensity, suggest that these structures are active. This is also implied by the observed neotectonic movements recorded in the Quaternary sediments and from the geomorphic studies of the region (Sridhar et al., 1994; Maurya et al., 1995, 1997; Tandon et al., 1997; Srivastava et al., 2001). However, no active volcanism in any of the three arms has been observed. A recent study (Minissale et al., 2000) employing chemical and isotopic signatures on a large number of thermal springs and the associated gas phase from the three arms of the triple junction has concluded that water emerging from these thermal springs is meteoric in origin with low equilibration temperatures (90–150 °C). No evidence of mantle-derived ^{3}He in the gas phase otherwise rich in N_2, He and Ar could be detected. These convectively circulating spring waters were therefore termed 'intracratonic thermal waters' (Minissale et al., 2000).

With this background, it is possible to construct a conceptual model that explains the observed features in the abundance of helium and groundwater temperature in the study area.

8. A tectono-hydrothermal model of the Cambay basin

At the micro-scale, helium is visualised to be released from the rocks and grains by diffusion, α-recoil and the weathering processes that include etching, dissolution and fracturing. The released helium migrates upwards due to concentration gradient (with lowest concentration in the atmosphere) by diffusion and temperature variations facilitated by micro- and macro-cracks, pores, fractures and fissures that act as collectors and conduits of helium from the underlying formations. The upward migration of helium can be further facilitated by mass flow of crustal liquids (e.g. groundwater and petroleum) which may also be present in these conduits.

On a regional scale, therefore, higher concentration of helium in soil-gas and groundwater are expected over regions where such preferred pathways lie close to the surface.

Near surface helium distribution is, however, modulated by inherent differences in the migratory pathways between the crystalline and sedimentary formations. Sedimentary formations are generally characterised by uniform and high density of pores that cause almost omnidirectional migration of helium. This is in contrast to crystalline rocks where a relatively small density of interconnected fractures and fissures dictate the migration. As a result, sedimentary formations cause dispersion of the upward migratory helium plume whereas the crystalline formations tend to act as sources of helium plumes.

The presence of deep-seated faults and fractures also facilitates percolation of groundwater to deeper layers which, in a high heat flow regime, establishes a convective circulation with thermal waters of meteoric origin emerging as springs. Often, this convective circulation of meteoric water will not emerge as springs but discharge the thermal waters back into the groundwater thereby giving rise to temperature anomalies. Thus, it is seen that though helium and groundwater have different sources, the faults and fractures in the crust can associate anomalous concentrations of helium and groundwater temperatures thereby providing an overall coupling between them. As the sources of the two anomalies are different, one may not expect a quantitative relationship between the two parameters. Geographical correlation is, however, expected because localisation of both anomalies is facilitated by fissures, fractures and faults at shallow (within 1–2 km) depth.

This conceptual model is depicted in Fig. 7 where a block diagram from western margin of the study area to the middle of the CG is schematically drawn. Two sets of braided fractures either joining into or emanating out from the major fault traces are shown. Those joining into are indicative of migration of helium from micro-cracks into macro-fractures, eventually joining the conduits provided by the major fractures and faults. Those emanating out are indicative of the pathways that upwardly migrating helium takes through the overlying sedimentary cover. In case of shallow depth of the basaltic layers, some of these pathways reach the surface and cause anomalous helium concentration in groundwater and soil-gas as seen on both flanks of the CG. In case of large thickness of the sedimentary cover, helium emanating from the fractures within or below the basaltic layer gets dispersed and diluted before reaching the surface. This explains the low concentration of groundwater helium as seen within the CG where the thickness of sedimentary cover is >3 km. It was, however, noted earlier that two areas of high groundwater temperature associated with geothermal springs but not associated

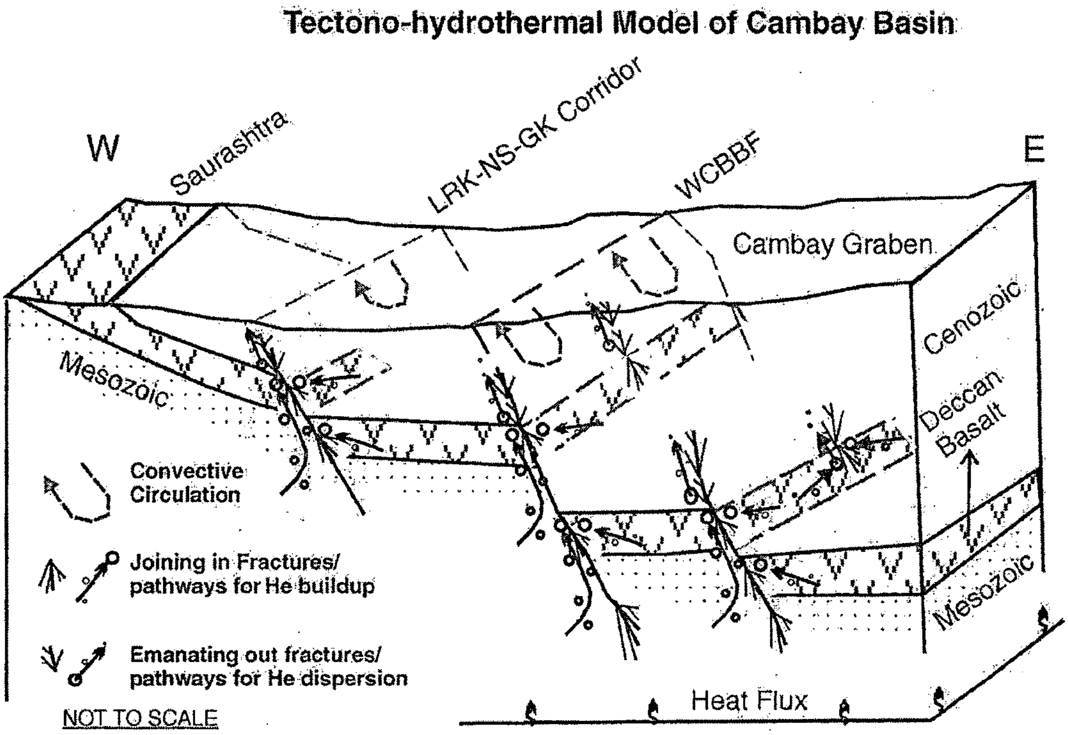

Fig. 7. A conceptual tectono-hydrothermal model for the origin of groundwater helium and temperature anomalies in the Cambay basin, Gujarat, India, is depicted schematically in an E–W block diagram across the Cambay graben. The set of braided fractures joining the major fault traces is indicative of migration of helium from micro-cracks into macro-fractures, eventually joining the conduits provided by the major fractures and faults. The joining in fractures thus acts as the pathway for helium build-up. Another set of braided fractures emanating out from the major fault traces is indicative of the pathway that the upwardly migrating helium takes through the overlying sedimentary cover leading to dispersion/diffusion. In both cases, the size of open circles schematically depicts the changing helium concentration during upward migration. The continuous arrows leading to major faults depict the preferred migration pathway of radiogenic helium derived from a large area. The broken arrows depict the shallow depth (~ 1–2 km) hydrothermal circulation facilitated by high heat flux and the ongoing tectonic movements along major fractures and faults.

with groundwater helium anomalies are seen across the CG between 23.5–24°N and 22–22.5°N. This is the most direct evidence that the localisation of helium anomaly is controlled not only by the presence of faults and fractures but also by the depth to the crystalline basement. The temperature anomalies, on the other hand, are localised by the existence of faults and fractures that may facilitate setting up of convective groundwater circulation.

Alternatively, the data could have also been explained by using a model wherein both helium and hydrothermal fluids had a common deep-seated origin possibly at the base of the crust (only ~ 40 km deep) and the faults/fractures were acting as conduits for the migration of the two towards the surface. However, this model is not tenable in view of the low equilibration temperature (90–150 °C) of the thermal spring waters and the absence of any ^{3}He signatures of mantle origin in the associated gas bubbles (Minissale et al., 2000).

9. Summary and conclusion

A commercially available portable helium leak detector has been converted into a sensitive soil-gas/water helium analyser by modifying the input port. A simple and cost-effective sample collection and storage system using commercially available soda-lime glass bottles with bromobutyl rubber stopper and triple protection aluminium cap has been shown to retain the vacuum and stored helium for reasonably long period with little loss for a groundwater helium survey. Calibration checks involving repeated dilution and water–helium equilibration testify the correctness and robustness of the standardised procedure for helium assays.

A survey of natural helium in groundwater and soil-gas was undertaken in the Cambay basin region. Several wells investigated in this study indicated higher than atmospheric equilibration concentration, referred to as anomalous helium concentration.

In most parts of the study area, high groundwater helium anomalies are seen to be associated with the enhanced groundwater temperatures except within the Cambay graben. The areas of high helium concentration and enhanced groundwater temperatures are seen to overlie some of the basement faults. This association of high helium anomaly, enhanced groundwater temperature and some of the basement faults is explained through a conceptual model wherein the fractures and fissures in the crystalline basement act as sources of helium plumes and the sedimentary cover as a dispersive media. The high heat flow in the region facilitates convective hydrothermal circulation of groundwater along the major faults and fractures within 1–2 km depth. The faults and fractures thus act to localise the helium and thermal emergences both on the western and eastern flanks of the CG. Within the CG, the presence of thick sedimentary cover disperses the helium plumes originating from deeper basement layers.

Acknowledgements

Dr. D.N. Yadav is thanked for his contribution during initial calibration experiments. We also thank the referee, Dr. Nilgun Gulec, and another unknown referee for suggestions on improvement of the final manuscript. **[SG]**

References

Arora, B.R., Reddy, C.D., 1991. Magnetovariational study over a seismically active area in the Deccan trap province of western India. Phys. Earth Planet. Inter. 17, 21–28.

Biswas, S.K., 1982. Rift basins in Western margin of India and their hydrocarbon prospects with special reference to Kutch basin. Am. Assoc. Pet. Geol. Bull. 66 (10), 1497–1513.

Biswas, S.K., 1987. Regional tectonic framework, structure and evolution of the western marginal basins of India. Tectonophysics 135, 307–327.

Burke, K., Dewey, J.F., 1973. Plume generated triple junctions: key indicators in applying plate tectonics to old rocks. J. Geol. 81, 406–433.

Craig, H., Lupton, J.E., 1976. Primordial neon, helium and hydrogen in oceanic basalts. Earth Planet. Sci. Lett. 31, 369–385.

Datta, P.S., Gupta, S.K., Jaisurya, A., Nizampurkar, V.N., Sharma, P., Plusnin, M.I., 1980. A survey of helium in groundwater in parts of Sabarmati basin in Gujarat state and in Jaisalmer district, Rajasthan. Hydrol. Sci. Bull. 26, 183–193.

Dikum, A.V., Korobeynik, V.M., Yanitskiy, I.N., 1975. Some indications of existence of transcrustal gas flow. Geochem. Int. 12 (6), 73–78.

Friedman, I., Denton, E.H., 1975. A portable helium sniffer. US Geological Survey, Open File Report 75-532.

Fry, V.A., Istok, J.D., Semprini, L., O'Reilly, L.T., Buscheak, T.E.,

1995. Retardation of dissolved oxygen due to a trapped gas phase in porous media. Groundwater 333, 391–398.

Golubev, V.S., Yeremeyev, A.N., Yanitskiy, I.N., 1975. Analysis of some models of helium migration in the lithosphere. Geochem. Int. 11 (4), 734–742.

GSI, 2000. Seismotectonic Atlas of India and its environs. Geological Survey of India, Calcutta, India. 87 pp.

Gupta, M.L., 1981. Surface heat flow and igneous intrusion in the Cambay basin, India. J. Volcanol. Geotherm. Res. 10, 279–292.

Gupta, S.K., Lau, L.S., Moravcik, P.S., El-Kadi, A., 1990. Injected Helium: A New Hydrological Tracer. Special Report 06.01:90 Water Resources Research Center, University of Hawaii at Manoa, Honolulu.

Kaila, K.L., Krishna, V.G., 1992. Deep seismic sounding studies in India and major discoveries. Curr. Sci. 62, 117–154.

Kaila, K.L., Krishna, V.G., Mall, D.M., 1981. Crustal structure along Mehmedabad–Billimora profile in the Cambay basin, India from deep seismic soundings. Tectonophysics 76, 99–130.

Kaila, K.L., Rao, I.B.P., Rao, P.K., Rao, N.M., Krishna, V.G., Sridhar, A.R., 1989. D.S.S. studies over Deccan traps along the Thuadara–Sendhawa–Sindad profile, across Narmada-Son lineament, India. In: Mereu, R.F., Mueller, S., Fauntain, D.M. (Eds.), Properties and Processes of Earth's Lower Crust. AGU Geophys. Monogr., vol. 51, pp. 127–141. IUGG6.

Lupton, J.E., Weiss, R.F., Craig, H., 1977. Mantle helium in the Red Sea. Nature 266, 244–246.

Mathur, L.P., Rao, K.L.N., Chaube, A.N., 1968. Tectonic framework of Cambay basin, India. Bull. ONGC 5 (1), 7–28.

Maurya, D.M., Chamyal, L.S., Merh, S.S., 1995. Tectonic evolution of the central Gujarat plain, western India. Curr. Sci. 69 (7), 610–613.

Maurya, D.M., Malik, J.N., Raj, R., Chamyal, L.S., 1997. Soft sediment deformation in the Quaternary sediments of the Lower Mahi river basin, Western India. Curr. Sci. 72 (7), 519–522.

Merh, S.E., 1995. Geology of Gujarat, Geological Society of India. 222 pp.

Minissale, A., Vaselli, O., Chandrasekharan, D., Magro, G., Tassi, F., Casiglia, A., 2000. Origin and evolution of 'intracratonic' thermal fluids from central-western peninsular India. Earth Planet. Sci. Lett. 181, 377–397.

Misra, K.S., 1981. The tectonic setting of Deccan Volcanism in southern Saurashtra and northern Gujarat. Deccan Volcanism and Related Basalt Provinces in Other Parts of the World. Geol. Surv. India Memoir, vol. 3, pp. 81–86.

Misra, K.S., 2001. Lineament fabric and its relation to the eruption of Deccan volcanics and seismicity of west-central India. Geol. Surv. India, Spec. Publ. 64, 209–221.

Negi, J.G., Agrawal, P.K., Singh, A.P., Pandey, O.P., 1992. Bombay gravity high and eruption of Deccan flood basalts India from a shallow secondary plume. Tectonophysics 206, 341–350.

Panda, P.K., 1985. Geothermal maps of India and their significance in resources assessments. Petrol. Asia J. VIII 2, 202–210.

Pandey, O.P., Agrawal, P.K., 2000. Thermal regime, hydrocarbon maturation and geodynamic events along the western margin of India since late Cretaceous. J. Geodyn. 30, 439–459.

Perry, J.H., 1984. Chemical Engineers' Handbook. McGraw-Hill, New York.

Ravi Shankar, J.H., 1988. Heat flow map of India and discussions on its geological and economic significance. Ind. Min. 42, 89–110.

Ravi Shankar, J.H., 1991. Thermal and crustal structure of "SONATA". A zone of mid-continental lifting in Indian shield. J. Geol. Soc. India 37, 211–220.

Ravi Shankar, J.H., 1995. Fragmented Indian shield and recent earthquakes. Geol. Surv. India, Spec. Publ. 27, 41–48.

Reimer, G.M., 1984. Prediction of central California earthquakes from soil-gas helium. PAGEOPH 122, 369–375.

Singh, A.P., 1998. 3-D structure and geodynamics evolution of accreted igneous layer in the Narmada-Tapti region. J. Geodyn. 252, 129–141.

Singh, A.P., Meissner, R., 1995. Crustal configuration of the Narmada-Tapti region India from gravity studies. J. Geodyn. 20, 111–127.

Sridhar, V., Chamyal, L.S., Merh, S.S., 1994. North Gujarat Rivers: remnants of super fluvial system. J. Geol. Soc. India 44, 427–434.

Srivastava, P., Juyal, N., Singhvi, A.K., Wasson, R.J., Bateman, M.D., 2001. Luminescence chronology of river adjustment and incision of Quaternary sediments in the alluvial plain of the Sabarmati river, north Gujarat, India. Geomorphology 36, 217–229.

Tandon, S.K., Sareen, B.K., Rao, M.S., Singhvi, A.K., 1997. Aggradation history and luminescence chronology of late Quaternary semi-arid sequences of the Sabarmati basin, Gujarat, Western India. Palaeogeogr. Palaeoclimatol. Palaeoecol. 128, 133–357.

Weiss, R.F., 1971. Solubility of helium and neon in seawater. J. Chem. Eng. Data 167, 235–241.

Dissolved helium and TDS in groundwater from Bhavnagar in Gujarat: Unrelated to seismic events between August 2000 and January 2001

S K GUPTA* and R D DESHPANDE

Physical Research Laboratory, P.O. Box 4218, Navrangpura, Ahmedabad 380 009, India

Temporal variations have been observed in both dissolved helium and TDS in the form of increase in basaltic and decrease in alluvial aquifers. The increase in basaltic aquifers has been explained by enhanced pumping of old groundwater with relatively higher concentration of dissolved helium and salt, whereas the decrease in alluvial aquifers has been explained by dilution from the post monsoon groundwater recharge. Therefore, the observed temporal variations cannot be ascribed to the contemporary enhanced seismic activity in this region since August–September 2000.

---

1. Introduction

Helium-4 is radiogenic, produced in decay of uranium and thorium series nuclides in soils and rock grains within the Earth. The gas is steadily released from grains by their etching, dissolution, fracturing and alpha recoil during weathering and then exhaled into the atmosphere by diffusion and temperature variations. The Earth's atmosphere has a small concentration of helium since it quickly escapes to the outer space. Since the production of both ^{4}He and radon occurs within the Earth, their concentrations show a gradient decreasing towards the ground-atmosphere interface. Before escaping to the atmosphere through fractures, these gases are intercepted by the omnipresent groundwater zone. Since the diffusivity of helium in water is small ($7.78 \times 10^{-5}\,\mathrm{cm^2 s^{-1}}$ at 25°C; CRC Handbook, 80th edition, 1999–2000), it generally follows groundwater flow.

While a part of the radiogenic helium is released to the atmosphere the remaining fraction continues to accumulate in grains. Episodes of rock dilation and fracturing may occasionally release this fraction. On such occasions, and for a short period of time, this fraction may dominate over steady-state release. Creation of micro-fractures due to slow build-up of strain resulting in escape of radiogenic helium and radon provides the basis of geochemical methods of earthquake prediction (Barsukov *et al* 1985a; Reimer 1985; Virk *et al* 2001). Tremors of significant magnitude can create new fractures in the crust and also unlock some that may already exist. Earthquakes can thus facilitate escape of helium through fractures and suddenly increase its concentration in the overlying groundwater zone. The sensitivity range of the gaseous components of groundwater including helium, radon, carbon dioxide and hydrogen sulphide has been estimated to be 300–500 km or more (Varhall *et al* 1985; Barsukov *et al* 1985b). On the basis of Tashkent precursor study during 1974–1980 an empirical formula (Log $RT = 0.63\,\mathrm{M} \pm 0.15$) relating time T to magnitude M and epicentral distance R had been put forward (Sultankhodzhayev *et al* 1980). Observations in helium content of Yavros flowing well waters in Dushanbe study area during 1977–79 have been useful in revealing that both precursor time and anomaly amplitude increased with magnitude of the following seismic event. The anomaly duration and amplitude decreased with epicentral distance. But in many other areas it is still uncertain if the observed anomalies were truly earthquake related or induced by other environmental

Keywords. Groundwater; Helium; TDS; Bhavnagar; seismicity.

Proc. Indian Acad. Sci. (Earth Planet. Sci.), **112**, No. 1, March 2003, pp. 51–60

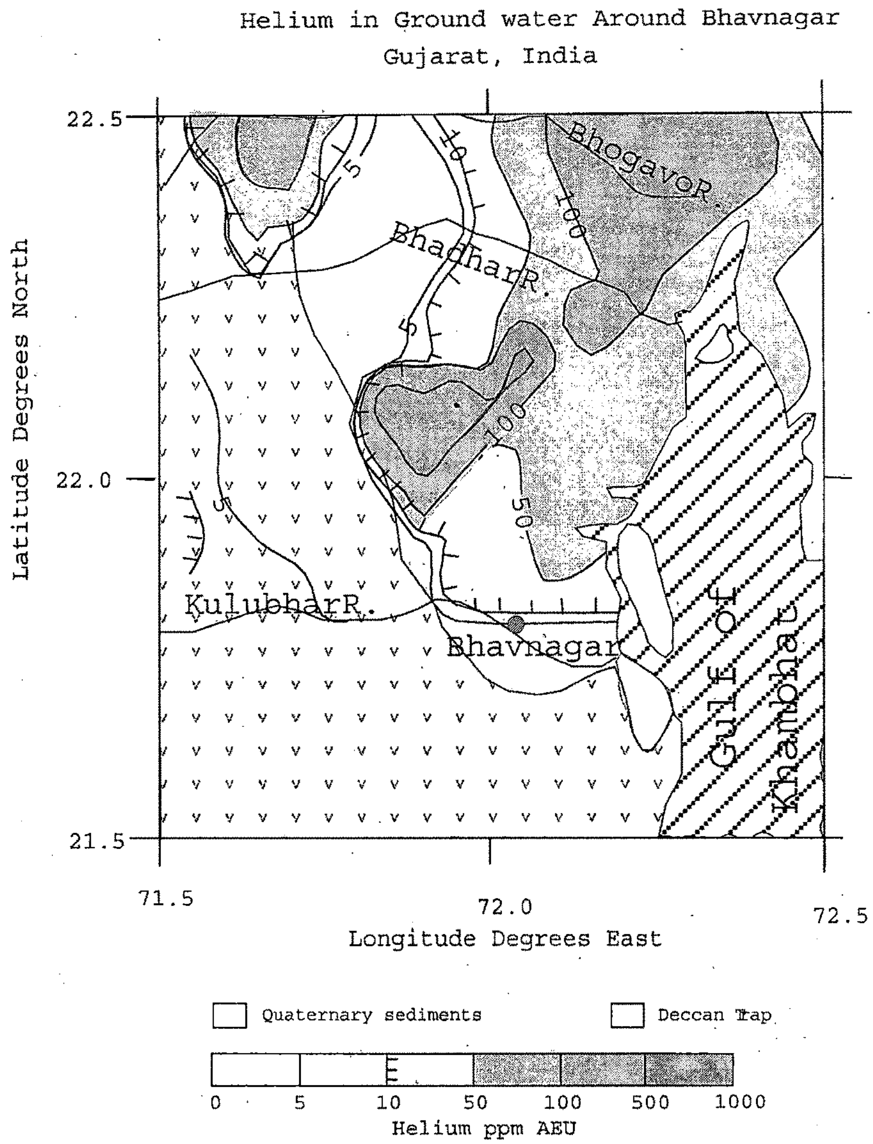

Figure 1. Contours of dissolved helium anomaly in groundwater in the region around Bhavnagar in March 1998, i.e., during a quiet seismic period.

variables such as weather and groundwater pumping (King 1985).

During the last two decades, Bhavnagar city (21.86°N; 72.04°E) in western India has intermittently experienced earthquakes of magnitude > 3 (Srivastava and Rao 1997). The city is located on the southern tip of Saurashtra, which is bound by the extension of Narmada geofracture in the south and western Cambay Basin fault in the east. During 1979 and 1982, several earthquakes with epicentres in Bhavnagar, Chandod, Gulf of Khambhat, Rajpipla etc., located along the Narmada geofracture were experienced. A survey of dissolved helium in groundwater from parts of Cambay Basin during 1999 did indeed show significantly high concentrations (figure 1) around Bhavnagar. During August–September, 2000 the frequency of small tremors around Bhavnagar increased significantly and presented an opportunity to test the earthquake induced helium release model in this part of the world.

Sixteen groundwater samples were collected from tubewells and hand pumps from different parts of the city (figure 2) on 16th and 17th September 2000. Some of the same stations were re-sampled on 22nd January 2001 after a long quiescence period for comparison. After the Bhuj earthquake of 26th January 2001, a repeat survey of these stations was conducted in March 2001. During the two repeat surveys,

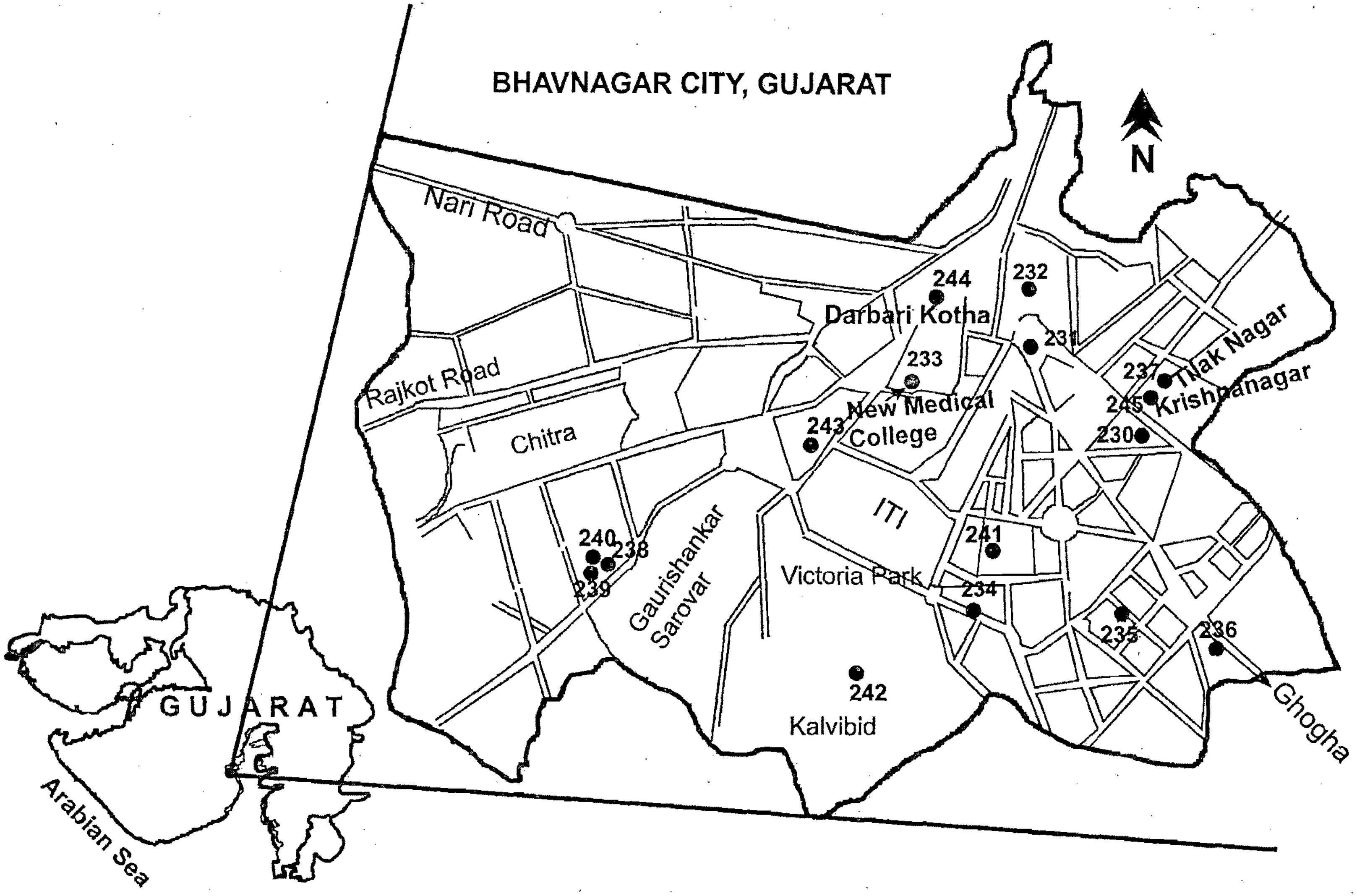

Figure 2. Map of Bhavnagar city with groundwater helium sampling stations.

some of the original wells could not be resampled and had to be abandoned because of a decline in the water table and drying up of the wells. In such cases wells in the vicinity were sampled.

2. Experimental

Water samples for analyses of dissolved helium were collected in 3-mm thick, 1.2-litre capacity, soda-lime glass bottles using procedures standardised in our laboratory for these analyses and described earlier (Gupta *et al* 2002). Briefly, after complete purging of air by groundwater, the bottles were filled by the water samples up to the top and then water above a pre-determined level was quickly sucked off, keeping headspace for exsolving gases. The bottles were immediately sealed. The temperature, TDS and pH of groundwater samples were measured at the sampling stations using standard pre-calibrated probes.

The helium analyses were made on the equilibrated air from the headspace of the sampling bottles within a day using a helium sniffer probe (ALCATEL Model ASM 100 HDS) with a modified inlet port to enable quantitative helium analyses (see Gupta *et al* 2002). The measured helium concentrations are corrected for

- volume of headspace,
- water volume,
- volume of air drawn-in during analysis and
- loss during storage.

The equilibrated air helium concentrations can be converted to the groundwater helium concentrations using Henry's Law and the respective volumes of water and air /gas in the sampling bottles. Henry's constant is defined by $H = C_g/C_w = \{$ (concentration of helium in gas phase)/(concentration of helium dissolved in water)$\}$. Using $H = 94.5$ (Fry *et al* 1995) at 25°C, the concentration of dissolved helium in equilibrium with air containing 5.3 ppmv helium is equivalent to 5.6×10^{-2} ppmv. However, for the sake of convenience the dissolved helium concentrations are expressed here in terms of Air Equilibration Units (AEU), i.e., helium concentration in air that was in equilibrium with the water at one atmospheric pressure. Helium anomaly is defined as concentration above the atmospheric equilibration value of 5.3 ppmAEU). The reproducibility of sampling and measured helium concentration variation is $< 5\%$ (table 1).

3. Results

Twelve of the sixteen groundwater samples collected for dissolved helium survey in September 2000 (figure 2) showed helium concentrations more than the air equilibration value of 5.3 ppmAEU (table 2). The values ranged between 11 and 498.2 ppmAEU. The highest value was found in a groundwater sample from a 60-m deep tubewell (#233) followed by 179.5 ppmAEU from a 43-m deep tubewell (#242). These values are much higher than those (~20ppmAEU) found even in deeper tubewells (#238, #239, #240) on the western outskirts of Bhavnagar. The groundwater temperatures ranged from 30° – 40°C and helium solubility changes due to these (Weiss 1971) cannot account for observed helium excesses.

Although a few studies (Datta *et al* 1980) had suggested that in alluvial aquifers, deeper groundwaters have higher helium concentration, subsequent measurements (Gupta and Deshpande 2003) and the present study indicate that in basaltic aquifers, this may not necessarily be the case. The present study, however, indicates that in the Bhavnagar city, high values of helium in groundwater are generally found in the basaltic aquifers and relatively low helium concentrations in the alluvial aquifer (see table 2). This observation is consistent with the understanding that interconnected pore space and high porosity in alluvial aquifers facilitate quick escape of helium from groundwater and the unconnected pore space and low porosity in basaltic aquifers limit the opportunity for groundwater helium to escape.

4. Discussion

The temporal variations of groundwater helium are plotted in figure 3. Some stations, particularly those with high levels of excess dissolved helium, showed a change by more than a factor of 2. From September 2000 to January 2001, except in case of stations #233 & #244 located in the basaltic aquifers, helium concentrations have either not changed or decreased marginally. Between January and March 2001, five out of seven stations, again located in basaltic aquifers, showed increase in helium concentration. This increase was also accompanied by an increase in TDS (except Stn. #238 & #239). It will also be noticed from figure 3 and table 2 that with respect to the data for September 2000, helium and TDS concentration changes in January and March 2001 have largely been in the same direction (increase/ decrease/ no change) for respective wells.

There also appears a certain pattern in the helium concentration and TDS between the three sets of sampling. It is seen that helium concentration changes (Sept. 2000 – March 2001; figure 4), at different stations are related to changes in (i)

Table 1. *Data of post-earthquake groundwater helium survey in Bhavnagar city, Gujarat, India.*

Sample code	Well type TW/HP	Location name	Near surface lithology AL/BAS	Depth (m)	Temperature (°C)			TDS (ppm)			Helium concentration (ppm AEU)		
					Sept. 2000	Jan. 2001	March 2001	Sept. 2000	Jan. 2001	March 2001	Sept. 2000	Jan. 2001	March 2001
CBGW-230	TW	Ambawadi	BAS	10	32	29	30	2800	2700	3500	5.3	5.3	6.2
CBGW-231	HP	Navapura	AL	21	30	28	28	500	500	500	5.9	5.3	5.9
CBGW-232	HP	Vorawad	AL	24	30	29	29	600	600	500	5.3	5.6	5.3
CBGW-233	TW	Medical College	BAS	61	32	31	32	3300	4100	3900	498.2	518.6	687.3
CBGW-234	TW	Kalvibid D-136	BAS	53	33	31	33	1100	1200	1200	5.3	5.3	5.9
CBGW-235	TW	Siddhipark	AL	18[α]/18[β]	33[α]	30[β]	31[β]	1700[α]	1400[β]	1300[β]	5.9[α]	5.3[β]	5.9[β]
CBGW-236	TW	Malanaka	AL	9	31.5	30	31	2400	2100	2000	5.3	5.3	5.3
CBGW-237	TW[α]/HP[β]	Tilaknagar	AL	20[α]/12[β]	31[α]	29[β]	30[β]	5100[α]	800[β]	1000[β]	10.6[α]	5.3[β]	5.3[β]
CBGW-238	TW	Chitra[γ]	BAS	229	40	–	39	2200		2200	22.9		53.7
CBGW-239	TW	Chitra	BAS	218	40	–	40	1200		1200	18.1		36.6
CBGW-240	TW	Chitra[δ]	BAS	293	39	–	40	1400		1600	26.3		18.8
CBGW-241	TW	Hill Drive	BAS	55	35	31	31	1000	1000	900	11.7	10.1	11.7
CBGW-242	TW	Kalvibid, Shantinagar	AL	43	33	28	31	7100	5900	6400	179.5	112.7	112.6
CBGW-243	TW	Vijayraj Nagar	BAS	21	32	–	30	900		1000	7.8		12.9
CBGW-244	HP	Darbari Kotha	BAS	34	31	30	30	1000	1300	1400	13.0	14.9	17.2
CBGW-245	HP	Krishnanagar	AL	15	31	α	α	2800	α	α	5.9	α	α
September 1998 sampling				Depth (m)	Temperature °C			TDS (ppm)			Helium concentration (ppm AEU)		
CBGW-47	TW	Chitra	BAS	127	–			–			6.6		
CBGW-48	TW	Chitra	BAS	229	39.5			–			100.2		

[α] Dried up and abandoned.

[β] Neighbouring tubewell to the one abandoned.

[γ] Repeat of CBGW-48.

[δ] Repeat of CBGW-47.

Table 2. *Reproducibility of measured helium concentration in groundwater samples.*

Sample location	Helium concentration (ppmAEU)		Variability(%)
	Sample-1	Sample-2	
Ranip	6.17	6.20	1
Bagodra	339.7	339.7	0
Roika^{X}	24.3	24.8	2
Tilaknagar	5.3	5.3	0

^{X} In this case eight samples in different sampling bottles were collected at the same time and analysed over a period of two years to estimate loss of helium during storage in sampling bottles. This loss has been estimated to be $< 0.15\%$ per day.

TDS of groundwater and, (ii) the lithology of the aquifer.

It is recalled that the sampling dates correspond to three distinct seismic phases at Bhavnagar:

- September 2000 – during this period low magnitude (< 4.2) tremors were repeatedly experienced;
- January 2001 – a long quiescent phase preceded the sampling;
- March 2001 – quiescent period following a major (26th January 2001) earthquake (magnitude: 7.6, IMD; 7.9 USGS) with epicentre > 300 km in NE.

Based on the reports of seismically induced geochemical changes in groundwater and local hydro-geological observations, two possible models to explain the observed variations in helium and TDS are examined.

- Seismically induced release of helium and/or forced injection of deep groundwaters (in general with higher helium and TDS concentrations) to shallow aquifers.
- Pumping of deep groundwaters due to decline in water table leading to progressive increase in helium and TDS.

The first model is based on several reported cases of increase in helium and salts in groundwater in response to earthquakes (Barsukov *et al* 1985a; Reimer 1985; Virk *et al* 2001). Also, in case of the Bhuj earthquake, large-scale liquefaction and resultant oozing of groundwater accompanied by release of gases at many places over a large area extending from Rajasthan to south Gujarat has been reported (Rajendran *et al* 2001). It may be useful to note that at Narveri (23.96°N;69.85°E); in the Great Rann of Kachchh an outflow of groundwater continued more than four months after the Bhuj earthquake (Gupta *et al* 2002). Air or gases bubbling through the freshly oozing water was observed at Narveri. Based on measurements of helium, radon, chloride, sulphate, sodium and temperature it was suggested that the outpouring water and escaping gases at Narveri had a deep confined source with a reservoir age in excess of $\sim 10^4$ years.

If seismically induced release of helium and/or forced injection of deeper groundwater were operative during the seismically active phase in September 2000, a decrease of helium concentration in the samples collected in January 2001 (quiescent phase) was expected. However, the decrease is observed only at three stations in alluvial terrain. In case of basaltic terrain, helium concentrations have either remained unchanged or have increased. This pattern of change in helium concentration has continued even in March 2001 (post Bhuj earthquake quiescent phase). This observed steady increase of helium concentration during quiescent phases in basaltic aquifers accompanied by no or marginal decrease in alluvial aquifers rules out the case of seismically induced injection of deep groundwater.

The second model is based on the observations that groundwater levels during successive sampling periods at Bhavnagar have steadily declined in basaltic terrain indicating pumping of progressively deeper (long resident) groundwater. As before, the deeper groundwater is expected to have higher concentrations of both helium and TDS due to longer residence in contact with aquifer material. This would explain the observed steady increase in both helium concentration and TDS in basaltic terrain. However, concurrent enhancement in helium and TDS concentrations in basaltic terrain and decrease or 'no change' in the alluvial terrain needs to be explained. One also needs to explain the nonlinearity of TDS and helium concentration variations (figure 4).

In aquifers comprising of secondary unconnected porosity in the form of fractures and fissures (e.g., the basaltic aquifers) groundwaters exhibit large spatial variability in dissolved constituents reflecting their largely local origin. This is clearly seen from table 2. The old groundwaters in such aquifers too will carry this spatial variability of dissolved constituents but with higher concentrations due to

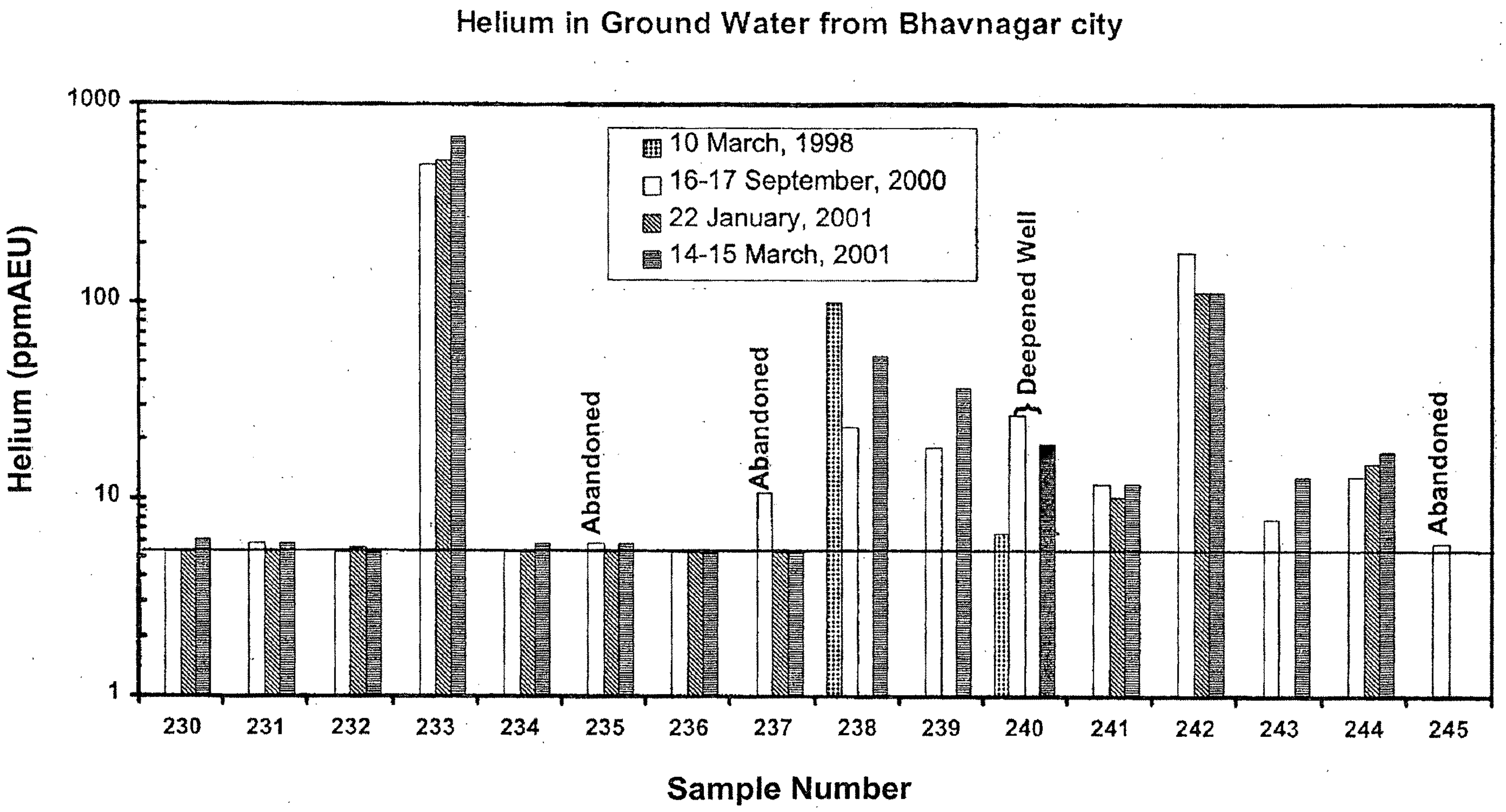

Figure 3. Temporal variation of groundwater helium concentration from Bhavnagar city during September 2000 to March 2001. Two analyses on samples collected in March 1998 are also shown. The horizontal line at 5.3 ppmAEU indicates the helium concentration expected in a water sample in equilibrium with atmosphere. Decline in groundwater level and drying up/ deepening of wells forced abandonment of three observation wells. In their place new wells were selected in the vicinity.

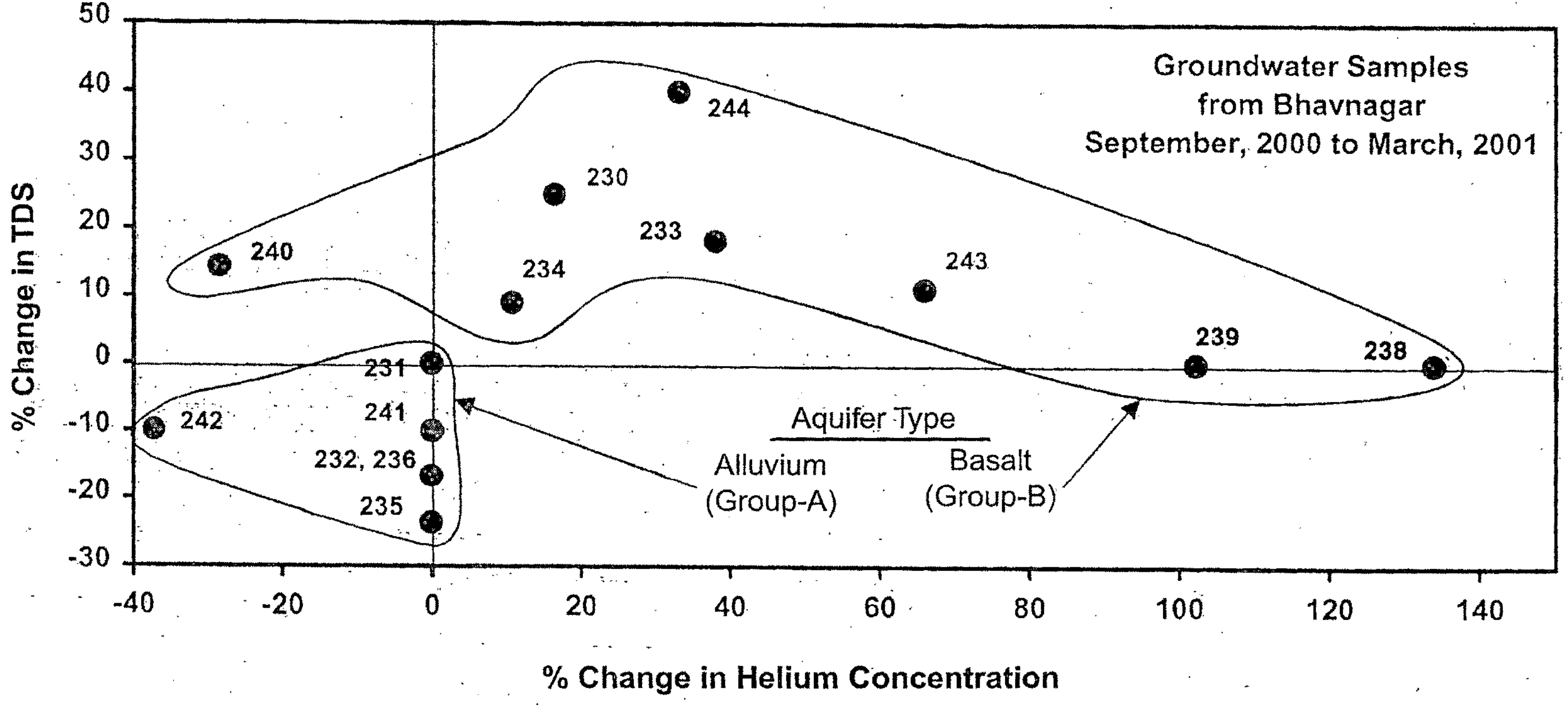

Figure 4. Bivariate plot of groundwater helium and TDS variation for different stations in Bhavnagar city between two sets of sampling. Samples derived from alluvial aquifers (Group-A) show decrease in TDS and/or helium concentration. Samples derived from basaltic aquifers (Group-B) show increase in TDS and/or helium concentration.

longer residence. The fractures and fissures quickly recharge these aquifers after the rain, but the amount is limited by the small availability of pore space. In post rainy season, excessive withdrawal of groundwater (as was indicated by decline in groundwater levels and drying up of some wells leading to their abandonment) results in pumping of old 'long resident' groundwater. This is in contrast to a relatively slow recharge that takes place during post monsoon period due to infiltration over a large area in regions of primary porosity such as alluvial aquifers. This recharge leads to slow but significant dilution of resident groundwater in alluvial aquifers in the post rainy season. Therefore, in a region having aquifers with both primary and secondary porosity correlation between variations of TDS and helium concentration in response to either mixing of old groundwater and/or post monsoon recharge may exhibit considerable variation. The variability of this relationship is due to the inherent spatial variability in dissolved constituents in groundwater, the porosity and the permeability.

It is seen from figure 4 that stations falling in Group-A, showing decrease in TDS and little or no decrease in helium are drawn from aquifers in the alluvial terrain. These stations had relatively lower values (table 2) of both TDS and helium in September 2000. The observed reduction in January and March 2001, therefore, represent dilution with slow post monsoon recharge through the overlying soil. It may be noted that the post monsoon recharge will have a 'fixed' low (= 5.3 ppmAEU) concentration of helium and low (though not necessarily a 'fixed' value) TDS. In contrast, stations falling in Group-B, showing a significant increase (except #240) in helium and moderate increase in TDS (except #238 & 239) are drawn from aquifers in the basaltic terrain. These stations, derived from the basaltic aquifers, had relatively high values of both TDS and helium in September 2000 (table 2). The observed increase in both TDS and helium in January and March 2001 represents pumping of relatively old groundwater with high but locally variable values of both TDS and helium due to the unconnected nature of secondary porosity.

5. Summary and conclusions

Temporal variations have been observed in both the concentration of dissolved helium and TDS of groundwaters at Bhavnagar following a period of locally enhanced seismic activity during August–September 2000. A significant aspect of the observed variation is the enhancement of helium and TDS concentrations in basaltic terrain and reduction in both parameters in alluvial terrain during the subsequent quiescent phases interrupted by a major Bhuj earthquake on 26th January 2001. Because of the large variability, it has not been possible to draw a quantitative relationship between the observed changes in TDS and helium concentration.

The observations have been explained by a model involving addition of deeper (old, long resident) groundwater in response to post-monsoon excessive pumping in the basaltic terrain and a concurrent dilution by slow post monsoon groundwater recharge in the alluvial terrain. The observed large variation is therefore due to the prevailing hydro-geological situation at Bhavnagar.

The steady increase of helium concentration in basaltic aquifers during quiescent phases, accompanied by little or marginal decrease in alluvial aquifers rules out the possibility that the observed variations were seismically induced.

Acknowledgements

The authors are thankful to Mr. G C Srivastava, Mr. P M Joshi, Mr. Y Sharma, Mr. S A Qureshi and Mr. D Dodia of GWRDC for identifying suitable sampling stations and fruitful discussions. We thank Prof. N Bhandari for critically reviewing the manuscript.

References

Barsukov V L, Varshall G M and Zamokina N S 1985a Recent results of hydrogeochemical studies for earthquake predictions in the USSR; *PAGEOPH* **122(2–4)** 143–156

Barsukov V L, Serebrennikov V S, Belaev A A, Bakaldin Yu A and Arsenyeva R V 1985b Some experience in unravelling geochemical earthquake precursors; *PAGEOPH* **122(2–4)** 157–163

Datta P S, Gupta S K, Jayasurya A, Nijampurkar V N, Sharma P and Plusnin M I 1980 A survey of helium in groundwater in parts of Sabarmati basin in Gujarat state and in Jaisalmer district, Rajasthan; *Hydrological Sciences- Bulletin* **25(2)** 183–193

Fry V A, Istok J D, Semprini L, O'Reilly L T and Buscheck T E 1995 Retardation of dissolved oxygen due to a trapped gas phase in porous media; *Groundwater* **33(3)** 391–398

Gupta S K, Bhandari N, Thakkar P S and Rengarajan R 2002 On the origin of the artesian groundwater and escaping gas at Narveri after the Bhuj earthquake in 2001; *Curr. Sci.* **82(4)** 463–468

Gupta S K and Deshpande R D 2003 Origin of groundwater helium and temperature anomalies in the Cambay region of Gujarat, India; *Chem. Geol.* (in press)

King Chi-Yu 1985 Earthquake hydrology and chemistry; *PAGEOPH* **122(2–4)** 141–142

Rajendran K, Rajendran C P, Thakkar M and Tuttle M P 2001 The 2001 Kutch (Bhuj) earthquake: coseismic surface features and their significance; *Curr. Sci.* **80(11)** 1397–1405

Rao G V, Reddy G K, Rao R U M and Gopalan K 1994 Extraordinary helium anomaly over surface rupture of September 1993 Killari earthquake, India; *Curr. Sci.* **66(12)** 933–935

Reddy G K, Rao G V, Rao R U M and Gopalan K 1994 Surface rupture of Latur earthquake: The soil-gas helium signature; *Mem. Geol. Soc. India* **35** 83–99

Reimer G M 1985 Prediction of central California earthquakes from soil-gas helium fluctuations; *PAGEOPH* **122(2–4)** 369–375

Srivastava S and Rao D T 1997 Present status of seismicity of Gujarat; *Vayumandal*, **27** (1–2) 32–39

Sultankhodzhayev A N, Latipov S U, Zarikov T Z, Zigan F G 1980 Dependence of hydrogeoseismological anomalies on the energy and epicentral distance of earthquakes; *Dokl. AN Uzb. SSR* **5** 57–59

Varshall G M, Sobolev G A, Barsukov V L, Kohsov A V, Kostin B I, Kudinova T F, Stakheyev Yu I and Tretyakova S P 1985 Separation of volatile components from rocks under mechanical loading as the source of hydrogeochemical anomalies preceding earthquakes; *PAGEOPH* **122(2–4)** 463–477

Virk H S, Walia V and Kumar N 2001 Helium/Radon precursory anomalies of Chamoli earthquake, Garhwal Himalaya, India; *Journal of Geodynamics* **31** 201–210

Weiss R F 1971 Solubility of helium and neon in seawater; *Journal of Chemical Engineering Data* **167** 235–241

MS received 1 January 2002; revised 30 August 2002

Groundwater in and Around Cambay Basin, Gujarat: Some Geochemical and Isotopic Investigations

Summary of the Thesis Submitted to

The Maharaja Sayajirao University of Baroda, Vadodara

For The Award of the Degree of

Doctor of Philosophy

in

Geology

By

R.D. Deshpande

Physical Research Laboratory
Ahmedabad, INDIA

November 2006

Groundwater in and around Cambay Basin, Gujarat: Some Geochemical and Isotopic Investigations.

Summary of the Thesis

Introduction

This thesis is based on the geochemical and isotopic investigations of groundwater from North Gujarat-Cambay (NGC) region in the Western India. The NGC region is characterized by a unique combination of geological, hydrological, tectonic and climatic features, namely (i) two major deep seated faults (East Cambay Basin Bounding Fault; ECBBF and West Cambay Basin Bounding Fault; WCBBF) defining the Cambay Graben and several sympathetic faults parallel and orthogonal to these; (ii) more than 3 km thick sedimentary succession forming a regional aquifer system in the upper part; (iii) higher than average geothermal heat flow; (iv) intermittent seismicity; (v) emergence of thermal springs; (vi) arid climate with high rate of evapotranspiration; and (vii) significant mining of groundwater over the past few decades.

As a result of extensive groundwater mining, the piezometric levels have declined by >3 m/yr during the last couple of decades. During the same period, progressive increase in groundwater fluoride concentrations with time and associated endemic fluorosis has been observed. In general, high fluoride in groundwater of the region has been associated with long residence time of the mined groundwater or subsurface injection of thermal waters. Very high amounts of dissolved helium and high groundwater temperatures from some parts of the NGC region were reported earlier but, their inter-relationship as well as their possible relationship with basement faults in the region was not understood in terms of tectonic framework and geothermal regime of the NGC region. The Late Quaternary sedimentary record of the region is indicative of increased aridity around Last Glacial Maxima (LGM; ~20 kaBP). However, no palaeoclimatic imprints were reported in hydrological studies.

Based on general topography, geology, lithologs of the drilled tubewells and the water level/ piezometric level data, the area of the foothills of the Aravalli Mountains in the NE was considered as the recharge area of the regional aquifer system with groundwater moving westwards towards the low lying tract linking Little Rann of Kachchh (LRK) – Nalsarovar (NS) – Gulf of Cambay (GC). However, this inference of groundwater recharge and movement, from conventional methods needed to be reinforced and substantiated by determining the age of groundwater by employing radiometric dating methods.

Objectives

The objective of this study was to bridge the existing gap in the knowledge as discussed above by carrying out specific geochemical and isotopic investigations. This study aimed to (i) determine the distribution of helium and temperature of groundwater and relate the anomalies with the tectonic framework of the region; (ii) determine the distribution of various geochemical tracers that could help identify the origin of groundwater fluoride; (iii) determine the direction and rate of movement of groundwater in the regional aquifer system; and (iv) search for hydrological proxies of past climates.

Methodology

To achieve the above objectives, following methodology was adopted.

- A survey of dissolved helium and temperature of groundwater in the NGC region was undertaken to delineate areas with anomalies in these parameters and to understand their inter-relationship with the regional tectonics. Simple procedures were developed and standardized for (i) sample collection and storage, and (ii) measurement of helium concentrations in soil-gas and groundwater using commercially available helium leak detector.

- A survey of dissolved groundwater fluoride and electrical conductivity (EC) was undertaken to identify areas of high concentration of fluoride, and to understand its origin. Dissolved fluoride and EC of modern rainfall were also measured to understand the role of dry deposition and/ or amount of rain in controlling the fluoride and EC of rainwater.

- Groundwater dating was undertaken employing ^{14}C decay, ^{4}He accumulation and $^{4}He/\,^{222}Rn$ ratio methods to determine regional groundwater flow parameters. Laboratory and field procedures for carbonate precipitation (for ^{14}C method) and water sample collection, storage and analyses for other groundwater dating methods were developed and standardized.

- Oxygen and hydrogen isotope ratios ($\delta^{18}O$ and δD) in thermal springs and groundwater samples were measured to identify the possible signatures of the past aridity and to identify the source of thermal spring water. Isotopic analyses of modern precipitation were also carried out to provide a reference for interpretation of the groundwater data.

- A groundwater CFC laboratory was set up as part of this study. Field and laboratory procedures for sample collection, storage, extraction of dissolved CFCs and injection for gas chromatographic analyses were standardized.

Results and Conclusions

Important observations from the above investigations and the conclusions drawn are summarized in the following.

Groundwater Helium and Temperature

Areas of high values of excess helium (He_{ex} >15 ppm AEU) in groundwater are generally associated with areas of high values of groundwater temperatures (>35 °C). Such areas are found to (i) lie along the major basement faults (ECBBF and WCBBF) on both flanks of the Cambay Graben; (ii) overlie sympathetic faults parallel or orthogonal to major faults; and (iii) overlie regions of thermal springs. Despite this geographical correlation between high He_{ex} and high temperature of groundwater, no quantitative correlation is seen between the two. Interpretation of such a high value of dissolved helium in groundwater pockets in terms of *in situ* accumulation would imply a long residence time (>100 kaBP) in aquifer. Such a long residence time of groundwater particularly in the recharge area and the observed inliers of old ground waters away from recharge area are not compatible with the hydrogeology and the ^{14}C age of groundwater. Evidence of near surface uranium mineralization was also not found from ^{222}Rn activity measurements and has also not been reported in any other study from this region ruling out the possibility of near surface uranium mineralization as the source for the observed He_{ex}. It is, therefore, inferred that observed high He_{ex} in certain groundwater pockets is due to injection from deeper sources that derive helium from much larger aquifer/rock volumes.

In this scheme of interpretation, deep subsurface faults provide pathways for upward migration of deeper fluids with high helium concentration and high temperature. Lack of quantitative relationship between He_{ex} and temperature, however, indicates that many localized sources with their varying helium concentration and fluid temperature may be involved in transferring helium and/ or heat from deeper levels to shallower aquifers. This interpretation is also presented in the form of a conceptual tectono-hydrothermal model for the NGC region. In this model, the radiogenic helium produced in a large volume of rocks within or below the basement migrates through micro-cracks into braided and interconnected fractures and dissolves in deep fluids/groundwater. Such deep fluids could either be of lower crust/ upper mantle origin or originate through downward migration of meteoric water from other locations using the pathways provided by deep fractures and fissures. This could result in setting up of a hydrothermal circulation along the deep seated fractures and fissures. The extent to which these deep fluids may have high concentration of helium is governed by interconnectedness of micro-cracks and fractures and the temperature is governed by the depth up to which any particular hydrothermal circulation cell penetrates.

Groundwater Fluoride

Based on the understanding that dissolved salt content of groundwater is to some extent related to leaching from the aquifer matrix, the high fluoride concentration in ground waters of NGC region was earlier believed to be related (i) either to the relatively high concentration of fluoride bearing minerals in certain sub-aquifer zones or (ii) to the higher residence time of groundwater. Geographical distribution of dissolved fluoride in groundwater of NGC region and its radiometric age, however, reveals that areas of high fluoride concentrations (>1.5 ppm) are not related to residence time. It is observed that the areas of high fluoride and high EC (>2 mS) are aligned around four linear belts. Three of these linear belts are trending NNW-SSE and roughly parallel to recharge zone in the Aravalli foothills. These groundwater belts of high fluoride are separated by low fluoride groundwater, forming alternate bands of high and low fluoride in groundwater. The fourth linear belt is trending EW from the region of thermal springs (Tuwa and Lasundra) to the low lying area around Nalsarovar.

This fluoride distribution in the NGC region is explained based on a hydrological model comprising a recharge area in the foothills of the Aravalli Mountains, grading into the confined aquifer south westwards towards LRK-NS-GC belt and general disposition of this semi-arid region to enhanced groundwater fluoride concentration. The groundwater in this aquifer system moves through the confined aquifer with the chemical characteristics acquired in the recharge area but progressively aging as it moves away from the recharge area.

The groundwater ages (using ^{14}C, ^{4}He and $^{4}He/^{222}Rn$ methods) progressively increase away from recharge area but the dissolved fluoride concentration does not increase progressively corresponding to groundwater age. Instead, alternating bands of high and low fluoride concentration in groundwater from confined aquifers are observed. This observation suggests the possibility of an additional control on fluoride concentration in groundwater of NGC region.

The confined groundwater in the central high fluoride groundwater belt within the Cambay Basin corresponds to groundwater ^{14}C age in the range 15-25 kaBP. The period around 20 kaBP, corresponding to the Last Glacial Maxima (LGM) is known to be a period of enhanced aridity in the NGC region. The enhanced aridity is generally associated with (i) increased evaporation; (ii) decreased rainfall; and (iii) increased dry deposition. Some imprints of evaporation and dry deposition even in the present climate are seen in the ionic concentration and stable isotopic composition of modern rainfall. The significant control of dry deposition is seen in the variation of fluoride and EC of fortnightly accumulated rain water samples. It is, therefore, inferred that groundwater recharged around LGM in the Aravalli foothills during the period of enhanced aridity has since traveled to its present position within Cambay Basin and corresponds to the central high fluoride groundwater belt. The groundwater, with relatively low fluoride concentration, on either side of this belt suggests recharge during less arid climatic regime.

The eastern high fluoride belt located in the recharge area corresponds to the modern recharge. The existence of high fluoride groundwater pockets in the recharge area is an indication that even under the present geo-environmental conditions, groundwater recharged to the regional aquifer system is predisposed to a certain degree of high fluoride content due to combination of (i) leaching; (ii) dry deposition and evaporation prior to recharge; and (iii) increased rock-water interaction at higher temperatures during hydrothermal circulation (as evidenced in thermal springs).

The western high fluoride belt overlies a low lying LRK-NS-GC tract which is the convergence zone for surface and subsurface drainage. The very high level of groundwater fluoride concentration in this belt is possibly due to evaporative enrichment of salts in the stagnant water in the topographically low area and its subsequent infiltration into shallower aquifers.

The high fluoride and EC in the E-W belt, linking the regions of thermal springs to the low lying area around Nalsarovar, can be attributed to additional source (hydrothermal fluids with relatively high concentration of ions including fluoride) steadily venting into the groundwater in the recharge area of the confined aquifers around Tuwa and Lasundra throughout the Late Quaternary period and the steady movement of the mixed groundwater in the regional aquifer system. The fluoride contribution by the hydrothermal fluids is so prominent and steady that imprints of the wet/arid excursions in climate are not visible along EW belt. Instead a continuous belt of higher fluoride (>1.5 ppm) and high EC (>2 mS) is seen.

It is, therefore, concluded that the high fluoride in groundwater of NGC region is not governed by its residence time in the aquifer but arises from a combination of (i) predisposition of this semi-arid region to high groundwater fluoride resulting from mineral assemblage in surface soils and aquifer matrix aided by general aridity, in particular the enhanced aridity around LGM; (ii) injection of hydrothermal fluids into groundwater; and

(iii) evaporative enrichment of salts in the stagnant water in the low lying convergence zone and its infiltration into groundwater.

Stable Isotopes of Oxygen and Hydrogen

The amount weighted average values for the modern rainfall in the NGC region are: $\delta^{18}O = -4.3 \pm 2.1‰$, $\delta D = -33 \pm 16‰$ and *d*-excess $=1.2 \pm 4.8‰$. This *d*-excess value and both the slope (7.6 ± 0.6) and the intercept ($-2.9 \pm 2.2‰$) of the local meteoric water line (LMWL) are lower than the average values of global meteoric water line (GMWL) and are interpreted as isotopic imprints of evaporation from falling raindrops under the present semi-arid climatic regime.

The groundwater samples exhibit a range of variation in isotopic composition significantly narrower than that for precipitation and both $\delta^{18}O$ and δD are higher than that for modern precipitation. The average value of *d*-excess of all groundwater samples ($-4.5 \pm 11‰$) is lower than that of precipitation samples. These isotopic characteristics for groundwater in the NGC region indicate mixing of rain water from different events in the soil and additional evaporation during the infiltration process confirming the predisposition of the region to evaporation, prior to groundwater recharge.

It is also seen from the geographical distribution of $\delta^{18}O$ and *d*-excess that groundwater around a linear belt within Cambay Basin is characterized by relatively lower values of *d*-excess and higher values of $\delta^{18}O$. Since evaporation of water results in low values of *d*-excess and higher $\delta^{18}O$, the groundwater around this belt within Cambay Basin represents relatively increased evaporation (indicative of enhanced aridity) either during rainfall or during groundwater recharge compared to groundwater on either side of this belt. The ^{14}C age of the confined groundwater around this belt has been estimated to be in the range 15-25 kaBP corresponding to the known arid phase in the past. Taking a holistic view of the data, i.e., 15-25 kaBP groundwater age, its lowered *d*-excess and higher $\delta^{18}O$, it is concluded that groundwater recharged in the Aravalli foothills around LGM with signatures of enhanced aridity has since traveled to its present position.

The isotopic characteristics of thermal waters indicate a trend towards isotopic equilibrium between ^{18}O depleted meteoric water and ^{18}O enriched rocks at higher temperatures.

Groundwater Dating

It is observed that the succession of sand/ silty-clay layers forming multilayered aquifer system is nearly parallel to the regional inclination of ground surface and the sampled tube wells tap almost the same set of water bearing formations across the NGC region. The groundwater in these nearly parallel layers of confined aquifers is recharged largely from the sediment-rock contact zone in the foot hills of Aravalli Mountains, and after the confinement becomes effective, moves with approximately the same velocity. This geohydrological model of the regional aquifer system appears to be justified because, the unconfined aquifers in the regions of Cambay Basin and farther westwards are almost completely dried up (as evident from several dried up and abandoned dug wells). Since the tubewells tap all the water bearing horizons intercepted within their maximum depth, these are treated as pumping a single aquifer unit, within which the groundwater ages progressively increase in the flow direction.

The estimated groundwater ^{14}C ages progressively increase from <2 kaBP in the ENE (along Aravalli foothills) to >35 kaBP in the WSW direction towards the low-lying tract linking LRK-NS-GC. From hydro-geological considerations, it seems that the confinement of the regional aquifers in the NGC region becomes effective near the ECBBF. Within the Cambay Basin, the age isolines are nearly parallel to each other and the horizontal distance between the successive 5 kaBP isolines is nearly constant giving a regional flow velocity in the range 2.5 – 3.5 m a^{-1} under the prevailing average hydraulic gradient of 1 in 2000. West of WCBBF, the ^{14}C ages increase rapidly, roughly in agreement with the distribution of transmissivity of the aquifers obtained from the pump test data, progressively decreasing from ~1000 m^2 d^{-1} east of the ECBBF to <200 m^2 d^{-1} west of the WCBBF.

The 5 ppmAEU He_{ex} isoline runs nearly along the WCBBF and corresponds to ^4He age of ~15 kaBP for helium release factor $\Lambda_{He} = 1$, and ~37 kaBP for $\Lambda_{He} = 0.4$. Except for pockets of anomalous groundwater helium concentrations, the ^4He ages are in close agreement with the ^{14}C ages for $\Lambda_{He} = 0.4$ when no crustal flux is considered. Ignoring the crustal flux is justified because the sampled wells up to the WCBBF in the in the NGC region tap shallow depth compared to total depth (~3 km) of the Cambay basin and hence are free from the crustal influence. For transmissivity values (~200 m^2d^{-1} – 1000 m^2d^{-1}) of the aquifers and crustal helium flux of 3.0 x 10^{-8} cm^3STPHe $cm^{-2}y^{-1}$ for sedimentary basin, the groundwater flow entrains insignificant amount of helium and therefore, groundwater ^4He ages are almost unaffected by the deep crustal ^4He flux.

A gradual $^4He/^{222}Rn$ age progression from the recharge area towards the WCBBF is also observed in the major part of the study area, similar to that for ^{14}C ages and ^4He ages.

Important Contributions of this Study

In the forgoing, main inferences from various geochemical and isotopic investigations of this study were summarised. The major contributions of this study are enumerated in the following.

A Geo-hydrological Model of Aquifer System in NGC Region

The regional aquifer system of NGC region comprises a sequence of unconfined and confined sub-aquifers. The recharge area of the confined aquifers lies in the foot hills of the Aravalli Mountains in the east. The confinement of aquifers becomes effective only towards west of the ECBBF. Beyond the region of effective confinement, the groundwater in the aquifer system preserves the geochemical and isotopic characteristics acquired at the time of recharge in the recharge area. The groundwater ages progressively increase in the general flow direction nearly along WSW up to the low lying tract of the LRK-NS-GC, which is also a zone of convergence with groundwater flow from its both the sides.

However, in certain pockets overlying the intersecting basement faults, deeper crustal fluids do get injected into the aquifer system and significantly alter some of the geochemical properties of the groundwater of the region.

A Conceptual Tectono-hydrothermal Model of NGC Region

Deeper crustal fluids injected into the groundwater of NGC region have been shown to affect temperature, dissolved helium, water isotopes, fluoride and EC of groundwater in certain pockets. The localization of these pockets along intersecting deep seated basement faults on the two flanks of the Cambay basin is conceptualised in the form of a tectono-hydrothermal model of the NGC region.

Origin of High Fluoride in Groundwater from NGC Region

The high fluoride concentration in groundwater of NGC region around the E-W line is explained by a continuous injection, throughout Late Quaternary, of hydrothermal fluids from around the thermal springs of Lasundra and Tuwa and the groundwater flow in the regional aquifer as governed by hydraulic gradient from the recharge area in the Aravalli foothills towards the Nalsarovar in low lying LRK-NS-GC tract. This mechanism, however, does not explain the observed distribution of enhanced groundwater fluoride around the three nearly NNW-SSE parallel lines. This distribution is explained by: (i) predisposition of this semi-arid region to high groundwater fluoride arising from mineral assemblage in surface soils and in aquifer matrix, aided by general aridity particularly in the recharge area; (ii) enhanced aridity around the LGM leading to recharge of groundwater enriched in fluoride resulting from enhanced evaporation as well as dry deposition and flow of this groundwater to its present location within Cambay Basin during the past 20 ± 5 kaBP; and (iii) evaporative enrichment of stagnant surface water in the low lying LRK-NS-GC convergence zone and infiltration of a part of it into groundwater.

Palaeo-climatic Imprints in Groundwater from NGC Region

The confined groundwater around a belt within Cambay Basin has characteristic geochemical (high fluoride and high EC) and isotopic (high $\delta^{18}O$ and low *d*-excess) signatures that are different from signatures of these parameters on either side. The alternating bands of groundwater with distinguishable geochemical and isotopic properties are explained as imprints of the past climate alternating between arid and humid phase, which modifies the geochemical and isotopic properties of the water infiltrating from the recharge area (Aravalli foothills) of the confined aquifer. The groundwater recharged during different climatic regime flows subsequently in the confined regional aquifer system giving rise to observed alternating bands of groundwater with distinctly different chemical properties. Thus, groundwater around the liner belt within Cambay Basin, indicate its recharge during enhanced aridity around LGM.